



NATIONAL TECHNICAL UNIVERSITY OF ATHENS

SCHOOL OF CHEMICAL ENGINEERING

DEPARTMENT OF SYNTHESIS AND DEVELOPMENT OF INDUSTRIAL PROCESSES

LABORATORY OF POLYMER TECHNOLOGY

DOCTORAL DISSERTATION

Development of environmentally friendly polymerization processes

Christina I. Gkountela

Chemical Engineer, NTUA

Supervisor: Stamatina N. Vouyiouka, Associate Professor NTUA

Athens, 2023

"The implementation of the doctoral thesis was co-financed by Greece and the European Union (European Social Fund-ESF) through the Operational Programme "Human Resources Development, Education and Lifelong Learning" in the context of the Act "Enhancing Human Resources Research Potential by undertaking a Doctoral Research" Sub-action 2: IKY Scholarship Programme for PhD candidates in the Greek Universities".



Operational Programme
Human Resources Development,
Education and Lifelong Learning
Co-financed by Greece and the European Union





ΕΘΝΙΚΟ ΜΕΤΣΟΒΙΟ ΠΟΛΥΤΕΧΝΕΙΟ
ΣΧΟΛΗ ΧΗΜΙΚΩΝ ΜΗΧΑΝΙΚΩΝ
ΤΟΜΕΑΣ ΣΥΝΘΕΣΗΣ ΚΑΙ ΑΝΑΠΤΥΞΗΣ ΒΙΟΜΗΧΑΝΙΚΩΝ ΔΙΑΔΙΚΑΣΙΩΝ
ΕΡΓΑΣΤΗΡΙΟ ΤΕΧΝΟΛΟΓΙΑΣ ΠΟΛΥΜΕΡΩΝ

ΔΙΔΑΚΤΟΡΙΚΗ ΔΙΑΤΡΙΒΗ

Ανάπτυξη φιλικών προς το περιβάλλον διεργασιών πολυμερισμού

Χριστίνα Ι. Γκουντέλα

Χημικός Μηχανικός, ΕΜΠ

Επιβλέπουσα: Σταματίνα Ν. Βουγιούκα, Αναπληρώτρια Καθηγήτρια ΕΜΠ

Αθήνα, 2023

«Η υλοποίηση της διδακτορικής διατριβής συγχρηματοδοτήθηκε από την Ελλάδα και την Ευρωπαϊκή Ένωση (Ευρωπαϊκό Κοινωνικό Ταμείο) μέσω του Επιχειρησιακού Προγράμματος «Ανάπτυξη Ανθρώπινου Δυναμικού, Εκπαίδευση και Διά Βίου Μάθηση», 2014-2020, στο πλαίσιο της Πράξης «Ενίσχυση του ανθρώπινου δυναμικού μέσω της υλοποίησης διδακτορικής έρευνας Υποδράση 2: Πρόγραμμα χορήγησης υποτροφιών ΙΚΥ σε υποψηφίους διδάκτορες των ΑΕΙ της Ελλάδας».



Ευρωπαϊκή Ένωση
Ευρωπαϊκό Κοινωνικό Ταμείο

Επιχειρησιακό Πρόγραμμα
Ανάπτυξη Ανθρώπινου Δυναμικού,
Εκπαίδευση και Διά Βίου Μάθηση

Με τη συγχρηματοδότηση της Ελλάδας και της Ευρωπαϊκής Ένωσης



ανάπτυξη - εργασία - αλληλεγγύη

Η έγκριση της διδακτορικής διατριβής από την Ανώτατη Σχολή Χημικών Μηχανικών του Εθνικού Μετσόβιου Πολυτεχνείου δεν υποδηλώνει αποδοχή των γνώμων του συγγραφέα (Ν. 5343/1932, Άρθρο 202).

Dans la vie, rien n'est à craindre, tout est à comprendre.

Marie Curie

Examination Committee

Stamatina N. Vouyiouka	Associate Professor, NTUA, Supervisor
Constantine D. Papaspyrides	Emeritus Professor NTUA, Member of the Advisor Committee
Evangelos Topakas	Associate Professor NTUA, Member of the Advisor Committee
Petroula Tarantili	Professor NTUA
Anastasia Detsi	Professor NTUA
Haralambos Stamatis	Professor University of Ioannina
Jasmina Nikodinovic-Runic	Full research Professor IMGGE, University of Belgrade

Acknowledgements

The Doctoral Thesis in hand was conducted at the Polymer Technology Laboratory, School of Chemical Engineering, NTUA, under the supervision of Stamatina Vouyiouka, Associate Professor NTUA. Part of the research was co-financed by Greece and the European Union (European Social Fund-ESF) through the Operational Programme "Human Resources Development, Education and Lifelong Learning" in the context of the Act "Enhancing Human Resources Research Potential by undertaking a Doctoral Research" Sub-action 2: IKY Scholarship Programme for PhD candidate in the Greek Universities.

Completing my doctoral studies has brought forth many emotions. Throughout this embracing journey, I had the privilege of collaborating with numerous colleagues and friends who have provided invaluable support in their unique ways, contributing significantly to fulfilling my academic quest.

First and foremost, I would like to express my heartfelt appreciation to my supervisor and mentor, Associate Professor Stamatina Vouyiouka. Her invaluable academic and personal guidance, unwavering support, and mentorship have been instrumental throughout this journey. Collaborating with her has not only enriched my skills as a researcher but also contributed significantly to my evolution as a person. I am particularly grateful for her patience, dedication, and persistent efforts in assisting me to overcome challenges, ensuring the successful completion of this step. The way of thinking and problem-solving mentality she taught me will always be a mindset model for me.

This endeavour would not have been possible without the support of Professor Emeritus NTUA Constantine Papaspyrides and Associate Professor NTUA Evangelos Topakas, both advisory committee members. Their influence extended beyond my PhD research as I had the opportunity to work with them on several scientific projects. I am thankful for our collaboration, which has significantly contributed to my academic and professional growth.

I would like to express my deepest gratitude to the four defense committee members. In particular, I am grateful to Petroula Tarantili, Professor NTUA, for trusting me as a member of her teaching team during the undergraduate laboratory courses, sharing her knowledge with me. I would also like to thank Anastasia Detsi, Professor NTUA, for her assistance, pivotal in completing my PhD research and broadening my horizons. Furthermore, I would like to sincerely thank the defense committee members, Professor Haralambos Stamatis, and Professor Jasmina Nikodinovic-Runic for graciously accepting this role. I am truly honoured by their presence and contribution, which have added immense value to this significant milestone in my academic endeavours.

My gratitude extends to the Polymer Technology Laboratory faculty members, Dr. Dimitrios Korres, for his support and assistance throughout these years, Dr. Elli-Maria Barampouti and Dr. Sofia Mai, for the fruitful conversations we had.

Special thanks go to the laboratory's post-doctoral researcher, Dr. Athanasios Porfyrus. His support and advice from the outset have been a driving force for me and played a crucial role in the progress of my research. I am grateful to have him as a mentor and friend.

I am deeply thankful to my fellow colleagues and friends Konstantina Chronaki, Aggeliki Mytara, Christos Zotiadis, Christos Panagiotopoulos, Vasilis Nikitakos and Panagiotis Ketikis for the time spent together in the lab. Their daily presence there made this journey enjoyable.

During these years, I worked with brilliant undergraduate students: Dimitrios Markoulakis, Marilena Mathioudaki, Ioannis Spanos, and Ourania Plaggessi. I thank them for our smooth and fruitful collaboration.

Beyond the lab walls, I am fortunate to have met colleagues who became friends during my doctoral studies. I would like to thank the members of the Industrial Biotechnology & Biocatalysts Group (IndBioCat), NTUA, under the guidance of Associate Professor Evangelos Topakas, particularly Dr. Efstratios Nikolaivits, George Taxeidis and especially Konstantinos Makryniotis. I would also like to thank the members of the Organic Chemistry Laboratory, NTUA, under the direction of Professor Anastasia Detsi, especially Ioanna Pitterou.

Words cannot express my gratitude to my family, my partner, Thanos, and those friends who became family during these years, supporting and encouraging me to complete this significant chapter of my life.

Publications

Publications in international peer-reviewed scientific journals

A) Publications relevant to the Doctoral Dissertation

1. C. I. Gkountela, O. Plaggese, S. N. Vouyiouka. Enzymatic prepolymerization combined with bulk post-polymerization towards the production of bio-based polyesters: The case of poly(butylene 2,5-furandicarboxylate). Under preparation.
2. C. Gkountela, K. Makryniotis, I. Spanos, E. Topakas, S. N. Vouyiouka. Enzymatic prepolymerization of poly(butylene succinate) using a thermostable variant of the Leaf and branch compost cutinase (LCC), along with melt post-polymerization as a finishing step. Under preparation.
3. C. I. Gkountela, D. Markoulakis, M. Mathioudaki, I. Pitterou, A. Detsi, S. N. Vouyiouka. Scalable enzymatic polymerization and low-temperature post-polymerization of poly(butylene succinate): Process parameters and application. Eur. Polym. J. 198 (2023) 112423. [DOI](#)
4. C. I. Gkountela and S. N. Vouyiouka. Enzymatic Polymerization as a Green Approach to Synthesizing Bio-Based Polyesters. Macromol. 2 (2022) 30-57. [DOI](#)
5. C. Gkountela, M. Rigopoulou, E.M. Barampouti, S. Vouyiouka. Enzymatic prepolymerization combined with bulk post-polymerization towards the production of bio-based polyesters: The case of poly(butylene succinate). Eur. Polym. J. 143 (2021) 110197. [DOI](#)

B) Publications relevant to the broader research activity

1. K. Makryniotis, E. Nikolaivits, C. Gkountela, S. Vouyiouka, E. Topakas. Discovery of a polyesterase from *Deinococcus maricopensis* and comparison to the benchmark LCC^{ICCG} suggests high potential for semi-crystalline post-consumer PET degradation. J. Hazard. Mater. 455 (2023) 131574. [DOI](#)
2. G. Taxeidis, E. Nikolaivits, R. Siaperas, C. Gkountela, S. Vouyiouka, B. Pantelic, J. Nikodinovic-Runic, E. Topakas. Triggering and identifying the polyurethane and polyethylene-degrading machinery of filamentous fungi secretomes. Environ. Pollut. 325 (2023) 121460. [DOI](#)
3. E. Nikolaivits, G. Taxeidis, C. Gkountela, S. Vouyiouka, V. Maslak, J. Nikodinovic-Runic, E. Topakas. A polyesterase from the Antarctic bacterium *Moraxella* sp. degrades highly crystalline synthetic polymers. J. Hazard. Mater. 434 (2022) 128900. [DOI](#)

International scientific conferences

(*speaker in oral presentations)

A) Presentations relevant to the Doctoral Dissertation

1. S. N. Vouyiouka*, C. I. Gkountela, K. Chronaki. Sustainable challenges to produce green polymers and manage their waste: solid state polymerization, Biopol 2022 – 8th International Conference on Bio-based and Biodegradable Polymers, November 14-16, 2022, Alicante, Spain

2. C. Gkountela* and S. Vouyiouka. Exploring enzymatic polymerization pathways for the production of aliphatic polyesters, Polymers 2022 – New Trends in Polymer Science: Health of the Planet, Health of the People, May 25-27, 2022, Turin, Italy. [Proceedings/Abstract](#)
3. C. I. Gkountela, D. M. Korres, S. N. Vouyiouka. A green enzyme-based process for the production of poly(butylene succinate). 13th Hellenic Polymer Society International Conference, December 12-16, 2021, online
4. C. I. Gkountela, D. N. Markoulakis, D. M. Korres, S. N. Vouyiouka. Evaluation of the parameters of poly(butylene succinate) enzymatic polymerization, The 2nd International Online Conference on Polymer Science – Polymers and Nanotechnology for Industry 4.0 (ICOPS 2021), November 01-15, 2021, online. [Proceedings/Abstract](#)

B) Presentations relevant to the broader research activity

1. K. Makryniotis, E. Nikolavaits, C. Gkountela, S. Vouyiouka, E. Topakas. Side to side comparison of a novel wild-type polyestherase from *Deinococcus maricopensis* with LCC^{ICCG} indicates promising degradation of semi-crystalline post-consumer PET, BIOTRANS 2023 – 16th International Symposium on Biocatalysis & Biotransformations, June 25-29, 2023, La Rochelle, France. [Proceedings/Abstract](#)
2. K. Makryniotis*, E. Nikolavaits, C. Gkountela, S. Vouyiouka, J. Nikodinovic-Runic, E. Topakas. An interdisciplinary approach for the discovery and utilization of novel polymer degrading enzymes, International Conference on Bio-based and Biodegradable Polymers, November 14-16, 2022, Alicante, Spain
3. C. Gkountela, E. Nikolaivits, G. Taxeidis, J. Nikodinovic-Runic, E. Topakas, S. Vouyiouka. Enzymatic depolymerization against polymers structure and properties in the perspective of biochemical recycling, Polymers 2022 – New Trends in Polymer Science: Health of the Planet, Health of the People, May 25-27, 2022, Turin, Italy. [Proceedings/Abstract](#)
4. K. Makryniotis, G. Taxeidis, E. Nikolaivits, C. Gkountela, S. Vouyiouka, J. Nikodinovic Runic, E. Topakas. Discovery of novel polyestherases capable of degrading a variety of synthetic polyesters. 21st European Meeting on Environmental Chemistry (EMEC21), November 30 – December 03, 2021, Novi Sad, Serbia. Best poster presentation award. [Proceedings/Abstract](#)
5. A.D. Porfyris*, C. Gkountela, C. Politidis, G. Messaritakis, P. Orfanoudakis, S. Pavlidou, D. M. Korres, S. N. Vouyiouka. Halogen-free flame retarded PP compounds designated for cable protection conduits. AMI Fire Resistance in Plastics, November 30 – December 02, 2021, Dusseldorf, Germany. [Proceedings/Abstract](#)
6. D. Porfyris, C. Gkountela, D. M. Korres, S. N. Vouyiouka. Polypropylene compounds for halogen-free low smoke (HFLS) conduits. European Meeting on Fire Retardant Polymeric Materials. August 29 – September 01, 2021, Budapest, Hungary. [Proceedings/Abstract](#)
7. G. Taxeidis, E. Nikolaivits, C. Gkountela, S. Vouyiouka, J. Nikodinovic Runic, E. Topakas. The ability of a known plant-biomass degrading fungus to break down polyurethane. European Federation of Biotechnology Virtual Conference (EBF 2021), May 10-14, 2021, online

National scientific conferences

A) Presentation relevant to the Doctoral Dissertation

1. C.I. Gkountela*, D. M. Korres, S. N. Vouyiouka. A sustainable approach to produce and upgrade poly(butylene succinate), 13^ο Πανελλήνιο Συνέδριο Χημικής Μηχανικής, 2-4 Ιουνίου 2022, Πάτρα, Ελλάδα. [Proceedings/Abstract](#)

B) Presentations relevant to the broader research activity

1. K. Makryniotis, E. Nikolaivits, G. Taxeidis, J. Nikodinovic-Runic, C. Gkountela, S. Vouyiouka. E. Topakas. Discovery of novel polyesterases capable to degrade plastic waste, 13^ο Πανελλήνιο Συνέδριο Χημικής Μηχανικής, 2-4 Ιουνίου 2022, Πάτρα, Ελλάδα. [Proceedings/Abstract](#)
2. Χ. Γκουντέλα, Α. Πορφύρης, Σ. Βασιλάκος, Δ. Κορρές, Σ. Παυλίδου, Σ. Βουγιούκα, Κ. Παπασπυρίδης. Σταθεροποίηση πολυ(γαλακτικού οξέος) για εφαρμογές διευρυμένου κύκλου ζωής, 12^ο Πανελλήνιο Συνέδριο Χημικής Μηχανικής, 29-31 Μαΐου 2019, Αθήνα, Ελλάδα

Industrial Reports in the context of collaborations with international industrial centers

1. C. Gkountela, S. Vouyiouka, C. Papaspyrides. Sustainable packaging for the beverage industry: Focus on primary packaging. Coca-Cola Hellenic Bottling Company (HBC) Greece S.A.I.C. Internal Report, 2019, 42 pp
2. C. Gkountela, S. Vouyiouka, C. Papaspyrides. Sustainable packaging for the beverage industry: Focus on secondary and tertiary packaging. Coca-Cola Hellenic Bottling Company (HBC) Greece S.A.I.C. Internal Report, 2019, 78 pp

Publication in technical journals - Conference paper

1. C. Gkountela, D. Markoulakis, D. Korres, S. Vouyiouka. Evaluation of the parameters of poly(butylene succinate) enzymatic polymerization. Mater. Proc. 7 (2021)11. [DOI](#)

Abbreviations

Abbreviation	Definition	Abbreviation	Definition
BDO	1,4-butanediol	N435	Novozym 435
BHMF	2,5-bis(hydroxymethyl)furan	pNPB	p-nitrophenyl butyrate
FDCA	2,5-Furandicarboxylic acid	PBF	poly(butylene 2,5-furandicarboxylate)
AEC	acyl-enzyme complex	PBA	poly(butylene adipate)
atRA	all-trans retinoic acid	PBI	poly(butylene isophthalate)
BSA	bovine serum albumin	PBP	poly(butylene pyridinate)
BHA	butylated hydroxyanisole	PBS	poly(butylene succinate)
BHT	butylated hydroxytoluene	PBS-DLS	poly(butylene succinate-dilinoleic succinate)
CALB	<i>Candida antarctica</i> lipase B	PBT	poly(butylene terephthalate)
LCR	<i>Candida rugosa</i> lipase	PEF	Poly(ethylene furanoate)
CAP	cellulose acetate phthalate	PEN	poly(ethylene naphthalate)
DEF	diethyl furan-2,5-dicarboxylate	PES	poly(ethylene succinate)
DES	diethyl succinate	PET	poly(ethylene terephthalate)
DSC	Differential Scanning Calorimetry	PLA	poly(lactic acid)
DMFDCA	dimethyl 2,5-furandicarboxylate	PPF	poly(propylene 2,5-furandicarboxylate)
DMS	dimethyl succinate	PTT	poly(trimethylene terephthalate)
eROP	enzymatic ring-opening polymerization	PVA	poly(vinyl alcohol)
EAM	enzyme-activated monomer	PVL	poly(δ -valerolactone)
EG	ethylene glycol	PCL	poly(ϵ -caprolactone)
FTIR	Fourier Transform Infrared Spectroscopy	PS	polystyrene
GPC	Gel Permeation Chromatography	ROP	ring-opening polymerization
ILs	ionic liquids	SSP	Solid state polymerization
LCC	Leaf and branch compost cutinase	SA	succinic acid
LBC	lipase from <i>Burkholderia cepacia</i>	TBT	tetrabutyl titanate(IV)
PPL	lipase from porcine pancreas	TbC	<i>Thermobifida alba</i> cutinase
MCs	microcapsules	TfC	<i>Thermobifida fusca</i> cutinase
MW	molecular weight	TGA	Thermogravimetric Analysis
NPs	Nanoparticles	TTIP	titanium tetraisopropoxide

Abstract

Given the fossil fuel crisis and the steady consumption of finite resources, green polymers are becoming necessary. The term “green” describes materials that present green properties (such as biological origin and/or biodegradability) and are produced *via* sustainable processes conducted under mild conditions and not requiring chemical catalysts or toxic solvents. Truly green materials must combine these characteristics; consequently, enzymatically synthesized bio-based and/or biodegradable polymers can be characterized as truly green. The main scope of this research work was to produce the bio-based polymers poly(butylene succinate) (PBS) and poly(butylene 2,5-furandicarboxylate) (PBF) in a sustainable route, i.e., enzymatic prepolymerization combined with low-temperature post-polymerization. In addition to their sustainability, other characteristics we aim for in these materials include high purity in terms of metal catalyst residues and side reactions’ by-products and controlled molecular weight. In this way, we create materials of increased research and industrial interest suitable for use in demanding applications such as high-purity encapsulation systems (e.g., in the food packaging and biomedical sector).

Enzymatic polymerization was conducted, and the immobilized *Candida antarctica* Lipase B was used as a biocatalyst in solvent-free systems to produce PBS and PBF *via* two-stage processes. The first step was conducted under milder conditions compared to chemical routes (40 or 50°C, atmospheric pressure, 24 h) to minimize possible monomers’ losses. The second stage’s conditions (reaction temperature, pressure, time) were thoroughly investigated. Based on the reaction temperature investigation, conducted under 200 mbar, 90°C was indicated as the optimum temperature for both PBS and PBF. The reduced pressure (20 mbar) slightly increased the molecular weight (MW) of PBS, reaching the values of 2500 and 6700 g·mol⁻¹ (\overline{M}_n and \overline{M}_w , respectively) and did not affect the MW of PBF, remaining 1800 and 1900 g·mol⁻¹. The investigated increased reaction times were found to negatively affect the enzymatic polymerizations of both PBS and PBF at both 90 and 95°C. The system may have reached equilibrium due to the active end groups consumption, while the increased by-product amounts requiring a higher vacuum to be removed, led to by-product accumulation within the reacting particles and alcoholysis reactions. At 95°C, the enzyme’s thermal inactivation was the main reason for the observed MW decreases.

Thanks to the simplicity of the applied processes (low-temperature bulk polymerization technique, not requiring multiple solvents for the final product isolation), both the prepolymers were synthesized at larger scales at their optimal synthesis conditions and up to 20 g PBS and 6 g PBF were received for the first time, thus filling the relevant gap in the open literature.

A novel, non-commercially available enzyme known for degrading plastic was also used as a biocatalyst in a solvent-free system to produce PBS for the first time. The protein expression and immobilization of a thermostable variant of the Leaf and branch compost cutinase (LCC), LCC^{ICCG}, as well as the biocatalyst characterization, were conducted by the Industrial Biotechnology & Biocatalysis group at the Biotechnology Laboratory of NTUA. Thus, the

immobilized biocatalyst was used in a two-step process. The reaction temperature of the first step was investigated (50-70°C), and it was conducted under atmospheric pressure for 24 h to study the enzyme's efficiency in the polymerization. The second stage was conducted at 80°C, under 200 mbar, for 2 h to favour the polymerization reaction. PBS was successfully synthesized in all the tested temperatures, and the achieved MW values reached 1400 and 1500 g·mol⁻¹ (\overline{M}_n and \overline{M}_w). The synthesized prepolymers presented several advantages, including narrow molecular weight distributions and increased susceptibility to post-polymerization ($\Delta\overline{M}_n$ and $\Delta\overline{M}_w$ up to 150 and 350 %, respectively), rendering them promising candidates for applications such as drug delivery systems.

The enzymatically synthesized PBS prepolymers were then subjected to different post-polymerization methods, including solid state polymerization (SSP) and low-temperature melt post-polymerization. SSP was examined for different reaction temperatures, but it was found ineffective in terms of significant MW increase. On the other hand, melt post-polymerization, conducted at 110°C under reduced pressure of 20 mbar for 4 h, with the addition of a drying step to remove any possible absorbed moisture from the prepolymer, led to $\Delta\overline{M}_n$ and $\Delta\overline{M}_w$ of 76 and 94 %, respectively. PBF was also submitted to melt post-polymerization at three different temperatures (85, 95 and 105°C). Its susceptibility to post-polymerization was confirmed, especially at 105°C; the monitored $\Delta\overline{M}_n$ and $\Delta\overline{M}_w$ were 6 and 12 %, respectively, and an increasing trend was observed.

Finally, the enzymatically synthesized, scaled-up and upgraded PBS was examined as a carrier for controlled release systems, in collaboration with the Organic Chemistry Laboratory, NTUA research team. Unloaded nanoparticles were firstly successfully formed (hydrodynamic diameter ca. 470 nm), and then, the naturally occurring antioxidant flavonoid, naringin was encapsulated with a sufficient encapsulation efficiency of 68 %. The system's controlled release was assessed *via* preliminary *in vitro* release experiments. Despite its low molecular weight, the enzymatically synthesized and upgraded PBS was a promising candidate carrier in controlled release systems, especially for long-term release applications.

Keywords: Biocatalysis, poly(butylene succinate), poly(butylene 2,5-furandicarboxylate), post-polymerization, SSP, encapsulation

Εκτεταμένη Περίληψη

Λαμβάνοντας υπόψιν τη συνεχή κατανάλωση των ορυκτών πόρων και το γεγονός ότι πρόκειται για πεπερασμένες πρώτες ύλες, η χρήση πράσινων πολυμερών κρίνεται πλέον αναγκαία. Ο όρος «πράσινα» περιγράφει υλικά που παρουσιάζουν «πράσινες» ιδιότητες (π.χ. βιολογική προέλευση και/ή βιοαποικοδομησιμότητα) και παράγονται μέσω βιώσιμων διεργασιών που διεξάγονται υπό ήπιες συνθήκες και δεν απαιτούν χημικούς καταλύτες ή τοξικούς διαλύτες. Τα πραγματικά πράσινα υλικά οφείλουν να συνδυάζουν αυτά τα χαρακτηριστικά. Συνεπώς, τα ενζυμικά συντεθειμένα, προερχόμενα από ανανεώσιμες πρώτες ύλες και/ή βιοδιασπώμενα πολυμερή δύνανται να θεωρηθούν πραγματικά πράσινα. Ο βασικός στόχος της παρούσας ερευνητικής εργασίας ήταν η παραγωγή των προερχόμενων από ανανεώσιμες πρώτες ύλες πολυμερών πολυ(ηλεκτρικός βουτυλεστέρας) (poly(butylene succinate) ή PBS) και πολυ(2,5-φουρανοδικός βουτυλεστέρας) (poly(butylene 2,5-furandicarboxylic acid) ή PBF) μέσω βιώσιμων οδών (ενζυμικός προπολυμερισμός σε συνδυασμό με χαμηλής θερμοκρασίας μεταπολυμερισμό). Εκτός του πράσινου χαρακτήρα τους, άλλα χαρακτηριστικά των υλικών στα οποία στοχεύουμε αποτελούν η υψηλή καθαρότητα ως προς υπολείμματα μεταλλικών καταλυτών και παραπροϊόντα παράπλευρων αντιδράσεων και το ελεγχόμενο μοριακό τους βάρος. Με τον τρόπο αυτό, παράγουμε υλικά υψηλού ερευνητικού και βιομηχανικού ενδιαφέροντος, καθώς είναι κατάλληλα για χρήση σε απαιτητικές εφαρμογές όπως υψηλής καθαρότητας συστήματα εγκλεισμού (π.χ. συσκευασία τροφίμων ή βιοϊατρική).

Ο ενζυμικός πολυμερισμός πραγματοποιήθηκε με τη χρήση του ακινητοποιημένου ενζύμου *Candida antarctica* Lipase B, χωρίς τη χρήση διαλυτών, για την παραγωγή των PBS και PBF, μέσω διεργασιών δύο σταδίων. Το πρώτο στάδιο πραγματοποιήθηκε σε ήπιες συνθήκες (40 ή 50°C, ατμοσφαιρική πίεση, 24 ώρες) ώστε να ελαχιστοποιηθεί η πιθανότητα απώλειας μονομερών. Οι συνθήκες του δεύτερου σταδίου διερευνήθηκαν ενδελεχώς. Αρχικά, τα προϊόντα ενζυμικού προπολυμερισμού τέθηκαν σε αναλύσεις φασματοσκοπίας πυρηνικού μαγνητικού συντονισμού ($^1\text{H-NMR}$) και φασματοσκοπία υπερύθρου με μετασχηματισμό Fourier (FTIR), ώστε να ταυτοποιηθούν οι επαναλαμβανόμενες δομικές μονάδες των πολυμερών. Στη συνέχεια, βάσει της διερεύνησης της θερμοκρασίας αντίδρασης σε πίεση 200 mbar, οι 90°C αναδείχθηκαν ως βέλτιστη θερμοκρασία τόσο για το PBS όσο και για το PBF, κυρίως μέσω του προσδιορισμού των μοριακών τους βαρών με χρωματογραφία διέλευσης μέσω πηκτής (GPC). Στην περίπτωση του PBS, τα μοριακά βάρη των προϊόντων των 90 και 95°C ήταν τα μέγιστα (\overline{M}_n έως 2300 και \overline{M}_w έως 5000 $\text{g}\cdot\text{mol}^{-1}$). Στην περίπτωση του PBF, εντοπίστηκαν δύο διακριτοί πληθυσμοί διαφορετικών μοριακών βαρών, οι τιμές των οποίων δεν διαφοροποιήθηκαν με αλλαγή της θερμοκρασίας αντίδρασης. Ωστόσο, διαπιστώθηκε ότι το ποσοστό του πληθυσμού με το μέγιστο μοριακό βάρος αυξήθηκε στους 90°C. Η εφαρμογή μειωμένης πίεσης (20 mbar) παρουσίασε ελαφρώς θετική επίδραση στα μοριακά βάρη του PBS (\overline{M}_n 2500 και \overline{M}_w 6700 $\text{g}\cdot\text{mol}^{-1}$), ενώ δεν επηρέασε τα μοριακά βάρη του PBF που παρέμειναν 1800 και 1900 $\text{g}\cdot\text{mol}^{-1}$ (\overline{M}_n και \overline{M}_w αντίστοιχα) για τους 90°C. Αυτή η διαφορετική συμπεριφορά των δύο συστημάτων αποδόθηκε στη διαφορετική δομή των

πολυμερών. Ο αλειφατικός πολυεστέρας PBS επιτρέπει την απομάκρυνση του σχηματιζόμενου παραπροϊόντος (αιθανόλη) μέσω εξάτμισης και διάχυσης ενόσω εφαρμόζεται το υψηλότερο κενό (20 mbar). Από την άλλη πλευρά, ο αλειφαρωματικός πολυεστέρας PBF, λόγω των ογκωδών δακτυλίων που περιέχει στην επαναλαμβανόμενη δομική του μονάδα, δυσχεραίνει την απομάκρυνση του παραπροϊόντος και ενδεχομένως απαιτείται εφαρμογή ακόμα υψηλότερου κενού. Ωστόσο, λόγω των σχετικά χαμηλών μοριακών βαρών του PBF, η εφαρμογή υψηλότερου κενού εμπεριέχει το κίνδυνο απώλειας ολιγομερών λόγω εξάχνωσης. Όσον αφορά στους 95°C, η μειωμένη πίεση επηρέασε αρνητικά και τα δύο συστήματα, γεγονός που αποδόθηκε στη μειωμένη ενεργότητα του ενζύμου στη συγκεκριμένη θερμοκρασία. Προϊόντα χαμηλότερου μοριακού βάρους σχηματίζονται και απομακρύνονται λόγω εξάχνωσης, διαταράσσοντας τη χημική ισορροπία της αντίδρασης. Επομένως, η διερεύνηση για τους χρόνους αντίδρασης συνεχίστηκε στα 20 mbar για το PBS και 200 mbar για το PBF για τις θερμοκρασίες των 90 και 95°C. Οι αυξημένοι χρόνοι αντίδρασης επηρέασαν αρνητικά τον πολυμερισμό των PBS και PBF, τόσο στους 90, όσο και στους 95°C, υποδεικνύοντας ότι το σύστημα έφτασε σε ισορροπία λόγω της κατανάλωσης των ακραίων δραστικών ομάδων και των αυξημένων ποσοτήτων παραπροϊόντων, για την απομάκρυνση των οποίων ενδεχομένως απαιτείται η εφαρμογή υψηλότερου κενού. Συνεπώς, το παραπροϊόν συσσωρεύεται μεταξύ των αντιδρώντων μορίων, καθιστώντας έτσι τα ολιγομερή ευάλωτα σε αλκοόλυση. Στους 95°C, παρατηρήθηκε περαιτέρω μείωση της ενζυμικής ενεργότητας, η οποία αποτέλεσε τον βασικό λόγο σχηματισμού προϊόντων χαμηλότερων μοριακών βαρών.

Χάρη στην απλότητα των διεργασιών που εφαρμόστηκαν (χαμηλής θερμοκρασίας πολυμερισμός μάζας χωρίς τη χρήση πολλών διαλυτών για την απομόνωση του τελικού προϊόντος), οι διεργασίες σύνθεσης και των δύο προπολυμερών στις βέλτιστες συνθήκες (PBS: 90°C, 20 mbar, 2 h και PBF: 90°C, 200 mbar, 2 h) κλιμακώθηκαν επιτυχώς. Έτσι, παραλήφθηκαν έως 20 g PBS και 6 g PBF για πρώτη φορά, καλύπτοντας το σχετικό κενό που έχει παρατηρηθεί στη βιβλιογραφία. Για το PBS των 20 g παρατηρήθηκε μικρή υποβάθμιση στις θερμικές ιδιότητες καθώς και στα μοριακά βάρη σε σχέση με το προϊόν της κλίμακας 1 g. Η υποβάθμιση αυτή αποδόθηκε στην επίδραση φαινομένων μεταφοράς μάζας, τα οποία είναι εντονότερα σε μεγάλες κλίμακες. Επί παραδείγματι, ο σχηματισμός μεγαλύτερης ποσότητας παραπροϊόντος, ενδεχομένως απαιτεί την εφαρμογή υψηλότερου κενού. Το προϊόν κλιμάκωσης 20 g αποτέλεσε το προπολυμερές που εν συνεχεία τέθηκε σε μεταπολυμερισμό. Από την άλλη πλευρά, η πιο περιορισμένη κλιμάκωση της διεργασίας σύνθεσης του PBF (έως 6 g), οδήγησε στον σχηματισμό προϊόντων με παρόμοιες ιδιότητες σε σχέση με τη μικρή κλίμακα (1 g). Στην περίπτωση αυτή, το προϊόν των 3 g επιλέχθηκε ως το προπολυμερές που τέθηκε σε μεταπολυμερισμό, λόγω της ελαφρώς καλύτερης μορφολογίας που παρουσίασε σε σχέση με το προϊόν των 6 g.

Στη συνέχεια, ένα καινοτόμο, μη διαθέσιμο εμπορικά ένζυμο, γνωστό για την ικανότητά του να αποικοδομεί πλαστικά, χρησιμοποιήθηκε για πρώτη φορά ως βιοκαταλύτης για τη σύνθεση PBS, χωρίς τη χρήση διαλύτη. Συγκεκριμένα, πραγματοποιήθηκε από την

ερευνητική ομάδα Industrial Biotechnology & Biocatalysis του Εργαστηρίου Βιοτεχνολογίας του ΕΜΠ, η έκφραση της πρωτεΐνης, καθώς και η ακινητοποίηση μιας θερμοσταθερής, τετραπλής μετάλλαξης της κουτινάσης Leaf and branch compost cutinase (LCC), LCC^{ICCG}. Επιπλέον, πραγματοποιήθηκε χαρακτηρισμός του ενζύμου, το οποίο εν συνεχεία χρησιμοποιήθηκε ως βιοκαταλύτης σε διεργασία δύο σταδίων. Η θερμοκρασία του πρώτου σταδίου διερευνήθηκε (50-70°C) για 24 ώρες ώστε να μελετηθεί η αποτελεσματικότητα του ενζύμου στον πολυμερισμό. Το δεύτερο στάδιο πραγματοποιήθηκε στους 80°C, σε μειωμένη πίεση 200 mbar, για δύο ώρες, ώστε να ευνοηθεί η αντίδραση του πολυμερισμού. Το PBS συντέθηκε επιτυχώς σε όλες τις θερμοκρασίες και τα MB που επιτεύχθηκαν ήταν 1400 και 1500 g mol⁻¹ (\overline{M}_n και \overline{M}_w). Μεταξύ των πλεονεκτημάτων των προϊόντων σημειώθηκαν στενές κατανομές μοριακών βαρών και αυξημένη επιδεκτικότητα σε μεταπολυμερισμό ($\Delta\overline{M}_n$ και $\Delta\overline{M}_w$ έως 150 και 350%, αντίστοιχα), που τα καθιστούν υποσχόμενους υποψήφιους για εφαρμογές όπως συστήματα αποδέσμευσης δραστικών ουσιών.

Το ενζυμικά συντεθειμένο προπολυμερές PBS (προϊόν κλίμακας 20 g) υποβλήθηκε στη συνέχεια σε διαφορετικές μεθόδους μεταπολυμερισμού, συμπεριλαμβανομένου του Πολυμερισμού Στερεάς Κατάστασης (ΠΣΚ ή SSP) και του χαμηλής θερμοκρασίας μεταπολυμερισμού τήγματος. Ο ΠΣΚ πραγματοποιήθηκε σε διαφορετικές θερμοκρασίες, ωστόσο κρίθηκε σε όλες τις περιπτώσεις αναποτελεσματικός ως προς την αύξηση του μοριακού βάρους, κυρίως λόγω των χαμηλών σημείων τήξεως. Αντίθετα, ο μεταπολυμερισμός τήγματος που πραγματοποιήθηκε στους 110°C υπό κενό 20 mbar για 4 ώρες, με την προσθήκη ενός σταδίου ξήρασης ώστε να απομακρυνθούν πιθανά υπολείμματα υγρασίας, οδήγησε σε αυξήσεις μοριακών βαρών $\Delta\overline{M}_n$ και $\Delta\overline{M}_w$ 76 and 94 %, αντίστοιχα. Οι συνθήκες του μεταπολυμερισμού τήγματος (χρόνος, θερμοκρασία) διερευνήθηκαν περαιτέρω και διαπιστώθηκε ότι τόσο σε μεγαλύτερους χρόνους (>6 ώρες, σε σταθερή θερμοκρασία 110°C) όσο και σε υψηλότερες θερμοκρασίες (>130°C, για σταθερό χρόνο αντίδρασης 4 ώρες) το προϊόν υποβαθμίζεται θερμικά και παρατηρείται μείωση στο μοριακό του βάρος, αλλά και υποβάθμιση των θερμικών ιδιοτήτων. Συνεπώς, οι συνθήκες αντίδρασης 4 ώρες, 110°C, 20 mbar κρίθηκαν ως βέλτιστες για το συγκεκριμένο σύστημα. Στη συνέχεια, μελετήθηκε ο μεταπολυμερισμός του PBF. Το PBF τέθηκε αποκλειστικά σε μεταπολυμερισμό τήγματος για τους εξής λόγους. Πρώτον, ο ΠΣΚ δεν κρίθηκε αποτελεσματικός στην αναβάθμιση του προπολυμερούς PBS. Δεύτερον, οι ογκώδεις υποκαταστάτες του PBF, καθώς και τα ιδιαίτερα υψηλά ποσοστά ακραίων υδροξυλομάδων που εντοπίστηκαν, είναι πολύ πιθανό να οδηγήσουν σε περαιτέρω παρεμπόδιση της διεργασίας. Συνεπώς, το PBF υπεβλήθη σε μεταπολυμερισμό τήγματος και συγκεκριμένα σε τρεις διαφορετικές θερμοκρασίες (85, 95 και 105°C). Βάσει των αποτελεσμάτων, επιβεβαιώθηκε η επιδεκτικότητα του προπολυμερούς σε μεταπολυμερισμό, ιδιαίτερα στους 105°C. Παρόλο που οι αυξήσεις των μοριακών βαρών $\Delta\overline{M}_n$ and $\Delta\overline{M}_w$ που καταγράφηκαν ήταν χαμηλές (6 και 12%, αντίστοιχα), σημειώθηκε αυξητική τάση.

Το ενζυμικά συντεθειμένο (προϊόν κλιμάκωσης) και αναβαθμισμένο PBS (προϊόν μεταπολυμερισμού τήγματος στους 110°C, για 4 ώρες) ελέγχθηκε ως φορέας σε συστήματα

ελεγχόμενης αποδέσμευσης, σε συνεργασία με την ερευνητική ομάδα του Εργαστηρίου Οργανικής Χημείας του ΕΜΠ. Στο πλαίσιο αυτό, αρχικά σχηματίστηκαν κενά νανοσωματίδια ώστε να επιβεβαιωθεί η καταλληλότητα της μεθόδου που επιλέχθηκε (γαλακτωματοποίηση/εξάτμιση διαλύτη). Από τη διαδικασία παρήχθησαν νανοσωματίδια υδροδυναμικής διαμέτρου περίπου 470 nm. Στη συνέχεια, πραγματοποιήθηκε εγκλεισμός φλαβονοειδούς αντιοξειδωτικού (ναρινγίνη), ως μοντέλο δραστικής ουσίας προς εγκλεισμό, σε σωματίδια του ενζυμικά συντεθειμένου (και αναβαθμισμένου) PBS, για πρώτη φορά. Η απόδοση εγκλεισμού κρίθηκε ικανοποιητική (68 %) σε σχέση με τιμές αντίστοιχων συστημάτων που συναντώνται στη βιβλιογραφία. Η ελεγχόμενη αποδέσμευση του συστήματος αξιολογήθηκε μέσω προκαταρκτικών *in vitro* πειραμάτων αποδέσμευσης. Συμπερασματικά, παρά το χαμηλό του μοριακό βάρος, το ενζυμικά συντεθειμένο και αναβαθμισμένο PBS απεδείχθη υποσχόμενος υποψήφιος για συστήματα ελεγχόμενης αποδέσμευσης, ειδικά για εφαρμογές παρατεταμένης αποδέσμευσης.

Λέξεις κλειδιά: Βιοκατάλυση, πολυ(ηλεκτρικός βουτυλεστέρας), πολυ(φουρανοδικός βουτυλεστέρας), μεταπολυμερισμός, ΠΣΚ, εγκλεισμός

Table of Contents

Chapter 1: Introduction	4
1.1 Introduction to Green Polymers.....	4
1.2 Introduction to Sustainable Polymerization Methods.....	7
1.2.1 Introduction to Enzymatic Polymerization	7
1.2.2 Introduction to post-polymerization: Solid State Polymerization (SSP)	32
1.3 Introduction to polymeric encapsulation systems	42
1.3.1 Introduction to nanoparticles: nanospheres and nanocapsules	42
1.3.2 Nanoparticles production methods.....	44
1.3.3 Nanoparticles applications	47
1.3.4 Advances in the active food packaging sector.....	48
1.4 Motivation	51
1.5 Thesis outline	51
Chapter 2: Enzymatic prepolymerization of poly(butylene succinate) using the immobilized <i>Candida antarctica</i> Lipase B (N435) as biocatalyst	53
2.1 Introduction.....	53
2.2 Scope	55
2.3 Experimental	55
2.3.1 Materials.....	55
2.3.2 Enzymatic prepolymerization experimental procedure for poly(butylene succinate) production	57
2.3.3 Characterization techniques.....	58
2.4 Results	61
2.4.1 Study of the key parameters influence on the small-scale (1 g) PBS enzymatic prepolymerization	61
2.4.2 Analysis of the scaling-up potential of the optimized PBS enzymatic prepolymerization process: 10 and 20g.....	74
2.4.3 Study of the monomers' ratio influence on the large-scale (20 g) PBS enzymatic prepolymerization process	75
2.5 Conclusions.....	78
Chapter 3: Enzymatic prepolymerization of poly(butylene 2,5-furandicarboxylate) using the immobilized <i>Candida antarctica</i> Lipase B (N435) as biocatalyst	81
3.1 Introduction.....	81
3.2 Scope	82
3.3 Experimental	82

3.3.1	Materials.....	82
3.3.2	Enzymatic prepolymerization experimental procedure for poly(butylene 2,5-furandicarboxylate) production.....	83
3.3.3	Characterization techniques.....	84
3.4	Results	85
3.4.1	Study of the key parameters influence on the small-scale (1g) PBF enzymatic prepolymerization	85
3.4.2	Analysis of the scaling-up potential of the optimized PBF enzymatic prepolymerization process: 3 and 6g.....	105
3.5	Conclusions.....	107
Chapter 4: Enzymatic prepolymerization of poly(butylene succinate) using a novel, non-commercially available enzyme.....		109
4.1	Introduction.....	109
4.2	Scope	110
4.3	Experimental	110
4.3.1	Materials.....	110
4.3.2	Experimental procedure of the heterologous expression of the LCC ^{ICCG} protein.....	110
4.3.3	Experimental procedure of the protein immobilization on the EziG ³ Amber carrier..	111
4.3.4	Biochemical characterization of the immobilized LCC ^{ICCG}	112
4.3.5	Enzymatic prepolymerization experimental procedure for poly(butylene succinate) production.....	112
4.3.6	Characterization techniques.....	113
4.4	Results	113
4.4.1	Biochemical characterization of the immobilized LCC ^{ICCG}	113
4.4.2	Enzymatic prepolymerization of PBS using the immobilized LCC ^{ICCG}	114
4.5	Conclusions.....	120
Chapter 5: Study of post-polymerization to increase the molecular weight of the enzymatically synthesized prepolymers: Evaluation of different methods and the most critical process parameters		122
5.1	Introduction.....	122
5.2	Scope	123
5.3	Experimental	123
5.3.1	Materials.....	123
5.3.2	Post-polymerization experimental procedure for the upgrade of enzymatically synthesized PBS and PBF	123
5.3.3	Characterization techniques.....	124

Table of Contents

5.4	Results	125
5.4.1	Study of the enzymatically synthesized PBS post-polymerization methods and key process parameters	125
5.4.2	Screening study of the enzymatically synthesized PBF melt post-polymerization: reaction temperature effect on the process	136
5.5	Conclusions.....	138
Chapter 6: End-use case study of the enzymatically synthesized and post-polymerization PBS: evaluation of suitability as a matrix for active agent encapsulation		140
6.1	Introduction.....	140
6.2	Scope	141
6.3	Experimental	141
6.3.1	Materials.....	141
6.3.2	Experimental procedure of naringin encapsulation in enzymatically synthesized and upgraded PBS	142
6.3.3	<i>Experimental procedure of in vitro</i> naringin release	142
6.3.4	Characterization techniques.....	142
6.4	Results	144
6.4.1	Formation of enzymatically synthesized PBS nanoparticles for naringin encapsulation	144
6.4.2	<i>In vitro</i> release tests of the encapsulated in enzymatically synthesized PBS nanoparticles naringin.....	146
6.5	Conclusions.....	147
Chapter 7: General Conclusions and Future Research		149
7.1	General Conclusions	149
7.2	Future Research.....	153
References		155
Appendix 1. Supplementary results.....		173
Appendix 2: Table of Figures		179
Appendix 3: Table of Tables		183

1.1 Introduction to Green Polymers

Even though most plastics are still fossil-based, the fossil fuel crisis has become more and more evident, especially since the late 1990s [1]. Given the steady consumption and the fact that fossil fuels are finite resources, their depletion seems unavoidable. As a result, greener materials, e.g., bio-based and/ or biodegradable polymers, and greener processes, e.g., enzymatic polymerization, are becoming necessary.

An illustrative example constitutes the increasing interest in the Twelve Principles of Green Chemistry, introduced in 1998 by Paul Anastas and John Warner [2]. The twelve Principles include: 1. Prevention: it is better to prevent waste than to treat or clean up waste after it is formed; 2. Atom Economy: Synthetic methods should be designed to maximize the incorporation of all materials used in the process into the final product; 3. Less Hazardous Chemical Synthesis: Whenever practicable, synthetic methodologies should be designed to use and generate substances that pose little or no toxicity to human health and the environment; 4. Designing Safer Chemicals: Chemical products should be designed to preserve the efficacy of function while reducing toxicity; 5. Safer Solvents and Auxiliaries: The use of auxiliary substances (e.g., solvents, separation agents, etc.) should be made unnecessary wherever possible and innocuous when used; 6. Design for Energy Efficiency: Energy requirements should be recognized for their environmental and economic impacts and should be minimized. Synthetic methods should be conducted at ambient temperature and pressure; 7. Use of Renewable Feedstocks: A raw material or feedstock should be renewable rather than depleting whenever technically and economically practicable; 8. Reduce Derivatives: Unnecessary derivatization (use of blocking groups, protection/deprotection, temporary modification of physical/chemical processes) should be minimized or avoided if possible because such steps require additional reagents and can generate waste; 9. Catalysis: Catalytic reagents (as selective as possible) are superior to stoichiometric reagents; 10. Design for Degradation: Chemical products should be designed so that at the end of their function, they break down into innocuous degradation products and do not persist in the environment; 11. Real-time analysis for Pollution Prevention: Analytical methodologies need to be further developed to allow for real-time, in-process monitoring and control before the formation of hazardous substances, and 12. Inherently Safer Chemistry for Accident Prevention: Substances and the form of a substance used in a chemical process should be chosen to minimize the potential for chemical accidents, including releases, explosions, and fires.

Demonstrating the timelessness of the issue, some years later, in 2014, Dubé and Salehpour [3] reviewed and applied the principles of Green Chemistry to polymer production. Focusing on the "Use of Renewable Feedstocks", the researchers presented the main renewable monomers classified from the following starting materials: 1. Vegetable oils (such as soybean oil, castor oil, palm oil), 2. Lignin fragments (such as cellulose, chitin, chitosan, starch, lactic

acid), 3. Sugars, 4. Rosin (resin acids), 4. Glycerol, 6. Furans (furfural, furfuryl alcohol), 7. Tannins, 8. Suberin, 9. Terpenes, and 10. Others (citric acid, tartaric acid, carbon dioxide). Even though renewable monomers are attractive due to their abundance and, in some cases, low cost, disadvantages like achieving a high monomer purity from bio-based sources and, therefore, high molecular weight polymer production still exist. In the context of the “Design of Degradation” principle, the authors also highlighted the value of biodegradable polymers such as PLA, polyhydroxyalkanoates (PHAs), and starch. The main disadvantages of these materials are their poor mechanical strength and barrier properties, increased vulnerability to hydrolysis, and significant sensitivity to solvents (including water) and temperature, respectively.

Since bio-based and/ or biodegradable polymers constitute significant parts of the Green Chemistry, it is worth focusing on and accurately defining the relevant terms. Bio-based polymers are defined as materials obtained from renewable resources [4]. Bio-based polymers include (a) natural polymers obtained from biomass (e.g., agropolymers originated from agroresources such as starch and cellulose); (b) polymers synthesized from microorganisms (e.g., PHAs); (c) polymers originated from bio-based monomers, synthesized in laboratories or by industry (e.g., PLA, PBS, PEF) [5]. When economically competitive, these polymers could replace conventional, fossil-based polymers [6]. It is of high essence that there is an increasing interest in bio-based materials in the open literature [7–9].

Biodegradable polymers are polymeric materials that can be degraded in the environment *via* the enzymatic action of microorganisms, which can be measured by standardized tests in a specific time interval reflecting available disposal conditions [10]. At the end of biodegradation, they are meant to be broken down into biomass, carbon dioxide and water [11]. A subset of biodegradable polymers may also be compostable with specific reference to their biodegradation in a compost system. These must be capable of undergoing biological decomposition in a compost site so that the plastic is not visually distinguishable and breaks down to carbon dioxide, etc., at a rate consistent with known compostable materials (e.g., cellulose) [10]. The use of biodegradable polymers, however, is not a “panacea”, given that when they are left to degrade on their own in anaerobic landfill leachate or marine conditions, the degradation kinetics is much slower and significantly higher times are required to reach a high degree of disintegration compared to industrial composting [12,13]. On that basis, biodegradable polymers seem to be a promising alternative to nondegradable fossil-based polymers, providing their end-of-life management options will be further studied, especially when they are to be released into the environment [14].

Among bio-based and/or biodegradable polymers, the most promising ones are the already commercially available aliphatic and aliphatic polyesters. In this context, we will focus on the enzymatic polymerization of the aliphatic PLA and PBS, as well as on a novel category of aliphatic furan-based polyesters (e.g., PBF) (Table 1). Even though furan-based polyesters are not biodegradable, their bio-based character and excellent properties make them promising sustainable candidates for future applications, especially when synthesized *via* a sustainable method such as enzymatic polymerization.

Table 1. Structures of PLA, PBS and PBF

Polymer	Structure
PLA	
PBS	
PBF	

In particular, poly(lactic acid) (PLA) is a bio-based, biodegradable and biocompatible polyester, able to be used for bioapplications and pharmaceutical applications (e.g., sutures, scaffolds and drug delivery systems) [6,15], as well as in packaging, as it is a promising alternative to polystyrene (PS) and poly(ethylene terephthalate) (PET) [16]. PLA is becoming increasingly popular as a packaging material, providing consumers with extra end-use benefits such as avoiding paying the “green tax” in Germany or meeting environmental regulations in Japan [17]. However, when PLA is conventionally produced – *via* direct condensation polymerization, azeotropic dehydration condensation or lactide ring-opening polymerization (ROP) [18] – either impurities or catalyst residues (organometallic, cationic, organic or bifunctional [19]) unavoidably remain in the final product, making it inappropriate to be used for food contact applications. Indicatively, according to the standards for compostable and biodegradable polymer packaging, the level of heavy metals should not exceed the maximum allowable level, which is $150 \text{ mg}\cdot\text{kg}^{-1}$ on dry substance [20]. The most commonly used industrial production method for PLA is ring-opening polymerization (ROP) of the lactone monomers, and tin(II) octoate (stannous bis(2-ethylhexanoate): $\text{Sn}(\text{Oct})_2$) is the most popular catalyst [21]. $\text{Sn}(\text{Oct})_2$ is biologically safe and approved by the FDA (the US Food and Drug Administration) for use in both food and medical applications [21]. However, the approval is dependent on empirical safety data and studies with long-term liberation and physiological effects of tin-ions from large tissue-embedded scaffold-matrices have not yet been conducted and may impose a different level of risk [22]. It becomes thus clear that there is a need to establish another PLA production method, not strictly requiring the removal of the used catalysts’ residues, such as enzymatic polymerization.

As a bio-based, biodegradable and biocompatible polyester, poly(butylene succinate) (PBS) can be used in the biomedical field. At the same time, it is also ideal for single-use food packaging, as it can degrade at high rates over short periods (see Chapter 2.1). Nevertheless, metal-based transesterification catalysts, including titanium(IV) tert-butoxide, tin(II) 2-ethylhexanoate, antimony(III) oxide, titanium(IV) isopropoxide, titanium(IV) isobutoxide, zirconium (IV) n-butoxide, antimony (III) n-butoxide, hafnium (IV) n-butoxide, bismuth (III) neo-

decanoate, germanium (IV) oxide, as well as high reaction temperatures are required for the conventional PBS synthesis [23]. The use of that kind of catalyst, along with the high reaction temperatures, usually causes the final product's yellowing as well as side reactions (e.g., the dehydration of 1,4-butanediol (BDO) towards THF) [24,25]. As a result, removing catalyst residues is unavoidable, especially when PBS is to be used for biomedical and food packaging applications. On the other hand, another approach is PBS enzymatic polymerization, where non-toxic enzymes are used as catalysts that do not have to be completely removed from the final product, making it appropriate for biomedical and (active) food packaging applications.

Poly(ethylene furanoate) (PEF) is a bio-based alternative to PET [26] specifically for packaging applications, presenting superior barrier properties compared to it (19 times decreased CO₂ permeability, 11x decreased O₂ permeability, 31x diffusivity) [27]. Up to date, PEF is produced *via* a two-stage melt polymerization method, carried out under hard conditions (e.g., high temperature of 230°C) in the presence of metal catalysts (Sb, Ti, Ge and Sn) [27,28]. However, this route negatively affects the final product's properties, including coloration, thermal instability and decreased electrical performance. Additionally, potential environmental and health problems may be caused mainly by the high applied temperatures and the metal catalyst residues that are hard to remove [28]. It is of high essence, though, that to obtain a sustainable polymer, the bio-based character of the final product is not sufficient; a sustainable synthetic route, conducted under mild conditions, not requiring the use of metal catalysts (e.g., enzymatic polymerization), can be established and followed to produce a truly green product. In light of the above, it is important to focus on sustainable polymerization methods, such as enzymatic polymerization, that can produce sustainable polymers.

1.2 Introduction to Sustainable Polymerization Methods

1.2.1 Introduction to Enzymatic Polymerization

Biotechnology is increasingly finding applications in industry, even though traditionally, it was restricted more to the research field. It encompasses a wide range of technologies and practices involving manipulating living materials. Biotechnology consists of five fields: red, dealing with medicine; green, dealing with agriculture; blue, dealing with marine and freshwater environments; white, dealing with the chemical industry; and yellow, dealing with environmental applications [29].

Focusing on white biotechnology, its main objective is to produce chemicals, materials or biofuels using renewable biological resources by utilizing microorganisms or isolated enzymes. These enzymes are highly significant due to their remarkable ability to catalyze specific chemical reactions while adhering to environmentally friendly (or green chemistry) principles. More specifically, in aqueous environments, lipases catalyze the hydrolysis of fatty acid esters by a two-step mechanism that involves nucleophilic attack by a serine residue located within the active site to produce an acylated enzyme and alcohol product, followed by nucleophilic addition of a water molecule to liberate the fatty acid (Figure 1). On the other hand, when

found in non-aqueous media, lipases can use other nucleophiles, such as methanol, to catalyze esterification and transesterification reactions [30].

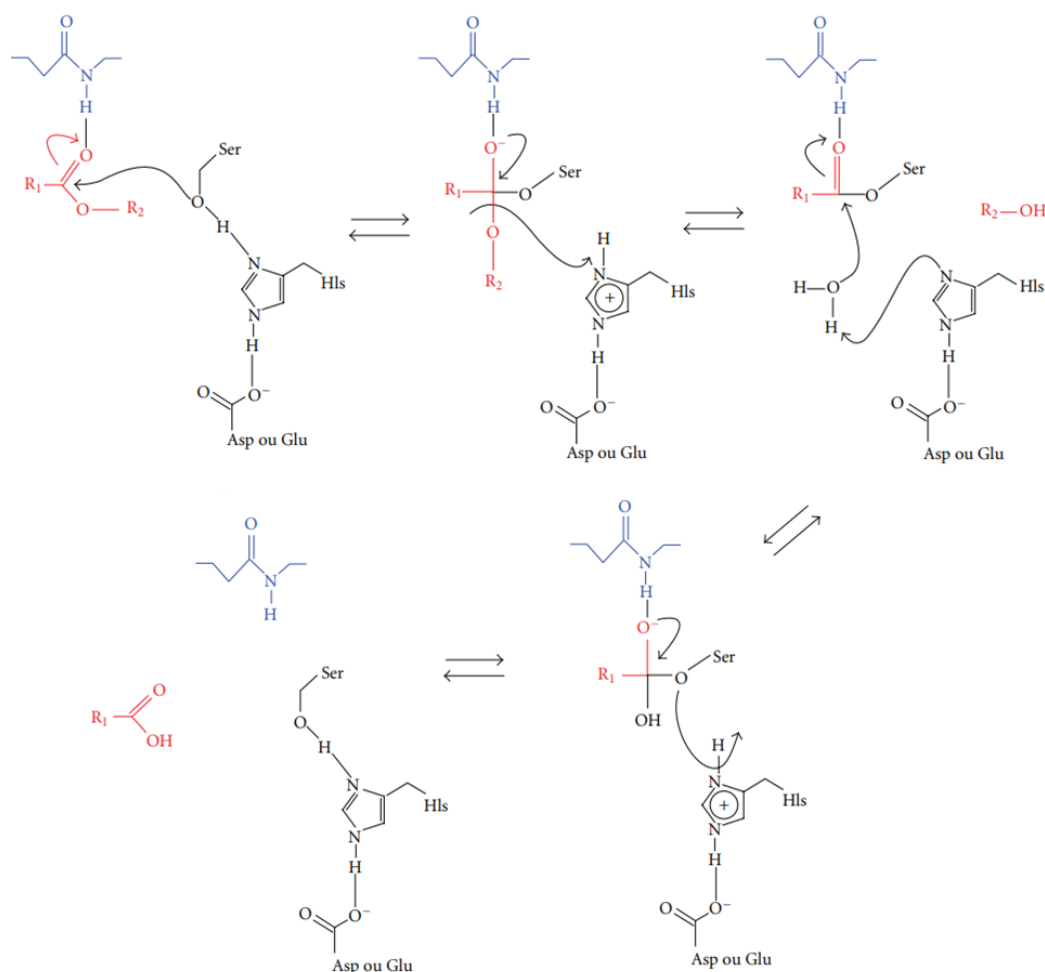


Figure 1. Mechanism of the hydrolysis reaction of ester bonds catalyzed by esterases and lipases [31].

Given the above, due to their remarkable selectivity and catalytic efficiency under mild conditions, enzymes are an attractive and sustainable alternative to toxic catalysts used in the polycondensation of functional monomers [32–35]. Bio-catalysis results in a high quality polymer due to enzyme high enantio-, chemo- and regioselectivity and to consequent restriction of side reactions. Furthermore, enzyme's removal from the polymers is not that stringent, something especially important for biomedical applications where organometallic catalysts based on Ti, Zn, Al, Sn or Ge should be completely removed [36,37].

It is important to investigate the most recent developments in the enzymatic polymerization of some of the most popular sustainable polymers (PLA, PBS, furan-based polyesters), greatly impacting society, including scientific and industrial. In this context, the appropriate enzymes to produce each polymer and their main characteristics are presented at the beginning of each following chapter. The key experimental conditions of each applied synthesis method are subsequently discussed. The applied synthetic methods are critically evaluated regarding their

environmental impact and capability to be used on an industrial scale. Finally, the most crucial monitoring variables of each synthesized polymer are analyzed.

1.2.1.1 Enzymatic polymerization of aliphatic polyesters

1.2.1.1.1 Type and characteristics of the used enzyme for PLA enzymatic polymerization

PLA can be enzymatically synthesized *via* either ROP of lactides or direct polycondensation of lactic acid (Figure 2). ROP is a propagation process of cyclic monomers initiated by different ions; for PLA production, the used cyclic monomer is a lactide, which is the cyclic dimer of lactic acid. Polycondensation of lactic acid occurs by connecting carboxyl and hydroxyl groups producing water simultaneously [38].

In most of the recently published works on the enzymatic polymerization of PLA, eROP is the most preferred synthesis method [15,16,47,48,39–46]. The same trend has been observed for the conventional synthesis of PLA, probably due to the wider range of molecular weight polymers that can be achieved *via* ROP by controlling the purity of lactide. Polycondensation is mostly used to produce PLA with low molecular weight using basic equipment and processes [38]. Given that the enzymatically synthesized polymers usually present low molecular weights, the eROP route seems to be more appropriate for the enzymatic synthesis of PLA. The crucial process parameters will be discussed in the following.

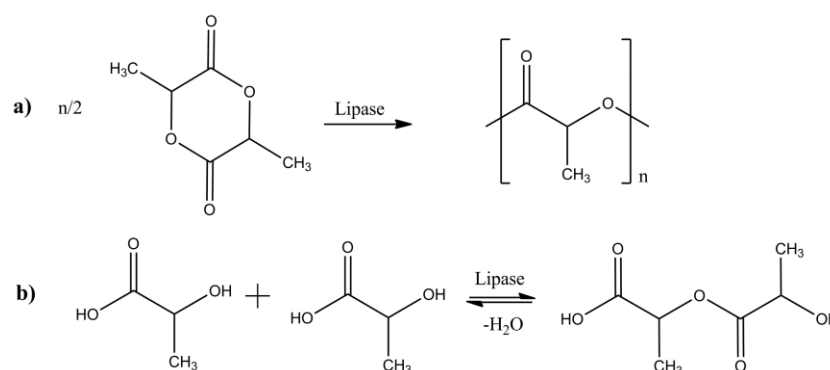


Figure 2. Enzymatic ROP of lactide (eROP) (a) and polycondensation of lactic acid (b).

Hydrolases and, more specifically, lipases are effective catalysts in the enzymatic polymerization of aliphatic polyesters [49]. The most widely used enzyme for the synthesis of PLA – *via* either eROP of lactones (cyclic esters) or direct polycondensation of lactic acid – is Novozym 435 (N435) [15,16,42,43,45–48,50], consisting of immobilized *Candida antarctica* lipase B (CALB) physically adsorbed within the macro-porous resin Lewatit VPOC 1600 (activity $10000 \text{ PLU}\cdot\text{g}^{-1}$, optimum temperature $30\text{--}60^\circ\text{C}$) (Table 2). Other commercially available enzymes that have been used for PLA enzymatic polymerization are *Candida rugosa* lipase (LCR) [39,51] and the lipase from *P. fluorescens* (lipase AK), as well as lipases from *Burkholderia cepacia* (LBC) and porcine pancreas (PPL) [41,43,44]. Another approach is to isolate, after screening, a strain of a microorganism that produces the desired enzyme and then isolate it in a crude form in the lab. In this context, Panyachanakul *et al.* [52] isolated a solvent-tolerant and thermostable

lipase-producing actinomycete strain (A3301), identified as *Streptomyces* sp. The obtained lipase's activity, optimum temperature and thermostability were $108 \text{ U}\cdot\text{ml}^{-1}$, 60°C and $45 - 55^\circ\text{C}$, respectively and it was able to tolerate 10 – 20% (v/v) hexane and toluene.

The mechanism of the lipases acting during the eROP of lactones has been studied in detail (Figure 3). In brief, the active site of CALB contains the amino acids Ser105-His224-Asp187, with Ser being the nucleophile, His the basic residue and Asp the acidic residue. Thus, a hydrogen-bonding network (serine – histidine and histidine – aspartic acid) is formed. An acyl-enzyme intermediate is formed by the reaction of the serine residue with the lactone, rendering the carbonyl group more prone to nucleophilic attack. The next step, initiation, includes the deacylation of the acyl-enzyme intermediate by an appropriate nucleophile such as water, producing the corresponding ω -hydroxycarboxylic acid/ester. When the nucleophile is an alcohol or amine, the product contains the corresponding ester or amide as an end-group. Finally, chain growth or propagation occurs by deacylation of the acyl-enzyme intermediate by the terminal hydroxyl group of the growing polymer chain to produce a polymer chain elongated by one monomer unit [53]. The mechanism of other types of reactions for the preparation of PLA – including (direct) polycondensation of lactic acid – is similar to the described above [54], starting with a stage of formation of an enzyme-activated monomer, which further participates in the stages of chain initiation and growth. The nucleophilic attack of the carbonyl carbon atom of the enzyme-activated monomer with the terminal hydroxyl group of the chain leads to the elongation of the polymer chain by one monomeric unit.

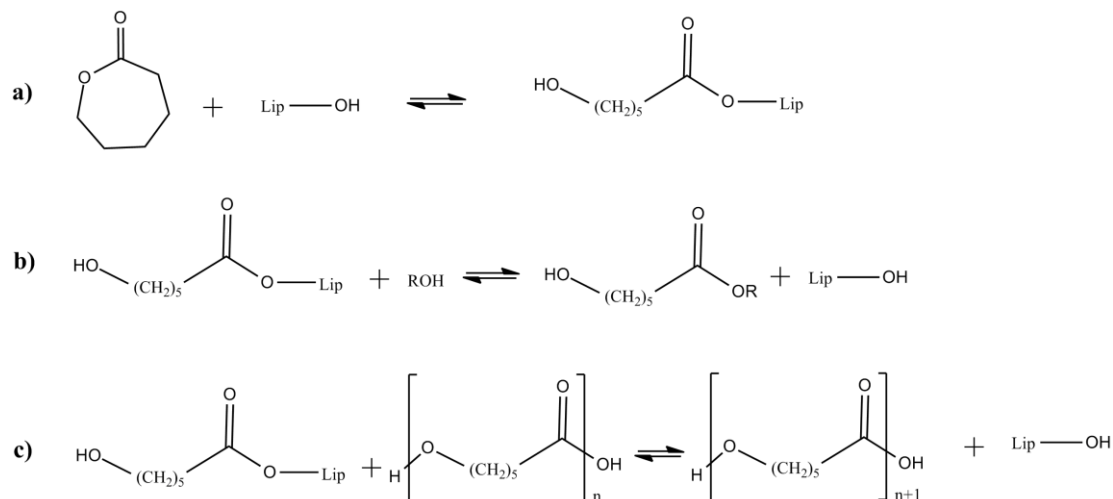


Figure 3. Mechanism of the lipase-catalyzed ROP of lactones: Formation of the acyl-enzyme intermediate (a); Initiation (b); Propagation (c).

However, eROP of lactones kinetics is usually slow and only some monomers are polymerized [43]. The type of enzyme obviously affects the polymerization rate, given that each enzyme presents specific stability and catalytic activity under the applied experimental conditions. Regarding lactide polymerization, N435 is the most efficient enzyme, presenting the highest activity. Duchiron *et al.* [43] determined the optimal activity temperature for four different lipases, including N435, by performing a simple esterification reaction and defined the initial

reaction rate at different temperatures. As expected, N435 presented (four times) higher activity compared to the other tested lipases (LBC, LCR, PPL) even at lower temperatures (e.g., 30°C, 50°C, 70°C). The effect of the type of the enzyme, which is strongly related to its activity, can be explained by the fact that the formation of the acyl-enzyme intermediate is the rate-determining step of the enzymatic polymerization [53]. Duchiron *et al.* [43] conducted eROP of lactide stereoisomers using N435 and *B. cepacia* to synthesize PLA. The authors stated that reactions kinetics were slow compared to metal-based catalysts or organocatalysts, as expected, since 80% monomer conversion was achieved after 24 and 48 h for N435 and LBC, respectively. N435 being more effective compared to LBC, resulted in a significant yield (90%) but slow kinetics and generally low molecular mass (less than 4000 g·mol⁻¹), probably attributed to a weak affinity between lipases binding site and lactide.

Even though in most of the published works on the enzymatic polymerization of PLA, the enzyme is not dried prior use, the water content in the enzyme has been found to play a crucial role in the polymerization process. There are two types of water molecules associated with enzymes; the "essential" or "free" or "hydration" water and the "bond" or "structural" water. Essential water is found at the surface layer of the enzyme, while bond water is embedded inside the enzymes' molecules [46]. Zhao *et al.* [46] measured the 'free water' content in N435, which was found in the range 0.77–1.97 wt%. The conducted eROP of L-lactide was catalyzed by different batches of N435. The researchers found that the molecular weight of PLA decreased with the increase in initial water content in the immobilized lipase. Only in a few works there is a reference to the drying process of the enzyme. Indicatively, N435 has undergone drying for one or two days under vacuum at room temperature [15,41] or for 2 h in a high vacuum pump (Vacuubrand, Germany) [48]. Otherwise, it has been stored under vacuum in a desiccator at 4°C [42]. On the other hand, using high vacuum for the enzyme's drying may be a significant obstacle to a possible process scaling up. Another drying option found in the open literature is freeze-drying [45,47]. Certain enzymes (e.g., *C. rugosa*) are commercially available in the form of freeze-dried powders [43]. In this context, Duchiron *et al.* [43] attempted to increase the PLA chains length and improve reaction kinetics *via* two different approaches: a. freeze-drying of the enzyme to significantly reduce the hydration water level without having a negative impact on the structural water content and b. addition of an amino base, TEA (anhydrous triethyl amine), as a co-solvent to toluene, which was used as solvent for the lactide's eROP. The first approach aimed at controlling the relative rate of the chain coupling (k_{cc}) reaction concerning the water reaction rate (k_w) and the water content in the medium (Figure 4). The second approach was used to increase the relative constant of coupling chain reaction ($k_{cc}/k_{cc'}$); by adding TEA, the lactide solubility was enhanced and the chain-ends of the formed oligomers were activated (Figure 5a). Due to its slight basic character and nucleophilicity, TEA probably increased the reaction rate also by activating the monomer for its ring-opening (Figure 5b). The enzymes' freeze-drying (approach a) resulted in an increase of 17 and 40% in the \overline{M}_n for N435 and LBC, respectively, while the TEA addition (approach b) permitted a significant kinetic improvement (reaction was five times faster for N435) and an increase of the molar mass (17% for N435).

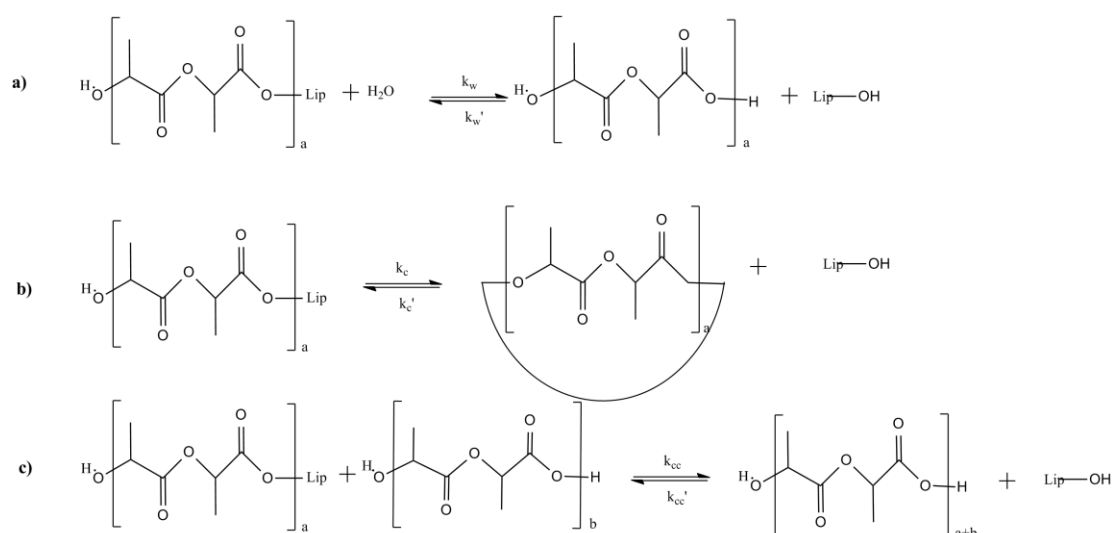


Figure 4. Reaction pathways for enzymatic ring-opening polymerization of lactide: Water reaction (a); Cyclisation reaction (b); Chain Coupling reaction (c).

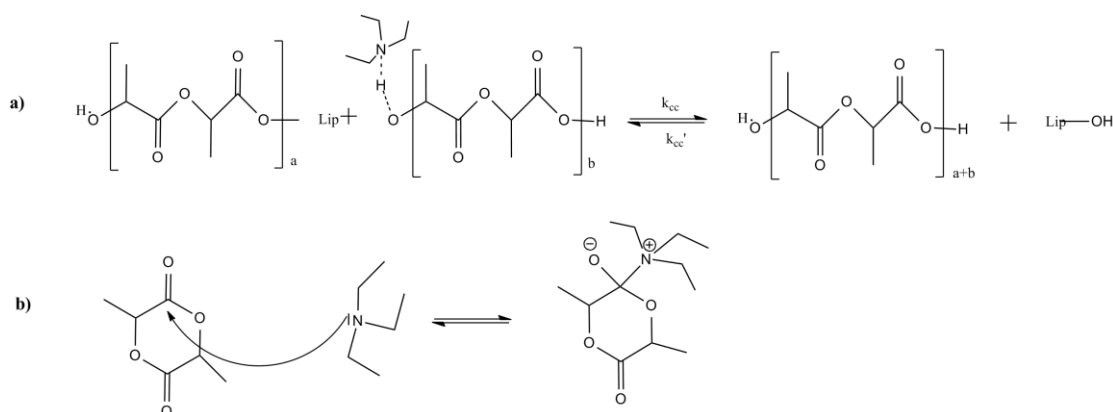


Figure 5. Oligomers chain-end activation (a) and nucleophilic activation of lactide (b)

Other approaches aiming at the improvement of enzymatic polymerization kinetics include the immobilization of the enzymes. Immobilization of an enzyme aims at avoiding the aggregation of the hydrophilic enzyme molecules, recycling the enzyme to reduce processing costs and, preventing the contamination of the product by the enzyme protein [55,56]. Additionally, immobilization enhances the enzyme properties by increasing the enzyme rigidity and heat tolerance, which is caused by the low conformational flexibility of the enzyme and is generally indicated by an increase in the optimum temperature and stability against inactivation [57]. When a non-immobilized lipase is submitted to heating, thermal deactivation occurs. The protein unfolding is considered a major cause of this kind of deactivation. However, *Rhizomucor miehei* lipase's thermal deactivation, which was studied by Noel and Combes [58] was attributed predominantly to the formation of aggregates rather than to protein unfolding. Several commercially available enzymes, such as the N435, are adsorbed within resins improving their stability and efficiency. Dsknkorur *et al.* [42] conducted eROP of D-, L- and D,L-lactide isomers while comparing free *Candida antarctica* lipase B (CALB) and its clay- and acrylic resin-immobilized forms. It was concluded that CALB immobilized on neat and organo-modified montmorillonite used for the D-lactide polymerization allowed to reach 70% of

monomer conversion after 4 days, but led to small oligomers. This slower polymerization kinetics compared with free CALB was partially attributed to hydroxyl groups at the clay surface that could be involved as co-initiators during polymerization.

Since N435 is immobilized, it can be reused up to ten times for numerous reactions [59] Loeker *et al.* [60] studied the eROP of poly(ϵ -caprolactone) (PCL) in supercritical carbon dioxide; it was found that reusing N435 led to the formation of high molecular weight values (\overline{M}_n 34000-37000 g·mol⁻¹) even after the enzyme's cleaning. On the other hand, the achieved mass yields were lower after the first recycling step. This was attributed to either leaching of the lipase B from the immobilization matrix or denaturation, leading to a partial loss in overall catalyst activity. Poojari *et al.* [61] reported the N435 recovery and reuse for up to ten reaction cycles during PCL synthesis in toluene at 70°C. High molecular weights (\overline{M}_w 50000 g·mol⁻¹) were constantly achieved. It was also stated that the multiple reuse cycles of N435 would be unattainable if leaching of CALB occurred due to physical desorption during polymer synthesis or if it was submitted to high mechanical shear (e.g., intense mechanical stirring). Very recently, Adhami *et al.* [62] conducted eROP of lactones to produce PCL and poly(δ -valerolactone) (PVL) using N435 in a flow tubular reactor. Due to the decreased reaction time of each cycle, the researchers synthesized PCL in toluene at 70°C while reusing the enzyme more than ten times. More precisely, high efficiency of the enzyme was proved, as it was used about twenty times in a flow tubular micro-reactor without the need for any extra step. The achieved molecular weight and conversion values were slightly lower than the fresh enzyme after the eight run.

1.2.1.1.2 PLA enzymatic polymerization key process parameters

The selected enzyme's concentration is one of the most important parameters of the enzymatic polymerization process. First, it has a considerable impact on the method's economical sustainability. As already discussed, immobilization aims at the enzymes' recycling; however, it is crucial to use as little as possible enzymes' quantity considering their high current cost [63,64]. In most of the published works with N435, lipase from the *B. cepacia* and lipase produced by *Streptomyces* sp. A3301, the selected average concentration is 10% relevant to the monomer's mass [16,41–45,52]. Of course, there are some exceptions; 2 and 3% of *C. rugosa* lipase has been also used for eROP and direct polycondensation of lactic acid [39,51], while 20% of N435 (0.5 g of lactide, 100 mg of N435) has been used by Zhao *et al.* [46] for eROP.

Second, the selected enzyme's concentration has a significant effect on the obtained product's properties. Zhao *et al.* [46] used 2% free CALB (0.5 g of lactide, 10 mg of free CALB) for the eROP of the L-lactide and obtained a product of \overline{M}_w 2800 g·mol⁻¹. When the enzyme's quantity increased to 10% (0.5 g of lactide, 50 mg of free CALB) the achieved \overline{M}_w of the product was 17500 g·mol⁻¹ under the same experimental conditions.

Table 2. Literature data on the enzymatic polymerization of PLA

Ref.	Enzyme	Polymerization method	Solvent	T(°C)	Range of achieved MW (g·mol ⁻¹)	
					\overline{M}_w	\overline{M}_n
[52]	<i>Streptomyces</i> lipase	polycondensation	Toluene	60	-	525
[51]	<i>Candida rugosa</i> lipase	Direct polycondensation	-	100	1430-1480	-
[40]	CALB redesigned	eROP	Toluene	60	-	780
[50]	Im. CALB	polycondensation	Isopropyl ether	60	-	2460
[42]	Im. CALB	eROP	Toluene	70	-	2600
[39]	<i>Candida rugosa</i> lipase	eROP	-	90	5400	2850
[43]	N435	eROP	Toluene, TEA	70	-	4900
[16]	N435	eROP	scCO ₂	65	12900	-
[46]	N435	eROP	<i>N,N</i> -Dimethylacetamide (DMA)	130	18800	-
[15]	N435	eROP	Toluene	60	-	12000
[44]	<i>B. cepacia</i> lipase	eROP	scR134a	105	-	14000
[47]	N435	eROP	Toluene	80	-	26000
[48]	Im. CALB	eROP	compressed R134a and the IL [C ₄ MIM][PF ₆] ¹	65	-	28000
[45]	N435	eROP	IL [HMIM][PF ₆] ²	90	-	37800
[41]	<i>B. cepacia</i> lipase	eROP	-	125	-	78100

¹1-butyl-3-methylimidazolium hexafluorophosphate, ²1-hexyl-3-methylimidazolium hexafluorophosphate

Another crucial parameter of enzymatic polymerization is the type of the used solvent when solution polymerization is selected. The most commonly used solvent for both eROP of the lactides and direct polycondensation of lactic acid is toluene [15,40,42,43,47,52]. In literature, toluene has been evaluated along with other conventional solvents based on their environmental risk. Toluene's environmental risk ranking was 0.7344, while water's 1.000 and benzene's 0.6098. Generally, toluene is characterized as usable but problematic [65], so not fully aligning with the principles of green polymerization. Toluene is a volatile, non-polar, aromatic hydrocarbon and along with hexane and benzene, they have been identified as hazardous air pollutants, carcinogens, mutagens and reprotoxins [66]. Especially for toluene, the primary target organ for chronic exposure is the central nervous system (CNS), gastrointestinal (GI) tract, cardiovascular system, hepatic, renal, hematological and dermal systems [67]. The replacement of toluene with a green solvent could be a solution to this problem. Gu and Jérôme, in their review paper [68], formulated the twelve criteria that a green solvent needs to meet: availability, price, recyclability, grade (technical grade solvents are preferred compared to highly pure solvents), synthesis, toxicity, biodegradability, performance, stability, flammability, storage and renewability. It is stated there, without being proven, that MeTHF, a commercially available solvent produced from renewable resources (lignocellulosic biomass) resembling in many ways to toluene in terms of physical properties, could theoretically replace it. However, it should always be considered that there is no absolutely green solvent, as it is a relative term, always depending on the context of each application. The only way to safely evaluate a solvent's level of greenness is to conduct an LCA [69].

Besides the sustainability issue, using low-polarity toluene is not ideal for eROP since lactides present high polarity and low solubility [48]. In this context, other alternative approaches, including ionic liquids (ILs) and supercritical fluids (SCFs), have been developed. ILs are considered green alternatives as they have a negligible vapor pressure and, as such, do not contribute to the volatile organic compounds problematic [69]. The term ILs includes chemically different solvents and liquid groups with different characteristics, except that they are all salts and liquids at low to moderate temperatures. Probably the most popular IL group contains N,N'-diacyl substituted imidazolium cations combined with a convenient counterion. The cations' synthesis, however, involves non-green reactions, and there is no enzyme known that could cleave the N-C- bonds. As a result, these cations are not biodegradable. Two other IL groups are considered greener; the first includes ILs consisting of cations found in the metabolism of living species or derived from them. Such cations can be based on choline, betaine, carnitine or amino acids. The second group includes ILs containing ethylene oxide groups. In contrast to other ILs, where the bulky cations energetically hinder crystallization, their low melting temperature is the consequence of high entropy contributions caused by the introduction of several ethylene oxide groups. Due to these structural features, these ions show high flexibility and favor the liquid state [69].

However, ILs have attracted great attention in the 21st century due to their ability to replace conventional solvents [65]. Most of the ILs that have been tested for ROP were inappropriate,

except for 1-butyl-3-methylimidazoliumhexa-fluorophosphate ([BMIM] [PF₆]) [46]. [BMIM] [PF₆] efficiency could be attributed to the relatively high miscibility of PLA with [BMIM][PF₆] (up to 10% by mass) and its low tendency to decompose the polymer matrix during melt-mixing, as it was studied by Gardella *et al.* [70]. [BMIM] [PF₆] has been used to some extent in eROP of lactides [45,46]. On the other hand, ILs present certain drawbacks that should be considered. Often their synthesis is not green at all and many of them are badly biodegradable and show significant toxicity. Additionally, their price is relatively high, especially for reasonably pure ILs, they often present high to very high viscosity and require high effort for their synthesis [69].

SCFs have also been used in eROP of lactides, probably due to the enhanced solubility of the monomer and the growing polyester chains in this kind of media [16,44]. Generally, eROP is conducted in a biphasic media system where the supercritical phase (e.g., supercritical carbon dioxide) coexists with a liquid organic phase mainly composed of melted monomer, wherein the formed PLA chains are soluble [16]. The polarity and hydrophobicity of SCFs such as 1,1,1,2-tetrafluoroethane scR134a contribute to this enhanced solubility of the monomer and subsequent polymeric products [44]. The use of SCFs may, however, influence enzyme activity by direct pressure effect, which may lead to denaturation and by indirect effects of pressure on enzymatic activity and selectivity; when supercritical CO₂ is used, lower catalytic activities may be observed due to the formation of carbonic acid [71].

Another approach aiming to develop a green process for the enzymatic synthesis of PLA is the combination of ILs and SCFs. According to Mena *et al.* [48], the use of a homogenous medium composed of the ionic liquid [C4MIM] [PF₆] with miscible compressed 1,1,1,2-tetrafluoroethane (R134a), above the critical points of the mixture, led to the successful enzymatic syntheses of linear and hyperbranched PLLA. The molecular weight of the obtained PLLA products were up to 3-fold higher than those obtained with the ionic liquid medium (up to 28000 g·mol⁻¹).

It is always preferable to avoid using a solvent when it is not necessary. Bulk systems have also been studied in the context of eROP of lactides [41,46,72]. Mälberg *et al.* [41] observed that lipase from *B. cepacia* was effective in both bulk and mini-emulsion eROP, while Zhao *et al.* [46], who used N435 for the L-lactide, stated that most of the tested organic solvents led to much lower molecular weights and yields compared to the bulk system, with the exception of xylene and DMA at a low concentration. This behavior could be attributed to the fact that the oligo(lactide) solidifies easily in bulk systems, creating a mass transfer barrier for continuing the enzymatic reaction. Additionally, the water content in solvents may lead to unfavorable side reactions, including polyester hydrolysis. On the other hand, using a solvent at a low concentration (e.g., 0.25 mL for 0.5 g L-lactide) may be beneficial to produce higher molecular weight PLA. Yoshizawa-Fujita *et al.* [72], who conducted eROP of the L-lactide, concluded that the achieved monomer conversions and molecular weights for certain ILs were better than the bulk and solution methods' and they attributed this to the fact that the anion of ILs has a molecular interaction during the polymerization. According to the researchers, the activity of lipases is strongly affected by the anion species of the IL; ILs having [BF₄], [PF₆], and [NTf₂] (from the IL 1-butyl-3-methylimidazolium bis(trifluoromethylsulfonyl)amide or [C4MIM] [NTf₂])

anions induce the polymerization activity of lipases. However, chloride and $[\text{N}(\text{CN})_2]$ anions have exhibited lipase deactivation due to the strong interaction of the lipase with the $[\text{N}(\text{CN})_2]$ anion. Additionally, stability studies have indicated that lipases exhibit greater stability in ionic liquids than in organic solvents, including hexane [73]. However, the polymer yields were relatively lower than those of bulk polymerization because PLLAs present great solubility in ILs, and it is thus difficult to be extracted at the end of the process.

The reaction temperature, time and pressure are also crucial factors for the properties of the product to be obtained. In general, the enzymatic polymerization reaction rate increases with temperature. The melting temperature of the L-lactide is 93°C , so when eROP takes place in solventless systems, the first step is usually the lactide's heating until it melts. In light of the above, Rahmayetty *et al.* [39] tested different temperatures in the range of $70 - 130^\circ\text{C}$ for eROP of L-lactide in the presence of *C. rugosa* lipase (CRL). They concluded that the highest CRL activity was obtained at 90°C for 72 h. The researchers noticed that above 90°C , the lipase underwent discoloration from yellowish-white to dark brown and confirmed that high temperatures caused denaturation of proteins of enzymes. Mälberg *et al.* [41] conducted bulk eROP for PLA synthesis at 100 and 125°C in the presence of lipase from *B. cepacia* for seven (7) days. The bulk direct polycondensation method, which was conducted by Rahmayetty *et al.* [51] in the presence of *C. rugosa* lipase, presents great interest regarding the applied experimental conditions; the mixture of the monomer and the enzyme was heated at different temperatures ($60 - 120^\circ\text{C}$) and vacuum pressure of 0.1 bar for 72 h. The researchers found out that the rising temperature causes the rising of viscosity and density of PLA solution. They also confirmed that PLA's yield is affected by temperature.

The applied reaction temperatures were slightly lower ($60-90^\circ\text{C}$) when enzymatic polymerization was conducted in toluene [15,40,42,43,47,52]. This could be attributed to the relatively low toluene boiling point (110°C). Indicatively, Takwa *et al.* [40] conducted eROP in the presence of wild type and redesigned CALB at 60°C , for 48 h, in D8-toluene, while Panyachanakul *et al.* [52] conducted polycondensation in the presence of a lipase produced by *Streptomyces* sp. A3301 at 60°C , for 8h, in toluene, under nitrogen atmosphere. Higher temperatures are sometimes applied when ILs are used. For example, Zhao *et al.* [46] noticed that a temperature of 130°C led to higher molecular weights and conversions than lower temperatures ($80-110^\circ\text{C}$) in $[\text{BMIM}][\text{PF}_6]$, so 130°C was the selected reaction for the polymerization process which was conducted for 7 days.

1.2.1.1.3 PLA enzymatic polymerization monitoring variables

The most important parameter to evaluate the level of success of an applied polymerization process is the molecular weight (MW) of the obtained product. Other important parameters include the thermal properties glass transition and melting temperature, crystallinity and the achieved process yield.

The MW of the obtained PLA grades of each research work could be classified into 3 categories; oligomers or low-molecular-weight (<5000 g·mol⁻¹) PLA grades, moderate-molecular-weight (5000-15000 g·mol⁻¹) and high- molecular-weight (> 15000 g·mol⁻¹) PLA grades.

The lowest obtained number-average molecular weight (\overline{M}_n) of the enzymatically synthesized PLA grades was 525 g·mol⁻¹, synthesized *via* polycondensation in the presence of a lipase from *Streptomyces* sp. (A3301), at 60°C, in toluene, by Panyachanakul *et al.* [52]. Based on their poor properties, the produced short oligomers would not be able to be used in any application. Still, as was suggested by the researchers, they could be applied as prepolymers for PDLLA synthesis in other experiments and applications. Similarly, Rahmayetty *et al.* [51], who applied direct polycondensation of lactic acid in the presence of *C. Rugosa* lipase, obtained low-molecular-weight products in the range 1400 – 1500 g·mol⁻¹. It could be very difficult to study and suggest a scaling up of this process, given that a relatively high vacuum (0.1 bar) is required. In general, the low molecular weights obtained in these works could be attributed to the applied direct polycondensation, which produces low molecular weight products even when conventional catalysts are used [38,74]. However, it is valuable that new enzymes were isolated and tested for the enzymatic polymerization of PLA, and the academic community can undoubtedly make good use of these data.

Lassalle and Ferreira [50] used immobilized CALB in isopropyl ether for 96 h to conduct direct polycondensation. The obtained products were solids, presenting values of \overline{M}_n between 400 and 2400 g·mol⁻¹ and LA conversion between 22 and 96%. The percentage of the solid PLA was in the range of 2-55%. Since a polymer of these properties can be used for a limited number of applications, a novel thermal treatment consisting of heating at 190°C, under vacuum, for 24 h was proposed to further increase the \overline{M}_n giving promising results.

Regarding eROP, Takwa *et al.* [40] synthesized PLA of 780 g·mol⁻¹, corresponding to a degree of polymerization (DP) of 4.5 lactide units at 60°C in toluene. They used the D-lactide and compared the efficiency of the wild type and several mutants of *Candida antarctica* of lipase B as biocatalysts. They found out that two mutants presented 90-fold increased activity compared to the wild type, and the achieved conversion was 89%. Based on a molecular dynamics simulation, the researchers concluded that the larger space created by a specific mutation altered the orientation of the dilactyl moiety in the tetrahedral intermediate, thus improving the deacylation step of the propagation in the ROP reaction drastically. On the other hand, the relevant low molecular weight that was obtained is not in complete accordance with the literature, as it is suggested that CALB has a good selectivity towards D-lactide (better than L-isomer) [40,43].

Rahmayetty *et al.* [39] performed eROP of L-lactide in the presence of *C. rugosa* lipase at 90°C. The resulting PLA presented \overline{M}_n of 2854 g·mol⁻¹ at a yield of 93%. The crystallinity of the enzymatically synthesized PLA was 31%, and its melting point (T_m) 120°C. It is known that PLA is a semicrystalline polyester with a melting temperature between 170 and 180°C [75]. The

lower melting point of the obtained PLA grade is attributed to its low molecular weight. This product was recommended for biomedical applications.

eROP of D- and L-Lactides was conducted by Duchiron *et al.* and Döskünkorur *et al.* [42,43]. Both the research groups used N435 and selected reaction temperatures of 90 and 115°C, respectively. Duchiron *et al.* [43] obtained oligomers of \overline{M}_n from 500 to 4900 g·mol⁻¹ and confirmed the selectivity of N435 towards D-lactide and *B. cepacia* towards L-lactide. The most important finding of this group was the activating role of TEA which, as an aprotic amino base, permitted a significant kinetic improvement (5 times faster enzymatic reactions) and an increase in the molar mass of the final product (17%). This approach could reveal new opportunities for lipase reverse catalysis and make eROP a competitive method, comparable with classical organometallic catalysis. Döskünkorur *et al.* [42] achieved the complete conversion of D-lactide to PDLA with \overline{M}_n of 2600 g·mol⁻¹.

Moderate-molecular-weight PLA grades were synthesized *via* eROP by Guzmán-Lagunes *et al.*, García-Arrazola *et al.* and Hans *et al.* [15,16,44]. Guzmán-Lagunes *et al.* [44] and García-Arrazola *et al.* [16] used the L-lactide and the enzymes *B. cepacia* lipase and N435, respectively. It is of high interest that both these groups used SCFs (scR134a and scCO₂) to synthesize PLA of \overline{M}_n 14000 g·mol⁻¹ (Đ < 2) and \overline{M}_w up to 12900 g·mol⁻¹, respectively. Of note that the grade of 14000 g·mol⁻¹ presented crystallinity of maximum 35% and melting temperature in the range of 170-180°C, in agreement with the reported values of PLA [75].

Hans *et al.* [15] obtained *via* eROP of D-lactide a narrowly distributed polymer (Đ 1.1) with \overline{M}_n of 12000 g·mol⁻¹. The reaction temperature was 70°C and the researchers used a monomer/toluene ratio of 1:2 (g:mL). They concluded that upon careful adjustment of the reaction conditions, it is possible to obtain PDLA with reasonable molecular weights in high yields enzymatically using the biocatalyst Novozyme 435.

Zhao *et al.* [46] conducted eROP at 130°C with the use of IL [BMIM][PF₆] to produce PLA grades of \overline{M}_w around 20000 g·mol⁻¹ or \overline{M}_n around 10000 g·mol⁻¹ (for an average Đ of 2), meaning medium-molecular-weight polymers. The researchers stated that this polyester type could be used as the soft block of thermoplastic elastomers or carriers for controlled drug delivery and release.

It is interesting to observe that several high molecular weight PLA grades have been synthesized enzymatically [41,45,47,48]. The highest molecular weight of enzymatically synthesized PLA grades \overline{M}_n 78100 g·mol⁻¹ was achieved by Mälberg *et al.* [41] with the use of a lipase from *B. cepacia* at 125°C for 7 days in bulk. Chanfreau *et al.* [45] used the IL [BMIM][PF₆] to obtain PLLA of \overline{M}_n 37800 g·mol⁻¹. The measured PLLA yield was 63% and it was attained at 90°C. Omay *et al.* [47] and Mena *et al.* [48] synthesized PDLA and PLLA grades of \overline{M}_n of 26000 g·mol⁻¹ and 28000 g·mol⁻¹, respectively. In both works, the used enzyme was N435, but PDLA was synthesized in toluene at 80°C, while PLLA was synthesized in a homogenous media composed of the ionic liquid [C4MIM] [PF₆] in combination with miscible compressed 1,1,1,2-tetrafluoroethane (R134a). This is very promising, given that the PDIs of the polymers were in

the range of 1.1–1.7, indicating narrow distribution, the percentages of crystallinity of the PLLAs were in the range 43–50%, which is expected for semicrystalline polymers, the T_g of the polymers were the range of 48.8–62°C, in agreement with published reports, the melting temperatures range between 109 and 138°C and the degradation temperatures of the polymers were between 155 and 122°C.

1.2.1.1.4 Type and characteristics of the used enzyme for PBS enzymatic polymerization

Since the 1990s PBS and its copolymers have been highlighted in polymer science mainly due to their ability to be used in biomedical and food packaging applications. PBS's biodegradability makes it an appropriate material for soft-tissue repair and tissue engineering, as well as in the single-use packaging sector. However, properties such as crystallinity play a major role in the degradation process and may limit its suitability for soft-tissue applications, mainly due to the relatively slow degradation and resorption rate [76]. Additionally, crystallinity degree and crystalline morphology significantly affect the gas barrier properties of a packaging material [77]. It is thus important to fine-tune the production process of PBS to obtain free of catalyst residue grades appropriate for use in biomedical and packaging applications while presenting controlled properties such as crystallinity. The most important parameters of the recently conducted enzymatic polymerizations of PBS will be discussed in the following.

N435 has been used for every conducted enzymatic PBS polymerization for the last 20 years (Table 3). There is only one work – published in 1998 – where the researchers used the lipase from *R. miehei* to produce biodegradable aliphatic polyesters, including PBS [78]. Even though the results were satisfying, and the lipase *R. miehei* generally seems adequate for esterification reactions due to its high stability in anhydrous media and good esterification activity [79], it has not been selected as a biocatalyst for the most recently conducted enzymatic polymerizations where we will mainly focus.

Enzymatic polycondensation and ring-opening polymerization that has been analyzed above for PLA occur through similar mechanisms and reaction intermediates (acyl-enzyme intermediates) [80]. The lipase mechanism during polycondensation has been described in detail by Hevilla *et al.* [80] and is depicted in Figure 6. In the first step, the primary alcohol from the nucleophilic serine ($-\text{CH}_2\text{OH}$) interacts with the carbonyl group of a substrate molecule (carboxylic acid or its esters) $\text{RC}(=\text{O})-\text{OR}'$, forming a tetrahedral intermediate (*I). This intermediate gets stabilized through three hydrogen bonds from glutamine (Gln 106, 1 hydrogen bond) and threonine (Thr40, 2 hydrogen bonds). Meanwhile, the imidazole group of His224 residue pulls the proton from Ser105. As a result, the nucleophilicity of the oxygen is increased enough to attack the carbonyl carbon of the substrate. In parallel, the carboxylate group of Asp187 helps the His224 residue to pull the proton. Consequently, the acyl-enzyme complex (AEC, *II), also known as enzyme-activated monomer specie (EAM), is formed while liberating $\text{R}'\text{O}-\text{H}$ (acylating step), which is removed from His224. In the deacylating step, a nucleophile, e.g., a primary alcohol from a diol ($\text{R}''\text{O}-\text{H}$), reacts with the AEC carbonyl carbon

forming a new tetrahedral intermediate (*III) which gets stabilized by the active site. Finally, the enzyme is deacylated and regenerated after releasing the product (ester, polyester).

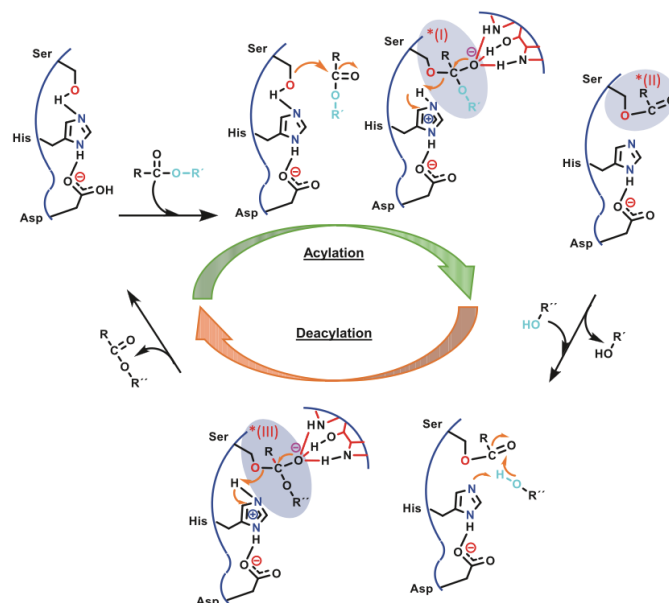


Figure 6. Enzymatic polycondensation in the presence of CALB. *I) Tetrahedral intermediate, *II) acyl-enzyme complex (AEC), *III) tetrahedral intermediate [80]

It has been observed that OH-rich PBS prepolymers are synthesized *via* enzymatic transesterification [49], probably attributed to DES low internal carbon chain length (2) and limited accessibility to the enzyme's active site.

To the best of our knowledge, there are no completed published studies on the kinetics of PBS enzymatic polymerization. The only exception is a reference to El Fray and Gradzik's work [81]: in this work, PBS was synthesized *via* enzymatic polymerization under varying pressures (0.3, 1 and 2 mmHg), in diphenyl ether at 80°C. The researchers observed that when the pressure of the polycondensation stage changed, the conversion of the reaction corresponding to the kinetics of polycondensation was altered. The highest molecular weight was obtained when the lowest pressure (0.3 mmHg) was applied, and the achieved yield under these conditions was 37%. The relevant low yield was attributed to the limited reaction time (9 h), and it was stated that it probably should be extended.

Sonseca *et al.* [82] synthesized poly(butylene succinate-dilinoic succinate) (PBS-DLS), a biodegradable copolymer that may be used for applications requiring contact with the human body. The researchers evaluated the kinetics of enzymatic transesterification using variable amounts of hard/soft segments (70 to 50 wt% butylene succinate hard segments and 30 to 50 wt% dilinoic succinate soft segments). Based on the ¹HNMR analysis, it was found that copolymer oligomers had been formed after 3 h of reaction (under atmospheric pressure and N₂). Additionally, the end groups of BDO, dimer linoleic diol (DLAOH) and DES were also identified; after 24 h of total reaction and the application of slight vacuum (600 Torr), the end groups from DLAOH disappeared, and the proton signals from ester formation increased, indicating that DLAOH was incorporated into the chains of the oligomers. At the end of this

low-vacuum stage, the BDO and DES end groups also decreased, indicating the conversion of the initially formed products into higher molecular weight oligomers. In the next step, the vacuum pressure increased, and a more than 2-fold increase in \overline{M}_n of all copolymers was observed from 21 to 48 h reaction time. It was concluded that the DLAOH had a significant effect on the molecular weights of the copolyesters; the high incorporation of DLAOH into the PBS backbone led to the formation of copolyesters of increasing molecular weights with an increasing amount of soft segments. It was also found, though, that the efficacy of the DLAOH incorporation was limited by the catalytic pocket size of the enzyme and its hydrophobic nature favoring the formation of long PBS sequences, especially at the early synthesis stages.

For N435 and PBS, it has been confirmed that the enzymes' drying before use is crucial for the polymerization process, as four modes of reversible reactions may occur during the lipase-catalyzed polyester synthesis, inducing hydrolysis, esterification, transesterification (alcoholysis and acidolysis) and interesterification [27]. On the other hand, even though a dry enzyme is usually more efficient and better resistant against microbiological degradation or chemical inactivation [83], the use of vacuum for the enzyme's drying is a limiting factor to a polymerization process scaling-up. In addition to that, the use of a solid, dried enzyme presents more drawbacks. Considering the cost aspect, it is quite expensive to evaporate water to obtain the enzyme in the solid form. Additionally, the enzyme could be inactivated by the drying process. Thus, liquid enzyme formulations are an alternative to the use of solid enzymes. The choice of solvent system for the liquid formulation is very important. Even though water is the common solvent for enzymes, co-solvents are often added to improve the stability of the native protein. They are often added in high concentrations and can either be other solvents (e.g., glycerol) or solids (e.g., sucrose), aiming to reduce water activity [83].

However, the usage of dried enzymes in enzymatic polymerization of PBS is widespread; Pellis *et al.* [33] dried N435 under vacuum for 96 h at 25°C and stored it in a desiccator before use, while Jiang *et al.* [84] placed CALB into a 25 mL flask and stored it in a desiccator with phosphorus pentoxide at room temperature under high vacuum for 16 h. P₂O₅ was used also by Sugihara *et al.* [85] for the enzyme's drying under vacuum at 25°C for 2 h. Azim *et al.* [86] and El Fray *et al.* [81] used N435, predried under 0.1 mmHg vacuum at 25°C for 24 h

Enzymatic polymerization's kinetics is usually slow, and thus, immobilization is an approach aiming at its improvement. Interestingly, the activity of polymer-immobilized CALB (N435) may depend on the enzyme storage time, as was recently stated by Pospiech *et al.* [87]. The researchers used lipase CALB for melt polycondensation of aliphatic polyesters, including PBS and observed that the enzymatic activity of immobilized CALB, which influenced the achieved molar mass of the obtained products, was affected by the time of the storage. Indicatively, the activity of CALB at 50°C stored for 2 years was found 1400±100 U·g⁻¹, while fresh CALB's was 2900±700 U·g⁻¹. PBS grades of \overline{M}_n 11000 g·mol⁻¹ and 2900 g·mol⁻¹ were synthesized using fresh and 2-year-stored CALB, respectively. Even though the measurements' standard deviations were significant (7-24%), the enzyme's degradation could probably be attributed to inappropriate storage conditions e.g., temperature above 25°C.

The reusability of N435 during transesterification reactions has been studied by Nasr *et al* [88]. The researchers used 1,6-hexanediol and diethyl adipate in bulk and solvent (diphenyl ether) systems to produce enzymatically poly(hexylene adipate). Constant \overline{M}_n values of the polyester were achieved over three consecutive cycles in bulk, even at relatively high temperatures (100°C), while a 17% decrease of the \overline{M}_n values was observed in the solution system. The decreased N435 activity was attributed to the better heat transfer in the solution system compared to the bulk, rendering the enzyme more prone to elevated temperatures leading to degradation or leaching. Additionally, given that N435 is prepared *via* interfacial activation of lipases to supports with hydrophobic surfaces, it becomes more susceptible to be released in the presence of organic solvents such as diphenyl ether.

1.2.1.1.5 PBS enzymatic polymerization key process parameters

PBS has been synthesized enzymatically *via* esterification or transesterification of succinic acid or diethyl succinate, respectively. In contrast to the conventional PBS synthesis, which usually includes esterification, transesterification is the most commonly applied enzymatic polymerization route. This is attributed to the fact that lipases, including N435, present higher specificity to esters and alcohols than acid substrates.

Typical monomers that have been used for PBS enzymatic polymerization *via* transesterification are BDO and diethyl succinate (DES) or dimethyl succinate (DMS) [33,36,81,84–86,89]. A commercial-scale process to produce bio-based BDO (from sugar) has already been developed and published [90], while bio-based DES has already been used for PBS enzymatic co-polymerization with dilinoleic succinate [91]. The use of these bio-based monomers is completely in line with the principles of green polymerization.

The selected enzyme's concentration for PBS enzymatic polymerizations is 10-40% relative to monomers [33,36,81,84–86,89,92]. Most researchers, especially in recent works, have used only 10% wt relative to monomers. Considering the principles of circular economy, the use of small quantity of reusable materials including enzymes is always desirable. On the opposite side, using large quantities of enzymes would significantly increase the whole process cost. Besides, it is well known that small quantities of an enzyme compared to their substrate are sufficient to lower down the activation energy of the reaction during catalytic action [93].

A crucial parameter for equilibrium reactions is removing the polycondensation by-product. The use of diesters such as DES or DMS instead of dicarboxylic acids can shift the equilibrium towards polymerization, as it results in much volatile by-products (alcohols) compared to water. In that sense, in most of the conducted PBS enzymatic polymerizations, two-stage polymerization routes with increasing vacuum/temperature are applied to achieve higher-molecular-weight polymers.

Table 3. Literature data on the enzymatic polymerization of PBS

Ref.	Enzyme	Solvent	T(°C)	Range of achieved MW(g·mol ⁻¹)	
				\overline{M}_w	\overline{M}_n
[33]	N435	-	85	1094	851
[49]	N435	Isooctane	50	2000	-
[94]	N435	-	60	2550	1700
[95]	N435	-	90	4000	1400
[81]	N435	Diphenyl ether	80	-	840-2550
[36]	N435	Diphenyl ether	75	-	3910
[84]	N435	Diphenyl ether	80	11520	4463-6017
[86]	N435	Diphenyl ether	60-90	-	2000-7000
[87]	N435	-	130	23600	11700
[86]	N435	-	80-95	38000	27340
[89]	N435	-	95	44000	-
[92]	N435	Toluene	95	73000	-
[85]	N435	Toluene	100-120	130000	81250

Pellis *et al.* [33] conducted two-step enzymatic polymerizations; the first stage was conducted at 85°C for 5 h under atmospheric pressure. Subsequently, a vacuum of 20 mbar was applied for 18 more hours while maintaining the reaction temperature at 85°C. At the end of the first stage, oligomerization was achieved, while during the second stage, the vacuum effectively removed the alcohol by-product and enabled the elongation of the polymeric chain length. Kanelli *et al.* [36] conducted PBS enzymatic polymerization through a two-stage route. The first one was applied at 75°C for 2 h under nitrogen atmosphere considering BDO high volatility and the second at 75°C for 2 h under a vacuum of 20 mbar. The researchers also observed that the product's morphology was improved when prolonging both stages (first stage: 5 h and second stage: 24 h). In the work of Azim *et al.* [86] the polycondensation reaction took place for 21 h and then, the polymerization temperature increased from 80 to 95°C. During the second stage, the polymer remained soluble in so that the reaction proceeded in a single liquid phase that facilitated further molecular weight increase. Sugihara *et al.* [85] applied direct polycondensation of BDO with dimethyl succinate at 100°C for 24h. They concluded that the ring-opening polymerization of lactones is probably a better method when aiming at high-molecular-weight polyesters, including PBS. The achieved molecular weight was low and it was

attributed to the reverse reaction and transesterification. A two-stage method was also selected by El Fray *et al.* [81]. The reaction occurred at 80°C for 2 h under atmospheric pressure, which was subsequently reduced to 0.03 mmHg. As a result, the obtained polyesters' molecular weight and melting points increased while the -OH groups number decreased.

1.2.1.1.6 PBS enzymatic polymerization monitoring variables

The achieved molecular weight of an enzymatically synthesized polymer is one of the most important parameters to evaluate the efficiency of the selected enzyme and the applied process. The MW of the synthesized PBS grades will be classified into 3 categories; oligomers or low-molecular-weight (<10000 g·mol⁻¹) PBS grades, moderate- (10000-80000 g·mol⁻¹) and high- (>80000 g·mol⁻¹) molecular-weight PBS grades.

The enzymatically synthesized PBS grade with the lowest weight-average molecular weight (1094 g·mol⁻¹) was obtained in a bulk system at 85°C for 24 h (under atmospheric pressure the first 6 h and 20 mbar for 18 h) [33]. The researchers tested different diesters and concluded that there is a strong effect of the selected alkyl group of the diester (dimethyl, diethyl and dibutyl) for all polyesters; more precisely, lower molecular weights and monomer conversions were obtained using dibutyl esters since it was more difficult to remove the butanol by-product during the reaction due to its higher boiling point (relative to methanol and ethanol). Uyama *et al.* [94] synthesized low molecular-weight PBS (\overline{M}_n 2550 g·mol⁻¹) in a bulk system at 60°C. The researchers confirmed that the methylene length of the monomers strongly affected the polymerization characteristics. Other low-molecular weight PBS grades (\overline{M}_n 2500-7000 g·mol⁻¹) were also obtained through solution polymerizations; diphenyl ether was used [36,81]. El Fray *et al.* [81] obtained PBS of \overline{M}_n 2500 g·mol⁻¹ and T_m 110°C, at a reaction temperature 80°C and pressure of 0.3 mmHg for 9 h with the use of diphenyl ether. They confirmed that the decreased pressure during the polycondensation reaction increased the molecular weight, reduced the -OH groups number and increased the melting point of the products. However, the achieved process yield (app. 40%) and the molecular weight were low, indicating that the reaction time should be extended. Kanelli *et al.* [36] synthesized a sticky PBS grade of \overline{M}_n 3900 g·mol⁻¹, which was subsequently upgraded *via* solid-state post-polymerization. The SSP process was examined under reduced pressure for 24 h at 84°C and a simultaneous increase in T_m and ΔH was observed, implying a crystal reorganization/perfectioning. Consequently, a two-step SSP process was conducted for 36 h; the first step, which served as a pre-crystallization step, was conducted at 77°C for 24 h while the second was conducted at 90°C for 12 h. The molecular weight and T_m were significantly enhanced ($\Delta\overline{M}_n$ 67%) with simultaneous improvement of prepolymer physical characteristics, as the stickiness disappeared. Gkountela *et al.* [49] recently synthesized PBS of \overline{M}_n 2000 g·mol⁻¹ and T_m 78°C, in isoctane at 50°C. This prepolymer was subsequently submitted to a post-polymerization stage, including a first step of heat treatment at 80°C for 2 h and then the second step at 90°C for 8 h to upgrade its quality

in terms of molecular weight and thermal properties. The final product presented an increase of 26°C in the T_m and 126% in the \overline{M}_w .

Concerning the moderate-molecular weight grades, Jiang *et al.* [84] synthesized fully bio-based poly(butylene succinate) and poly(butylene succinate-co-itaconate), given that all the used building blocks and catalysts were generated from renewable resources. The synthesized PBS grade presented \overline{M}_w 11500 g·mol⁻¹ and T_m of 112.9°C, which is very close to a commercial PBS T_m of \overline{M}_w 75000 g·mol⁻¹ (ca. 114°C [96]). The applied process included a first step at 80°C for 2–24 h under atmospheric pressure and a nitrogen atmosphere. A second step under very low pressure (2–40 mmHg) was applied for another 94 h at the same temperature. Azim *et al.* [86] synthesized PBS of \overline{M}_w 38000 g·mol⁻¹. However, the researchers used diphenyl ether as the solvent and applied a very high vacuum; the process was carried out first at 80°C for 5–21 h at 1.8–2.2 mmHg to form PBS oligomers and subsequently, the reaction temperature was raised to 95°C at 1.8–2.2 mmHg. An *et al.* [89] also applied a very high vacuum of 10 mmHg at 95°C for 25 h to produce PBS with a molecular weight of \overline{M}_n 44000 g·mol⁻¹. Ren *et al.* [92] applied a two-step route for the synthesis of bio-based PBS using succinic anhydride and BDO. In the first step, the polycondensation reaction took place for 12 h at 95°C in the presence of succinic acid. The nucleophilic attack to succinic anhydride by BDO facilitated the polycondensation *via* esterification between di-acidic and diol units. A linear oligomer was formed, enabling the solvation of monomers and thus paved the way for the following lipase-catalyzed polymerization in the presence of N435 in toluene. The researchers did not apply vacuum to remove the by-product, but a hydrous azeotrope (water with toluene) was formed, facilitating the reuse of both the lipase and the solvent while minimizing energy consumption. The obtained PBS grade presented \overline{M}_w 73000 g·mol⁻¹. It is of high essence that the recovered lipase catalyst was tested and presented a similar performance after six cycles.

An interesting approach to synthesize high-molecular-weight PBS (\overline{M}_w 130000 g·mol⁻¹) was suggested by Sugihara *et al.* [85]. The researchers developed a new strategy for the green production of bio-based plastics, including PBS. In the first step, a cyclic oligomer was produced by the lipase-catalyzed condensation of dimethyl succinate and BDO in a dilute toluene solution. In the next step, ring-opening polymerization of the cyclic oligomer took place in a more concentrated solution or in bulk with the same lipase. The conventional, direct polycondensation route was compared to this new strategy. In this context, PBS was synthesized enzymatically through polycondensation of BDO and dimethyl succinate. During polycondensation, methanol was removed using molecular sieves 4Å and the obtained polyester presented \overline{M}_w of 45000 g·mol⁻¹. However, it was stated that lipase itself contains water and thus, complete removal of the small molecules, such as methanol and water, is difficult. So, the researchers concluded that to obtain a higher molecular weight polyester, the ring-opening polymerization of cyclic oligomers is the most effective route for such a lipase-catalyzed polymerization.

1.2.1.2 Enzymatic polymerization of aliphatic polyesters

1.2.1.2.1 Type and characteristics of the used enzyme for furan-based polyesters enzymatic polymerization

2,5-Furandicarboxylic acid (FDCA) is a bio-based compound consisting of two carboxylic acid groups attached to a furan ring. FDCA's chemical structure, along with its thermal stability and aromatic nature, make it capable of replacing terephthalic acid, which is used to produce polymers such as PET and poly(butylene terephthalate) (PBT). FDCA is one of the monomers for poly(ethylene 2,5-furandicarboxylate) (PEF) and poly(butylene 2,5-furandicarboxylate) (PBF) [97]. Avantium catalytically converts plant-based sugars into FDCA to produce 100% plant-based, 100% recyclable and degradable PEF, which presents superior performance, including barrier properties, compared to PET. According to Gert-Jan M. Gruter and Thomas B. van Aken from Avantium [98], "a strong barrier preventing oxygen from entering the bottle (relevant for juice and beer) and CO₂ leaving the bottle (relevant for any carbonated beverage) was an unmet need in the market". As a result, special coatings, additives (scavengers) or nylon layers were used for PET bottles to improve this barrier. This practice increased the process and final product's cost and made PET's recycling more difficult. PEF monolayer was a great step toward solving this unmet market need.

Furan-based polyesters have been gaining popularity very recently and their conventional synthesis has started being studied. Papadopoulos *et al.* [99] synthesized PEF from FDCA and ethylene glycol (EG) and tested two different antimony catalysts (antimony oxide and antimony acetate) and different reaction temperatures while applying a two-step polycondensation method. The authors concluded that for the first step of the polymerization, i.e., the esterification of FDCA with EG to afford PEF oligomers, Sb₂O₃ was more active than Sb(CH₃COO)₃ at lower temperatures (160°C), while in the second step of the polymerization, Sb₂O₃ exhibited the highest activity. Zhu *et al.* [100] synthesized PBF with the use of titanium tetraisopropoxide (Ti[OCH(CH₃)₂]₄) as a catalyst at temperatures in the range 150-200°C by melt condensation polymerization. It was concluded that the synthesized PBF presenting excellent thermal stability, strength and ductility could probably replace PBT. Pouloupoulou *et al.* [101] synthesized bio-based PBF with the use of tetrabutyltitanate (TBT) by melt polycondensation. The researchers also prepared blends with its terephthalate counterpart, PBT and studied the thermal properties of the homopolymers and the blends by employing both conventional and fast scanning calorimetry. Thus, amorphous samples were obtained to reveal the glass transitions of the polymers and improve the blends miscibility.

It is important, though, to investigate all the alternative furan-based polyesters' synthetic routes that could provide us with truly green products – in terms of performance properties and synthesis process. In that sense, even though furan-based polyesters' enzymatic synthesis has not been studied greatly, the most important parameters of the synthesis processes will be discussed to provide valuable guidance on their enzymatic synthesis in the coming years.

The only enzyme that has been used for the synthesis of the furan-based polyesters so far is Novozyme 435 (N435) (Table 4). Even though numerous aliphatic polyesters have already been successfully synthesized *via* N435-catalyzed polymerization, the number of the enzymatically synthesized aliphatic and aromatic polyesters is limited. This is attributed to the high melting temperature (T_m) of aliphatic and aromatic polyesters and their low solubility in the reaction media, as well as the lack of reactivity of aromatic monomers in enzymatic polyesterification [27].

Table 4. Literature data on the enzymatic polymerization of furan-based polymers

Ref.	Polymer	Enzyme	Solvent	T(°C)	Range of achieved MW(g·mol ⁻¹)	
					\overline{M}_w	\overline{M}_n
[102]	PBF	N435	-	50	600	500
[103]	PBF	N435	Diphenylether	80-140	5500	1600
[104]	Furan-based copolyesters (P(FMF-co-OF))	N435	Diphenylether	80-95	35000	-
[105]	Furanic-aliphatic poly(ester amide)s (PEAF12)	N435	Toluene	90	21000	-

It can be assumed that the enzymatic production of furan-based polyesters in the presence of lipase N435 occurs through the already described enzymatic polycondensation mechanism and reaction intermediates. Maniar *et al.* [104] who used dimethyl 2,5-furandicarboxylate (DMFDCA), 2,5-bis(hydroxymethyl)furan (BHMF), aliphatic linear diols and diacid ethyl esters to synthesize furan-based copolyesters, studied in detail the synthetic mechanism of the copolymerization, firstly by varying the aliphatic linear monomers: the methylene units of the tested diols were 4, 6, 8, 10 and 12. The results indicated that *Candida antarctica* lipase B (CALB) prefers longer linear diols ($n = 8, 10$ and 12) compared to shorter linear ones ($n = 4$ and 6). The copolyester P(FMF-co-OF), synthesized with the use of 1,8-ODO, presented the highest degrees of polymerization. The researchers observed that when the chain length was decreased to 6 and 4 (1,6 hexanediol (or 1,6-HDO) and 1,4-BDO), the \overline{DP}_n and \overline{DP}_w of furan-based copolyesters significantly decreased. A second approach of the researchers to evaluate the synthetic mechanism was by changing the aliphatic monomers from diols to diacid ethyl esters. Based on the obtained results, a significant decrease in the molecular weight was observed. In light of the above, the researchers presented the proposed copolymerization mechanism, depicted in Figure 7. The polymerization starts with the formation of the acyl-enzyme complex and continues with polycondensation. During the polycondensation, an intermediate product (b) that can inhibit the polymerization is formed. Steric hindrance of (b) creates structure incompatibility with the enzyme active site and consequently, the polymer growth is terminated. When diacid ethyl ester is used, the OH functionality in (b) may also transform into BHMF ether, eventually terminating the copolyester chain elongation.

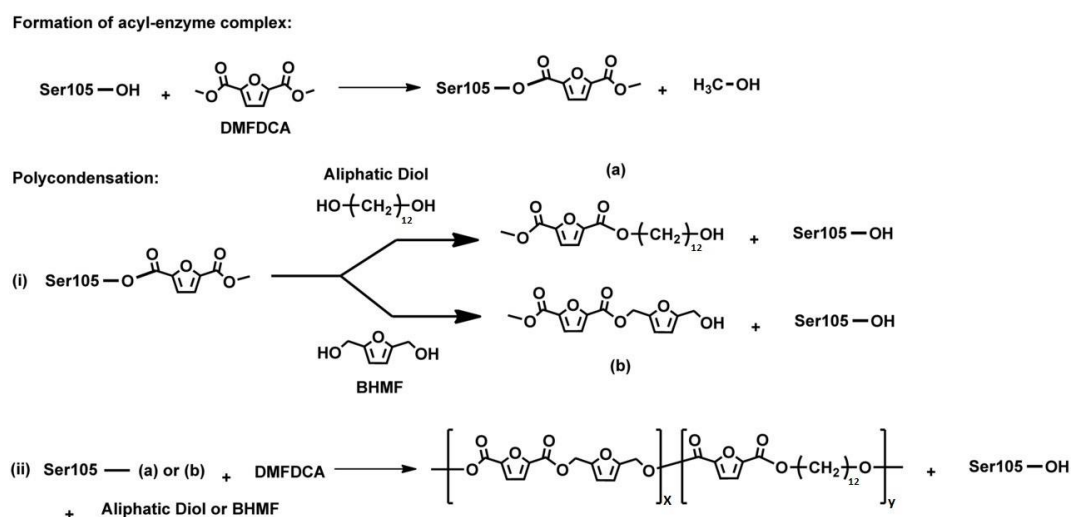


Figure 7. Proposed copolymerization mechanism of CALB-catalyzed formation of P(FMF-co-DOF) [104].

The enzymatic polymerization kinetics of furan-based polyesters has not been studied yet. However, Jiang *et al.* [106] studied the kinetics of the enzymatic synthesis of 2,5-furandicarboxylic acid-based aliphatic polyamides. The relevant conclusions could be valuable information for a future furan-based polyesters enzymatic polymerization kinetics study. The researchers produced a series of FDCA-based aliphatic polyamides using N435, bio-based DMFDCA and aliphatic diamines differing in chain length (C4–C12).

A one-stage method (90°C in toluene) was applied, and the researchers found that N435 presented the highest selectivity towards 1,8-octanediamine (1,8-ODA) among the tested aliphatic diamines. Based on the results of the enzymatic polymerization kinetics study, \overline{M}_w increases significantly with the increase of polymerization time. Additionally, phase separation of the FDCA-based oligoamides/polyamides occurs in the early stage of polymerization and the resulting product undergoes a subsequent enzymatic solid-state polymerization. However, due to the phase separation and the low efficiency of the enzymatic solid-state polymerization, a large proportion of the resulting polyamides possess low molecular weights. As a result, only less than 50% of the products can be obtained after purification.

The water content seems to be the most important factor for the enzymes' efficiency in polymerization processes. Jiang *et al.* [103] who produced furanic-aliphatic polyesters including PBF, used CALB, which was predried overnight in the presence of phosphorus pentoxide (P₂O₅) at room temperature under high vacuum. Comerford *et al.* [102] who produced oligoesters such as PBF, used CALB, which was submitted to drying under vacuum for 48 h at 25°C and stored in a desiccator prior use. Maniar *et al.* [104] who synthesized furan-based copolyesters and furanic-aliphatic poly(ester amide)s, used CALB, predried in the presence of P₂O₅ in a desiccator at room temperature under high vacuum for 16h. In addition to eliminating the enzyme's water content, selecting an immobilized enzyme such as N435 aims to improve the enzymatic polymerization kinetics, which is expected to be slow.

1.2.1.2.2 Furan-based enzymatic polymerization key process parameters

DMFDCA is a bio-based diester that is used as a monomer in all the furan-based enzymatic polymerizations [102–105]. This is attributed to its better solubility in the reaction medium (e.g., diphenyl ether) under mild conditions and the lower melting temperature of DMFDCA (T_m 112°C) than FDCA (T_m 342°C) [103]. It is also known that lipases including N435 present higher specificity to esters and alcohols than acid substrates. Various potentially renewable aliphatic diols, BHMF and diamines or amino alcohols are used too as monomers/comonomers.

There doesn't seem to be a specific trend regarding the most appropriate enzyme concentration. For PBF synthesis, Jiang *et al.* [103] used 0.4 g of CALB with 5.4304 mmol (0.999 g) of DMFDCA corresponding to 40 wt% of the monomer, while Comerford *et al.* [102] used 10% of the total amount of the monomers. Maniar *et al.* [104,105] used 20 wt% and 15 wt% in relation to the total amount of the monomer for the synthesis of furan-based copolyesters and furanic-aliphatic poly(ester amide)s respectively.

The by-product removal, strongly affecting polycondensation reactions' equilibrium, is achieved firstly with the use of diesters resulting in much volatile by-products (alcohols) compared to water from dicarboxylic acids and secondly with the application of vacuum, usually *via* a two-stage synthesis route. Jiang *et al.* [103] conducted enzymatic polymerization of DMFDCA and different aliphatic diols in diphenyl ether and tested two different synthetic routes. The first route included a first stage at 80°C for 2 h under an atmospheric nitrogen environment and a second at 80°C under reduced pressure (2 mmHg) for 72 h. The second tested route was a temperature-varied two-stage method; the first stage was performed at 80°C for 2 h under a nitrogen atmosphere. At the second stage, the pressure was reduced to 2 mmHg while maintaining the reaction temperature at 80°C for the first 24 h. The temperature was subsequently increased to 95°C for another 24 h. Finally, the reaction temperature was regulated at 95, 120 or 140°C for the last 24 h. Based on the enzymatic synthesis process which was applied by Comerford *et al.* [102] the reaction occurred at 50°C for 6 h at a pressure of 1000 mbar. A vacuum of 20 mbar was subsequently applied for an additional 18 h, maintaining the reaction temperature at 50°C. The total reaction time was 24 h. According to Maniar *et al.* [104] in the first step of the reaction, the monomers mixture (e.g., DMFDCA, BHMF, diethyl succinate) in the presence of diphenyl ether was heated 80°C for 2h under a nitrogen atmosphere. At the subsequent second stage, the pressure was reduced stepwise to 2 mmHg while maintaining the reaction temperature at 80°C for the first 48h. Finally, the reaction temperature was increased to 95°C under full vacuum for the last 24h. Maniar *et al.* [105] produced furanic-aliphatic poly(ester amide)s *via* a one-stage method; the reaction took place at 90°C in the presence of toluene under a nitrogen atmosphere for 72 h.

The main disadvantage of the applied enzymatic polymerization/copolymerization methods is using the high-boiling point diphenyl ether as already discussed, along with the high vacuum requirement, impeding a process scaling up. Lower-boiling point toluene for the furanic-aliphatic poly(ester amide)s synthesis seems more promising; however, toluene is still not a

green solvent. In this context, Maniar *et al.* [105] performed the polymerization to produce furanic-aliphatic poly(ester amide)s in an ionic liquid ([BMIM][PF₆] and [EMIM][BF₄] or 1-ethyl-3-methylimidazolium tetrafluoroborate) as the reaction solvent.

1.2.1.2.3 Furan-based enzymatic polymerization monitoring variables

The enzymatically synthesized PBF grades presented weight-average molecular weight values of 600-5500 g·mol⁻¹. Comerford *et al.* [102] synthesized the lowest molecular weight PBF grade (\overline{M}_w 600 g·mol⁻¹, \overline{M}_n 500 g·mol⁻¹) and the polymerization was conducted in a solventless system. The achieved low molecular weight could probably be attributed to the selected polymerization method. More precisely, higher molecular weight polymers are usually synthesized enzymatically *via* solution polymerization, given that the solution reaction system presents lower viscosity, decreasing diffusion constrictions among polymer chain reactants, monomers and oligomers. On the other hand, in bulk, the reaction medium has a higher viscosity, reducing the diffusion of the reactants [107]. To upgrade the enzymatically synthesized PBF oligoester, the researchers subsequently performed a thermal, catalyst-free treatment. A \overline{M}_w 3.3 times higher than the initial oligomer was achieved. Jiang *et al.* [103] synthesized *via* a two-stage method (1st stage: 80°C, 2h, N₂ atmosphere and 2nd stage: 80°C, 72 h, 2 mmHg) a PBF grade of \overline{M}_w 1700 g·mol⁻¹ and \overline{M}_n 1200 g·mol⁻¹. Considering that the major obstacle for enzymatic synthesis of furanic-aliphatic polyesters at mild temperatures is the phase separation mainly caused by the high T_m and the low solubility of the final products, the researchers performed the enzymatic polymerization at higher reaction temperatures. Thus, they applied a temperature-varied two-stage method (1st stage: 80°C, 2 h, N₂ atmosphere and 2nd stage: a. 80°C, 24 h, 2 mmHg, b. 95°C, 24 h, c. 95, 120 or 140°C, 24 h). When the reaction temperature of the last 24 h of the 2nd stage (c) was increased from 80°C to 140°C, the corresponding \overline{M}_w and \overline{M}_n values increased from 1700 and 1200 g·mol⁻¹ to 5500 and 1600 g·mol⁻¹, respectively. The significant increase of molecular weights with reaction temperature is first attributed to the fact that phase separation was delayed at higher reaction temperatures. It can also be attributed to the fact that eliminating alcohol by-products and the residual water is easier at higher temperatures, thus improving the enzymatic polycondensation efficiency. Finally, the mobility of the amorphous phase of furanic-aliphatic polyesters, which is enhanced at higher temperatures, facilitates the CALB-catalyzed solid-state polymerization. Concerning the melting point of the synthesized PBF grade, it increased from 145 to 168°C when its \overline{M}_w increased from 1700 to 5500 g·mol⁻¹. This indicates that the chain growth of PBF was limited at the tested temperatures. As a result, the molecular weights of the obtained PBF increased with reaction temperature but couldn't reach higher values.

Maniar *et al.* [104] used DMFDCA, BHMF and different aliphatic linear diols to synthesize various furan-based copolyesters with \overline{M}_w up to 35000 g·mol⁻¹. More exactly, when 1,8-ODO was used, P(FMF-co-OF) with \overline{DP}_n and \overline{DP}_w 122 and 269 was formed, which was the highest amongst the tested aliphatic diols.

The first novel FDCA-based poly(ester amide)s were enzymatically synthesized by Maniar *et al.* [105] and poly(dodecamethylene furanoate-co-dodecamethylene furanamide) (PEAF12) presented the highest \overline{M}_w (21000 g·mol⁻¹). This material presented T_m and T_d of 92 and 395°C, respectively, comparable to PEF, presenting T_m of 211°C and T_d of around 389°C [107].

1.2.2 Introduction to post-polymerization: Solid State Polymerization (SSP)

Solid state polymerization (SSP) belongs to the bulk polymerization techniques used for both step- and chain-growth polymers with a strong industrial (and academic) interest in condensation polymers. SSP includes the starting material heating in an inert atmosphere or vacuum at a temperature below its melting point but permitting the initiation and propagation of typical polymerization reactions.

The different versions of the SSP family are presented below. Direct SSP, the first version, includes using dry monomers (e.g., polyamide salt, amino acids) as the starting material to form polymers [108,109]. The second version, post-SPP, also known as SSP finishing, requires as starting material a solid prepolymer, i.e., a low-molecular-weight polymer synthesized through another polymerization technique, usually conventionally [110]. A very interesting case is the combination of post-SSP with enzymatic prepolymerization, as these methods can be considered eco-friendly [36,49,111,112] (Chapter 5.1). SSP is indeed a green method, given that it is usually conducted at relatively low temperatures (below the prepolymer melting point); it is also a solventless method and can be effective without catalysts. Post-SSP aims to increase the prepolymer molecular weight and improve processability and end-product properties. On that basis, SSP can be applied as an efficient recycling technique [25]. In this case, the starting material can be a postconsumer polymer grade needing a molecular weight increase to be processed without severe recycled material deterioration.

The main SSP rate-limiting steps are the following: the intrinsic kinetics of the *chemical reaction*, the *diffusion* of functional *end groups*, the diffusion of the condensate in the solid reacting mass (*interior diffusion*), and the diffusion of the condensate from the surface of the reacting mass to the surroundings (*surface diffusion*) [110,113].

Regarding the mechanism of the post-SSP, Zimmerman and Kohan [114] suggested a two-phase model according to which the polymerization proceeds by stepwise reactions in the amorphous regions of the semi-crystalline polymer, where the end groups and low-molecular-weight substances such as the condensates are excluded (Figure 8). It is assumed that reactions and equilibrium in the amorphous regions are the same as for a completely amorphous or molten polymer at the same temperature. The diffusion of end groups in the amorphous phase is considered to occur either through the low-molecular-weight molecules (oligomers), through the motion of the terminal segments (segmental diffusion) or through exchange reactions (chemical diffusion) that allow reactive end groups to approach up to an appropriate distance for reaction. Based on the two-phase model, it has also been proposed that two categories of end groups exist in the amorphous polymer regions: active and inactive end

groups include chemically dead chain ends and functional groups trapped in the crystalline structure and cannot participate in the reaction. Based on the above, a more accurate definition of SSP could be the following: heating of the prepolymer at a temperature between the glass transition and the melting point (T_g and T_m , respectively) to make the end groups mobile enough to react and promote condensation reactions in the amorphous regions.

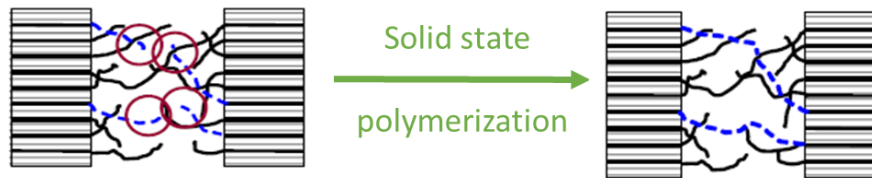


Figure 8. Solid state polymerization: Two-phase model

The most critical parameter affecting the SSP process is the reaction temperature, interfering with the chemical reaction, the mobility of the functional end groups and the by-product diffusivity. It is thus crucial to optimize the $T_m - T_r$ to achieve increased polymerization rates while avoiding undesirable phenomena such as sintering or agglomeration. It is also typical to apply temperature-step processes aiming for gradual increases in the prepolymer softening temperature, thus avoiding agglomeration and removing initial moisture and impurities [115].

The initial end-group concentration is a crucial parameter for SSP, affecting segmental mobility and diffusion of the active chain ends [25]. It has been indicated that the lower the end group concentration, the higher the achieved number-average molecular weight increase. This is because the lower molecular weight prepolymers' short chains can easily fit into crystal lattices and form rigid crystals; as a result, a greater number of the end groups will get trapped and become inactive.

Other important factors affecting the SSP effectiveness are the prepolymer geometry and the gas flow rate. The first one affects the (interior) diffusion of the by-product within the polymer particle. However, this influence gets weaker when diffusion and reaction control the process. The inert gas flow affects the surface by-product diffusion. Acceleration of the gas flow increases the mass and heat transfer rates in the gas-solid system and decreases resistance to the by-product diffusion from the particle surface to the bulk of the gas phase. These two parameters strongly depend on the chemical reaction characteristics, such as the equilibrium constant, which is proportional to the by-product removal requirements [110].

Crystallinity also influences the SSP rate due to its interaction with other controlling critical parameters, including end-group mobility and by-product diffusion. Based on the two-phase model, an increase in crystallinity leads to a higher concentration of end groups rejected in the amorphous phase and, thus, to an increase in the reaction rate. On the other hand, a very high degree of crystallinity could limit the by-products' removal from the reacting mass due to rigidity and the well-organized crystal lattice and thus it is not desired in most SSP processes [113].

The last factor that may increase the slow SSP reaction rates is the use of appropriate catalysts. The SSP reaction rate is generally low without catalysts as it is limited to the diffusion of the autocatalyzing acid chain end groups. Typical catalysts are acidic compounds (e.g., H_3PO_4 , H_3BO_3 , H_2SO_4) that can easily be diffused into the reacting mass [110].

The relatively slow reaction rates that are expected during SSP may sometimes lead to the selection of melt polymerization, especially when using catalysts is to be avoided. However, except for its green character (low temperature, solventless process, can be a continuous operation), SSP presents several advantages over melt polymerization. Thanks to the relatively low reaction temperatures, side reactions are usually avoided, and as a result, the products usually present increased thermostability compared to the grades prepared in the melt state. Regarding the economic aspect, using uncomplicated, inexpensive equipment renders it viable.

The most typical fossil-based polymers that have been submitted to SSP include polyamides and polyesters including poly(ethylene terephthalate) (PET), poly(butylene terephthalate) (PBT), poly(ethylene naphthalate) (PEN) and poly(trimethylene terephthalate) (PTT) [108]. Especially PET is the most studied polyester submitted to SSP due to its industrial importance. The factors of the highest interest include reaction temperature, pellet size, crystallinity level, nature and rate of carrier gas and catalyst concentration. An interesting finding is the increased diffusivity of water instead of ethylene glycol (EG), rendering the SSP diffusion controlled. Due to this phenomenon, an optimal COOH/OH molar ratio (typically 0.3-0.8 depending on the SSP conditions) in the starting prepolymer is usually required to reduce the SSP time and achieve high MW values. Another approach to reach high MW values is to stop SSP after a given time, melt the polymer, and then restart SSP on the particle obtained after solidification of the molten polymer. In this case, issues such as the reduced segmental mobility of end groups during SSP are solved.

In light of the above, SSP is an industrialized method typically used to produce or upgrade fossil-based polyamides and thermoplastic polyesters. Besides, it was not considered feasible in the open literature for the case of aliphatic polyesters due to their low melting points [116], rendering the by-product removal very difficult. However, our research group has successfully applied it to bio-based and biodegradable linear polyesters such as PLA and PBS.

1.2.2.1 PLA Solid State Polymerization

Regarding bio-based and biodegradable linear polyesters, it is crucial to study the influence of the most critical parameters affecting the SSP process to avoid sintering phenomena usually occurring at reaction temperatures close to the melting point and to achieve high post-polymerization rates. Starting with PLA, indicative works dealing with SSP are presented in Table 5. It is interesting that in some works, SSP also served as a monomer removal method from ROP-derived PLA. In other words, crystallization occurring simultaneously with SSP may result in excluding reactive ends and monomers in the amorphous regions and reaching a polymerization conversion of 100%. Emphasis is also put on prepolymer pretreatment.

Table 5. Indicative literature conditions for melt synthesized PLA solid state polymerization [115]

	Prepolymer	Precrystallization conditions			SSP conditions			Range of MW (g·mol ⁻¹)		
		Temperature (°C)	Time (min)	Pressure (torr)	Temperature (°C)	Time (h)	Vacuum (torr)	Catalyst	Initial	Final
[117]	PLLA				100-140	9	n.a.	Stannous 2-ethyl hexanoate	40000-10000	52000-74000
[118]	PLAA	105	60-120	0.5	130-155	10-55	0.5	SnCl ₂ 2H ₂ O/TSA	13000	670000
[119]	PLAA	60	60	0.5	150	10	0.5	SnCl ₂ 2H ₂ O/TSA	13000	320000
[120]	PLAA	105	15-90		135	15-50	n.a.	SnCl ₂ 2H ₂ O/TSA	18000	80000
[121]	PLA				98-150	5-12	n.a.	tin octanoate	26000	228000
[122]	PLA nanocomposites (clay)				150-160	5-10	n.a.	tin octanoate clay: cloisite 20 A	21000	138000
[123]	PLAA/PDLA				140-160	30	0.5	SnCl ₂ 2H ₂ O/TSA	22000	141000
[124]	PLLA/PDLA (1:1 wt)				140-160	30	0.5	SnCl ₂ 2H ₂ O/TSA	31000	202000

n.a.: not available

More exactly, precrystallization seems important to be conducted before PLA SSP to increase prepolymer melting point and to avoid sintering phenomena, as well as to exclude monomer and catalyst in the amorphous regions of the polymer to accelerate SSP reactions, similar to PET SSP.

Vouyiouka *et al.* [115] submitted PLA to solid state polymerization (SSP) in a fixed bed reactor under nitrogen flow (gas flow rate at ca. 150 mL·min⁻¹) to examine technique efficiency for increasing the molecular weight and hence permitting the reduction of the melt polymerization residence times. In this context, prepolymers were produced through solid state hydrolysis of high-molecular-weight commercial PLA to provide starting materials of appropriately reactive carboxyl and hydroxyl end groups. The fine-tuning of the reaction temperature indicated that temperatures below 130°C are the most appropriate, as above 130°C, sintering phenomena occur, especially when $T_m - T_{SSP}$ reaches very low values (<2.5°C). Additionally, at 140°C, despite the quasi-melt transition of reacting particles, theoretically favoring reacting groups' mobility and by-product removal, the SSP rate was low independently of starting MW, and the change in MW varied from 5 to 22%. Similar SSP rates were indicated for the lower temperatures of 120 and 130°C.

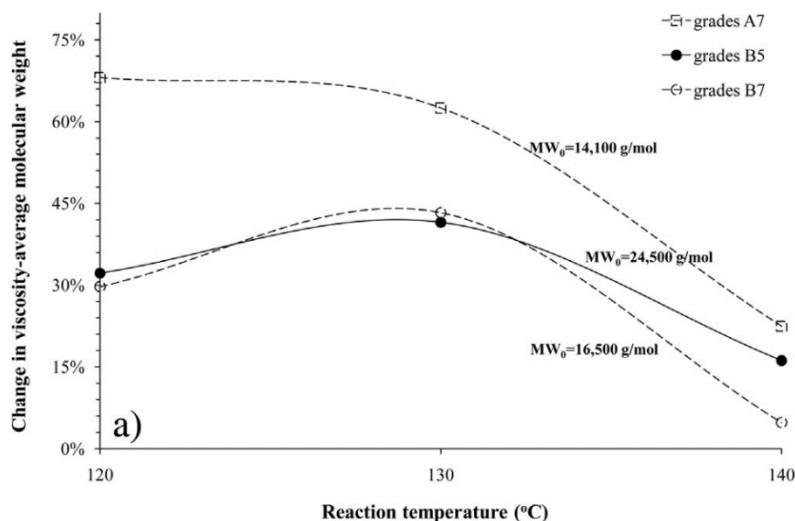


Figure 9. Change of viscosity-average molecular weight with respect to reaction temperature during SSP under flowing nitrogen nitrogen for 32h, with starting PLA grades of $\overline{M}_v < 25000$ g·mol⁻¹[115]

The initial molecular weight of the prepolymer was the next factor for PLA SSP to be investigated. For the effective reaction temperatures (i.e., 120 and 130°C), it was found that the lower molecular weight grades presented increased susceptibility to SSP and a critical starting \overline{M}_v of 25000 g·mol⁻¹ was revealed. More specifically, a PLA grade of initial \overline{M}_v of 14100 g·mol⁻¹ after being submitted to SSP at 120 for 32 h, reached 23700 g·mol⁻¹, i.e., a 68% increase in molecular weight was achieved (Figure 9). On the contrary, the grades of higher MW (presented significantly lower MW increases after SSP. For instance, a PLA grade of initial \overline{M}_v of 55600 g·mol⁻¹ reached 64800 g·mol⁻¹ and was thus limited to a 16% increase. Finally, in some cases, SSP resulted in reduced molecular weight values compared to the initial, attributed to

degradation reactions, such as hydrolysis of ester groups due to water traces, lactide formation and/or vinyl chain ends formation, that may occur during SSP. The high impact of the MW of the PLA prepolymer on the SSP effectiveness has been explained as follows. The low MW PLA, presenting a relatively low T_g , possesses a high chain end concentration, leading to greater free volume and, thus, greater segmental mobility. As the prepolymer MW increases (higher T_g), the concentration of chain ends decreases, as does the free volume. Given these, the by-product diffusivity also decreases, thus leading to lower SSP rates.

The use of a catalyst during PLA SSP was also investigated [125]. More specifically, commercial phosphorous-containing organic additives (trisphenylphosphite, tris(nonylphenyl)phosphite, trislaurylphosphite, tris(octadecyl)phosphite, tristearylsorbitoltriphosphite, tris(octadecyl)phosphate, trislaurylphosphate, or mixtures of them), typically used as processing stabilizers were used and found effective leading to MW increases by 15-30% depending on the initial molecular weight of the prepolymer. Besides, the degree of crystallization and the branching density of the prepolymer increased after the SSP.

Interestingly, SSP has also been applied as a post-polymerization step for PLA microcapsules (MCs) [126]. PLA MCs were submitted to SSP to tailor the polymeric shell properties, i.e., MW and crystallinity, significantly affecting the release profile of the encapsulated substance. Semi-crystalline PLA MCs (\overline{M}_v 21.200 - 150.200 g·mol⁻¹, particle size at ca. 2.8 μm, T_m 163-168°C) were formed. The SSP was conducted at 135°C, and even though the spherical topology of the microcapsules was not fully maintained since particle aggregation occurred, the achieved MW increase was 70 % for the MC of the lowest initial molecular weight, along with an increase in crystallinity up to 60%. It was thus concluded that adapting the SSP process from the conventional bulk polymer scale to the microcapsule geometry scale is feasible and valuable to overcome the conventional encapsulation drawbacks and produce customized application products.

1.2.2.2 PBS Solid State Polymerization

Melt polymerization products such as PBS usually suffer from drawbacks associated with the high reaction temperatures and residence times in the melt and yellowing caused by titanium-based catalysts. PBS synthesis requires high esterification temperatures for prolonged times and the application of vacuum favoring BDO loss (boiling point, T_b 230°C), its dehydration to tetrahydrofuran, and other side reactions, all resulting in a disturbed end-group balance and impaired properties such as hydrolysis stability. Thus, investigating alternative PBS synthesis methods conducted at milder conditions is necessary. Except for the PBS enzymatic polymerization, discussed in Chapter 2, an alternative could be the SSP. Even though PLA SSP has been studied to an extent in the open literature (see Chapter 1.2.2.1), the SSP of PBS is very limited. This is probably attributed to the lower operating temperatures (<114°C) compared to PET (T_m 260°C) and even PLA (T_m 150–160°C), which are anticipated to result in slower overall process kinetics. Some works of our group focusing on the application of SSP on PBS as a

finishing step after enzymatic prepolymerization are presented in Chapter 5.1. Besides these works, Paspaspyrides *et al.* [25] studied the feasibility of SSP on fossil- and bio-based PBS.

More precisely, fossil-based and true bio-based poly(butylene succinate) (PBS) prepolymers were synthesized and submitted to solid-state polymerization (SSP) in the proximity of the polyester melting point (T_m) for reaction times up to 29 h under flowing nitrogen. Starting with the fossil-based grade, the effect of the reaction temperature was the first parameter to be examined. When SSP was conducted at 8.2°C below the melting point of the prepolymer (113.2°C), no significant MW increase was achieved (i.e., $\Delta\overline{M}_w$ 9%). However, for a T_m-T_{SSP} of 3.2°C \overline{M}_w increased by 169%. Interestingly, when SSP was conducted at the lower temperature, 8.2°C below the T_m , an increase in the crystallinity was observed, implying crystal thickening.

The next examined parameter was the prepolymer MW, and therefore, three different MW PBS grades (\overline{M}_w 18000, 46500 and 85700 g·mol⁻¹) were submitted to SSP at ca. 3°C below the prepolymers' melting points for 24 h. The low MW grade presented the highest \overline{M}_w increase of 64%, followed by the medium and the highest MW grades (21 and 8% respectively). In agreement with the PLA SSP results, this trend was attributed to the high chain end concentration in the amorphous regions of the low MW prepolymer, increasing the free volume, segmental mobility and byproduct diffusivity.

One of the most important parameters of the PBS SSP is the end-group imbalance. To study the effect of this parameter, two similar MW PBS grades with different initial [COOH] (Figure 10) were submitted to SSP at ca. 3°C below the prepolymers' melting points for 24 h. The grade with the higher initial [COOH], F3, presented significantly limited SSP effectiveness ($\Delta\overline{M}_w$ 5%), in contrast to the almost balanced structure grade, F2, which presented an MW increase of 64%. It was thus indicated that the COOH-terminated macromolecules were inactive for further polycondensation.

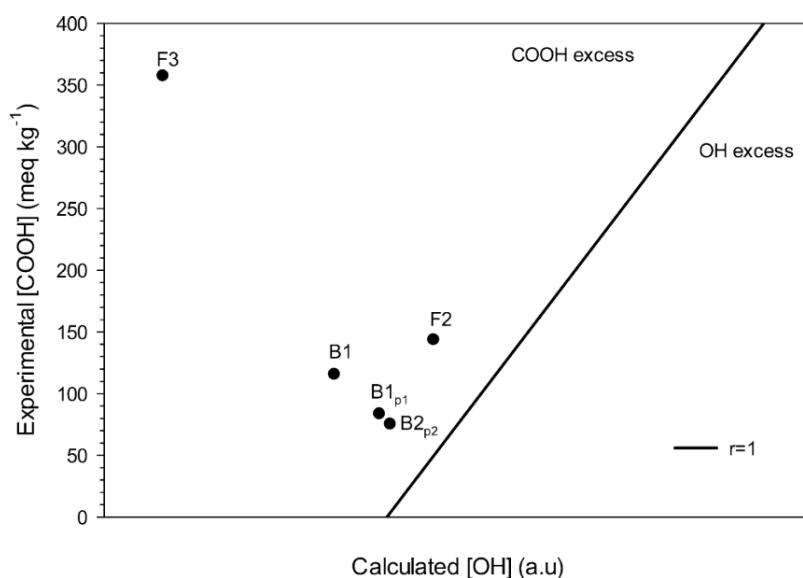


Figure 10. Mapping of the susceptibility of PBS prepolymers to SSP [25]

The last parameter to be examined was the addition of a precrystallization step. With the low MW, almost balanced PBS grade as initial material and taking advantage of the SSP-increasing T_m , a two-step process was conducted for a total time of 29 h, with the first step (5 h, 113°C) serving as a precrystallization step, similar to PET and PLA technology, and the second step reaching higher reaction temperature (118°C) to favor MW build-up. The SSP rate was found to increase and a higher than triple increase in the \overline{M}_w was monitored. In addition, there was a significant increase in the prepolymer melting point ($\Delta T_m \sim 13^\circ\text{C}$) and the degree of crystallinity.

A precrystallization step was necessary for the bio-based PBS grade due to its high T_m deviation ($115.7 \pm 2.9^\circ\text{C}$). The optimized precrystallization step (105°C, 4h) followed by the SSP stage (114°C, 24 h) led to no sintering issues, but the relevant MW increase was lower than the fossil-based grades ($\Delta\overline{M}_w$ 23 %). Additionally, even though there was a significant increase in the T_m , for the first time after the SSP process, a multiple-melting behavior was observed; the first endotherm was attributed to secondary crystallization or thinner/imperfect lamellae, developed in the case of bio-based PBS, whereas the second endotherm may be attributed to the isothermally grown crystals or dominant lamellae.

The decreased susceptibility of the bio-based PBS grade was attributed to the dominating COOH-rich polymer chains, attributed to either BDO loss during melt polymerization or acidic impurities of the bio-based SA monomer. Different approaches were examined, including prepolymer purification and blending with PBS oligomers rich in OH end groups to approach stoichiometric balance ($r=1$). Both the tested approaches resulted in a slight improvement in terms of the achieved $\Delta\overline{M}_n$ ranging between 27-33 %, while sticking problems arose after the second approach, probably due to the oligomer incorporation.

Since PBS is sensitive to hydrolytic degradation, SPP was effective as a PBS recycling/repairing technique. The hydrolyzed PBS grades presented a significant increase in the defined IV, with the fossil-based reaching the value of the initial material and the bio-based a 27% increase. The prepolymers' thermal properties were also upgraded with a ΔT_m of almost 8°C and ΔT_d of 9°C , returning to the relevant value of the initial material. A slight decrease in the crystallinity of the post-polymerized samples was monitored and attributed to the short SSP time, which was inadequate for reorganizing the polymeric chains into thicker crystalline domains. However, longer SSP times further improved the crystallinity values, reaching up to 90%.

Jbilou *et al.* [127] also applied SSP on PBS and monitored it using a fluorescent probe: 9-2-carboxy-2-cyanovinyljulolidine or CCVJ. CCVJ is a molecular rotor incorporated in the PBS bulk (100 ppm) for fluorescent labeling. Different commercial and synthesized PBS grades with different MW were used; the commercial grade presented \overline{M}_n and \overline{M}_w of 36000 and 136000 $\text{g}\cdot\text{mol}^{-1}$, respectively, while the synthesized grades were in the ranges 5600-44000 $\text{g}\cdot\text{mol}^{-1}$ \overline{M}_n and \overline{M}_w 9100-72000 $\text{g}\cdot\text{mol}^{-1}$. Single- and two-step SSP processes were examined. After the single-stage SSP, conducted at 110°C for 24 h, the PBS grades presented $\Delta\overline{M}_w$ increases of up to 22%, while a slight increase in the prepolymers T_m of almost 4°C was monitored,

accompanied by a significant increase in the crystallinity (from 58 to 96 %). When the PBS-labeled grades were submitted to a two-step SSP (1st step: 5 h at 113°C, 2nd step: 24 h at 118°C), a MW increase of 2.75-4.2 times was monitored. The melting points increased with SSP time, displaying a fast initial increase followed by a slower rise, probably within DSC errors (Figure 11). In particular, T_m increased linearly with SSP time within the first 7 h, reaching values above 121°C. This was attributed to the linear increase of the spherulite radius over time at a fixed temperature. After 7 h of SSP, the melting point increase rate was significantly reduced, obviously due to the performed MW build-up, which restrains the perfecting/thickening of the crystals (more entanglements at the expense of chain foldings).

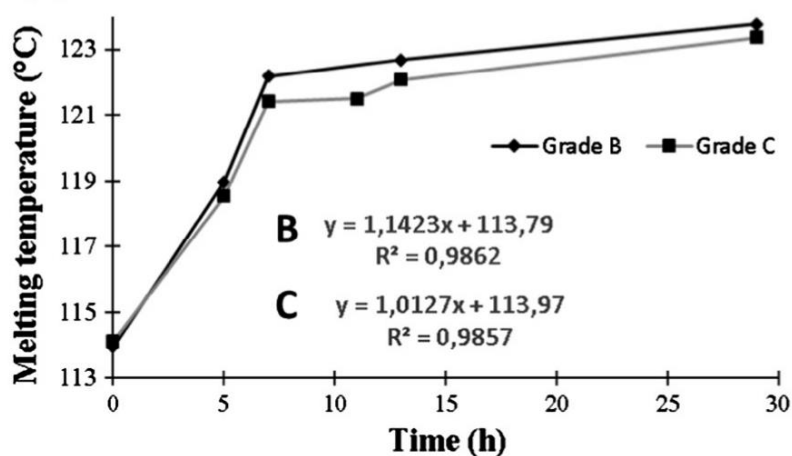


Figure 11. Melting point change of different PBS grades in the course of SSP [127]

1.2.2.3 PBF Solid State Polymerization

Even though the SSP of poly(ethylene furanoate) has been examined to an extent in the open literature [128–130], the SSP of poly(butylene 2,5-furandicarboxylate) is almost absent with only one relevant work dealing with the SSP of PBF.

PEF seems susceptible to SSP, as significant MW and IV increases have been reported in the open literature. Knoop *et al.* [131] showed that after 72 h of SSP, the molecular weight of PEF presented a ten-fold increase, while Hong *et al.* [132] applied SSP for 48 h, and the initial intrinsic viscosity of PEF 0.6 dL·g⁻¹ reached 0.72 dL·g⁻¹. In addition, the Bikiaris research group has thoroughly investigated the effect of different nano inclusions [130] and different catalysts on the molecular weight of the polyester [128,129,133], the effect of which has also been studied by other research groups [134,135].

Papadopoulos *et al.* [136] synthesized PBF with the conventional two-step melt polycondensation (in the presence of tetrabutyl titanate(IV) (TBT) as catalyst), followed by solid-state polycondensation conducted at different temperatures and times. The procedure of solid-state polymerization took place in an apparatus containing four test tubes, connected to a vacuum line and submersed in a thermostated salts bath. 3 g of milled polymer were placed in a glass tube under vacuum (3–4 Pa). The reaction was carried out at a constant temperature of

155, 160 or 165°C, and the tubes were removed from the bath after 1, 2, 3 and 4 h. Given the amorphous character of the synthesized PBF, before the SSP process, it was annealed overnight at 100°C to increase crystallinity and remove any water that could interfere with SSP.

The first parameter to be examined was the IV, and it was concluded that increasing the reaction temperature the IV increase is favored since both transesterification and esterification are accelerated (Figure 12). These reactions are regulated by the diffusion of the respective glycol and water, and as the SSP temperature decreases, the diffusion of the glycol becomes slower. This explains the slow increase of IV at 155 and 160°C. At 165°C a rapid rise of the intrinsic viscosity values was observed during the first two hours, attributed to enhanced mobility of the macromolecular chains of PBF, resulting in an increased reactivity of the hydroxyl and carboxyl end-groups, and, thus, higher molecular weights.

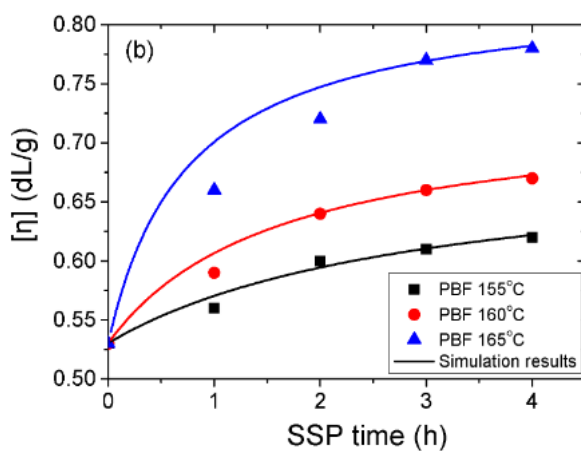


Figure 12. Evolution of the intrinsic viscosity (IV) with time during SSP of PBF at different temperatures. The continuous line represents simulation results [136]

Another factor studied was the concentration of carboxyl end-groups, which decreased with time and increased temperature. The evolution of the carboxyl end-group concentration, however, depends essentially on time: there is a continuous downward trend with increasing time, whereas the variation is less significant when increasing the temperature.

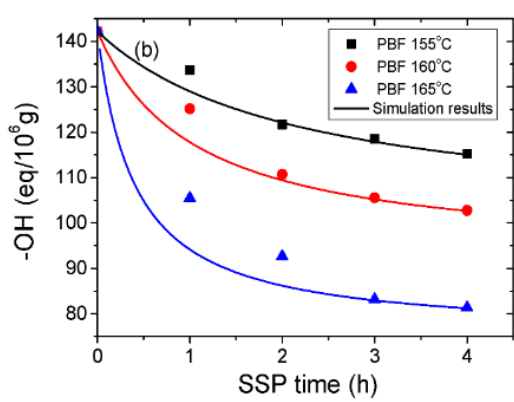


Figure 13. Evolution of hydroxyl (-OH) end-groups concentration with time during SSP at different temperatures. The continuous line represents simulation results [136]

The hydroxyl end group concentrations were also studied regarding the reaction temperature and time during SSP. In agreement with the IV monitored trend, there is a rapid reduction in the calculated hydroxyl end-group concentration during the first 2 h, which becomes slower afterward (Figure 13).

Regarding the SSP products' thermal properties, both melting temperature and crystallinity reached higher values with increasing SSP time and temperature following the molecular weight increase (Figure 14). Except for PBF, poly(propylene furanoate) (PPF) was also synthesized and submitted to the identical SSP processes. Interestingly, PBF reached a higher crystallinity degree than PPF (44.8 and 41.5, respectively), even though the starting degree of crystallinity was lower for PBF (28.7 and 32.4 % for PBF and PPF, respectively). The researchers thus confirmed that SSP takes place in the amorphous regions of the polymer. As crystallinity greatly influences the diffusion rate and the mobility of the polymer chain end-groups, which are located in the amorphous phase of semi-crystalline polyesters, it was stated that the rapid increase in molecular weight of PBF was linked to its lower degree of crystallinity. The unwanted byproducts were removed more easily, thus, the molecular weight increased faster.

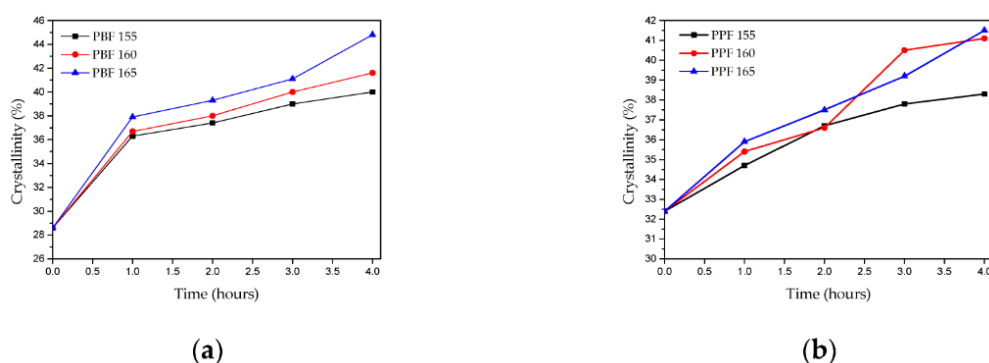


Figure 14. Evolution of the crystallinity degree with time and temperature of SSP for (a) PBF and (b) PPF [136].

1.3 Introduction to polymeric encapsulation systems

1.3.1 Introduction to nanoparticles: nanospheres and nanocapsules

Nanoparticles (NPs) are dispersions or solid particles with sizes typically ranging from 10 to 100 nm and sometimes up to 1000 nm [137–141]. The impact of the nanoscale on materials and systems is often related to the surface-to-volume ratio, which leads to increased surface activity. Nanomaterials present unique physical and chemical characteristics such as diffusivity, strength, solubility, chemical, mechanical and kinetic stability and lower density [142]. Overall, nanomaterials represent a powerful interdisciplinary tool for developing innovative products.

Nanoparticles for bioactive compounds are continuously evolving and find applications in various fields. Their primary role is to protect the encapsulated compound from the environment and, consequently, degradation while simultaneously modifying the

physicochemical characteristics of the entire system. Drug delivery systems play a crucial role in the pharmacological action of the molecule, as they can influence its pharmacokinetics, the drug release rate, the region and duration of its action and thus its side effects. The different metal nanoparticles and other nano-size materials that have been introduced as drug delivery systems and diagnostics are presented in Figure 15 [143].

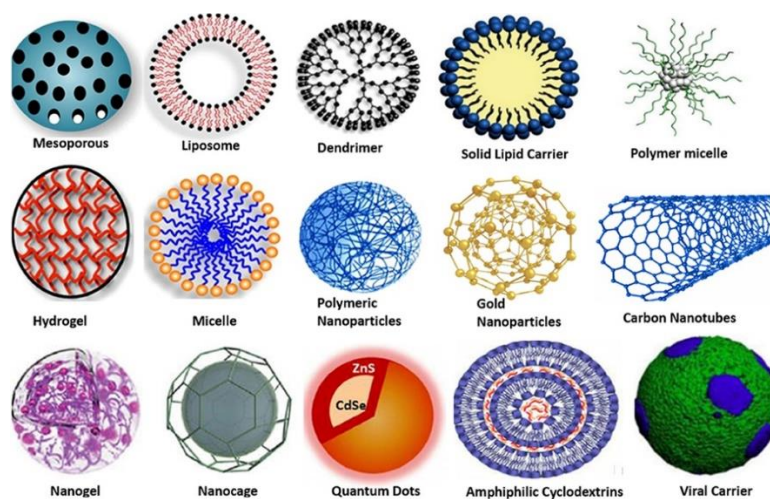


Figure 15. Different types of nanocarriers (nanoparticles) serve as drug delivery [143].

Among the different types of nanocarriers, polymeric nanoparticles (NPs) have attracted the scientific community's interest in recent years due to their promising properties. They can be derived from either synthetic polymers (such as poly(lactic acid), poly(glycolic acid), poly(lactic-co-glycolic acid), poly(ϵ -caprolactone)) or natural polymers (such as collagen, chitin, chitosan, keratin, silk, elastin, starch, cellulose, pectin, etc) [144].

Polymeric NPs can maintain high stability in systemic circulation with an enhanced half-life, which can be further optimized by controlling the release of therapeutic agents from the NPs. Moreover, polymeric molecules have various solubility profiles in various solvents. This is advantageous for surface modification or functionalization to achieve different purposes of delivery and targeting. Subsequently, both doses and frequency of administration of therapeutic agents can be reduced due to high payloads into nanocarriers, leading to superior efficacy and minimizing the side effects. Besides, polymeric NPs of desired physicochemical properties can preserve their content from hepatic metabolism and enzymatic degradation [145].

It is useful at this point to note that the term nanoparticle is a collective name for both nanospheres and nanocapsules. Nanospheres have a matrix type of structure (Figure 16). Drugs may be absorbed at the sphere surface or encapsulated within the particle. Nanocapsules are vesicular systems in which the drug is confined to a cavity consisting of an inner liquid core surrounded by a polymeric membrane. In this case, the active substances are usually dissolved in the inner core but may also be adsorbed to the capsule surface [139].

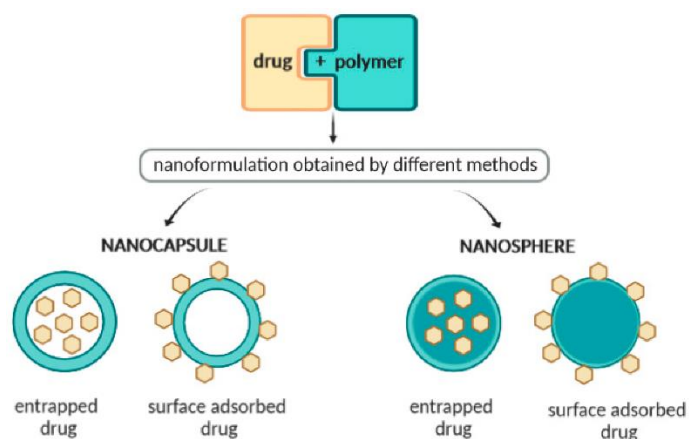


Figure 16. Different possibilities of the drug association with nanospheres and nanocapsules [146].

1.3.2 Nanoparticles production methods

To receive NPs in the desired form, the appropriate production method has to be selected. Emulsification-solvent evaporation was the first method developed to prepare polymeric NPs from a preformed polymer (Figure 17). It is one of the most popular methods thanks to its easiness [147] and the one selected in this work to form enzymatically synthesized PBS nanoparticles. In this method, the preparation of an oil-in-water (o/w) emulsion is initially required, leading to nanospheres production. Firstly, an organic phase is prepared, consisting of a polar organic solvent in which the polymer is dissolved, and the active ingredient (e.g., drug) is included by dissolution or dispersion. Dichloromethane and chloroform are the most commonly selected solvents, which, however, due to their toxicity, recently have been replaced by ethyl acetate [36], presenting a better toxicological profile and, therefore, being more suitable for biomedical applications. An aqueous phase containing a surfactant (e.g., polyvinyl alcohol; PVA) has also been prepared frequently. The organic solution is emulsified in the aqueous phase with a surfactant, and then it is typically processed by using high-speed homogenization or ultrasonication, yielding a dispersion of nanodroplets. A suspension of NPs is formed by evaporation of the polymer solvent, which is allowed to diffuse through the continuous phase of the emulsion. The solvent is evaporated either by continuous magnetic stirring at room temperature (in case of more polar solvents) or in a slow process of reduced pressure (as happens when using e.g., dichloromethane and chloroform). After the solvent has evaporated, the solidified nanoparticles can be washed and collected by centrifugation, followed by freeze-drying for long-term storage. This method leads to the formation of nanospheres [146].

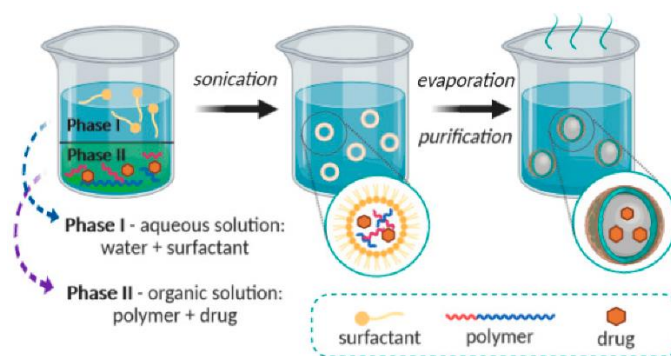


Figure 17. Schematic representation of the solvent evaporation method [146].

Another method leading to nanospheres is the emulsification/solvent diffusion method (Figure 18). This method forms an o/w emulsion between a partially water-miscible solvent containing polymer and drug and an aqueous solution with a surfactant. The internal phase of this emulsion consists of a partially hydro-miscible organic solvent, such as benzyl alcohol or ethyl acetate, which is previously saturated with water to ensure an initial thermodynamic balance of both phases at room temperature. The subsequent dilution with a large amount of water induces solvent diffusion from the dispersed droplets into the external phase, forming colloidal particles. Generally, this method produces nanospheres, but nanocapsules can also be obtained if a small amount of oil (such as triglycerides: C6, C8, C10, C12) is added to the organic phase. Finally, depending on the boiling point of the organic solvent, this latter stage can be eliminated by evaporation or filtration. In the end, obtaining NPs with dimensions ranging from 80 to 900 nm is possible. This method is frequently applied for polymeric NPs production despite the requirement of a high volume of the aqueous phase, which must be eliminated from the colloidal dispersion, and despite the risk of diffusion of the hydrophilic drug into the aqueous phase [146,147].

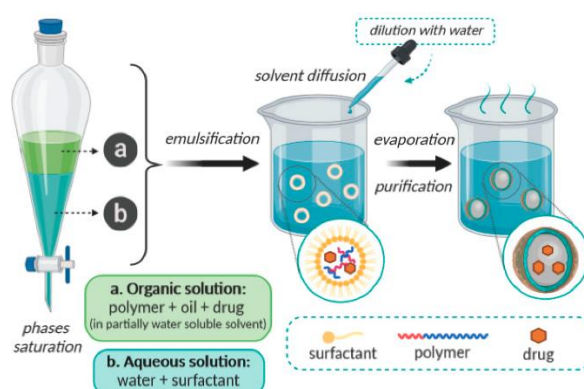


Figure 18. Schematic representation of the emulsification/solvent diffusion method [146].

The above-described emulsification/solvent diffusion method can be considered a modification of the emulsification/reverse salting-out method. The salting-out method separates a hydro-miscible solvent from an aqueous solution through a salting-out effect that may form nanospheres (Figure 19). The main difference is the composition of the o/w emulsion, formulated from a water-miscible polymer solvent, such as acetone or ethanol, and the aqueous phase contains a gel, the salting-out agent and a colloidal stabilizer. Examples of

suitable salting-out agents include electrolytes, such as magnesium chloride (MgCl_2), calcium chloride (CaCl_2) or magnesium acetate [$\text{Mg}(\text{CH}_3\text{COO})_2$], as well as non-electrolytes, e.g., sucrose. The miscibility of acetone and water is reduced by saturating the aqueous phase, which allows the formation of an o/w emulsion from the other miscible phases. The o/w emulsion is prepared under intense stirring at room temperature. Then, the emulsion is diluted using an appropriate volume of deionized water or an aqueous solution to allow the diffusion of the organic solvent to the external phase, the precipitation of the polymer, and, consequently, the formation of nanospheres. The remaining solvent and salting-out agent are eliminated by cross-flow filtration. The condition of complete miscibility between the organic solvent and water is not essential, but it simplifies the execution process. The dimensions of the nanospheres obtained by this method vary between 170 and 900 nm. The average size can be adjusted to values between 200 and 500 nm by varying the polymer concentration of the internal phase/volume of the external phase [146,148].

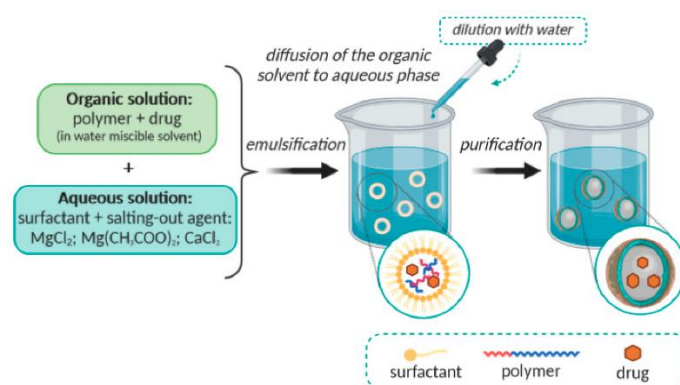


Figure 19. Schematic representation of the emulsification/reverse salting-out method [146].

Nanoprecipitation is also designated as a solvent displacement method, requiring two miscible solvents (Figure 20). The internal phase consists of a polymer dissolved in a miscible organic solvent, such as acetone or acetonitrile. Because of immiscibility in water, they can be easily removed by evaporation. The principle of this technique relies on the interfacial deposition of a polymer after the displacement of the organic solvent from a lipophilic solution to the aqueous phase. The polymer is dissolved in a water-miscible solvent of intermediate polarity, and this solution is added stepwise into an aqueous solution under stirring (in a dropwise way) or by controlled addition rate. Due to the fast spontaneous diffusion of the polymer solution into the aqueous phase, the nanoparticles form instantaneously to avoid the water molecules. As the solvent diffuses from the nanodroplets, the polymer precipitates in nanocapsules or nanospheres. Generally, the organic phase is added to the aqueous phase, but the protocol can also be reversed without compromising the nanoparticle formation. Usually, surfactants can be included in the process to guarantee the stability of the colloidal suspension, although their presence is not required to ensure the formation of nanoparticles. The obtained nanoparticles are typically characterized by a well-defined size and a narrow size distribution, better than those produced by the emulsification solvent evaporation procedure. Nanoprecipitation is a method frequently used to prepare polymeric NPs with around 170 nm dimensions, but it also allows the acquisition of nanospheres or nanocapsules. Nanospheres

are obtained when the active principle is dissolved or dispersed in the polymeric solution. Nanocapsules are obtained when the drug is previously dissolved in an oil, which is then emulsified in the organic polymeric solution before the internal phase is dispersed in the external phase of the emulsion [146,148].

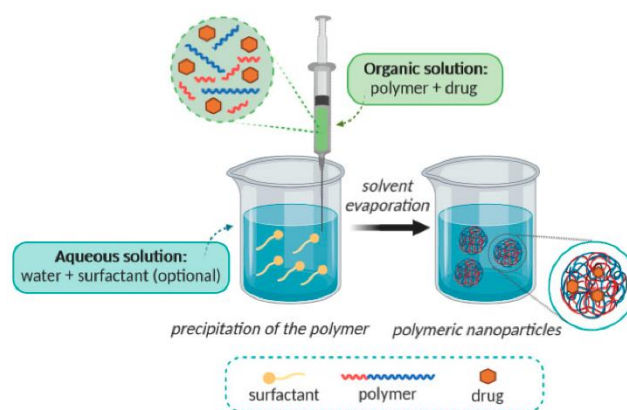


Figure 20. Schematic illustration of the nanoprecipitation method [146].

1.3.3 Nanoparticles applications

Nanoparticles are known to be used in the biomedicine and pharmaceutical sector. As effective drug delivery systems, different NPs have been used to treat diseases such as asthma, cancer, lung infections [149,150], and as transdermal delivery patches, designed to provide the controlled and sustained release of active substances to the systemic circulation after crossing the skin barrier, mostly by diffusion and resulting in a prolonged and adequately constant absorption [151] rate. Some of the most commonly selected polymers for NP applications include poly(lactic acid) (PLA), cellulose acetate phthalate (CAP), poly(ϵ -caprolactone) (PCL) and poly(D, L- lactide-co-glycolide) (PLGA)[139].

Except for the biomedical sector, nanoparticles, and especially polymeric nanoparticles, are promising candidates for the packaging sector too, as they can be used for the protection of nutraceutical ingredients from decomposition, bioactive transport, controlled release of analyte from coatings, unwanted taste masking, and as smart packaging of food materials.

It is important at this point to define the term smart packaging. Smart packaging is a broad term that describes new packaging concepts, most of which can be classified in one of two main categories: active or intelligent packaging (Figure 21). An active package is the one that modifies the condition of packaged foods to extend shelf-life or improve their safety or sensorial properties, keeping their quality. Sometimes this is achieved by the intrinsic properties of the polymer and others adding some specific additives in the packaging material or in the headspace in order to attain a better package yield [152,153]. In this sense, the European Community regulation defines active materials and components as those aimed at extending shelf-life or keeping or improving the condition of packaged foods, designed to deliberately incorporate components that release or absorb substances toward or from the

packaged foods and the environment surrounding the foods (Framework Regulation on Food Contact Materials 1935/2004 and 450/2009, 2020). Although bioactive packaging can also be considered in this category, they have another purpose that is to provoke a direct and positive impact on consumers' health through the generation of healthier packaged foods. On the other hand, an intelligent package as a packaging system capable of carrying out intelligent functions, such as detecting, registering, locating, communicating and applying scientific logics, in order to ease decision-making, extend shelf-life, improve safety and quality, provide information and warn of possible problems. The European Community Framework Regulation (Framework Regulation on Food Contact Materials 1935/2004 and 450/2009, 2020) acknowledges them as those materials and objects that control the state of packaged foods or the environment surrounding them. These systems, which are attached as labels or incorporated or printed on the food packaging material, offer better possibilities to check product quality, track critical items and provide more detailed information during the food supply chain (storage, transport, distribution and sale). They can also inform about product history such as storage conditions, composition of headspace, microbial growth, etc. Intelligent packages do not act directly to extend food shelf-life and do not aim at releasing their components onto the food, as active packaging does. Instead, intelligent packages have the aim to convey information related to food quality to manufacturers, retailers, and/or consumers. These definitions imply product-package-environment interactions. Thus, active packaging would be considered as an extension of the protection and preservation function of traditional food packaging, while intelligent ones can be considered as an extension of their communication and marketing function. So, smart packaging gives a total packaging solution: on the one hand, it monitors changes in the product or the environment (intelligent packaging), and on the other hand, it acts upon these changes (active packaging).

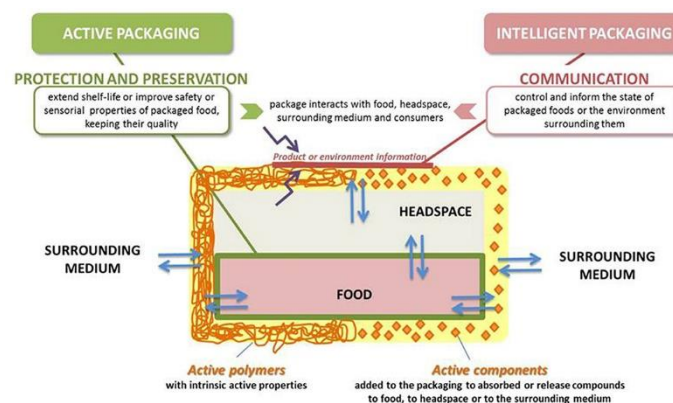


Figure 21. Schematic diagram of active and intelligent packaging concepts [154].

1.3.4 Advances in the active food packaging sector

When active agents are incorporated into the packaging material, coated on its surface, or also inside certain elements associated with the package, such as bags, labels, pads, bottle caps instead of being applied directly on foods, lower concentrations are achieved, thus limiting

undesired flavors and smells to foods [155]. These active compounds are added to release or absorb substances to/from the packaged food or its surrounding environment, or to make changes in food composition or organoleptic features as long as these changes adjust to current regulations. These active agents may migrate (partially or completely) through gradual diffusion into the food or headspace or act only when the food is in direct contact with the packaging [154].

Active agents incorporated into polymer matrices may include antimicrobials, antioxidants, moisture absorbers, oxygen, carbon dioxide (CO₂) and ethylene (C₂H₄) scavengers, carbon dioxide generators, flavor/smell capturers.

Among the above-mentioned active agents, it is worth focusing on the antioxidants, as lipid oxidation is the second cause of food spoilage after microbial growth. Foods with high lipid content, and especially those with a high unsaturation degree, such as nuts, vegetable and fish oils, meat and fishing products, are susceptible to oxidation. Lipid oxidation in food products results in the development of rancid smells, making the product unacceptable for human consumption. Other negative effects are aldehyde formation and nutritional quality loss produced by the degradation of polyunsaturated fatty acids. There are two main action methods for antioxidant packages: (i) the addition of antioxidant compounds or (ii) the elimination of undesired compounds that can accelerate oxidation reactions, such as O₂ [154].

Synthetic antioxidants, such as butylated hydroxytoluene (BHT) or butylated hydroxyanisole (BHA), have been added to PLA, gelatin, carrageenan, gum cordia and carboxymethyl cellulose films proving to effectively reduce lipid oxidation in several foods. However, the use of natural antioxidants like pure compounds (e.g., tocopherols, caffeic acid, chlorogenic acid, ferulic acid, rosmarinic acid, salvianolic acid, carnosic acid and ascorbic acid carvacrol, thymol, carnosol, quercetin, luteolin, apigenin, eriodictyol, catechin, rutin), plant and fruit extracts (e.g., rosemary, grape seed, green tea, oregano, murta, mint, marjoram, savory, and pomegranate peel), and essential oils or oleoresins from herbs and spices (e.g., cinnamon, lemongrass, clove, thyme, ginger, sage, oregano, pimento and bergamot) is currently preferred. Likewise, it is important to mention the potential use of extracts obtained from plant by-products like barley husks, pomegranate peel, olive leaves, as sources of antioxidant agents. The antioxidant properties of peptides obtained from diverse food proteins were also. Over the last years, several studies have been published dealing with addition of different antioxidant compounds to biodegradable and biobased polymers and their assessment in diverse food systems [154].

Acting as antioxidants, free-radical scavengers can donate hydrogen to reactive free radicals and convert them into (fairly) stable products unable to participate in initiation or propagation reactions. In addition to primary antioxidants, other additives like chelating agents, ultraviolet absorbers, singlet oxygen quenchers, and oxygen scavengers are also used to reduce the oxidation rate in active packaging. Metal pro-oxidants (e.g., iron or copper derivatives) could be converted into stable products using metal chelators such as ethylenediaminetetraacetic acid (EDTA), poly (acrylic acid), citric acid, and lactoferri). Some examples of UV absorbers are

lignin, naringin, boric acid, bixin, α -tocopherol, ellagic acid, natural extracts rich in phenolic compounds, and pigments like phtalocyanine and TiO_2 .

The adequate selection of the antioxidant compound to be incorporated in the polymeric matrix is very important and should be considered for each application. The antioxidant compound and polymer matrix should be compatible to achieve a homogeneous distribution, and the antioxidant partition coefficients in the different phases must that favor their release toward the food or headspace [154]. Once released, the antioxidant solubility features could determine its efficacy, so in turn the antioxidant must be selected depending on food type.

Interestingly, PBS has recently been used as a matrix for active agents, including antioxidants (Table 6). As discussed in Chapter 2.1, the tested active agents include quercetin, a natural polyphenolic antioxidant [156] and kesum, a new antimicrobial active agent [157]. In both cases, PBS films acted as food packaging materials (e.g., chicken fillet package). Solution casting was the selected method for active agent incorporation and film processing. PBS has also been processed by melt extrusion to disperse the active agent (melt mixing) and compression moulding at relatively low temperatures and short times to form the film [158]. Only in one research work PBS (homopolymer) has been used as a matrix for an encapsulation system in a tissue engineering application. The used method was the double emulsion/solvent evaporation, and the selected agents were a hydrophilic and a hydrophobic bioactive agent (i.e., bovine serum albumin (BSA) and all-trans retinoic acid (atRA), respectively) [159].

Table 6. Active agents incorporated in PBS matrices, incorporation methods and formulations

Reference	Active agent	Activity	Incorporation method	Formulation
[156]	Quercetin	Antioxidant	Solution casting	Film
[157]	Kesum	Antimicrobial	Solution casting	Film
[158]	CD-lim inclusion complex	antimicrobial	Extrusion (135°C, 3 min, 40 rpm)	Film (after compression moulding)
[159]	bovine serum albumin (BSA) and all-trans retinoic acid (atRA)	Cell differentiation agents	Double emulsion/solvent evaporation	Microcapsules

Considering the compatibility of PBS with different active agents, its potential to act as a matrix, along with its green character (biobased and biodegradable) and its approval as a food contact material, it seems that PBS emerges as a promising alternative for fossil-based polyolefins (mainly PP) to be used in the (active) food packaging sector.

1.4 Motivation

Nowadays, environmental concerns that were once theoretical are becoming more and more evident in our everyday lives. Plastic pollution is probably the major concern as it is known that plastics can take hundreds of years to decompose, leading to widespread pollution in the oceans, rivers and landfills. At the same time, they are typically derived from petroleum, which is a finite and non-renewable resource. It becomes thus clear that actions need to be taken to eliminate these phenomena affecting people and the planet's future.

Part of the problem could be addressed by using green materials. Green plastics, i.e., highly modified polymeric materials originating from renewable resources (bio-based) and presenting sustainable disposal options (e.g., biodegradable, compostable), are gaining increasing academic and industrial interest. However, the green properties of these materials are not enough to ensure their truly green character, as their conventional production process is conducted under hard conditions (i.e., usually temperatures higher than 200°C are applied), in the presence of metal catalysts, the residues of which are difficult to be totally removed from the final products. These requirements negatively affect not only the final products' properties (e.g., coloration, thermal instability) but also the environment and the people's health.

It is thus challenging to deal with the establishment of one (or more) method(s) aiming at sustainably synthesizing sustainable materials. Enzymatic polymerization was selected to be the heart of this research. The target polymers to be enzymatically synthesized were the aliphatic, bio-based and biodegradable poly(butylene succinate) and the alipharomatic, bio-based poly(butylene 2,5-furandicarboxylate), as representatives of their categories.

Considering the limitations of the enzymatic polymerization, i.e., the low molecular weights achieved, we decided to focus on the enzymatically synthesized prepolymers upgrade through sustainable methods conducted at relatively low temperatures, not requiring the use of solvents, such as solid-state (SSP) and melt post-polymerization.

To produce green and competitive materials, their capability to be used in applications should have been examined. In this context, this research would be completed with a case study using an enzymatically synthesized and upgraded polymeric material in some application (e.g., active food packaging).

1.5 Thesis outline

The present work aimed to synthesize and upgrade poly(butylene succinate) and poly(butylene 2,5-furandicarboxylate) *via* sustainable methods, i.e., enzymatic polymerization and solid-state or low-temperature melt post-polymerization.

In this context, the first chapter presented an overview of the advances in enzymatic polymerization of the most promising, aliphatic (PLA, PBS) and alipharomatic (furan-based) green polymers. Additionally, the main aspects of solid state polymerization (SSP) were

analyzed, focusing on its application on PBS and PBF. Finally, an introduction to the polymeric encapsulation systems was conducted with an emphasis on PBS.

In the second chapter, the enzymatic polymerization of PBS was examined using the commercially available, immobilized enzyme N435. The applied process was solventless, and the most critical parameters (i.e., reaction temperature, pressure, and reaction time) were investigated. Emphasis was put on scaling up the process to fill the relevant gap in the open literature.

In Chapter 3, the enzymatic polymerization of PBF was examined using N435, similar to the second chapter. The most critical process parameters (i.e., reaction temperature, pressure and reaction time) were investigated, and the process potential of scaling up was studied.

The next Chapter examined a novel, non-commercially available enzyme, LCC^{ICCG}, on the PBS synthesis. It is of high interest that this enzyme is known for its plastic-degrading activity, and to the best of our knowledge, it has never been used as a biocatalyst for polymer synthesis.

After completing the prepolymers enzymatic prepolymerization investigation, the synthesized prepolymers were submitted to post-polymerization, and the results are presented in Chapter 5. PBS was used as a model-prepolymer and submitted to solid-state and low-temperature post-polymerization; the critical parameters (reaction temperature and time) were investigated. PBF was also submitted to low-temperature melt-post polymerization to study its susceptibility to the process.

Chapter 6 examined the enzymatically synthesized and upgraded PBS as a carrier in controlled release systems. As analyzed in Chapter 6, PBS nanoparticles were formed, and the naturally occurring antioxidant flavonoid, naringin, was selected as a model-bioactive agent to be encapsulated. Preliminary *in vitro* release tests were conducted to monitor the system's release rate, considering the matrix's relatively low molecular weight.

In the last chapter, the general conclusions of this research were presented, along with several suggestions for future work.

2.1 Introduction

PBS is a semicrystalline, thermoplastic polyester presenting glass transition temperature of -30°C, melting point of 114°C, thermal stability up to 220°C and decomposition temperature above 390°C. Thanks to its thermal properties and structure, PBS presents increased flexibility and satisfactory processability, being thus appropriate for film applications, e.g., in biomedicine and the food packaging sector [32,49,160,161].

As regards biomedical applications, PBS-based polymers are emerging as candidate biomaterials since they possess interesting physical properties, such as high crystallization ability with mass fraction crystallinity (x_c) in the range of 65–71% [162], tailored surface wettability (water contact angle = 25–117°) [162–165] as well as mechanical properties that can be properly tuned influencing material biodegradation rate and biocompatibility. PBS can be used in bone tissue engineering and has been found superior to PLA regarding human mesenchymal stem cell attachment, proliferation and osteogenesis [166]. Furthermore, except for the satisfactory processability, PBS excellent hydrolytic degradability and hydrophilicity, render it an alternative candidate novel biomaterial also for soft tissue repair [163]. Regarding the packaging sector, according to the European Commission, packaging waste increased by more than 20% over the last ten years and is forecast to soar by another 19% by 2023 [167]. PBS emerges as a promising alternative for polyolefins (mainly PP), considering its green character (bio-based and biodegradable) and its approval as a food contact material [168]. PBS has recently been introduced in the active food packaging sector too. PBS films modified with quercetin, a natural polyphenolic antioxidant, have been tested as antimicrobial and antioxidant food packaging materials [156], while PBS films filled with kesum, a new antimicrobial active agent, have been submitted to *in vivo* direct food contact analysis in a chicken fillet package [157]. In these studies, the incorporation of active agents and film formation was achieved *via* solution casting method. PBS has also been submitted to melt extrusion and compression moulding at relatively low temperatures and short times in a work aiming at preparing bioactive packaging films [158]. More precisely, melt extrusion was conducted in a twin screw extruder under mild conditions (135°C, for 3 min, 40 rpm) to disperse the active agent CD-lim inclusion complex in a PBS matrix (melt mixing). CD-lim inclusion complex consists of limonene, a volatile essential oil with antimicrobial properties, encapsulated in β -cyclodextrins (β -CD) to protect limonene from oxidative degradation. The composite was placed in a compression moulding press at 130°C, thus forming packaging films.

All the abovementioned PBS grades were commercial or synthesized in labs, using chemical catalysts with all the relevant drawbacks discussed in Chapter 1.1. Especially when it comes to the packaging sector, where according to the compostable and biodegradable polymers

packaging standards, heavy metals should not exceed the maximum allowable level of 150 mg kg⁻¹ (i.e., 150 ppm) on dry substance [20], the conventional PBS production process becomes problematic, given that heavy metals catalysts in metal amounts between 100 and 1500 ppm (e.g., Ti 100-360 ppm, Sb 350-450 ppm, and Sn 450-1500 ppm) are required.

An alternative approach to producing high molecular PBS is the combination of polycondensation with a finishing step of chain extension [169]. A chain extender with two functional groups reacts with the terminal –OH or –COOH of PBS and couples two PBS chains. However, the biosafety and biodegradability of PBS can be negatively affected and, thus, impair the use of the chain-extended PBS as a food-contacting material [161].

The most common methods to remove metal-based catalyst residues from polymers, especially when destined for food packaging applications, include solvent extraction and leaching. However, these methods require several steps and many organic solvents and acids. Modern approaches that have been found effective, such as using a high-pressure CO₂/water binary system as a green solvent to dissolve and remove zinc-based catalysts from polymers, present high operation costs and need to be further optimized [20].

On the other hand, enzymatically synthesized PBS grades with a wide range of MW, from oligomers (\overline{M}_n 800 g·mol⁻¹) [33] to high molecular weight grades (\overline{M}_n 81000 g·mol⁻¹) [85], have been reported in the open literature (Chapter 1.1.1). The by-product removal, strongly affecting the reaction equilibrium, has been indicated as one of the most crucial parameters of the process. In this context, high-boiling point diphenyl ether is the most commonly used solvent, permitting the application of a high vacuum to remove polycondensation by-products. However, using various solvents (e.g., diphenyl ether for solution polymerization, chloroform for filtration, methanol for precipitation) impedes the enzymatic polymerization processes' scaling up [102]. Additionally, the requirement of high vacuum (i.e., 10 mmHg) [89] and temperatures (>90°C) [85,87] for prolonged reaction times leads to increased MW but increases the operating costs and energy consumption, thus opposing the green chemistry principles. An alternative approach, permitting the process scale-up, has been suggested by our group and included using low-boiling point solvents (e.g., isooctane), which are easy to remove from the system. At the same time, mild conditions were applied (40–60°C, atmospheric pressure), but the achieved molecular weights and melting points were low (\overline{M}_w 2000 g·mol⁻¹ and T_m 78°C [49]). In a recent paper, PBS enzymatic polymerization was conducted in a solventless system, favoring scaling-up, at a "pre-melting" temperature (i.e., 90°C), and the achieved MW reached the values of 1500 and 4000 g·mol⁻¹ (\overline{M}_n and \overline{M}_w , respectively) [95]. The main drawbacks of this process, probably hindering a significant MW build-up, are the co-existence of melted and solid oligomers' chains impeding the uniform mixing of the reacting mass and the possible monomers' loss before esterification at 90°C considering also the applied high vacuum (0.1 atm).

Summing up, it seems that the main disadvantage of all the published works is their non-scalability, attributed to the requirement of various solvents and/or the very high vacuum, even

for the small scales, considering that mass transfer limitations (e.g., higher by-product removal rate could be required) are expected to be more intense on large scales. In addition, the requirement of high vacuum and temperatures for prolonged reaction times reduces the environmental friendliness of the enzymatic polymerization. Thus, it can be concluded that there's a need to synthesize enzymatically a PBS grade in larger quantities, always in line with green chemistry, thus increasing not only the research but also its industrial interest.

2.2 Scope

The main objective of this chapter was to optimally synthesize PBS in a scalable enzymatic polymerization process, in line with the green chemistry guidelines. On that basis, the process was selected to be solvent-free and conducted under mild conditions.

In the first part of the chapter, the most critical parameters of the process, including reaction temperature, pressure, and time, were thoroughly studied on a small scale of 1 g of the final prepolymer. The prepolymers' molecular weight, thermal properties, and morphology were assessed for every process parameter.

Based on the optimized conditions, two consecutive scaling-up attempts followed in the second part of the chapter. The first was to receive 10 g, and the second 20 g of the final product. The scope of this study was to investigate the effect of the relative scaling up on the prepolymer's properties.

In the last part of this chapter, the effect of the monomers' ratio was investigated. Since OH-rich prepolymers are expected to present increased susceptibility to post-polymerization (see Chapter 5), different molar BDO excesses from 5 to 20% were examined based on the relevant data of the literature.

2.3 Experimental

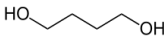
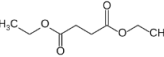
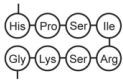

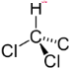
2.3.1 Materials

The monomers used for PBS synthesis were diethyl succinate or DES ($C_8H_{14}O_4$, purity 98%) and 1,4-butanediol or BDO ($C_4H_{10}O_2$, purity 99%), both purchased from Alfa Aesar, Germany (Table 7). Both monomers were in the form of liquids under room temperature (RT) conditions.

It is worth noting that BDO and succinic acid (SA), used for DES production, can be fossil-based or bio-based (e.g. when produced by fermentation [170]). Bio-SA is already produced on an industrial scale by companies such as Succinity GmbH (a joint between Corbion Purac and BASF), Reverdia, BioAmber and Myriant. Bio-BDO can be produced on an industrial scale indirectly through bio-SA hydrogenation [171] or directly from carbohydrate feedstocks using *Escherichia coli* strains [90].

The used biocatalyst was the commercial product Novozym®435 (N435), supplied by Novozymes, Denmark. N435 is the immobilized *Candida antarctica* Lipase B (CALB), which is physically absorbed within the macroporous resin Lewatit VPOC 1600. The enzyme's activity is 10.000 PLU·g⁻¹, and its optimum temperature is 30–60°C. N435 presents increased specificity with esters and alcohols as substrates. Thus, PBS is herein synthesized *via* transesterification of DES and BDO, even though the conventional synthesis (in the presence of chemical catalysts) typically begins with the esterification of SA and BDO. Chloroform (HPLC grade, purity ≥ 99.8%) was purchased from Fisher Scientific (U.K.). All chemicals were used without further purification.

Table 7. Compounds used for the prepolymerization of PBS

Compound	Molecular Formula	Structure	MW (g·mol ⁻¹)	Other characteristics	Supplier
BDO	C ₄ H ₁₀ O ₂		90.12	Purity 99%	Alfa Aesar, Germany
DES	C ₈ H ₁₄ O ₄		174.19	Purity 98%	Alfa Aesar, Germany
N435			33 kDa [172]	Activity 10000 PLU·g ⁻¹	Novozymes, Denmark
Chloroform	CHCl ₃		119.38	Purity ≥99,8%	Fisher Scientific, U.K.

2.3.1.1 Assay of the immobilized *Candida antarctica* Lipase (B) activity experimental procedure

The activity of the lipase N435 assay was conducted at the Biotechnology Laboratory by the Industrial Biotechnology & Biocatalysis group (NTUA). The protocol followed is described below.

For the esterolytic activity determination, *p*-nitrophenyl butyrate (*p*NPB) was used as a substrate. The esterolytic activity of the biocatalyst was assessed through reactions with *p*NPB at 35°C for 35 min under agitation (1400 rpm), in an Eppendorf Thermomixer Comfort (Eppendorf, Germany). Reactions consisted of 1 mL substrate solution containing 1.0 mM of the substrate in 0.1 M citrate-phosphate pH 6.0, buffer, and 1 mg of biocatalyst. The release of *p*-nitrophenol (*p*NP) was monitored at 410 nm, in a SpectraMax-250 microplate reader (Molecular Devices, Sunnyvale, CA, USA), connected with the SoftMaxPro software (version 1.1, Molecular Devices, Sunnyvale, CA, USA).

To calculate the biocatalyst activity, the enzyme (protein) loading onto the support must be known. Based on the open literature, the loading of the CALB on the Lewatit support ranges between 8.5 and 20% wt [173,174], while in some works, it is reported as 10% wt [36,175]. Considering that the ratio range is wide, the biocatalyst activity was calculated for the boundary concentrations of 8.5 and 20%, as well as for the reported ratio of 10% wt and the results are presented in Table 8.

Table 8. Calculated activity values of N435, based on the different protein contents

Loading ($W_{\text{protein}}/W_{\text{carrier}}$, %)	Activity (Units·mg ⁻¹)	Standard deviation (Units·mg ⁻¹)	Relative Standard Deviation (RSD, %)
8.5	$1.63 \cdot 10^{-2}$	$9.38 \cdot 10^{-4}$	6
10	$1.39 \cdot 10^{-2}$	$7.98 \cdot 10^{-4}$	6
20	$6.94 \cdot 10^{-3}$	$3.99 \cdot 10^{-4}$	6
	* $1.24 \cdot 10^{-2}$	* $7.12 \cdot 10^{-4}$	6

*Mean value

Based on the assay results, the N435 activity ranges between $6.94 \cdot 10^{-3}$ and $1.63 \cdot 10^{-2}$, i.e., by an order of magnitude. The measurement is considered reliable given the relatively low RSD of 6%, and an estimation of the mean value is $1.24 \cdot 10^{-2} \pm 7.12 \cdot 10^{-4}$ Units·mg⁻¹.

2.3.2 Enzymatic prepolymerization experimental procedure for poly(butylene succinate) production

Stoichiometric amounts of DES (6 mmol, 1.04 g) and BDO (6 mmol, 0.54 g) were premixed in a round-bottom flask and stirred (75 rpm) at 40°C in a rotary evaporator (Rotavapor R-210, Buchi, Switzerland) under atmospheric pressure. 10% wt N435 (relative to monomers) was subsequently added, and a two-step prepolymerization process was applied. The first step was conducted at 40°C, under atmospheric pressure for 24 h to minimize BDO losses through limited transesterification reactions. Then, the temperature increased, and vacuum was applied. At the end of the reaction, chloroform was added (4:1 wt relative to monomers) to dissolve the formed polyester and the enzyme was subsequently filtered off. The remaining chloroform was evaporated in a high-vacuum pump (Edwards RV5 Rotary Vane Pump, Edwards, U. K.) and the formed polyester (w_{exp}) in the form of a colorless, free-flowing powder was stored in a desiccator. The process yield (%) was calculated by Eq. (1):

$$\text{Process yield (\%)} = \frac{w_{\text{exp}}}{w_{\text{theor}}} \cdot 100 \quad (1)$$

where w_{exp} is the experimental amount of the product (g), and w_{theor} the theoretical weight of the product predicted by stoichiometric calculations (g).

The variation of enzymatic prepolymerization conditions resulted in three sets of prepolymers (Table 9): samples A (reaction temperature, 80–95°C), samples B (reduced pressure value, 200 and 20 mbar), samples C (reaction time, 2 and 6 h). The sample B-90 was scaled up to prepare adequate amounts (ca. 10 and 20 g) for the following post-polymerization attempts (Chapter 5).

Table 9. Conditions of PBS enzymatic prepolymerization

Sample	1 st step			2 nd step			Process yield (%)
	T (°C)	P (mbar)	t (h)	T (°C)	P (mbar)	t (h)	
A-80	40	1000	24	80	200	2	56
A-85	40	1000	24	85	200	2	84
A-90	40	1000	24	90	200	2	75
A-95	40	1000	24	95	200	2	91
B-90 ¹	40	1000	24	90	20	2	81
B-95	40	1000	24	95	20	2	70
C-90	40	1000	24	90	20	6	83
C-95	40	1000	24	95	200	6	94

¹B-90_10g, B-90_20g: scaled-up prepolymers (10 and 20g) with process yields 95 and 96%, respectively and B-90_20g_5%, B-90_20g_10%, B-90_20g_20%: prepolymers synthesized using BDO excess (5, 10 and 20%) with process yields 99, 99 and 100% respectively.

2.3.3 Characterization techniques

2.3.3.1 ¹H-NMR Spectroscopy

¹H-NMR spectroscopy was performed in CDCl₃ on a Bruker DRX 400 spectrometer, equipped with a 5 mm ¹H/¹³C dual inverse broad probe operating at 400 MHz to verify the structure of the formed polyesters. The number-average molecular weight (\overline{M}_n , g·mol⁻¹) and number-average degree of polymerization (\overline{x}_n) were also calculated by Eqs. (2) and (3) respectively [176]

$$\overline{M}_n = \frac{I_a - I_d - \frac{2}{3}I_e \cdot 88.10 + \frac{I_c}{4} \cdot 84.07 + \frac{I_d}{2} \cdot 89.11 + \frac{I_e}{3} \cdot 45.06}{0.5 \cdot \left(\frac{I_d}{2} + \frac{I_e}{3}\right)} \quad (2)$$

where 88.10 is the molar mass (g·mol⁻¹) of 1,4-butyl segments, 84.07 is the molar mass (g·mol⁻¹) of succinate segments, 89.11 is the molar mass (g·mol⁻¹) of 1,4-BDO end-groups, 45.06 is the molar mass (g·mol⁻¹) of ester end-groups and I_a is the integral of the 1,4-butyl segment signal at 4.12 ppm, I_c is the integral of the succinate segment signal at 2.62 ppm, I_d is the integral of the BDO end-group signal at 3.67 ppm and I_e is the integral of the ester end-group signal at 1.25 ppm.

$$\overline{x}_n = 2 \cdot \frac{\overline{M}_n}{m_0} \quad (3)$$

where m_0 is the molecular weight of the repeating PBS unit (172 g·mol⁻¹).

The percentage of the ester-end group in respect to the total number of prepolymer ends was calculated by Eq. (4):

$$\text{ester end groups percentage (\%)} = \frac{\frac{I_e}{3}}{\frac{I_e}{3} + \frac{I_d}{2}} \cdot 100 \quad (4)$$

2.3.3.2 Fourier Transform Infrared Spectroscopy (FTIR)

FTIR was performed on an Alpha II (Alpha II, Bruker, Germany) using the ATR method with a diamond crystal in the range of 400 to 4000 cm^{-1} wavenumber region and a resolution 4 cm^{-1} (Figure 22). The prepolymers' being in the form of powder, were submitted to the FTIR analysis without prior processing.



Figure 22. Spectrometer Platinum-ATR ALFA II Bruker

2.3.3.3 Gel Permeation Chromatography (GPC)

GPC was carried out with the use of Agilent 1260 Infinity II instrument (Agilent Technologies, Germany), equipped with a guard column (PLgel 5 μm) and two PLgel MIXED-D 5 μm columns (Figure 23). Elution was carried out with chloroform ($\geq 99.8\%$ purity, Fisher Scientific, U.K.) at a flow rate of 1 $\text{mL}\cdot\text{min}^{-1}$. The analysis was performed using an Agilent 1260 Infinity II refractive index detector (RID) (G7162A). The calibration of the instrument was carried out with polystyrene standards of molecular weight from 162 to 500000 $\text{g}\cdot\text{mol}^{-1}$ (EasiVial PS-M 2 mL, Great Britain) and a universal calibration curve was constructed.



Figure 23. Agilent 1260 Infinity II instrument

2.3.3.4 Differential Scanning Calorimetry (DSC)

Differential scanning calorimetry (DSC) measurements were performed in a Mettler DSC 1 STARe System (Figure 24). Heating – cooling – heating cycles from 30 to 150°C, cooling to –10°C and finally heating to 150°C were conducted. All measurements were conducted under N₂ flow (20 mL·min⁻¹), with a rate of 10°C·min⁻¹. The melting points derived from the first and second heating cycle are represented as T_{m1} and T_{m2} , and the relevant mass fraction crystallinity was computed from the cooling and the second heating DSC curves (x_c and x_{cf} %) according to Eq. (5a) and (5b). The melt crystallization point (T_c), as well as the crystallization enthalpy (ΔH_c , J·g⁻¹) were obtained from the DSC cooling cycle.

$$x_c(\%) = \frac{\Delta H_c}{\Delta H_0} \cdot 100 \quad (5a)$$

$$x_{cf}(\%) = \frac{\Delta H_f - \Delta H_{cc}}{\Delta H_0} \cdot 100 \quad (5b)$$

Where ΔH_f is the heat of fusion (J·g⁻¹), ΔH_{cc} is the cold crystallization enthalpy (J·g⁻¹), ΔH_0 is the heat of fusion of 100% crystalline PBS (J·g⁻¹) equal to 110.5 J·g⁻¹ [177].



Figure 24. Mettler DSC 1 STARe System

2.3.3.5 Thermogravimetric Analysis (TGA)

Thermogravimetric analysis (TGA) was conducted in a Mettler TGA/DSC 1 thermobalance (Figure 25) from 30 to 600°C, at a heating rate 10°C·min⁻¹ under N₂ flow (10 mL·min⁻¹). The onset decomposition temperature was defined as the temperature at 5% weight loss ($T_{d,5\%}$), the degradation temperature (T_d) was determined at the maximum rate of weight loss, and the char yield as the % residue at 600°C.

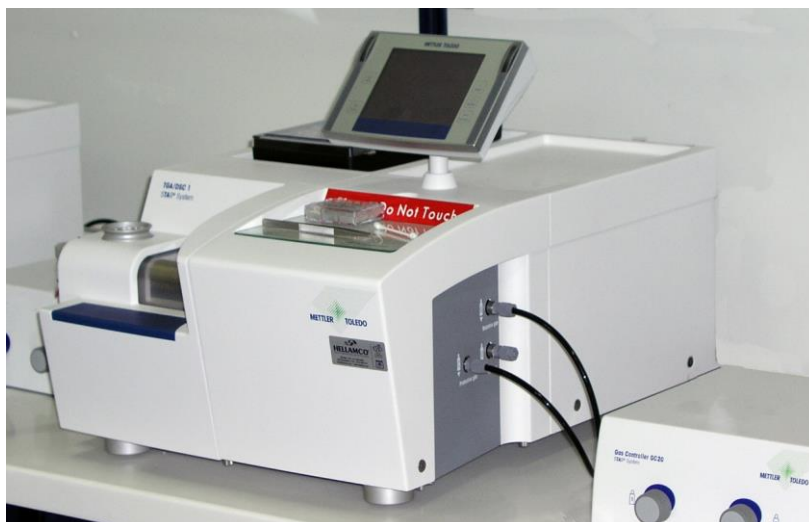


Figure 25. Mettler TGA 1 STARe System

2.4 Results

2.4.1 Study of the key parameters influence on the small-scale (1 g) PBS enzymatic prepolymerization

2.4.1.1 Investigation of the reaction temperature impact on the PBS enzymatic prepolymerization process

The enzymatic prepolymerization process was conducted in two steps to minimize the monomers' loss, especially due to the BDO's high volatility. The selected reaction temperature of the first stage was 40°C, based on previous studies of the group, where BDO and DES's enzymatic polycondensation was studied in solvent-based (low boiling point solvents, namely isooctane and toluene) and solvent-free systems at three reaction temperatures (40, 50 and 60°C) in the presence of N435 [49]. The bulk system was found more effective than the examined solvent-based systems; this is attributed to the fact that a polar solvent may deactivate the enzyme due to conformational changes and be responsible for releasing water bound to the enzyme leading to hydrolysis reactions. Thus, the PBS prepolymer synthesized in bulk at 40°C presented the highest \overline{M}_n (2800 g·mol⁻¹), probably indicating increased enzyme activity at this temperature.

The second stage's reaction temperature (80-95°C, samples A) was firstly investigated for the enzymatic polymerization of PBS. The relevant process yields were in the range of 56-91%, with the lowest and the highest value for 80°C and 95°C, respectively (Table 9). For all samples A, PBS repeating unit was verified *via* ¹H-NMR spectroscopy (Figure 26).

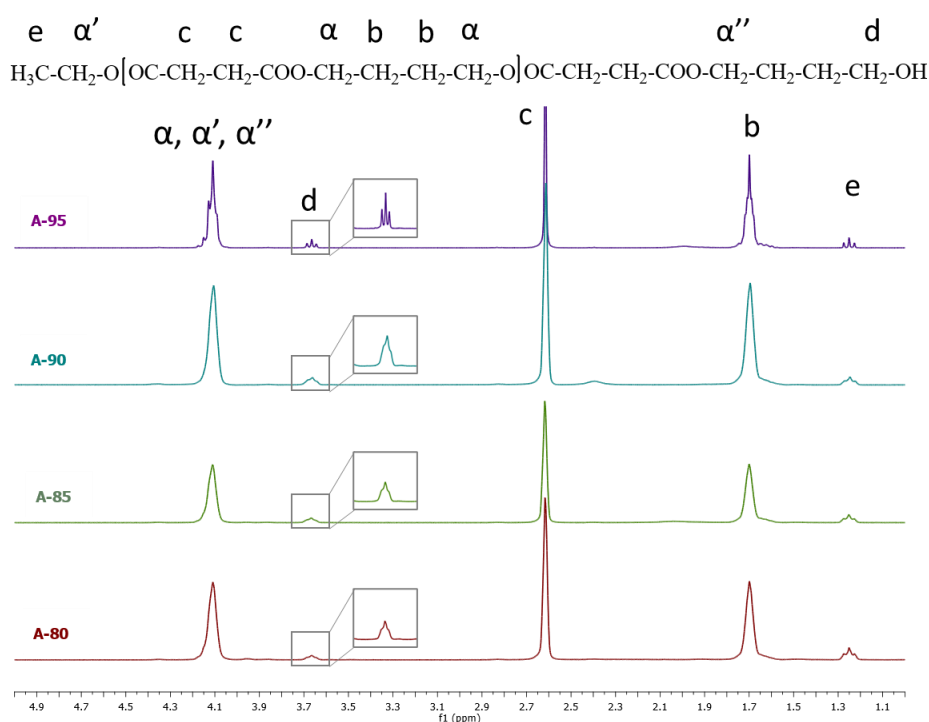


Figure 26. ^1H NMR spectra of the prepolymers A-80, A-85, A-90 and A-95

The determined shifts were: 4.11–4.18 ppm (4H, $-\text{O}-\text{CH}_2-\text{CH}_2-\text{CH}_2-\text{CH}_2-\text{O}-$ from the 1,4-butyl segment of BDO), 2.62 ppm (4H, $-\text{CO}-\text{CH}_2-\text{CH}_2-\text{CO}-$, from the succinate segment of DES), 1.65–1.75 ppm (4H, $\text{O}-\text{CH}_2-\text{CH}_2-\text{CH}_2-\text{CH}_2-\text{O}$, from the 1,4-butyl segment of BDO), 3.65–3.69 ppm (2H, $\text{HO}-\text{CH}_2-\text{CH}_2-\text{CH}_2-\text{CH}_2-\text{O}$, from the BDO end-groups) and 1.23–1.28 ppm (3H, $\text{CH}_3-\text{CH}_2-\text{O}-\text{CO}-$, from the ester end-groups). The BDO end-group $\text{HO}-\text{CH}_2-\text{CH}_2-\text{CH}_2-\text{CH}_2-\text{O}$ (α'') and the ester end-group $\text{CH}_3-\text{CH}_2-\text{O}-\text{CO}-$ (α') both give a signal at 4.12 ppm which is overlapped with the main butylene signal ($-\text{O}-\text{CH}_2-\text{CH}_2-\text{CH}_2-\text{CH}_2-\text{O}-$) of the repeating unit. Except for the PBS repeating unit verification, the ^1H -NMR spectra indicated no residual BDO in the final products. The hydroxyl end group peak (signal at about 3 ppm [178]) monitored in the BDO spectrum, is absent in all prepolymers spectra (Figure 27). The resonance signal of the end unit ($-\text{OH}$) proton is typically not detectable in polymers' spectra due to intra-molecular hydrogen bonding (e.g., between hydroxyl groups and the ester bonds) [179]. It can be thus considered that there is no residual unreacted BDO in the prepolymers.

A-95 spectrum presented a typical morphology, with multiple, distinguished peaks at 4.12 and 1.7 ppm [49,176]. On the contrary, the A-80, A-85, and A-90 spectra presented different morphology with single, unsplit peaks at 4.12 ppm and 1.7 ppm. This difference indicates decreased chain length of the A-80, A-85 and A-90 prepolymers compared to A-95, given that there is a minimum polymerization degree above which the ^1H NMR peaks distinguish [180].

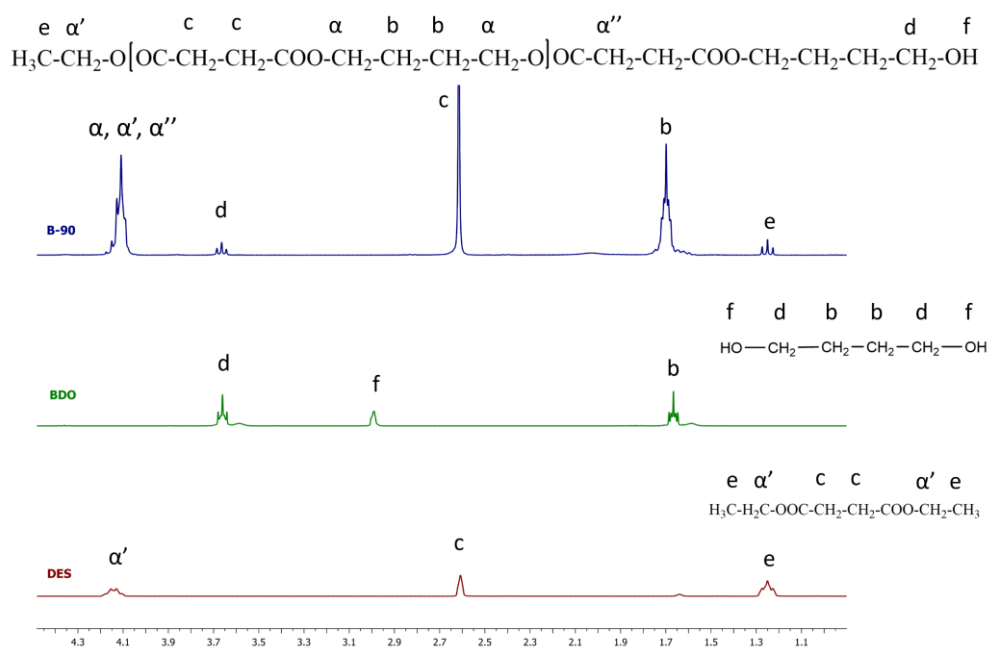


Figure 27. ^1H NMR spectra of the prepolymer B-90 and the monomers BDO and DES

The ^1H NMR-based molecular weight calculations (Figure 28) verified this observation, since decreased values were found for the A-80, A-85 and A-90 prepolymers compared to A-95. Based on the results, for \overline{M}_n and \overline{X}_n values lower than 1200 g mol^{-1} and 14 respectively (A-90 prepolymer), the monitored peaks in the spectrum do not distinguish. A similar trend has been observed for different enzymatically synthesized PBS grades by the group and the relevant results have already been published. More precisely, higher molecular weight PBS oligomers (e.g., \overline{M}_n 2000 g mol^{-1}) presented spectra with clearly separated peaks at 4.12 and 1.7 ppm in contrast to the spectrum of lower molecular weight PBS oligomers (e.g., \overline{M}_n 1250 g mol^{-1}), where the same peaks were slightly separated. Similarly, Kang-Jen Liu used oligomers ($n = 3$ to 10) and high molecular weight grades of poly(dimethyl siloxane) (PDMS) to prove the strong “short-range near-neighbor effect” on the NMR spectra as a function of chain length in bulk and solution. The researcher interestingly observed that the “internal” methyl groups of the polymer were distinguishable only when the chain length increased to $n \geq 5$. The main polymer NMR peaks of the polymers were also affected by chain length when aromatic solvent media were used. It was concluded that these phenomena should be considered, especially when low molecular weight polymer samples are measured.

Interestingly, the A-prepolymers \overline{M}_n values defined *via* GPC significantly differed (33-92%) from the relevant ^1H NMR-derived values (Figure 28, Table S1). This phenomenon is already observed in the literature. Adams *et al.* [181] used ^{15}N NMR and GPC to calculate the molecular weight of polyaniline samples. The GPC-calculated molecular weight values were found artificially higher due to either incomplete polyaniline chain disentanglement in solution or the polyaniline's stiffer nature compared to the used standard (PVP). Da Costa *et al.* [182] used four PBS samples of different molecular weights to compare the ^1H NMR- and the GPC-calculated molecular weight values. The values presented significant deviations (3-100%). It was concluded that NMR presents absolute, more accurate results than GPC.

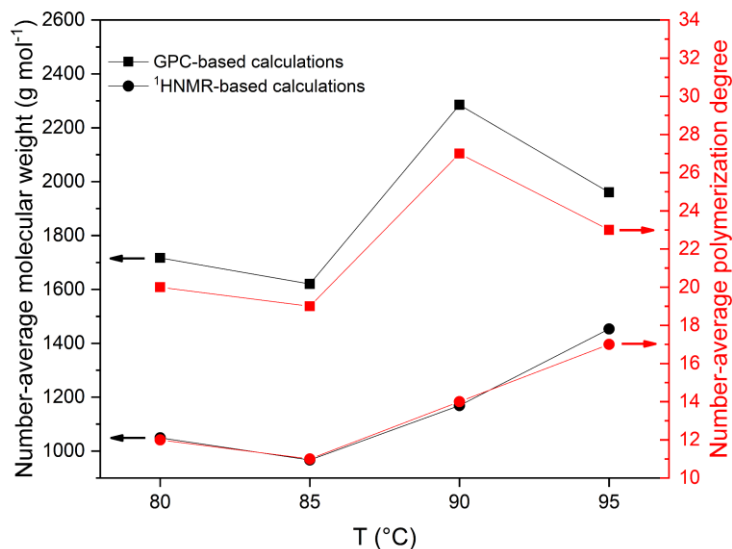


Figure 28. ¹H-NMR- and GPC-calculated \overline{M}_n and \overline{X}_n of the A-80, A-85, A-90 and A-95 prepolymers

Similarly, Izunobi and Higginbotham [183] assessed the molecular weight values of the homopolymer α -methoxy- ω -aminopolyethylene glycol (MPEG-NH₂) and the block copolymer α -methoxy-polyethylene glycol-block-poly- ϵ -(benzyloxycarbonyl)-L-lysine (MPEG-b- PLL(Z)) *via* different methods including GPC (calibrated with PS and PEG standards) and ¹H-NMR. The strong dependence of the GPC results on the calibrant was proved as the \overline{M}_n values obtained from the PS-calibrated curve were lower than the theoretical molecular weights of the measured samples, whereas the opposite scenario occurred for the PEG standards. In agreement with the abovementioned published works, the researchers concluded that ¹H-NMR is the most reliable technique to assess the molecular weight values, considering that there is no need for calibration. In any case, in the present work, the trend of the monitored molecular weights through ¹H-NMR and GPC is identical for every temperature except for 95°C. This inconsistency of A-95 could probably be attributed to inhomogeneity of the prepolymer due to partial loss of the enzyme's reactivity at elevated temperatures.

The A-prepolymers' chemical structure was also verified *via* PBS FTIR characteristic peaks (Figure 29): 1712 cm⁻¹, C=O stretching vibrations; 1154 cm⁻¹, C-O-C stretching vibration from the ester groups; 1045 cm⁻¹, O-C-C vibration in the BDO segment; 953 cm⁻¹, C-O symmetric stretching mode and 805 cm⁻¹, CH₂ in the succinate in-plane bending mode [96,176]. The broad band at around 3400 cm⁻¹ is attributed to the O-H stretch in the BDO end-group. The intensity of the carbonyl stretch C=O band (1712 cm⁻¹) is proportional to the concentration of the ester bonds (COO) along the polymer backbone and at the end of the polymer chain. In this work, where the synthesized PBS grades were oligomers, the contribution of the ester end-groups to the overall carbonyl stretch C=O band signal intensity is expected to be significant.

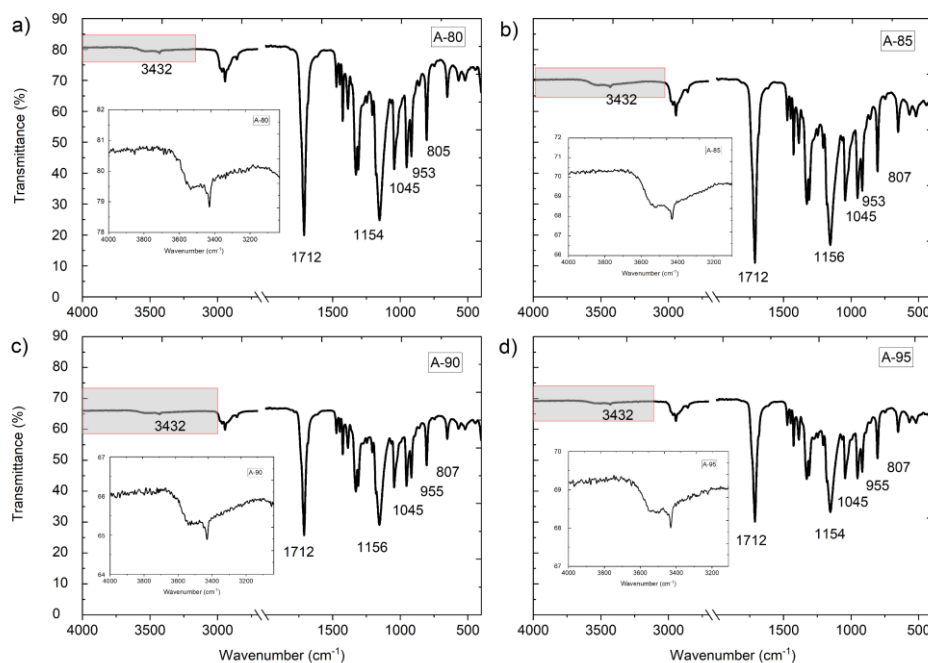


Figure 29. FTIR spectra of the prepolymers A-80 (a), A-85 (b), A-90 (c) and A-95 (d).

Indeed, the carbonyl content, defined qualitatively based on the intensity at 1712 cm⁻¹, was found to decrease with temperature (Figure 30), showing that the peak intensity is mainly related to the chain-end ester groups which are consumed with polymerization. The same trend is also observed for the ¹HNMR-calculated ester end groups percentage, which was also found to decrease (eq.4, Figure 30). More precisely, the COO peak intensity and the ester end groups percentage decreased slightly (3 and 11%, respectively) from 80 to 85°C, indicating that the reaction temperatures below 85°C are insufficient to reach effective polymerization rates. On the other hand, the highest percentage decrease of the carbonyl content (30%) and the highest decrease of the ¹HNMR-calculated ester end groups percentage (21%) were detected above 85°C, indicating that increased polymerization rates and chain-end ester groups consumption were achieved. The kinetic energy of the enzyme and the substrate chains was sufficient, and the most successful collisions due to higher diffusion rates between the enzyme's active site and the substrates were favored at 90°C. Further increase of the reaction temperature (from 90 to 95°C) did not have a significantly positive effect on the polymerization rate, as the carbonyl content further decreased slightly by 4%, while the ¹HNMR-calculated ester end groups percentage remained almost constant.

The intensity of the hydroxyl end-groups peak at 3400 cm⁻¹, which is much weaker and broader than the COO band at 1712 cm⁻¹, was also examined for the A-prepolymers (Figure 30). The most intense change was detected when the reaction temperature increased from 85 to 90°C (50% decrease), similar to the carbonyl content. It is thus confirmed that above 85°C, increased transesterification rates were achieved. At the lower temperatures of 80 and 85°C, the transesterification rates were significantly lower, and OH groups appeared to increase at 85°C compared to 80°C. This OH-end group concentration increase may indicate the initial formation of OH-rich oligomers during lipase-catalyzed polymerization [49,184]: due to the

low internal carbon chain length of DES its accessibility to the active site is limited, while diol presence permits the nucleophilic attack of the intermediate complex.

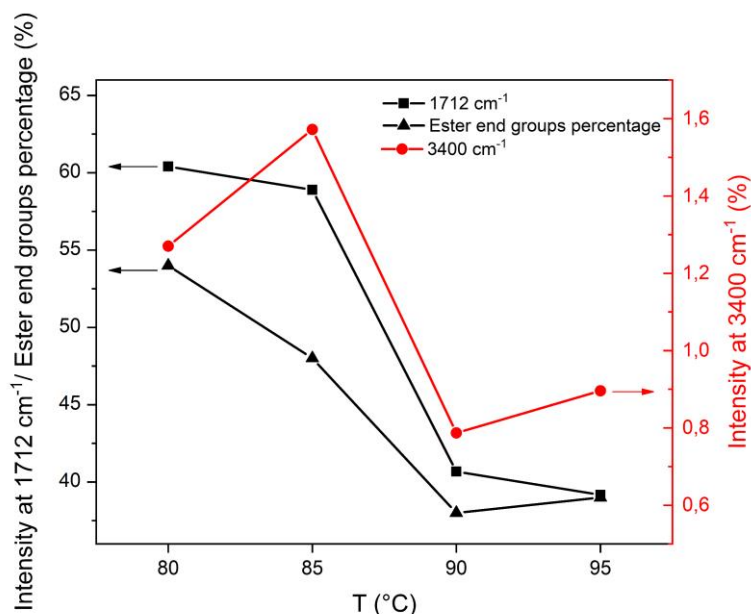


Figure 30. ¹HNMR-calculated ester end groups percentage (eq.4) and peak intensities (transmittance percentage) at 1712 and 3400 cm⁻¹ for the prepolymers A-80, A-85, A-90, A-95.

In agreement with the decrease of COO intensity with temperature, the obtained GPC-calculated average molecular weights significantly increased for reaction temperatures above 85 °C (Figure 30, Table S1). In particular, the highest GPC-calculated \overline{M}_n (2300 g mol⁻¹) and \overline{M}_w (5100 g mol⁻¹) were observed at 90 °C with a dispersity of 2.2, being close to the most probable molecular weight distribution value. At 95 °C, the average molecular weights seemed to decrease (by 15%) compared to 90 °C remaining though higher than the values at 80 and 85 °C. This behavior of lower polymerization rate at 95 °C may be due to partial loss of the enzyme's reactivity, while dispersity remained at similar values (2.1). A recent paper correlated this effect of biocatalysis temperature to the melting of the formed PBS chains above 84 °C [95]. More precisely, based on the DSC results, the solid state of PBS below 83.6 °C limited the diffusion of polymer chains through the porous support to reach the enzyme's active site. According to the researchers, PBS melting was possible above this temperature, and 90 °C was thus found as the optimal reaction temperature. Similarly, 90 °C has been indicated as the optimal reaction temperature of N435 in different polymerization systems (e.g., ring-opening polymerization of ϵ -caprolactone in toluene [185] and furanic-aliphatic polyamides synthesis in toluene [186]).

The percentage increase of the GPC-calculated average molecular weights for a ΔT of 5 °C was calculated to find the temperature coefficient values (Figure 31). A temperature coefficient (α) describes the relative change of a property depending on a given change in temperature, and it can be calculated as follows (Eq. 6).

$$a = \frac{\overline{MW} - \overline{MW}_{ref}}{\overline{MW}_{ref} \cdot (T_r - T_{ref})} \quad (6)$$

Where α is the temperature coefficient ($^{\circ}\text{C}^{-1}$), \overline{MW} the \overline{M}_n or \overline{M}_w at a selected reaction temperature T_r (g mol^{-1}), \overline{MW}_{ref} the reference \overline{M}_n or \overline{M}_w (at 80°C , in g mol^{-1}), T the selected reaction temperature ($^{\circ}\text{C}$), T_{ref} the reference reaction temperature (80°C).

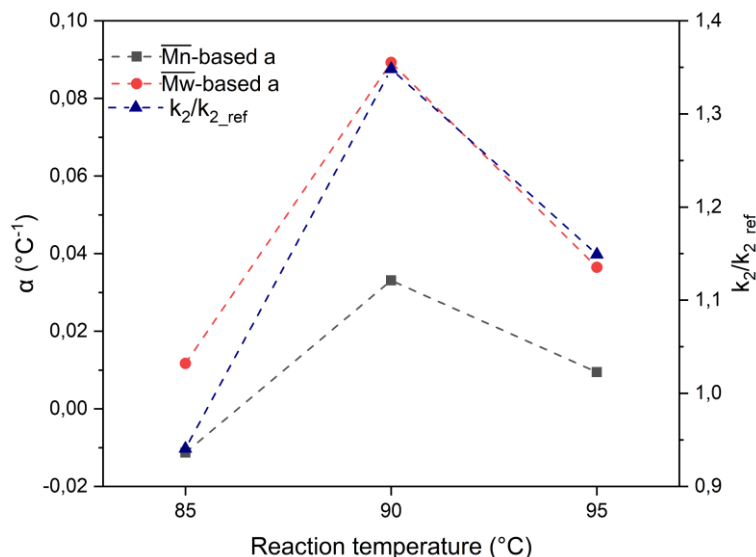


Figure 31. Temperature coefficient (α) and the ratios of the constants of the 2nd order kinetics (k_2/k_{2_ref})

The negative and low \overline{M}_n - and \overline{M}_w -based calculated temperature coefficients ($-0.01^{\circ}\text{C}^{-1}$ and $0.01^{\circ}\text{C}^{-1}$ respectively) at 85°C (Figure 31), confirm that the polymerization reaction was not favored at reaction temperatures below 85°C , probably due to decreased enzyme activity along with the diffusion limitations due to the products' solid state, considering the decreased \overline{M}_n values and process yields, especially at 80°C (Figure 28, Table 9). On the other hand, the temperature increase from 85 to 90°C seems crucial for the system, as the temperature coefficient maximizes at 90°C . Following the FTIR results, the further temperature increase up to 95°C does not positively affect the polymerization rate, as the temperature coefficient decreases, remaining though higher compared to the relevant value at 85°C .

The herein conducted polymerization is anticipated to follow the kinetics of a second order reaction due to the presence of the enzyme as a catalyst. The polymerization kinetics were analyzed under the assumptions of stoichiometric balance and no side reactions (including hydrolysis), based on the following Flory theory-based equation (Eq. 7).

$$\overline{X}_n = 1 + k_2 C_0 t \quad (7)$$

Where k_2 the rate constant of the polymerization reaction ($\text{kg meq}^{-1} \text{h}^{-1}$), C_0 the initial concentration of the ester- or hydroxyl-end groups ($t=0$) and t the reaction time (h).

The reaction temperature 80°C was considered as the reference reaction temperature and based on Eq. 7, the ratios $\frac{k_n}{k_{ref}}$ (where n: the different reaction temperatures and ref: 80°C) were calculated (Figure 31). It is confirmed that the rate constants ratios increase with temperature up to 90°C . In the range $80\text{--}90^\circ\text{C}$ the temperature increase from 85 to 90°C is the most crucial, as the ratio $\frac{k_{90}}{k_{ref}}$ is 1.4 times higher than $\frac{k_{85}}{k_{ref}}$ indicating that 90°C is the most promising reaction temperature. On the other hand, the ratio $\frac{k_{95}}{k_{ref}}$ was found 12% decreased compared to $\frac{k_{90}}{k_{ref}}$ probably due to the beginning of the protein denaturation as it remained higher (26%) than $\frac{k_{85}}{k_{ref}}$.

Turning to the thermal properties (Figure 32, Table S2), all the enzymatically synthesized samples were submitted to a first heating cycle to erase their thermal history, which was followed by cooling up to -10°C . The A-prepolymers crystallization temperatures (T_c) were correlated to prepolymerization temperature and thus to the achieved molecular weights (Figure 33). The higher molecular weight prepolymers (A-90 and A-95) presented higher crystallization temperatures (61 and 64°C respectively) in contrast to the lower molecular weight A-80 ($T_c = 53^\circ\text{C}$) and A-85 ($T_c = 55^\circ\text{C}$). This trend is attributed to the increased ease of chain folding of longer macromolecules and the decreased number of end groups that may act as crystal defects, slowing down the crystallization process.

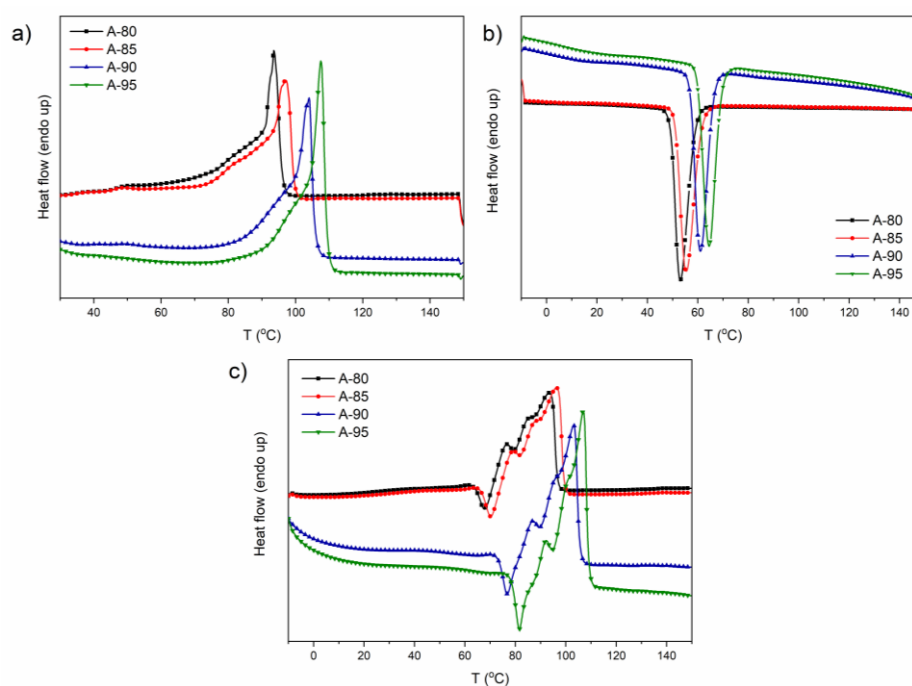


Figure 32. First heating (a), cooling (b) and second heating (c) of the prepolymers A-80, A-85, A-90 and A-95.

The calculated crystallinities, however, were found similar (x_c 72-74%) during cooling (Table S2) and in agreement with the relevant values reported in the open literature [162]. During the second heating, cold crystallization occurred for all the A-prepolymers at 68-81°C, indicating the formation of small crystals that didn't have enough time to be formed during cooling from the melt. The higher molecular weight prepolymers (A-90 and A-95) presented increased ΔH_{cc} values (8 and 12 J·g⁻¹ respectively), confirming again their enhanced tendency to crystallize. Multiple melting peaks were then monitored for all the A-prepolymers, indicating the existence of different crystal populations (e.g., different lamellar thickness) with different melting stability, a typical phenomenon for PBS. The first two melting peaks (77-92 and 84-100°C respectively) are attributed to the original crystalline melting [187], while the third one, monitored at the highest temperatures (93-107°C) corresponds to the recrystallization of the partially melted crystals during heating and was found close to the typical T_m (114°C) of a commercial PBS grade. As expected, the higher molecular weight prepolymers (A-90 and A-95) presented the higher melting points (Figure 33) and sharper endothermic peaks (Figure 32c) similarly to typical PBS thermographs. The melting enthalpies were also found increased for the higher molecular weight grades A-90 and A-95, i.e., 88 and 86 J·g⁻¹ respectively.

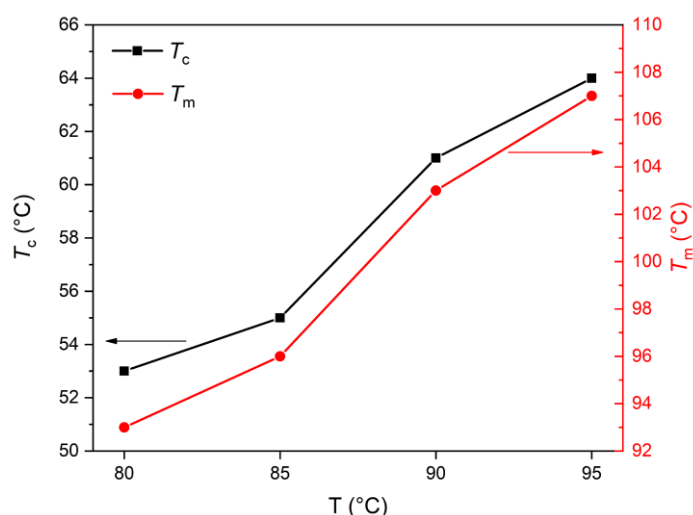


Figure 33. Crystallization temperature (T_c) and melting point from the second heating (T_{m2}) of the prepolymers A-80, A-85, A-90 and A-95.

Turning to TGA results, all A-prepolymers presented a single-step decomposition profile (Figure 34), with $T_{d5\%}$ and T_d from 303 to 326°C and 382 to 398°C (Table S3). The monitored T_d values were found similar to a commercial PBS grade (T_d at ca. 400°C) [96], and no mass loss was monitored at temperatures related to the monomers evaporation (T_b of BDO: 205°C, T_b of DES: 179°C) indicating also no residual monomers in the products (Figure 35b). The achieved high thermal stability of the enzymatically synthesized PBS grades, despite their low molecular weight, can be evidenced and attributed to the enzymes' selectivity, the applied mild polymerization conditions and the absence of undesirable by-products and metal catalyst residues that may accelerate thermal degradation reactions lowering thus the T_d .

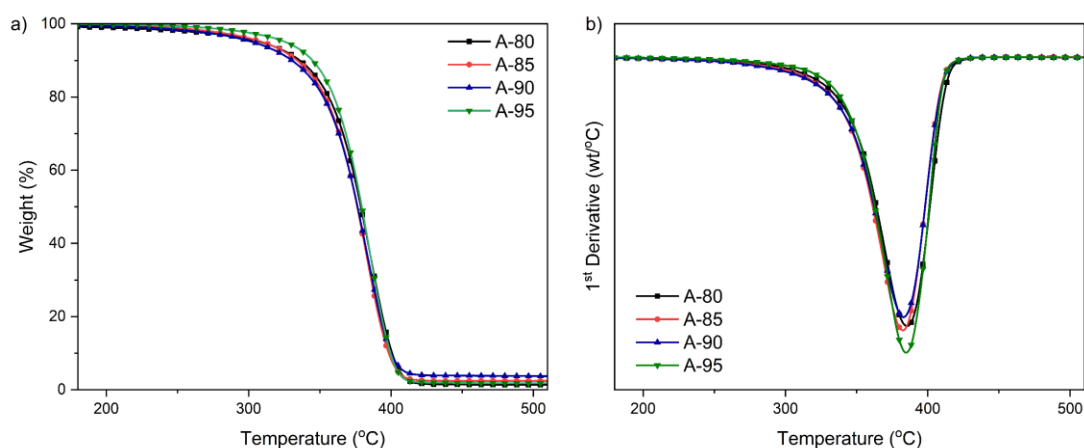


Figure 34. TGA curves and 1st derivatives of the prepolymer samples A-80, A-85, A-90 and A-95.

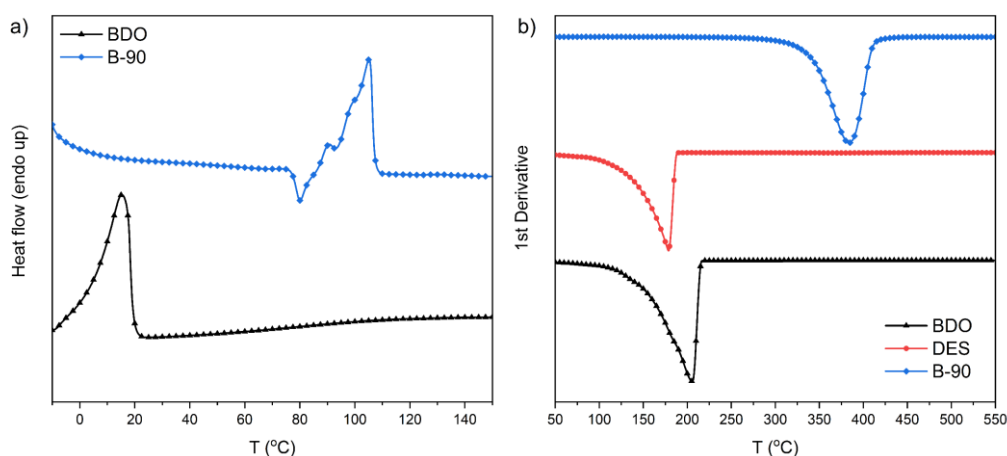


Figure 35. 2nd heating DSC thermogram of B-90 and the monomer BDO (a) and 1st derivative of the TGA curve of B-90, DES and BDO (b).

2.4.1.2 Investigation of the pressure impact on the PBS enzymatic prepolymerization process

Given the improved characteristics of the A-90 and A-95 prepolymer samples, the reduced pressure effect was studied at 90 and 95°C in order to enhance the rate of by-product (ethanol) removal *via* evaporation and diffusion. In samples B-90 and B-95, the pressure was set at 20 mbar, and the reference prepolymer samples were A-90 and A-95 (200 mbar).

Concerning the macroscopic observations, B-90 was a colorless solid in contrast to B-95, which was in the form of a sticky bulk material, indicating a lower degree of polymerization. The process yield slightly increased at 90°C (81%) compared to A-90 (75%), while it significantly decreased at 95°C (Table 9): from 91% (A-95) to 70% for B-95. At the end of the reaction at 95°C under 20 mbar, the enzyme presented yellowish color (Figure 36a), indicating the beginning of its denaturation, which probably led to the formation of lower molecular weight

oligomers that are more susceptible to sublimation, justifying also the lower yield. The chemical structure of the prepolymers was again verified *via* ^1H NMR, and the molecular weights were calculated *via* ^1H NMR and GPC (Table S1).

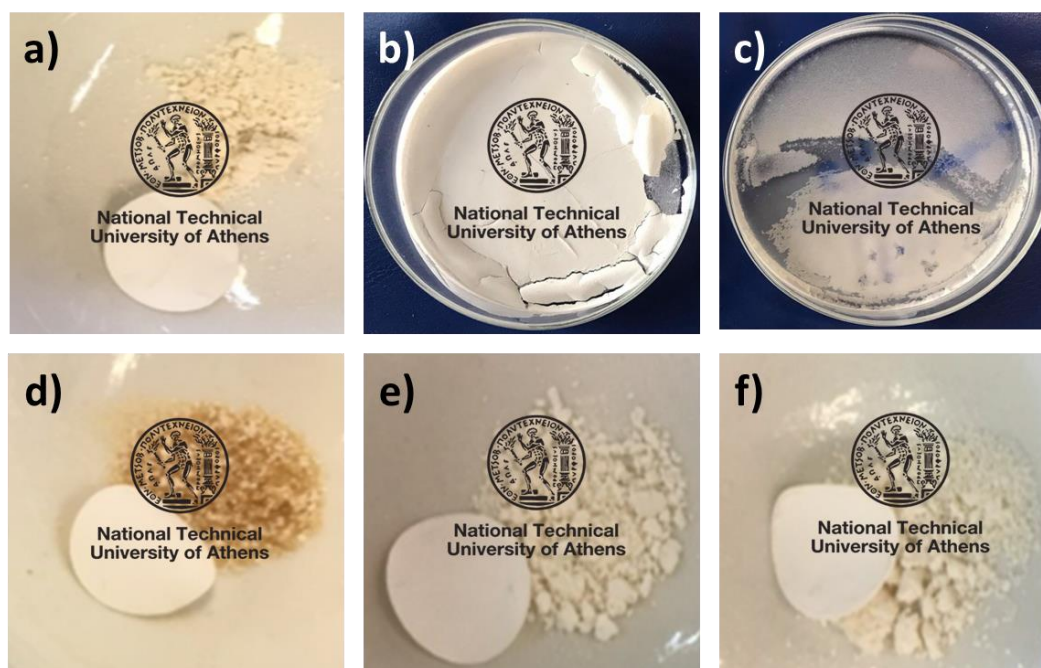


Figure 36 Morphology of the enzymes at the end of the reactions for the production of the prepolymers B-95 (a), C-95 (d), B-90 (e) and C-90 (f). Morphology of the prepolymers C-90 (b) and C-95 (c)

According to the process yield values, GPC-calculated \overline{M}_n slightly increased with the reduced pressure for the prepolymers synthesized at 90°C . On the other hand, B-95 presented significantly lower molecular weight values, and GPC showed a narrower MWD (dispersity 1.5), something that may also confirm the removal of the lower molecular weight oligomers through sublimation under the high vacuum of 20 mbar, thus disturbing the chemical reaction equilibrium. As regards DSC analysis, A-90 and B-90 behaved similarly (Table S2). Melt crystallization (T_c) occurred at ca. $61\text{--}64^\circ\text{C}$, and the presence of three melting peaks, all slightly higher for B-90 (91 , 99 and 105°C) is in line with the slightly increased molecular weight of B-90 compared to A-90. On the other hand, the prepolymers synthesized at 95°C , presented significantly different thermal properties. B-95 had significantly decreased T_c (45°C) compared to A-95 (64°C), and similar ΔH_c 81 and $84\text{ J}\cdot\text{g}^{-1}$ (Figure 37). The faster crystallization kinetics of A-95 verified its higher molecular weight compared to B-95. For the same reason, during the second heating, B-95 presented significantly broader endothermic peaks and severely lower T_m compared to A-95. Indicatively, the third melting endotherm was found 107°C and 83°C for A-95 and B-95 respectively. The ΔH_m values of B-95 were also found decreased ($72\text{ J}\cdot\text{g}^{-1}$) compared to A-95 ($86\text{ J}\cdot\text{g}^{-1}$).

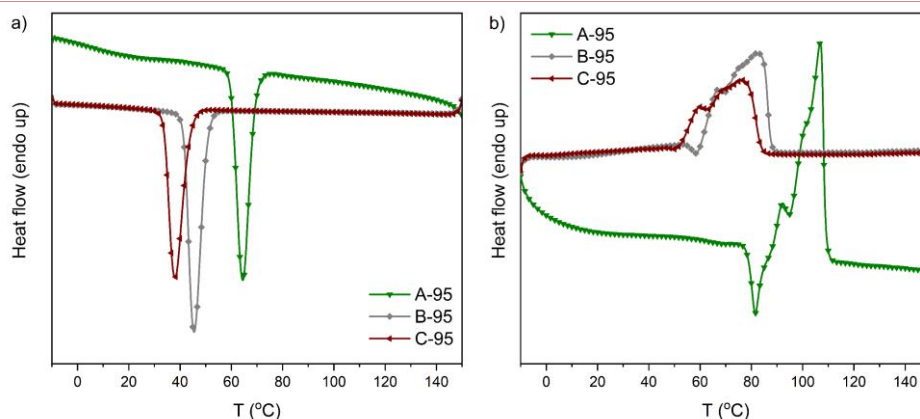


Figure 37. Cooling (a) and second heating (b) of the prepolymers A-95, B-95 and C-95.

The B-90 prepolymer also presented increased $T_{d,5\%}$ (327°C, Table S3) compared to the A-90 (303°C), while the B-95 presented significantly decreased $T_{d,5\%}$ (272°C) compared to A-95 (326°C). The $T_{d,5\%}$ is highly sensitive and correlated to the molecular weight changes; the simultaneous increase of reaction temperature and vacuum in B-95 had a negative effect on the achieved molecular weight and on the prepolymer thermal stability. On the other hand, at the temperature of 90°C, the higher vacuum resulted in a slightly higher overall quality of the prepolymer, i.e., in terms of molecular weight, melting characteristics and thermal stability.

2.4.1.3 Investigation of the reaction time impact on the PBS enzymatic prepolymerization process

Given the positive effect of the reduced pressure at 90°C and its negative effect at 95°C, a higher reaction time (6 h) was also studied as parameter at 90°C, 20 mbar (C-90) and 95°C, 200 mbar (C-95). On that basis, the reference prepolymers were B-90 and A-95 respectively.

Regarding prepolymers morphology, C-90 was a colorless solid (Figure 36b) similar to B-90. On the contrary C-95 was sticky (Figure 36c), indicating a low degree of polymerization. Additionally, the enzyme collected at the end of the reaction at 95°C presented yellow color, an indication of its thermal denaturation (Figure 36d). The process yield increased slightly for C-90 and C-95 (Table 9) with the increase in the reaction time. For C-90, \overline{M}_n increased up to 3100 g·mol⁻¹ being close to the B-90 value (2500 g·mol⁻¹). However, \overline{M}_w was found to decrease, indicating the existence of competitive phenomena. The system may have reached equilibrium due to increased end-groups consumption, while the high by-product amounts, requiring a higher vacuum to be removed, led to by-product accumulation within the reacting particles and alcoholysis reactions. Considering also the solid state character of the products at 90°C, it is easier for the shorter macromolecules to be recombined *via* diffusion and reaction on the enzymatic support, compared to the longer macromolecules which present decreased mobility being thus more susceptible to downgrade. As a result, \overline{M}_n of C-90 slightly increased in contrast to \overline{M}_w , which was found to decrease due to the longer macromolecules' higher contribution to the weight-average molecular weight calculation. For C-95°C, both molecular weight averages

significantly decreased, confirming the enzyme's time-dependent thermal inactivation at 95°C indicated by its yellow color at the end of the reaction.

B-90 and C-90 presented similar thermal properties as evidenced by DSC and TGA analyses (Tables S2, S3). On the contrary, C-95 presented significant differences to A-95 including slower crystallization kinetics, (26°C lower T_c , 8 J·g⁻¹ lower ΔH_c). The increased ΔH_c of the higher molecular weight prepolymer A-95 confirms its enhanced tendency to crystallize compared to the lower molecular weight C-95, attributed to the increased lamellar crystal thickness derived from the increased ease of chain folding of the longer macromolecules. Song and Sung [188] who studied the crystallization of different PBS grades as a function of molecular weight (4600 – 27000 g·mol⁻¹) also noticed a significant increase at the ΔH_c (from 18.1 to 19.7 cal·g⁻¹) when the molecular weight increased from 4600 to 6300 g·mol⁻¹. Then ΔH_c remained almost constant up to 11000 g·mol⁻¹ and finally decreased at higher molecular weight values (18.7 cal·g⁻¹ at 27000 g·mol⁻¹). The fact that the higher molecular weight grade (27000 g·mol⁻¹) presented lower T_c and ΔH_c values, can be attributed to the limited ease of chain folding due to the increased viscosity of the medium. C-95 also presented significantly different melting points, crystallinity and $T_{d,5\%}$, all attributed to its lower molecular weight (Figure 37, Table S3). Interestingly, the T_d of the prepolymers C-90 (383°C) and C-95 (383°C) were found similar to the B-90 (384°C) and A-95 (385°C), respectively. Even though C-90 and B-90 presented similar MW values, while C-95 presented a significantly decreased MW compared to A-95, the T_d in both cases was not affected and the decomposition process was conducted in a single-stage. This non-dependence of the T_d and the MW is attributed to the fact that the \overline{M}_n of all the prepolymers is higher than 1000 g·mol⁻¹. More precisely, in a work of the group, it was proved that the enzymatically synthesized PBS grades with low molecular weights ($\overline{M}_n < 1000$ g·mol⁻¹) decomposed at temperatures lower than 450°C and presented a two-stage decomposition in most cases. On the contrary, higher molecular weight grades (\overline{M}_n 1000 - 3000 g·mol⁻¹) decomposed at temperatures higher than 450°C in a single-stage process. A similar trend has been reported by Chrissafis *et al.* [189] for poly(ethylene succinate) or PES; it was proved that PES of \overline{M}_n 2300-3000 g·mol⁻¹ decomposed at temperatures lower than 200°C, with a three-stage decomposition process. On the contrary, PES of \overline{M}_n 3560-21480 g·mol⁻¹ presented a clear mass loss stage at temperatures higher than 290°C. The enhancement mechanism of thermal stability above a specific MW is rather complex and has not been studied in detail in the open literature. Unger *et al.* [190] investigated the effect of molecular weight on the thermal degradation of poly(ϵ -caprolactone) or PCL by TGA and FTIR. The researchers discovered that the lower molecular weight PCL grade (10000 g·mol⁻¹) decomposed in a three-step mechanism in contrast to the higher molecular weight (80000 g·mol⁻¹) for which a two-step decomposition was monitored. The products formed at each stage were defined through FTIR, and it was found that in the low molecular weight PCL decomposition during the first step, which was not observed for the high molecular weight grade, the monomer ϵ -caprolactone was formed. It was considered that the depolymerization was conducted *via* an unzipping mechanism of the PCL chains. This reaction was restricted to low molecular weight PCL because an increased concentration of (hydroxyl and carboxyl) end groups was present. All the other products

formed during the second and third decomposition steps were detected in low and high molecular PCL grades. Summing up, there seems to be a critical molecular weight value above which each polymer's decomposition is less (or even not at all) affected by the molecular weight variations.

2.4.2 Analysis of the scaling-up potential of the optimized PBS enzymatic prepolymerization process: 10 and 20g

The prepolymers synthesized at 90°C under 20 mbar for 2 and 6 h (B-90 and C-90) presented the highest performance in terms of molecular weight (\overline{M}_n 2500 and 3100 g·mol⁻¹, \overline{M}_w 6700 and 5200 g·mol⁻¹), thermal properties (T_{m2} 105 and 107°C) and morphology (colorless, free-flowing powders). Even though their characteristics were similar, B-90 was selected to be scaled up (10 and 20 g) as its synthesis reaction time was shorter (2 h), permitting thus lower energy requirements in line with the main principles of green chemistry. It is also important that the herein applied process can be easily scaled up, considering that it is a low-temperature bulk polymerization technique not requiring multiple solvents for the final product isolation. The scaled-up prepolymers were also received as colorless, free-flowing powders, and the achieved process yields were 95-96%. The obtained molecular weight values were found to be lower compared to the smaller scale grades (Table S1); especially the \overline{M}_w presented the highest decrease (53%) from the 1g- to the 20g-scale, indicating that the formation of the longer chains was restricted, while the relevant decrease in the \overline{M}_n values was less intense. This phenomenon can be attributed to mass transfer limitations that are more intense on large scales. For instance, the rate of by-product removal decreases as the produced ethanol is increased (constant vacuum of 20 mbar). Additionally, the scaled-up prepolymers' OH end groups were slightly lower than B-90 (52 and 53% for the 10 g and 20 g prepolymers instead of 60% for the B-90, see Figure 30), showing that mass transfer limitations may also affect the reactants' concentration and accessibility in the enzyme active site leading to a diverse distribution of end groups on large scales.

The scaled-up prepolymers' thermal properties were also lower compared to B-90 (Figure 38, Table S2). The melting points derived from the first heating of the scaled-up prepolymers, critical for the subsequent post-polymerization step, were found to decrease (103°C for the 10g and 98°C for the 20g) compared to B-90 (106°C). Slower crystallization kinetics, lower crystallinity, second-heating melting points and $T_{d,5\%}$ were monitored for the scaled-up prepolymers. On the contrary, the obtained decomposition temperatures were similar, as they are not that sensitive to molecular weight differences (Table S3).

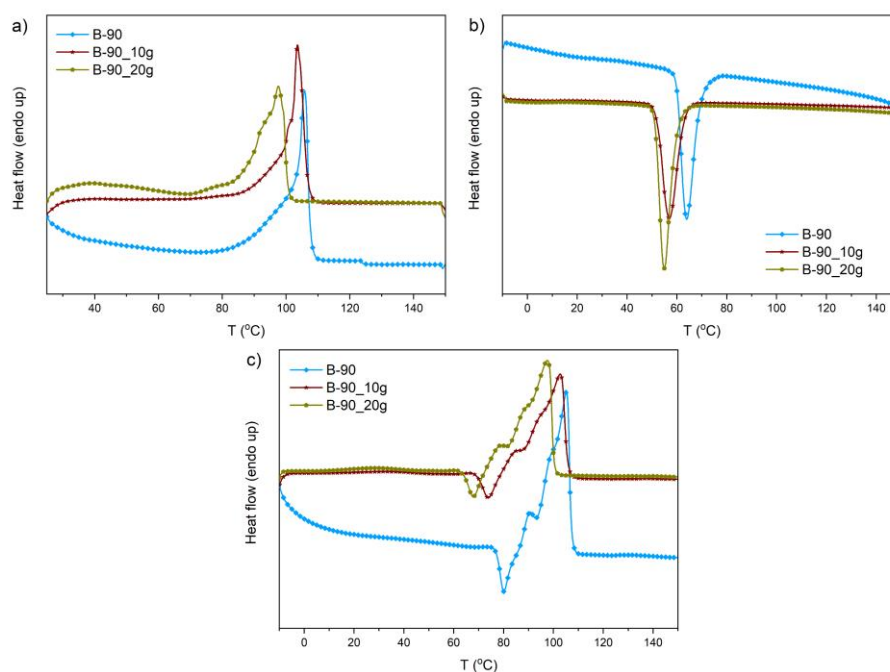


Figure 38. First heating (a), cooling (b) and second heating (c) of the prepolymer B-90 and the scaled-up prepolymers (10 and 20 g)

The prepolymer B-90_20g was selected as the starting material for the following post-polymerization tests (Chapters 5.4.1.1 and 5.4.1.2) due to its adequate available amount, good thermal performance and morphology to permit applying and examine SSP as a possible upgrading method.

2.4.3 Study of the monomers' ratio influence on the large-scale (20 g) PBS enzymatic prepolymerization process

In typical metal-catalyzed systems of esterification and trans-esterification stages for poly(alkylene succinate) production, reaction mixture composition is tuned by adding butanediol in slight excess. Thus, the equilibrium of the esterification reaction is shifted towards the formation of the diester, and the formation of OH-rich oligoesters that will further react during transesterification leads to a high yield of the final product. Jacquelin *et al.* [23] synthesized PBS with different chemical transesterification catalysts and used a molar excess of butanediol of 5%. Bikiaris *et al.* [24] synthesized different aliphatic polyesters, including PBS, using a higher butanediol excess of 20% (molar ratio of acid/glycol 1/1.2). High reactive groups' (such as OH) concentrations are also usually required during SSP as they affect the reaction rates [115]. In this context, the monomers' ratio was studied as a parameter for enzymatic prepolymerization on the large scale of 20 g, and the selected conditions were identical to the scaled-up prepolymer's synthesis (Table 9). The selected BDO molar excesses to be examined were 5, 10 and 20%, and the relevant products are coded as B-90_20g_5%, B-90_20g_10% and B-90_20g_20%, respectively.

The obtained products were colorless solids, with the B-90_20g_20% being stickier than the 90_20g_5% and B-90_20g_10%, probably indicating a lower degree of polymerization. This morphology aligns with the achieved process yields; the lower BDO excess products (5 and 10%) presented a 99% process yield, similar to the B-90_20g prepolymer's (96%, Table 9). On the other hand, the B-90_20g_20% product's process yield was calculated at 100% (Table 9), which is extremely high and probably indicates a remarkable quantity of unreacted BDO in the prepolymer mass, which could lead to a lower polymerization degree.

The products' chemical structures were verified *via* $^1\text{H-NMR}$ and FTIR, and the OH end groups of the synthesized prepolymers were monitored (Figure 39). As was expected, the OH end groups percentage significantly increased using BDO in excess, reaching the values from 64 to 81% (for the 5 and the 20% excess, respectively), all significantly higher than the stoichiometric prepolymer B-90_20g (OH end groups percentage 53%). In agreement with the $^1\text{H-NMR}$, a similar trend was observed in the FTIR results, with the intensity of the hydroxyl end-groups peak at 3400 cm^{-1} increasing with the BDO excess increase. It was thus confirmed that the BDO excess overcame the large-scale mass transfer limitations, typically leading to diverse distribution of end groups in the final products, as discussed in 2.4.2.

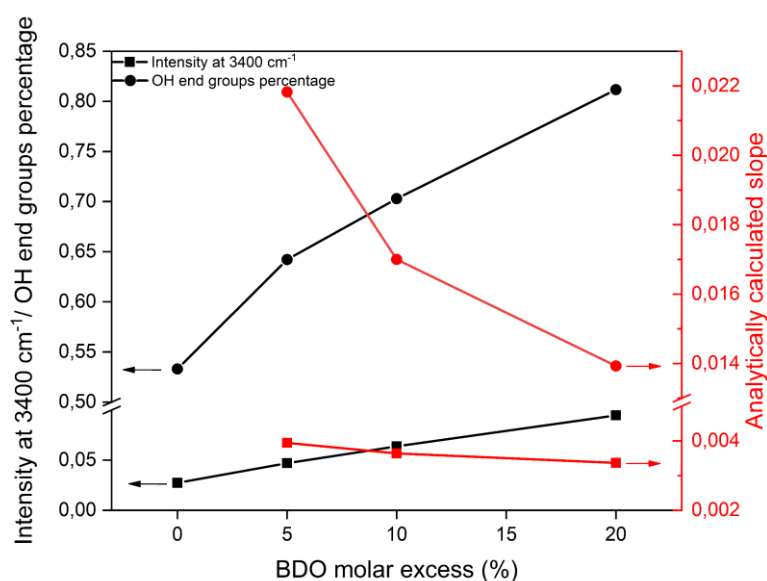


Figure 39. Peak intensity at 3400 cm^{-1} , $^1\text{H-NMR}$ -calculated hydroxyl end groups percentage and the analytically calculated slopes for the prepolymers B-90_20g, B-90_20g_5%, B-90_20g_10% and B-90_20g_20%.

The OH end groups increased linearly with the BDO excess increase based on both the $^1\text{H-NMR}$ and FTIR methods (R^2 : 0.9701 and 0.9968 for the $^1\text{H-NMR}$ and FTIR, respectively). However, when the slope was analytically calculated at each BDO molar excess, it was found to decrease after 5% (Figure 39). This trend can be attributed to the very high abundance of BDO (for excesses higher than 5%), probably leading to competing side reactions, leading to the formation of undesirable byproducts (including short-chain oligomers such as dimers), as the system tries to counteract the intense change in the monomers' concentrations.

The prepolymers' molecular weight values were defined *via* $^1\text{H-NMR}$ and GPC, and the results are presented in Figure 40. Based on the GPC-calculated results, the \overline{M}_n did not show significant changes, with the 20% BDO excess product presenting the highest decrease of 8% compared to the stoichiometric B-90_20g. The decreasing trend of the prepolymers' \overline{M}_n was depicted more clearly in the $^1\text{H-NMR}$ results, especially at the B-90_20g_20% prepolymer, which reached the value of $600\text{ g}\cdot\text{mol}^{-1}$, thus confirming the negative effect of the high BDO excess on the prepolymer in agreement with the abovementioned macroscopical observations (sticky morphology). The \overline{M}_w of the prepolymers was significantly affected by the BDO excess reaching up to a 35% decrease for the 20% BDO excess. The lower molecular weights are generally expected in step-growth polymerization when there are significant deviations from the stoichiometric ratio of the monomers. In our system, the presence of high amounts of the residual unreacted BDO could also negatively affect the enzyme's function, leading to the formation of numerous short-chain oligomers (e.g., dimers), as already discussed. The formation of these shorter oligomers negatively affects the MW (especially the \overline{M}_w) and consequently, the polymer's dispersity, which was also decreased and significantly lower than the most probable molecular weight distribution value.

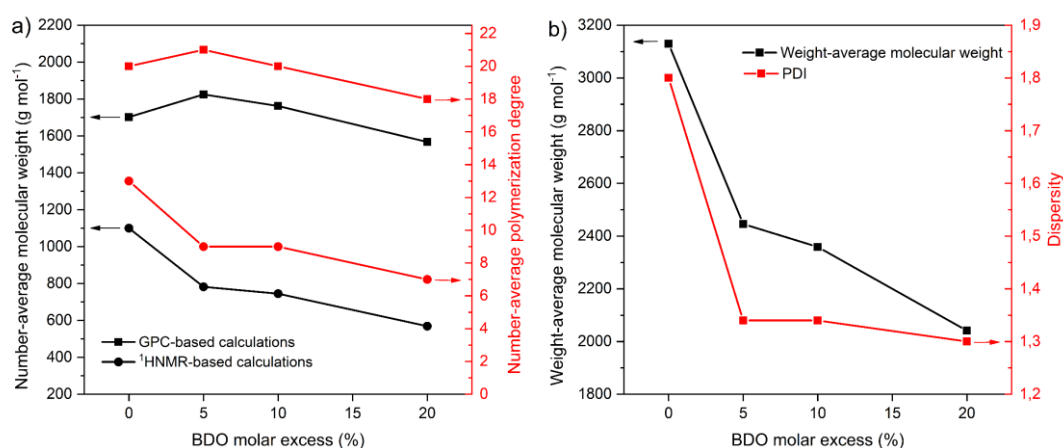


Figure 40. Number-average molecular weight values defined by GPC and $^1\text{H-NMR}$ (a) and weight-average molecular weight values and dispersity values (b)

As regards the prepolymers' thermal properties monitored *via* DSC, B-90_20g_20% presented the lowest melting point during the first and the second heating (96 and 94°C respectively) compared to the stoichiometric B-90_20g (98°C). The slowest crystallization kinetics and the lowest crystallinity were also monitored for the 20% excess product (Table S2). The decomposition temperatures of all the BDO excess products, defined through TGA, were increased (T_d 400 - 401°C) compared to B-90_20g presenting T_d of 384°C (Table S3). This behavior could be related to the increased OH-end group concentrations of the BDO excess products, as these polar groups can form during heating intermolecular hydrogen bonds (e.g., with the PBS ester bonds) and thus increase the overall stability of the oligomer but further investigation is required. The lowest $T_{d,5\%}$ was also monitored for the B-90_20g_20% (233°C instead of 315°C for B-90_20g), attributed to its lower molecular weight.

Overall, the prepolymer B-90_20g_5% was selected as the starting material for the following post-polymerization tests (Chapter 5.4.1.2.3) due to its adequate thermal performance and OH-end groups percentage to study the effect of the OH-end group concentration on the post-polymerization process.

2.5 Conclusions

This chapter examines PBS prepolymers synthesis *via* enzymatic polymerization using immobilized *Candida antarctica* Lipase B as a biocatalyst in a solvent-free system. The enzymatic synthesis was conducted in two stages, with the first at milder conditions (40°C, atmospheric pressure, 24 h) to minimize possible monomers' losses. The second stage's conditions (reaction temperature, pressure, time) were thoroughly investigated.

Starting with the reaction temperature, the examined temperature window was 80-95°C. All the synthesized prepolymers' structure was verified *via* ¹H-NMR and FTIR. The prepolymers synthesized at 90 and 95°C (A-90 and A-95, respectively) presented superior properties compared to the products of the lower reaction temperatures. More precisely, the molecular weight values, were found to increase above 85°C, reaching the values of 2300 g·mol⁻¹ and 5000 g·mol⁻¹ (\overline{M}_n and \overline{M}_w , respectively) at 90°C. This behavior of higher polymerization rate at 90°C agreed with the open literature where 90°C has been indicated as the optimal reaction temperature of N435 in different polymerization systems. At 95°C, the average molecular weights decreased slightly (compared to 90°C), probably implying partial loss of the enzyme's reactivity, but were still higher than the MW at 80 and 85°C. The different products were also qualitatively compared based on the carbonyl and hydroxyl band intensities (transmittance percentage), given that the contents are proportional to the relevant values. The highest percentage decrease of the carbonyl content (30%) and the highest decrease of the ¹H-NMR-calculated ester end groups percentage (21%) were detected above 85°C, indicating that the contribution of the ester end-groups to the overall carbonyl stretch C=O band signal intensity is significant when oligomers are examined. In line with the GPC results, it was shown that increased polymerization rates and chain-end ester groups consumption were achieved at 90°C. At this temperature, the kinetic energy of the enzyme and the substrate chains was sufficient, and the most successful collisions due to higher diffusion rates between the enzyme's active site and the substrates were favored. Further increase of the reaction temperature (from 90 to 95°C) did not significantly affect the polymerization rate. The thermal properties of the prepolymers synthesized at 90 and 95°C were also superior, with higher crystallization temperatures (T_c up to 64°C) and higher melting points (T_{m2} up to 107°C).

Given the improved characteristics of the A-90 and A-95 prepolymers, the reduced pressure effect was studied at 90 and 95°C (prepolymers B-90 and B-95, respectively) to enhance the by-product (ethanol) removal rate *via* evaporation and diffusion. The applied reduced pressure had a positive effect at 90°C, but a negative effect at 95°C. The morphology of B-90 was similar

to that of A-90, namely free-flowing powder. Higher MW were determined for the B-90, namely 2500 and 6700 g·mol⁻¹ (GPC-derived \overline{M}_n and \overline{M}_w , respectively) and similar thermal properties (e.g., T_{m2} 105°C). On the contrary, B-95 was a sticky bulk material, significantly different from A-95. B-95 also presented significantly reduced MW compared to A-95, reaching the values of 1400 and 2000 g·mol⁻¹ (GPC-derived \overline{M}_n and \overline{M}_w , respectively). The thermal properties of B-95 were also downgraded, with broad endotherm peaks, decreased T_{m2} (83°C), and decreased thermal stability, indicated by the significantly lower $T_{d,5\%}$, which is highly sensitive and correlated to the molecular weight changes. Finally, at the end of the reaction at 95°C under 20 mbar, the enzyme presented yellowish color, indicating the beginning of its denaturation, which probably led to the formation of lower molecular weight oligomers that are more susceptible to sublimation, leading also to a lower yield.

Higher reaction time (6 h) was also studied as parameter at 90°C, 20 mbar (C-90) and 95°C, 200 mbar (C-95), with the reference prepolymers being B-90 and A-95 respectively. Reaction time did not significantly affect polymerization at 90°C, in contrast to 95°C, where a clearly negative effect was monitored. For C-90, \overline{M}_n increased up to 3100 g·mol⁻¹ being close to the B-90 value (2500 g·mol⁻¹), but \overline{M}_w was found to decrease, indicating the existence of competitive phenomena. The chemical reaction equilibrium may have been reached due to increased active end-group consumption. High by-product amounts were formed requiring a higher vacuum to be removed, thus leading to ethanol accumulation within the reacting particles and alcoholysis reactions. The thermal properties of B-90 and C-90 were found similar. On the other hand, for C-95°C, both molecular weight averages significantly decreased to 1100 and 3800 g·mol⁻¹ (\overline{M}_n and \overline{M}_w , respectively), confirming the enzyme's thermal inactivation at 95°C also indicated by its yellow color at the end of the reaction. Regarding the C-95 thermal properties, it presented slower crystallization kinetics, significantly lower melting points, crystallinity and $T_{d,5\%}$, all attributed to its lower molecular weight.

The prepolymers synthesized at 90°C under 20 mbar for 2 and 6 h (B-90 and C-90) presented the highest performance in terms of molecular weight, thermal properties and morphology. Even though their characteristics were similar, B-90 was selected to be scaled up (10 and 20 g) as its synthesis reaction time was shorter (2 h), permitting thus lower energy requirements in line with the main principles of the green chemistry. The herein applied process was successfully scaled up, thanks to its simplicity as it is a low-temperature bulk polymerization technique not requiring multiple solvents for the final product isolation. Thus, 20 g of enzymatically synthesized PBS were received for the first time, filling the relevant gap in the open literature as discussed in the introduction part. The scaled-up prepolymers' morphology was as expected (colorless, free-flowing powders), but the obtained molecular weight values were found to be lower compared to the smaller scale grades due to mass transfer limitations that are more intense on large scales. Additionally, the scaled-up prepolymers' OH end groups were slightly lower than B-90 probably due to the mass transfer limitations affecting the reactants' concentration and leading to a diverse distribution of end groups on large scales. The scaled-up prepolymers' melting points derived from the first heating, critical for the

subsequent post-polymerization step, were found to decrease (103°C for the 10g and 98°C for the 20g) compared to B-90 (106°C). Slower crystallization kinetics, lower crystallinity, second-heating melting points and $T_{d,5\%}$ were monitored for the scaled-up prepolymers. On the contrary, the obtained decomposition temperatures were similar, as they are not that sensitive to molecular weight differences.

The last examined parameter was monomers' ratio, studied on the large scale of 20 g, applying the optimized prepolymerization conditions. The selected BDO molar excesses to be examined were 5, 10 and 20%. The OH end groups increased linearly with the BDO excess increase based on $^1\text{H-NMR}$ and FTIR. However, when the slope was analytically calculated at each BDO molar excess, it was found to decrease after 5%. The \overline{M}_w of the prepolymers was significantly affected by the BDO excess reaching up to a 35% decrease for the 20% BDO excess. The observed MW decrease can be attributed to deviation from the stoichiometric ratio of the monomers, while the high amounts of the residual unreacted BDO could negatively affect the enzyme function, leading to the formation of numerous short-chain oligomers (e.g., dimers). The 20% BDO excess product presented the lowest melting points, the slowest crystallization kinetics and the lowest $T_{d,5\%}$, all attributed to its lower molecular weight.

Summing up, PBS prepolymers were enzymatically synthesized through a process designed in line with the green chemistry guidelines, i.e., solvent-free process, easiness of workup, and low energy requirements due to low reaction temperatures and times. The main advantage of this process is its scalability potential, thanks to its simplicity. The herein prepared pure, controlled low molecular weight and crystallinity PBS permits tunable degradation rates needed in controlled release applications, and it is thus appropriate for biomedical materials and biodegradable plastics for packaging. It is thus a product presenting increased primarily research and secondarily industrial interest.

Chapter 3: Enzymatic prepolymerization of poly(butylene 2,5-furandicarboxylate) using the immobilized *Candida antarctica* Lipase B (N435) as biocatalyst

3.1 Introduction

In 2004, the US Department of Energy published a list of 12 high-value-added chemicals obtained from sugars (updated in 2010), among which 2,5-furan dicarboxylic acid (2,5-FDCA) can be found. This monomer has attracted the attention of important companies, such as ADM, DuPont, Avantium and BASF, interested in its industrial production, as it is characterized as “a sleeping giant” due to its structural similarity with terephthalic acid employed in the production of important thermoplastic polyesters like poly(ethylene terephthalate) (PET) and poly(butylene terephthalate) (PBT) [191].

Among the FDCA-based polyesters (i.e., poly(ethylene 2,5-furandicarboxylate) (PEF), poly(propylene 2,5-furandicarboxylate) (PPF), poly(butylene 2,5-furandicarboxylate) (PBF)), PBF undoubtedly occupies a privileged position due to its resemblance to the engineering plastic poly(1,4-butylene terephthalate) [192]. Although PBF presents similar morphological, thermal, and mechanical properties to PBT due to their similar chemical structures (the furan ring replaces the benzene ring), it is more hydrophilic than PBT and, therefore, more prone to attack by microorganisms [193]. PBF has also shown potential for usage in multilayer packaging materials due to its exceptional gas barrier properties [136]. Guidotti *et al.* [191] synthesized homopolyesters of 2,5-FDCA with high molecular weight by two-stage melt polycondensation, starting from dimethyl ester of 2,5-FDCA and glycols of different lengths (the number of methylene groups ranged from 3 to 6). The synthesized polyesters were then processed into free-standing thin films (thicknesses between 150 to 180 μm) by compression molding. The researchers concluded that the polyesters containing short glycolic subunits, i.e., PPF and PBF, could be suitable to produce rigid packages with outstanding barrier properties to CO_2 , as in the case of bottles for soft drinks.

A 2010 patent has already mentioned PBF synthesis, albeit no specific detail was reported then [194]. Later, several independent studies [195,196] reported its synthesis by reacting FDCA with 1,4-butanediol through a two-stage approach in the presence of titanium-based catalysts, including TBT (tetrabutyltitanate) and TTIP (titanium tetraisopropoxide) as catalysts (See Chapter 1.2.1.2.1). As already discussed, using metal catalysts can be a significant drawback, especially when the final product is used for food contact applications, as they can be toxic to the environment and people.

A promising alternative is enzymatic polymerization, which avoids using toxic catalysts. However, the relevant literature is very limited, with only two published works enzymatically synthesizing PBF with \overline{M}_n and \overline{M}_w up to 1600 and 5600 $\text{g}\cdot\text{mol}^{-1}$.

Thus, PBF seems to be a polymer with great potential to be used as a packaging material in the coming years. It is thus crucial to invest in green methods to safely synthesize it and probably upgrade PBF, for instance, when produced *via* enzymatic polymerization.

3.2 Scope

The main objective of this chapter was to examine the immobilized *Candida antarctica* Lipase B as a biocatalyst in a solvent-free system to produce poly(butylene 2,5-furandicarboxylate) (PBF) in a scalable process.

In the first part of the chapter, the most critical parameters of the process, including reaction temperature, pressure, and time, were studied on a small scale of 1 g of the final PBF prepolymer. The prepolymers' molecular weight, thermal properties, and morphology were assessed for every process parameter. Additionally, an assay of the recyclability potential of the enzyme was conducted.

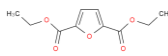

In the second part of the chapter, two consecutive scaling-up attempts to receive 3 and 6 g of the PBF prepolymer and study the scalability of the process occurred. This study also aspired to investigate the relative scaling-up effect on the prepolymer's properties.

3.3 Experimental

3.3.1 Materials

For PBF synthesis, diethyl furan-2,5-dicarboxylate or DEF ($C_{10}H_{12}O_5$, purity >95%) was used. DEF was purchased from Biosynth, Switzerland (Table 10) and was in the form of a yellow powder. It is worth noting that DEF (also known as DEFDCA) and dimethyl furan-2,5-dicarboxylate (DMF or DMFDCA) are the most common FDCA derivatives that are usually preferred over FDCA to facilitate polymerization reactions; these derivatives present increased reactivity, solubility in the reaction mixtures and lower melting temperatures [197]. Additionally, using a diester such as DEF is crucial for our case, where enzymatic polymerization is conducted using biocatalyst N435, presenting increased specificity with esters.

Table 10. Compounds used for the prepolymerization of PBF

Compound	Molecular Formula	Structure	MW ($g \cdot mol^{-1}$)	Other characteristics	Supplier
DEF	$C_8H_{14}O_4$		212.2	Purity >95%	Biosynth, Switzerland
Hexane	C_6H_{14}		86.18	Purity 95%	Fisher Scientific, U.K.

BDO and the N435, both presented in Chapter 2.3.1, Table 7, were also used for the PBF polymerization. Hexane was purchased from Fisher Scientific, U.K. All chemicals were used without further purification.

3.3.1.1 Experimental procedure for the Assay of the immobilized *Candida antarctica* Lipase (B) activity

The assay of the N435 activity was conducted as described in Chapter 2.3.1.1. Since the reusability potential of the biocatalyst N435 was to be assessed (Chapter 3.4.1.2), the protein loading was considered 10% wt (see Chapter 2.3.1.1) for every calculation included in the reusability study.

3.3.2 Enzymatic prepolymerization experimental procedure for poly(butylene 2,5-furandicarboxylate) production

Stoichiometric amounts of DEF (6 mmol, 1.27 g) and BDO (6 mmol, 0.54 g) were premixed in a round-bottom flask and stirred (75 rpm) at 50°C in a rotary evaporator (Rotavapor R-210, Buchi, Switzerland) under atmospheric pressure. 10% wt N435 (relative to monomers) was subsequently added, and a two-step prepolymerization process was applied.

Table 11. Conditions of PBF enzymatic prepolymerization

Sample	1 st step			2 nd step		
	T (°C)	P (mbar)	t (h)	T (°C)	P (mbar)	t (h)
D-75	50	1000	24	75	200	2
D-80	50	1000	24	80	200	2
D-85	50	1000	24	85	200	2
D-90 ¹	50	1000	24	90	200	2
D-95	50	1000	24	95	200	2
E-90	50	1000	24	90	20	2
E-95	50	1000	24	95	20	2
F-90	50	1000	24	90	200	6
F-90_24	50	1000	24	90	200	24
F-95	50	1000	24	95	200	6

¹D_90_3g, D-90_6g: scaled-up prepolymers (3 and 6 g respectively)

The first step was conducted at 50°C, under atmospheric pressure, for 24 h to minimize BDO losses. Then, the temperature increased, and vacuum was applied. At the end of the reaction, chloroform was added (4:1 wt relative to monomers) to dissolve the formed polyester and the enzyme was subsequently filtered off. The remaining chloroform was evaporated in a high-

vacuum pump (Edwards RV5 Rotary Vane Pump, Edwards, U. K.), and the formed polyester, a yellowish sticky gel, was stored in a desiccator. The process yield (%) was calculated as in 2.3.2. When needed, the product was dispersed in hexane to dissolve residual DEF and the undissolved oligomer was subsequently filtered off.

The variation of enzymatic prepolymerization conditions resulted in three sets of prepolymers (Table 11): samples D (reaction temperature, 75-95°C), samples E (reduced pressure value, 200 and 20 mbar), samples F (reaction time, 2 and 6 h). The sample D-90 was scaled up to prepare a higher amount (ca. 3 g) for the following post-polymerization attempts (see Chapter 5).

3.3.3 Characterization techniques

3.3.3.1 ¹H-NMR Spectroscopy

¹H-NMR spectroscopy was performed in CDCl₃ on a Bruker DRX 400 spectrometer, equipped with a 5 mm ¹H/¹³C dual inverse broad probe operating at 400 MHz to verify the structure of the formed polyesters. The number-average molecular weight (\overline{M}_n , g·mol⁻¹) was calculated by Eq. (8):

$$\overline{M}_n = \frac{I_b - I_d - \frac{2}{3}I_e \cdot 88.10 + \frac{I_a - \frac{1}{3}I_{e'}}{2} \cdot 122 + \frac{I_d}{2} \cdot 89.11 + \frac{I_e}{3} \cdot 45.06}{0.5 \cdot \left(\frac{I_d}{2} + \frac{I_e}{3}\right)} \quad (8)$$

where 88.10 is the molar mass (g·mol⁻¹) of 1,4-butyl segments, 122 is the molar mass (g·mol⁻¹) of furanoate segments, 89.11 is the molar mass (g·mol⁻¹) of 1,4-BDO end-groups, 45.06 is the molar mass (g·mol⁻¹) of ester end-groups and I_b is the integral of the 1,4 butyl segment signal at 4.35-4.43 ppm, I_a is the integral of the furanoate segment signal at 7.20 ppm, I_d is the integral of the BDO end-group signal at 3.67 ppm, I_e is the integral of the ester end-group signal at 1.25 ppm and $I_{e'}$ is the integral of the ester signal at 1.40 ppm.

The number-average degree of polymerization (\overline{x}_n) was calculated by Eq. (3) (see Chapter 2.3.3.1) for a m_0 of 210 g·mol⁻¹ (i.e., the molecular weight of the repeating PBF unit).

The percentage of the hydroxyl-end group in respect to the total number of prepolymer ends was calculated by Eq. (9):

$$\text{hydroxyl end groups percentage (\%)} = \frac{\frac{I_d}{2}}{\frac{I_e}{3} + \frac{I_d}{2}} \cdot 100 \quad (9)$$

3.3.3.2 Fourier Transform Infrared Spectroscopy (FTIR)

FTIR was performed as described in 2.3.3.2. The prepolymers, in the form of sticky powders, were submitted to the FTIR analysis without prior processing.

3.3.3.3 Gel Permeation Chromatography (GPC)

GPC was carried out as described in 2.3.3.3. The calibration of the instrument was carried out as described in 2.4.3. The calibration curve was not used for the MW determination due to lacking Mark-Houwink (K and a) constants for the specific polymer-solvent system.

3.3.3.4 Differential Scanning Calorimetry (DSC)

Differential scanning calorimetry (DSC) measurements were performed in the system described in 2.3.3.4. Heating – cooling – heating cycles from 20 to 180°C, cooling to –90°C, and heating to 200°C were conducted. All measurements were conducted under N_2 flow (20 mL·min⁻¹), with a 10°C·min⁻¹ rate. The relevant mass fraction crystallinity (x_c) was computed from the cooling DSC curves according to Eq. (5a), for the heat of fusion of 100% crystalline PBF (ΔH_0) equal to 129 J·g⁻¹ [198].

3.3.3.5 Thermogravimetric Analysis (TGA)

Thermogravimetric analysis (TGA) was conducted as presented in 2.3.3.5.

3.4 Results

3.4.1 Study of the key parameters influence on the small-scale (1g) PBF enzymatic prepolymerization

3.4.1.1 Investigation of the reaction temperature impact on the PBF enzymatic prepolymerization process

Similarly to PBS (Chapter 2), the PBF enzymatic prepolymerization was conducted in two steps to minimize BDO loss due to its high volatility. The selected reaction temperature of the first stage was 50°C instead of 40°C, which was the optimum first-stage reaction temperature for the case of PBS. This temperature was selected to have DEF in the liquid (melt) state, thus ensuring that the monomers mixing and diffusion into the enzyme's support to reach the enzyme's active site would be facilitated. The reaction temperature of the second step (75-95°C, samples D) was the first parameter of the PBF enzymatic polymerization to be studied. All the calculated process yields were higher than 100%, indicating the presence of residual monomers in the oligomers' mass, probably the solid DEF, as liquid BDO is expected to be removed during drying.

All the products' repeating unit was verified *via* ¹H-NMR spectroscopy, and the obtained spectra were similar. Indicatively, the D-90 spectrum is presented in Figure 41 compared to the relevant blank sample, the monomers (BDO and DEF), and the monomers' mixture spectra. The determined shifts of the herein synthesized prepolymers were: 7.20 (2H, -CH=, protons **a** from the furan segment of DEF), 4.35-4.43 (4H, -O-CH₂-CH₂-CH₂-CH₂-O-, protons **b** from the butyl

segment of BDO), 1.80-1.91 (4H, $-\text{CO}-\text{O}-\text{CH}_2-\text{CH}_2-$, protons **c** from the butyl segment of BDO), all verifying the repeating unit of PBF [103]. Regarding the end-group protons, the determined shifts were: 3.68-3.75 (2H, $\text{HO}-\text{CH}_2-\text{CH}_2-\text{CH}_2-\text{CH}_2-\text{O}$, protons **d** from the BDO end-groups) and 1.25-1.28 (3H, $\text{CH}_3-\text{CH}_2-\text{O}-\text{CO}-$, protons **e** from the ester end-groups, Figure 41 and Figure 42a) [49]. The BDO end-group $\text{HO}-\text{CH}_2-\text{CH}_2-\text{CH}_2-\text{CH}_2-\text{O}$ (**b''**) and the ester end-group $\text{CH}_3-\text{CH}_2-\text{O}-\text{CO}-$ (**b'**) both give a signal at 4.35-4.43 ppm, which is overlapped with the main butylene signal $-\text{O}-\text{CH}_2-\text{CH}_2-\text{CH}_2-\text{CH}_2-\text{O}-$ (**b**) of the repeating unit [199].

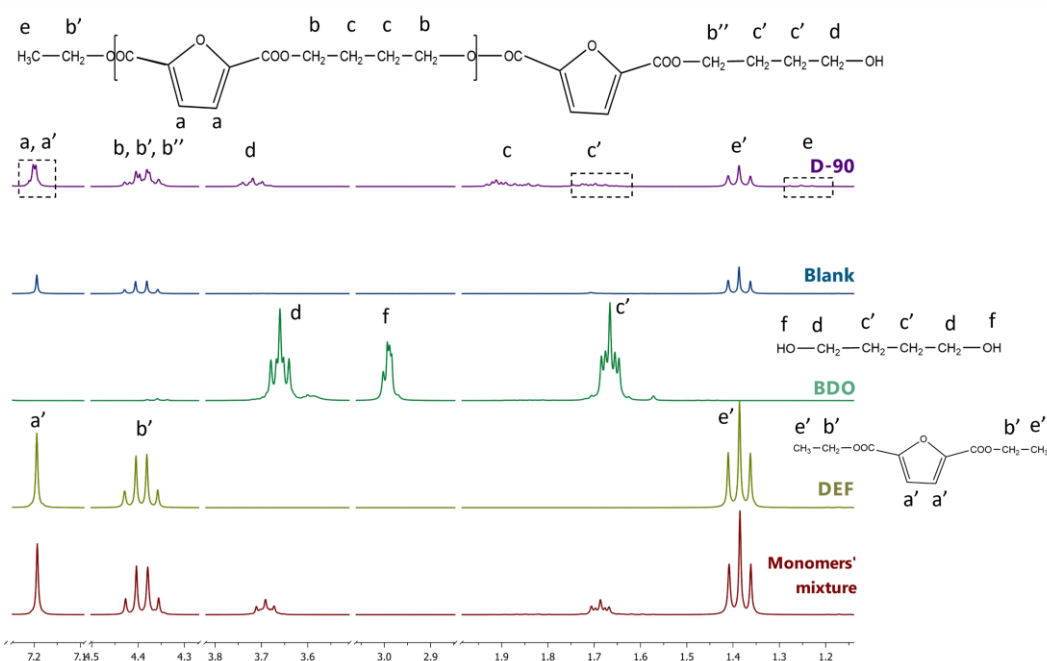


Figure 41. ^1H NMR spectra of the prepolymer D-90, the blank sample, the monomers, and the monomers' mixture. The signals in boxes are zoomed in Figure 42.

Secondary peaks were also monitored, except for the main shifts of the repeating unit (protons *a*, *b* and *c*) and the end groups (protons *d* and *e*). As regards the furan segment at 7.20, in the prepolymer's spectrum, a double peak was monitored (*a* and *a'* protons). The first one, *a*, is attributed to the prepolymer furan segment, as discussed above. The other, *a'*, which is also monitored in pure DEF, monomers' mixture and the blank sample's spectra as a single peak (Figure 42b), is attributed to the DEF furan ring, indicating residual DEF in the prepolymer's mass. The presence of residual DEF in the prepolymers is also indicated by the *e'* protons (shift at about 1.40), which are also monitored in DEF, monomers' mixture and the blank sample's spectra. This peak at about 1.40 is attributed to the DEF group CH_3-CH_2- , which differs from the *e* protons (shift at 1.25-1.28) of the prepolymer's ester end groups (Figure 41 and Figure 42a). Even though the chemical structures of the pure DEF (protons *e'*) and the prepolymers ester end group (protons *e*) are identical, this difference could be associated with the different chemical environments of the oligoester compared to the shorter, pure diester. Interestingly, a similar phenomenon was not observed in the case of PBS, where the signals of the end group protons of the oligomer and the diester (diethylene succinate) were identical (Chapter 2.4.1.1, Figure 26). This different behaviour between the two systems is probably attributed to the

different nature of the oligoesters. The furan ring is more susceptible to chemical interactions (e.g., hydrogen bonding) that may lead to shifts in the ^1H NMR spectrum compared to the aliphatic PBS. Montejo *et al.* [200] discovered the existence of different intermolecular contacts between adjacent molecules in furan by a topological analysis of the theoretical electron density and by a natural bond orbital (NBO) calculation. The researchers stated that these results could be extrapolated to the polyfuran, suggesting possible interactions between end groups of neighbouring polymer chains that could affect its properties. It was stated that these conclusions can also be extended to other conjugated polymers in which charge transfer between chains could affect properties such as conductivity. The increased tendency of the furan ring to interact (intermolecular and intramolecular interactions), especially when found in a polymer chain, could contribute to a significant shift in the ^1H NMR spectra of the polymer compared to the relevant monomer. As regards the other monomer, BDO, the hydroxyl end group peak (3 ppm), monitored in the BDO spectrum, is absent in all prepolymers spectra (Figure 41). The resonance signal of the end unit ($-\text{OH}$) proton is typically not detectable in polymers' spectra due to intra-molecular hydrogen bonding (e.g., between hydroxyl groups and the ester bonds), as discussed in Chapter 2.5.1. It is thus considered that there is no residual unreacted BDO in the prepolymers.

Finally, the c' protons (shift at about 1.64-1.75), monitored in the prepolymer, the BDO and the monomers' mixture spectra correspond to the BDO end-group protons $\text{HO}-\text{CH}_2-\text{CH}_2-\text{CH}_2-\text{CH}_2-\text{O}$ (Figure 42c). The difference between the c (butyl segment from BDO of the repeating unit) and c' (BDO end group) protons is attributed to the fact that the first ones are more protected as part of the repeating unit.

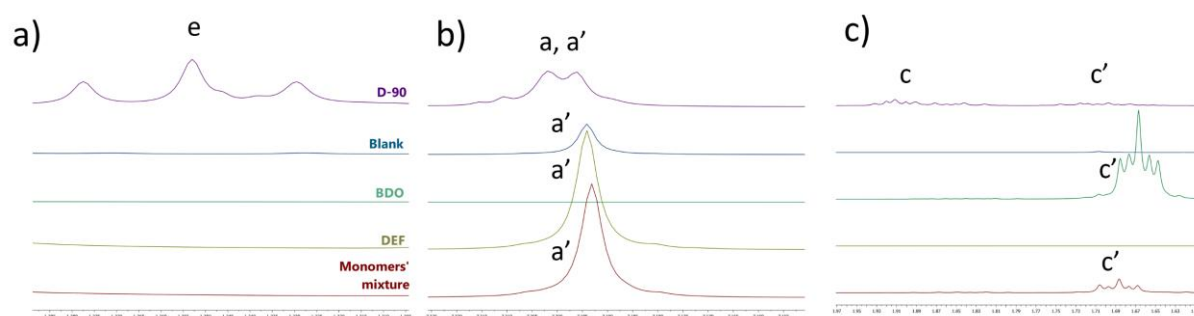


Figure 42. Zoomed ^1H NMR spectra of the prepolymer D-90, the blank sample, the monomers DEF, BDO and the monomers' mixture for the e (a), a and a' (b), c and c' (c) protons' shifts.

Summing up, the presence of the protons a , c and e explicitly in the prepolymer's spectrum confirms the formation of PBF after the herein-conducted enzymatic polymerization. Additionally, the identical spectra of the blank sample and the DEF indicate that no polymeric product was formed without using the enzyme, and BDO was removed during drying. Thus, any possible BDO residues in the prepolymers are expected to be removed during the applied drying process, in contrast to the solid DEF residues that have already been monitored in the prepolymers. The identical spectra of DEF and the blank sample align with the morphology of the obtained products: a sticky gel for the enzymatically synthesized prepolymers and a dried powder, similar to the starting material DEF, for the blank sample (Figure 43).

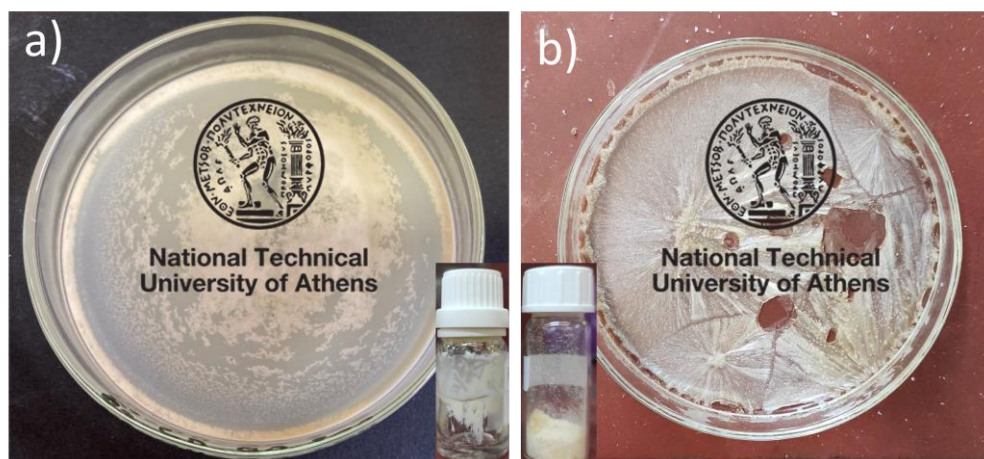


Figure 43. Morphology of the prepolymer D-90 and the relevant blank sample

The D-prepolymers' chemical structure was also verified *via* FTIR [103,201] (Figure 44a): 3153 cm^{-1} , symmetric stretching vibration of the furan C-H; 3118 cm^{-1} , asymmetric stretching vibration of the furan C-H; 2963 cm^{-1} , methylene C-H stretching vibrations; 1722 cm^{-1} , ester C=O stretching vibrations; 1574 cm^{-1} , C=C ring stretching vibrations of the furan rings; 1272 cm^{-1} , asymmetric stretching vibrations of the ester C-O-C groups; 1222 cm^{-1} , =C-O-C= ring vibrations of the furan ring; 965, and 768 cm^{-1} , C-H out-of-plane deformation vibrations of the furan ring. The broad band at around 3375 cm^{-1} is attributed to the O-H stretch in the BDO end group.

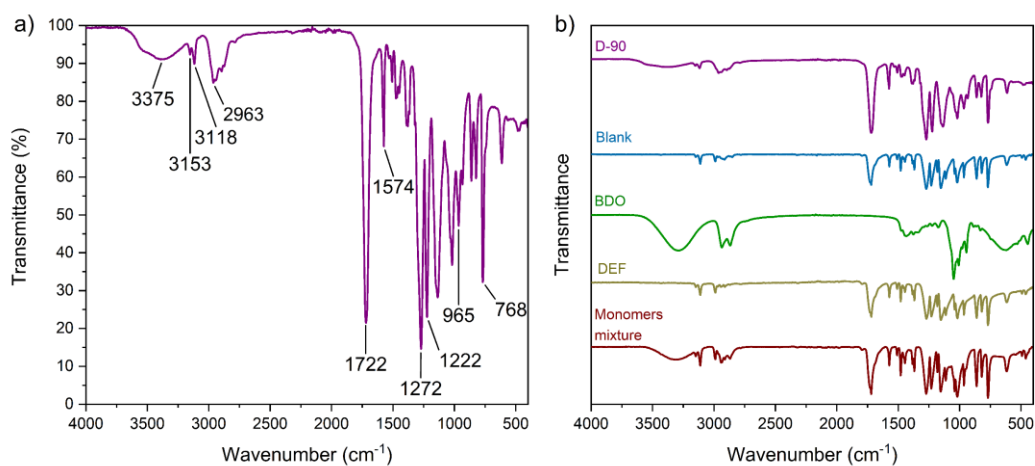


Figure 44. FTIR spectrum of the prepolymer D-90 (a) compared to the blank sample, the monomers DEF, BDO and the monomers' mixture (b).

All the obtained spectra, except for the BDO, exhibited significant similarity, especially in regions 400 to 1750 cm^{-1} , due to their comparable structural characteristics (Figure 44b). For instance, the band at 1722 cm^{-1} , attributed to the ester C=O stretching vibrations, is monitored in the prepolymer and DEF (and the monomers mixture) spectra, given that the herein-conducted polycondensation reaction is a transesterification, where the starting material is an ester and the final product a polyester. It is of high essence that the blank and the DEF spectra

are identical, thus confirming the effectiveness of the conducted polymerization and the removal of any residual BDO during drying, in agreement with the abovementioned ^1H NMR results and the macroscopical observations.

In the next step, the intensities of the hydroxyl stretch band at around 3375 cm^{-1} (monitored in every sample except for the blank and DEF) and the intensities of the ester stretching vibrations at 1722 cm^{-1} were investigated. As expected, pure BDO presented the highest OH intensity (transmittance 37%), followed by the monomers mixture (transmittance: 14%) and the prepolymer (transmittance $\sim 5\%$). In this context, the OH end group and the ester contents, proportional to the relevant intensities, were qualitatively defined. Five measurements were conducted for each sample, and the averages were calculated and presented in Figure 45 boxplots.

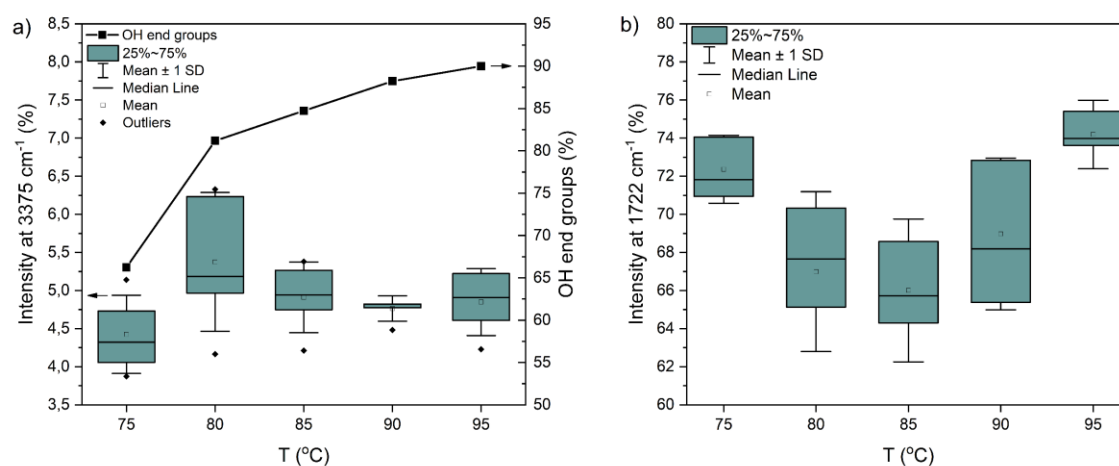


Figure 45. ^1H NMR-calculated BDO end groups percentage and peak intensities at 3375 cm^{-1} (a) and 1722 cm^{-1} (b) for the prepolymers D-75, D-80, D-85, D-90, D-95.

Starting with the OH content, it can be observed that it was similar for all the D prepolymers based on the FTIR results, while a high dispersity was monitored, indicating decreased repeatability of the measurement, probably due to the sticky morphology of the samples (Figure 45a). However, the OH end groups were also defined *via* ^1H NMR, and a clearer trend was monitored. The OH end group percentage increased almost linearly (R^2 0.828) with temperature, especially after 75°C (R^2 0.980 for $80\text{--}95^\circ\text{C}$). Extremely high OH end group percentages were reached, such as 88% at 90°C , indicating the formation of OH-rich end group oligomers. This behavior could mainly be attributed to sterical factors affecting the herein-conducted lipase-catalyzed polymerization; the low internal carbon chain length (4) and the bulky furan rings of DEF limit its access to the enzyme's active site, while permitting diol nucleophilic attack in the intermediate complexes present at lower extent compared to DES. Additionally, increased OH-end groups are expected, as BDO is more reactive than DEF, mainly due to its highly reactive hydroxyl groups. Besides this, aromatic monomers present decreased reactivity in enzymatic polyesterification [27]; aliphatic monomers (such as the herein used DEF) present lower aromaticity compared to aromatic substrates (e.g., benzene [202]), but

the furan ring is expected to show increased stability compared to a linear molecule such as BDO. Maniar *et al.* [104] investigated the impact of aromatic unit content on enzymatic copolymerization of DMFDC, BHMF, aliphatic linear diols, and diacid ethyl esters. It was shown that the furan co-polyester's MW was restricted by incorporating aromatic units in the backbone, implying that the enzyme's substrate specificity determines the total enzyme catalytic activity depending on the structural compatibility of the active site and the monomer transition state. More specifically, the researchers used N435 to synthesize different furan-based copolyesters in diphenyl ether *via* the following temperature-varied two-stage process: 80°C, under nitrogen atmosphere for 2 h (1st stage) and 80°C, at a reduced pressure of 2mmHg, for 48 h, followed by 24 h at 95°C under full vacuum (2nd stage). According to the researchers, when 2,5-furan di-methylene furanoate (FMF) molar feed fraction increased (from 25 to 50%), the \overline{DP}_n and the \overline{DP}_w of the examined co-polyester (poly(2,5-furandimethylenefuranoate-co-dodecamethylenefuranoate) or P(FMF-co-DOF)) significantly decreased from 86 and 160 to 11 and 14, respectively. The corresponding \overline{M}_n and \overline{M}_w values were 13150 to 1860 and 24500 to 2300 g·mol⁻¹, respectively.

Interestingly, after 90°C, the OH content remained almost constant; only a 2% increase was monitored when the temperature was turned from 90 to 95°C. Even though the reactants' reactivity is expected to increase with increasing temperature [103], N435 has been found to present decreased reactivity due to the beginning of protein denaturation and deactivation at temperatures above 90°C. On that basis, the efficiency of the enzymatic polymerization decreases, leading to the formation of products with properties (including the OH-end groups concentration) similar to or lower than the 90°C product's properties. The same conclusion was reached in the case of PBS (see Chapter 2.4.1.1, Figure 30). The ¹HNMR-defined ester end-group percentages at 90 and 95% were 38 and 39% (i.e., the OH end-group percentages were 62 and 61%, respectively), indicating the formation of products with similar properties.

Regarding the FTIR results and its decreased sensitivity to record the evolution of the OH end groups, a baseline shift from 4000 cm⁻¹ (Transmittance: 99%) to 400 cm⁻¹ (Transmittance: 75%) was monitored in all the prepolymers spectra (see Figure 44b), possibly implying surface-crystal contact issues. The baseline shift in ATR is a defect fostering stronger signals at lower wavenumbers (due to infrared penetration within the sample depending on the wavenumber), thus leading to intense baseline shifts [203]. This defect's intensity depends on the acquisition quality, mainly due to the surface-crystal contact. Even though during spectra acquisition, emphasis has been put on the ATR measurement protocol to minimize surface-crystal contact issues, the sticky morphology of the materials is probably responsible for inhomogeneity in the surface and thickness of the material. It is of high essence that the baseline shift phenomenon in the FTIR spectra was not obvious for PBS (see Chapter 2.4.1.1), which was in the form of a free-flowing powder providing a high, homogenous surface area.

Regarding the intensity at 1722 cm⁻¹ (Figure 45b), which is proportional to the concentration of the ester bonds (COO) along the polymer backbone and at the end of the polymer chain,

FTIR provided similar values, too. In the case of PBS, it has been found that the COO peak intensity is mainly related to the chain-end ester groups (see Chapter 2.4.1). However, in this case, as discussed above, the prepolymers present very high OH-end group concentrations (OH end group percentages up to 90%, Figure 45a); thus, the polymer backbone ester bonds are expected to dominate regarding the carbonyl stretch C=O band at 1722 cm^{-1} . On that basis, all the D-prepolymers' similar ester contents indicate similar molecular weight values. Small differences between the ester contents probably couldn't be monitored, considering the gel morphology of the samples hindering the flowless surface-crystal contact.

The molecular weights were defined *via* GPC, and the prepolymers were washed with hexane before being submitted to the analysis to remove the monitored in $^1\text{H NMR}$ residual DEF. The monomers, BDO and DEF, were also submitted to GPC analysis for comparison. In the obtained GPC chromatograms, three peaks (I, II and III) were monitored for all the tested prepolymers (Figure 46). Peaks I and II, monitored at 16.6 - 17.1 and 17.2 - 17.8 mL, respectively, correspond to PBF, in contrast to peak III, monitored at 17.8 - 18.8 mL, which is attributed to residual DEF. The molecular weights (\overline{M}_n and \overline{M}_w) of this last peak were calculated at $500\text{ g}\cdot\text{mol}^{-1}$. The difference between the real molecular weight of DEF ($212\text{ g}\cdot\text{mol}^{-1}$) and the GPC-derived values is attributed to the different chemistry of the standards used in calibration (PS) and the examined sample. The relationship between molecular weight and size depends on the type of polymer; thus, accurate molecular masses can only be obtained if the calibration standards and the samples are the same type. However, as regards the prepolymers' molecular weight values, the deviations are expected to be small since the molecule structures of the prepolymers and the standards are not significantly different (e.g., linear and branched polymers).

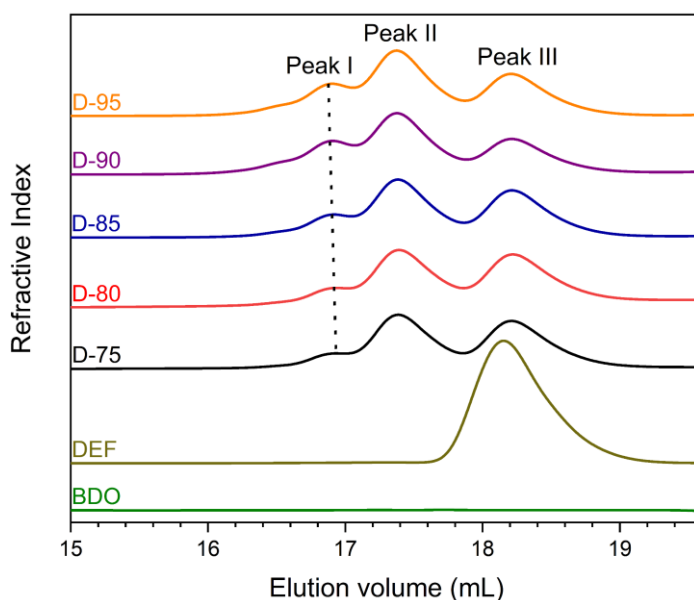


Figure 46. GPC chromatograms of the prepolymers D-75, D-80, D-85, D-90, D-95.

The presence of two different peaks corresponding to the prepolymer indicates the existence of two PBF populations of different molecular weights. The first peak represents the highest molecular weight population, while peak II indicates the presence of lower molecular weight

oligomers in all the prepolymers. In GPC, each peak intensity strongly depends on the concentration of the examined solutions. Even though the solutions have been prepared with identical concentrations, the latter may be changed during dissolution, filtration or even the measurement. As a result, the absolute intensities cannot be used to define the percentage of each population in the final products. However, the ratios of the highest-molecular-weight population (Peak I) to the lower-molecular-weight population (Peak II) and the monomer residues (Peak III) can be calculated and considered reliable indications of the different MW populations' distributions in each product.

In this context, the ratios of the intensities of Peak I/Peak II, Peak I/Peak III and Peak II/Peak III were calculated (Figure 47). Even though peak II is the dominant, presenting the highest absolute intensity values, the ratio of Peak I/Peak II intensities increases with temperature increase and reaches the highest value at 90°C. Above 90°C, the same ratio slightly decreases, remaining though higher than 75-85°C. This behavior could depend on the enzyme's efficiency, which is probably increasing above 85°C, maximizing at 90°C and slightly decreasing at 95°. The same trend was monitored for the Peak I/Peak III ratio. Even though the monomer residues are present in all the prepolymers, the intensity of the peak I ratio to the monomer residues significantly increases at 90°C. Then, it lowers at 95°C in agreement with all the abovementioned results, indicating the beginning of the enzyme's deactivation, leading to increased unconsumed monomer concentrations in the final products.

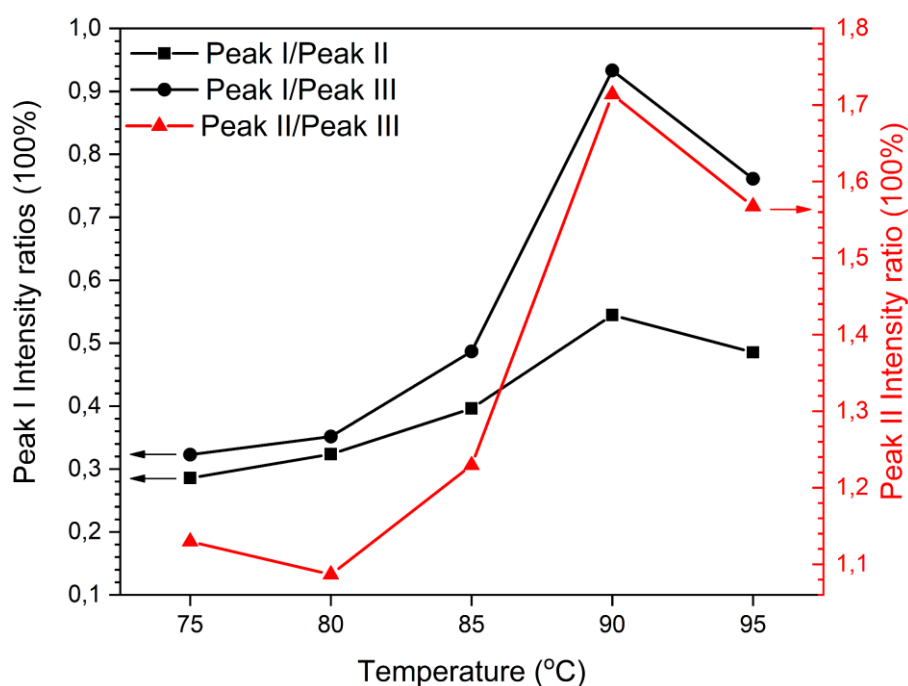


Figure 47. Intensity ratios of peaks I and II of the prepolymers D-75, D-80, D-85, D-90, and D-95, monitored *via* GPC.

The Peak II intensity is also affected by the temperature. Even though it depicts the lower molecular weight PBF fraction, its percentage inside the product mass increases at temperatures above 85°C compared to the monomer residues intensity (Peak III), and

decreases after 90°C (Figure 47). This trend means that thanks to the enzyme’s high activity at 90°C, the highest quantity of the monomers is expected to be consumed, thus leading to less residual DEF in the final product and, probably, higher molecular weight values.

The molecular weight values, defined through GPC and ¹HNMR, are presented in Figure 48. Both the \overline{M}_n and \overline{M}_w of Peak I were found similar up to 85°C, and a small increase was monitored at 90°C, reaching the values of 1700 and 1900 g·mol⁻¹, respectively. Above 90°C, no positive effect on the PBF enzymatic polymerization was noticed, confirming that the enzyme’s efficiency maximized at 90°C and then thermal deactivation began. The same trend was monitored in ¹HNMR, with lower molecular weight values defined. This phenomenon is already mentioned in the open literature and is mainly attributed to the strong dependence of the GPC results on the calibrant (see Chapter 2.4.1.1). In addition, in ¹HNMR, the distinct populations of different molecular weights cannot be detected, resulting in average MW values in contrast to GPC.

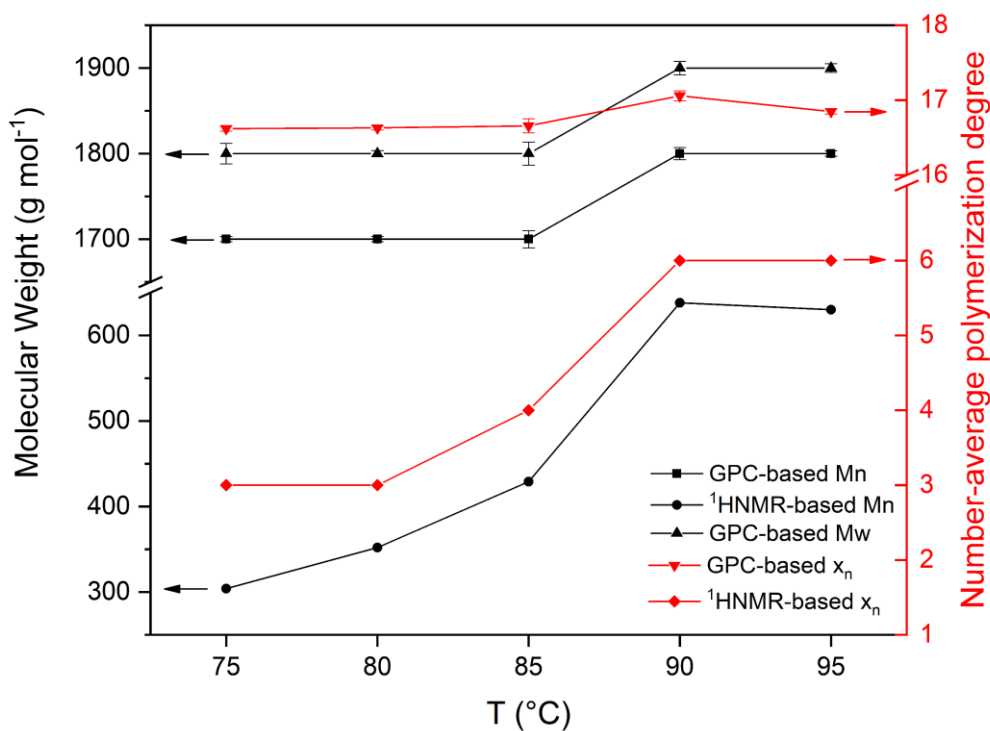


Figure 48. Molecular weights (\overline{M}_n and \overline{M}_w) and number-average polymerization degree of the prepolymers D-75, D-80, D-85, D-90 and D-95 (Peak I).

In contrast to the high-molecular-weight population (Peak I), the lower molecular weight values (Peak II) didn’t seem affected by the reaction temperature. More exactly, the dominant population presented no shifts in the chromatogram and stable molecular weight values of 1000 g·mol⁻¹ for both \overline{M}_n and \overline{M}_w (Table 12). The non-dependency of the lower molecular weight population is in line with the step-growth polymerization main principles. During the first hours, the slow reaction between the monomers leads to the formation of very low MW oligomers and insignificant MW increase. The formed oligomers react with each other for higher reaction times, leading to a noticeable MW increase.

Table 12. ¹HNMR- and GPC-calculated \overline{M}_n , \overline{M}_w and dispersity \mathcal{D} of the enzymatically synthesized PBF prepolymers

Sample	¹ HNMR-calculated			GPC-calculated			\mathcal{D}			
	\overline{M}_n (g mol ⁻¹)	\overline{M}_n (g mol ⁻¹)	\overline{M}_w (g mol ⁻¹)	\overline{M}_n (g mol ⁻¹)	\overline{M}_w (g mol ⁻¹)	\overline{M}_w (g mol ⁻¹)				
D-75	300	1700	1000	500	1800	1000	500	1.02	1.03	1.05
D-80	400	1700	1000	500	1800	1000	500	1.02	1.03	1.05
D-85	400	1700	1000	500	1800	1000	500	1.03	1.03	1.04
D-90	600	1800	1000	500	1900	1000	500	1.04	1.03	1.04
D-95	600	1800	1000	500	1900	1000	500	1.04	1.03	1.04
E-90	400	1800	1000	500	1800	1000	500	1.02	1.03	1.05
E-95	200	1400	800	400	1400	800	400	1.03	1.03	1.05
F-90	300	1600	900	400	1600	900	400	1.04	1.03	1.05
F-90_24	400	1700	900	400	1800	900	400	1.06	1.03	1.03
F-95	200	1500	900	400	1600	900	400	1.04	1.03	1.05
D-90_3g	300	1600	900	400	1700	900	400	1.06	1.03	1.05
D-90_6g	n.d.	1600	900	400	1600	900	400	1.04	1.03	1.05

Even though the achieved MW values are not considered high, they seem satisfying compared to relevant values reported in the open literature. Comerford *et al.* [102], synthesized PBF oligomers in the presence of N435 based on the following solvent-free process: 50°C for 6 h at atmospheric pressure and 18 h at 20 mbar maintaining the reaction temperature. The achieved MW values were 600 and 500 g·mol⁻¹ (\overline{M}_w and \overline{M}_n , respectively). The low achieved MW was probably due to the low reaction temperature compared to the herein-applied process.

It is of high essence that even though the enzymatic polymerization of PBF is very limited in the open literature, the phenomenon of the co-existence of two molecular weight PBF populations has been mentioned once. More precisely, Jiang *et al.* [103] synthesized PBF using N435 in diphenyl ether. The first stage was conducted at 80°C for 2 h under nitrogen atmosphere. Then, the pressure was reduced to 2 mmHg for 24 h while maintaining the reaction temperature at 80°C, and then the reaction temperature was increased to 95°C for another 24 h. Finally, the reaction temperature was regulated at 95, 120 or 140°C for the last 24h. The researchers found that the proportion of the low molecular weight fraction, which was named oligo(butylene furanoate) or OBF and presented \overline{M}_w of about 500 g·mol⁻¹, increased as the reaction temperature increased from 80 to 140°C. This trend was attributed to different reasons, including the high crystallization ability of OBF and the lower catalytic reactivity of

CALB at temperatures above 90°C. Another factor leading to the increase of the low molecular weight fraction, could be the diol dehydration due to the elevated reaction temperatures [103]. Since BDO could not react with the ester monomer at higher temperatures, the enzyme catalyzed the recombination of the short-chained oligomers, increasing the low molecular weight fraction. On the contrary, in our case, at 95°C, a decrease in both the high and low molecular weight fractions was monitored, as mentioned above (Figure 47). This trend could indicate that due to the decreased efficiency of the enzyme at 95°C the monomers' reaction was catalyzed by the enzyme, thus producing some oligomers of even lower MW (e.g., dimers) and leading to decreased high- and low-molecular-weight fractions (of \overline{M}_n 1900 and 1000 and \overline{M}_w 1900 and 1000 g·mol⁻¹).

Turning to the thermal characteristics of the products, all the prepolymers were submitted to DSC before and after washing with hexane (Figure 49). Also, the monomers BDO and DEF were submitted to DSC for comparison reasons. During the first heating (Figure 49a), a broad endotherm, indicating the formation of an oligomer, was monitored for the D-90 sample at 30 to 85°C. It is of high essence that after washing with hexane, there was a clearer distinction of the endotherm into two broad but separated melting peaks. The first endotherm, at 48°C, indicates residual DEF, in line with the abovementioned results; pure DEF presented a sharp melting point at about 50°C. The second endotherm, at 75°C, is attributed to the PBF oligomer melting. The first heating curves were similar for all the D-prepolymers.

During cooling, the hexane-washed D-90 crystallized slightly (ΔH_c 2 J·g⁻¹) at 18°C (Figure 49b, Table S4). For the unwashed D-90, crystallization occurred at 13.5°C (ΔH_c 1 J·g⁻¹), closer to the DEF crystallization temperature (T_c 9.5°C), probably indicating that crystallization of both the oligomer and the residual DEF occurred, with the latter being more intense for the unwashed D-90. The monitored crystallization temperatures are significantly lower than the chemically synthesized PBF reported values in the open literature (T_c ~108°C [204]), which is attributed to the low molecular weight of the herein synthesized oligoesters. As already discussed (Chapter 2.4.1), the high molecular weight polymers typically present higher crystallization temperatures due to increased ease of chain folding compared to the lower molecular weight grades and the decreased number of end groups, acting as defects slowing down the crystallization process. In addition, the presence of residual DEF in the prepolymer matrix may also hinder the alignment of the formed chains. Except for the crystallization, another thermal transition was monitored from -20 to -40°C during cooling for both the unwashed and washed with hexane D-90 samples.

The same transition from -20 to -40°C was also monitored during the second heating of the samples. Interestingly, Jiang *et al.* [103] who enzymatically synthesized PBF oligomers of \overline{M}_w 5500 g·mol⁻¹ and submitted it to DSC analysis, received an identical thermal transition at about -30 to -40°C. Even though the morphology of this transition resembles a glass transition temperature, the PBF T_g is reported to be significantly higher in the open literature (ca. 36–44°C) [204–207]. This transition could be related to the existence of two molecular weight populations observed in the present and the abovementioned work. More precisely, the lower

molecular weight population, having minimal energy requirements, could acquire enough mobility at very low temperatures to transition from a solid to a more flexible state. On the other hand, the expected T_g (at about 36-44°C) is not monitored in the prepolymers' DSC curves, probably because the higher molecular weight population is not dominant in the oligomer mass, as evidenced by GPC. During the second heating, cold crystallization occurred for the unwashed and hexane-washed D-90, which was followed by melting at about 75°C, significantly lower than the chemically synthesized PBF melting point of 164-173°C [204–208], attributed again to its lower molecular weight values. The monitored melting point after washing was hexane was slightly higher than before (72°C). A shoulder is also monitored in the product's endotherm due to the residual DEF melting. Based on the second heating DSC curve, the amorphous character of the herein synthesized PBF oligomers can be assumed even though DEF residues melt in the same temperature window.

No BDO residues are observed since BDO presents its main melting peak at 19°C and an endotherm at -30°C, probably attributed to impurities. More exactly, crude 1,4-butanediol is known to contain impurities of low freezing points (e.g., 1,4-hydroxyacetoxybutane: -65°C; γ -butyrolactone: -44°C) and impurities forming azeotropic mixtures with 1,4-butanediol, being thus difficult to separate through distillation [209]. Another explanation of the BDO double endotherm could be the presence of two distinct solid forms [210], a phenomenon already reported in the literature for 1,4-butanediol; however, this is not highly possible as the reported melting points have been close to each other (16 and 19°C).

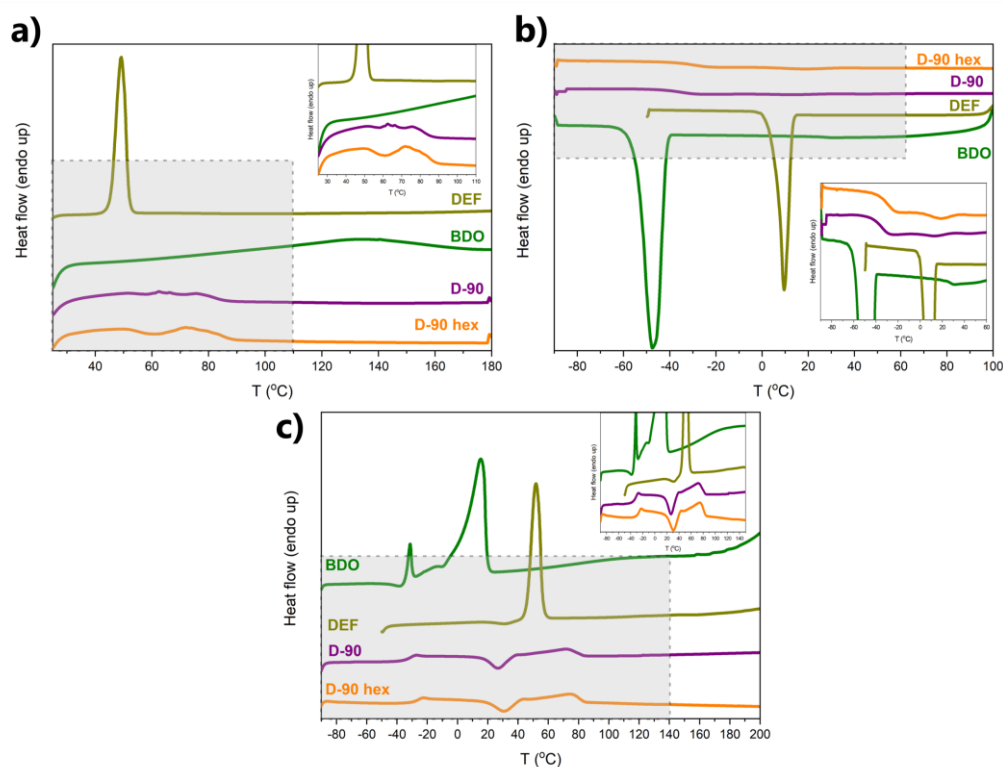


Figure 49. DSC curves of the monomers BDO, DEF and the prepolymer D-90 before and after washing with hexane: (a) first heating; (b) cooling; (c) second heating

Regarding TGA, all grades presented a two-step decomposition profile (Figure 50). Molecular weight is a critical parameter influencing polymers' thermal decomposition (see Chapter 2.4.1.3). More precisely, lower molecular weight polymer (and oligomer) grades such as PBS and PCL have been found to decompose in multiple-step mechanisms in contrast to the higher molecular weight grades that usually decompose in single- and sometimes two-step mechanisms. The main reason for this different behavior is that the lower molecular weight grades are more easily involved in different decomposition reactions due to increased end-group concentration. However, the effect of the molecular weight on the decomposition mechanisms seems to eliminate above a critical molecular weight. The first decomposition step was conducted for all the prepolymers at 278°C and the second at about 384°C (Table 13), slightly lower than the relevant value of the chemically synthesized PBF in the open literature (i.e., 387°C) [204]. It is of high essence that Jiang *et al.* [103] reached similar conclusions, as the enzymatically synthesized PBF grade presented a two-step decomposition profile, with the first step before 350°C being attributed to the lower molecular weight population.

Table 13. Thermal properties (TGA) of the enzymatically synthesized PBF prepolymers

Sample	$T_{d,5\%}$ (°C)	T_d (°C)	T_d (°C)	Residue (%)
D-75	174	281	386	5.31
D-80	226	280	380	2.75
D-85	178	275	384	2.37
D-90	211	278	382	3.39
D-95	181	268	382	3.24
E-90	203	271	385	0.66
E-95	183	272	384	2.73
F-90	159	275	382	1.15
F-90_24	199	282	385	2.19
F-95	180	278	384	1.47
D-90_3g	178	275	370	4.8
D-90_6g	169	274	385	2.28

Even though washing with hexane does not affect the decomposition temperature (T_d) of the prepolymers, $T_{d,5\%}$ was significantly affected as expected. D-90 presented $T_{d,5\%}$ of 182°C, 29°C lower than D-90 hex ($T_{d,5\%}$ of 211°C). The DEF mass loss in D-90 was more intense due to its higher amount. The monomers' mass loss (due to evaporation) occurs at about 200°C, significantly lower than the first decomposition step of the products. The monomers' mixture decomposes at 253°C, higher than the pure substances, probably indicating intermolecular interactions (e.g., hydrogen bonding between the BDO hydroxyl groups and DEF ester bonds) requiring additional energy to decompose, but still lower than the first decomposition step of the products.

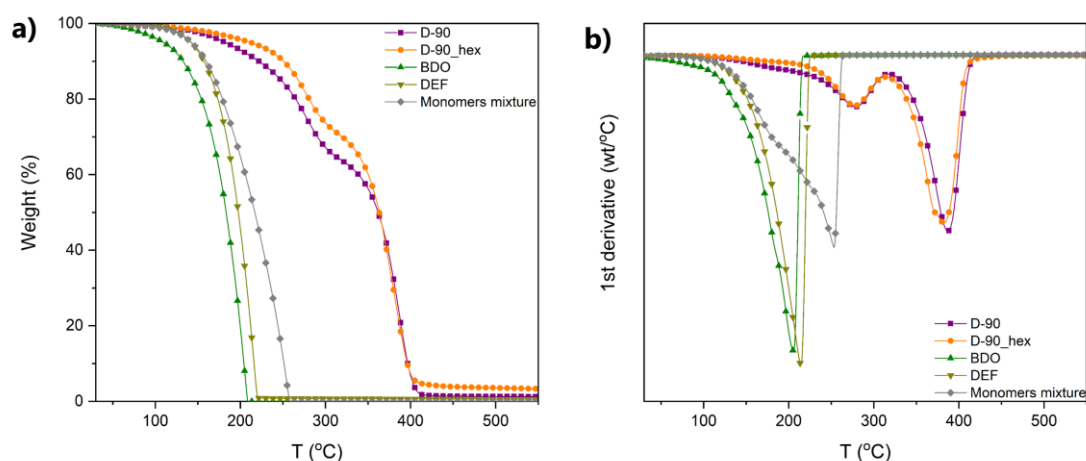


Figure 50. TGA curves of the monomers BDO, DEF, monomers' mixture and the prepolymer D-90 before and after washing with hexane: (a) weight curves; (b) 1st derivatives

3.4.1.2 Study of the recyclability potential of the immobilized *Candida antarctica* Lipase B (N435) for PBF enzymatic prepolymerization

The recyclability of the biocatalyst N435 has been studied to an extent in the open literature on enzymatic polymerization systems for the production of aliphatic polyesters, including PBS, as will be discussed later. However, we decided to focus on the recyclability of the enzyme on a more challenging polymerization system, i.e., for the production of furan-based polyesters such as PBF. In order to study the recyclability potential of the biocatalyst, its activity before and at the end of the reactions conducted under different temperatures (80, 85, 90 and 95°C) was defined (Figure 51). As discussed in Chapter 3.3.1.1, the protein loading of N435 was considered 10% wt and the relevant initial activity was calculated at $1.39 \cdot 10^{-2} \pm 7.98 \cdot 10^{-4}$ Units·mg⁻¹, with an RSD of 6%.

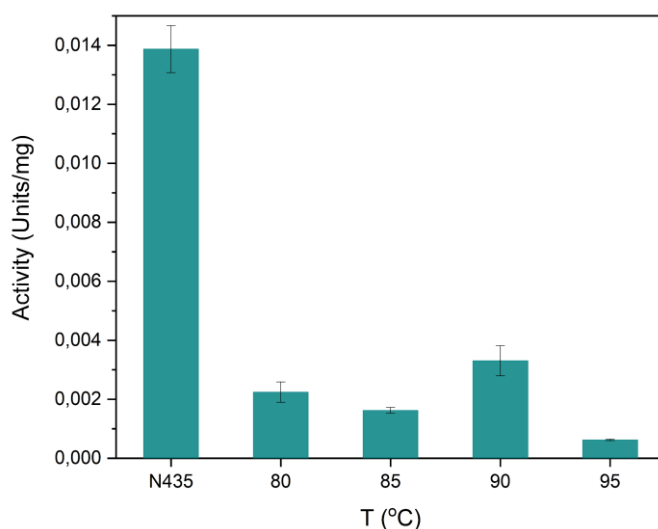


Figure 51. Initial activity of N435 compared to the defined activity at the end of the PBF enzymatic prepolymerization reactions at 80, 85, 90 and 95°C

Based on the assay results, the enzyme was significantly downgraded after the prepolymerization reactions. Even for the temperature of 80°C, the enzyme activity decreased by 76%, while at 95°C it decreased by more than 90%. Thus, the enzyme cannot be reused after being submitted to these conditions in this system.

A recyclability study of N435 has been conducted by Guckert *et al.* [95], who used 10% of the enzyme relevant to the monomers mass in polymerization reactions to synthesize PBS at 90°C for a reaction time of 90 min. The recyclability of the enzyme was evaluated by its reuse in different PBS synthesis cycles; the amount of the by-product in each cycle was monitored. The researchers found that the amounts of the by-products were similar for the first four cycles, while a small reduction was observed after the fifth and sixth cycles. The end of the reuse process was defined after the seventh cycle, where a decrease of 56% in the by-products' amount was reached. The enzyme's activity was assessed after seven cycles, and almost 88% decreased compared to the initial activity. To increase the enzyme's recyclability, the researchers conducted a make-up procedure with 25% of its mass replaced by a new enzyme. When it was submitted to a new synthesis cycle, the results obtained were higher than the fifth cycle. As regards the MW of the obtained products, the \overline{M}_w was unaffected until six reuse cycles, in contrast to the \overline{M}_n being in line with the monitored by-product amounts, remaining similar for the first four cycles. Very low molecular weight oligomers (dimers or trimers) were monitored after seven reuse cycles.

Other relevant studies focusing on the reuse of N435 are presented below. Nasr *et al.* [88] used diethyl adipate (DEA) and 1,6-hexanediol in bulk and solution systems (diphenyl ether) at 100°C with 10% wt of the enzyme. They concluded that the poly(hexylene adipate) \overline{M}_n remained constant over three cycles in bulk, while a decrease of 17% was observed in solution. Poojari *et al.* [61] reported the N435 recovery and reuse for up to ten reaction cycles during PCL synthesis in toluene at 70°C for 4h. High molecular weights (\overline{M}_w 50000 g·mol⁻¹) were constantly achieved. It was also stated that the multiple reuse cycles of N435 would be unattainable if leaching of CALB occurred due to physical desorption during polymer synthesis or if it was submitted to high mechanical shear (e.g., intense mechanical stirring). Weinberger *et al.* [211] used N435 for the enzymatic polymerization of dimethyl adipate (DMA) and BDO at 70°C and 70 mbar for 4 h. The researchers found the enzyme stable for over nine cycles, with conversion rates between 92 and 94%. Finally, Adhami *et al.* [62] conducted eROP of lactones to produce PCL using N435 in a flow tubular reactor. Due to the decreased reaction time of each cycle, the researchers synthesized PCL in toluene at 70°C for a reaction time of 30 min (for each cycle) while reusing the enzyme more than ten times. The achieved molecular weight and conversion values were slightly lower than the fresh enzyme after the eighth run.

Interestingly, even though N435 seems stable for several cycles in the open literature, in our case, it was proved incapable of reusing after the first cycle. The common characteristic of all the abovementioned systems is the monomers' aliphatic character. Considering this, one could assume that the presence of the bulk furan rings in our system could affect the overall stability of the enzyme. For instance, the increased tendency of the furan ring to interact (intermolecular

and intramolecular interactions), especially when found in a polymer chain, could affect the enzyme's stability and lead to a faster decrease in its activity. To the best of our knowledge, only Jiang *et al.* [103] have attempted to synthesize PBF and investigate the enzyme's recyclability. CALB was recycled from a temperature-varied two-stage enzymatic polymerization with DMFDCA in diphenyl ether using the following conditions: (1) 80°C, 26 h; (2) 95°C, 24 h; (3) 120°C, 24 h. Enzymatic ring-opening polymerization of ϵ -caprolactone (CL) was performed with fresh and recycled CALB to verify the enzymatic catalytic reactivity of the recycled CALB. The polymerization reactions were conducted in toluene at 70°C for 24 h under a nitrogen environment. The obtained PCL products formed with the recycled enzyme presented the \overline{M}_n and \overline{M}_w up to 62 and 60% decreased, compared to the fresh enzyme product. Thus, it was concluded that the reactivity of the used CALB decreased and was attributed mainly to the elevated temperatures leading to the unfolding and/or inactivating.

3.4.1.3 Investigation of the pressure impact on the PBF enzymatic prepolymerization process

Given the improved characteristics of the D-90 and D-95 prepolymers, the reduced pressure effect was studied at 90 and 95°C to enhance the by-product (ethanol) removal rate *via* evaporation and diffusion. In samples E-90 and E-95, the pressure was set at 20 mbar, and the reference prepolymers were D-90 and D-95 (200 mbar).

The chemical structure of the prepolymers was verified *via* FTIR and ^1H NMR, and the hydroxyl and ester contents were also monitored. Regarding the FTIR results, the ester and hydroxyl contents were found to be similar for both 90 and 95°C (Figure 52a and b, respectively), probably indicating surface-crystal contact issues, as an intense baseline shift was observed in this case, too (see Chapter 3.4.1.1). On the other hand, ^1H NMR revealed several differences in the hydroxyl end groups of the prepolymers. In both E-90 and E-95, the OH end groups decreased; this reduction can be attributed to the loss of unreacted BDO, leading to ester end group richer oligomers. Another reason could be the sublimation of several already formed OH-rich oligomers due to the applied high vacuum. The most intense reduction (from 90 to 31%), monitored at 95°C, can be also related to the enzyme thermal deactivation, which is expected to begin at this temperature. Due to a slow reaction rate at 95°C, the recombination through diffusion and reaction on the enzymatic support of the existing, non-sublimated OH-rich oligomers, which would increase the calculated OH percentage of the prepolymer, did not proceed sufficiently. On the contrary, at 90°C, where a higher reaction rate is expected (due to increased enzyme activity), the recombination of a sufficient amount of the existing OH-rich oligomers led to a less significant hydroxyl end group decrease in the final product (from 88 to 59%), as some of the ester end groups were consumed leading to a less intense OH-end groups reduction.

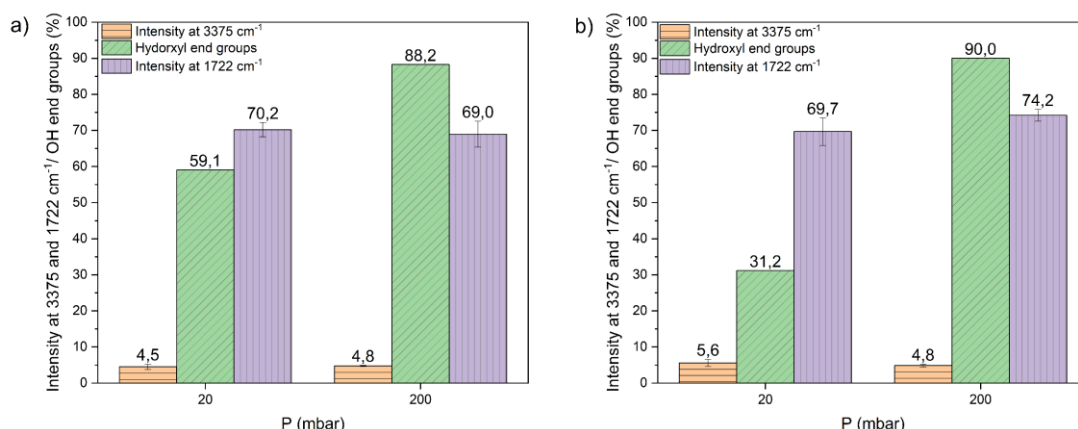


Figure 52. Peak intensity at 3375 cm⁻¹ and 1722 cm⁻¹ and ¹H-NMR-calculated hydroxyl end groups percentage for the prepolymers (a) E-90 compared to D-90 and (b) E-95 compared to D-95

The molecular weights of the samples, calculated *via* ¹H-NMR and GPC (Table 12), were also affected by the reduced pressure. Based on the GPC results, E-90 presented similar molecular weight values to D-90 (\overline{M}_n 1800 g·mol⁻¹; \overline{M}_w 1900 and 1800 g·mol⁻¹ for D-90 and E-90, respectively). On the contrary, E-95 presented significantly lower molecular weight values than D-95, reaching 1400 g·mol⁻¹ (\overline{M}_n and \overline{M}_w of D-95 were 1800 and 1900 g·mol⁻¹, respectively). The \overline{M}_n and \overline{M}_w of the second peak were also affected, both reaching 800 g·mol⁻¹ (instead of 1000 g·mol⁻¹ of the D-95). A significant reduction (about 66%) was also monitored in the ¹H-NMR-calculated \overline{M}_n at 95°C in line with the abovementioned GPC results. The intense MW reduction at 95°C can be attributed to the following interdependent reasons: first, the unreacted BDO loss due to high vacuum disrupts the reaction's stoichiometric balance, leading to low polymerization degrees. Second, the decreased enzyme efficiency at 95°C (due to thermal deactivation) leads to a reduced reaction rate and formation of only low molecular weight oligomers with any remaining BDO. On the contrary, the high enzyme efficiency at 90°C leads to the formation of higher molecular weight oligomers and the recombination of the existing ones, thus balancing the sublimated oligomers loss and resulting in similar MW values with D-90. Finally, the extended sublimation of the lower molecular weight oligomers that are formed, disturbs the reaction equilibrium as part of the reactants is removed.

The thermal properties of the prepolymers weren't significantly affected by the reduced pressure (Table 13). The decomposition occurred in two stages, attributed to the different molecular weight populations, at 271-278°C (1st stage) and 382-385°C (2nd stage) for the prepolymers synthesized at 90°C (D-90 and E-90) and at 268-272°C (1st stage) and 382-384°C (2nd stage) for the prepolymers synthesized at 95°C (D-95 and E-95). The E-90 prepolymer's $T_{d,5\%}$ was found to be slightly lower than D-90 (203 vs 211°C), while $T_{d,5\%}$ was found similar for the E-95 and D-95 (183 and 181°C, respectively). On that basis, it can be considered that the prepolymers synthesized at 90°C are superior to those synthesized at 95°C, and the reaction temperature is the most crucial parameter affecting their quality. It can be thus concluded that

the process is mainly controlled by the chemical reaction itself, and not the by-product removal rate through vacuum application.

It is of high essence that for the case of PBS, it was concluded that at the temperature of 90°C, the higher vacuum resulted in a slightly higher overall quality of the prepolymer, i.e., in terms of molecular weight, melting characteristics and thermal stability (Chapter 2.4.1.2), while a similar conclusion was not reached for the case of PBF. The noticeable difference between the two systems is the nature of the reacting monomers; the bulky furan rings of the aliphatic DEF and PBF compared to the aliphatic DES and PBS probably limit the ethanol molecules' movement through the reaction mixture, thus impeding the ethanol removal *via* (evaporation and) diffusion.

3.4.1.4 Investigation of the reaction time impact on the PBF enzymatic prepolymerization process

Given the insignificant effect of the reduced pressure at 90°C and its negative effect at 95°C, a higher reaction time (6 h) was then studied as a parameter at 90 and 95°C, at a pressure of 200 mbar (F-90 and F-95, respectively). The reference prepolymers were D-90 and D-95 (2 h, 200 mbar).

The chemical structure of the prepolymers was verified *via* ¹HNMR and FTIR, and the hydroxyl and ester contents were also monitored. Regarding the ¹HNMR results, the hydroxyl end group percentage decreased slightly at 90°C and significantly at 95°C (Figure 53a and b, respectively). The slight decrease in the F-90 sample compared to D-90 can be attributed to slightly greater BDO consumption after 6 than 2 h of reaction; the enzyme efficiency has been found to maximize at 90°C (see Chapter 3.4.1.1), meaning that BDO was participating in the occurring reactions and after 6 h it was not as abundant as it was after 2 h. It is interesting to note that the defined OH-end group percentage of F-90 (75%) was lower than D-90 (88%) but higher than E-90 (59%), confirming the effect of the lower pressure (i.e., loss of unreacted BDO) on the end-group distribution discussed in Chapter 3.4.1.2. The significant decrease in the OH-end group percentage at 95°C for 6 h of reaction is related to the time-dependent thermal inactivation of the enzyme. As the reaction time increases, the enzyme efficiency decreases, forming (OH-rich) oligomers with very low molecular weights. These oligomers are prone to sublimation and/or degradation, thus decreasing the hydroxyl-terminated oligomers number. Regarding the FTIR results, the hydroxyl contents were similar for the prepolymers formed at 90°C and 95°C (Figure 53a and b, respectively), probably implying the already discussed surface-crystal contact issues, considering also that an intense baseline shift was observed. Similar ester contents were also monitored for the prepolymers synthesized at 90°C, while a small but noticeable reduction was observed in the ester content of the prepolymer synthesized at 95°C after 6 hours of reaction. This reduction indicates the decreased molecular weight of the F-95 prepolymer; the ester band signal is proportional to the backbone ester

bonds and not to the ester-end groups, given that OH-end groups dominate in PBF prepolymers.

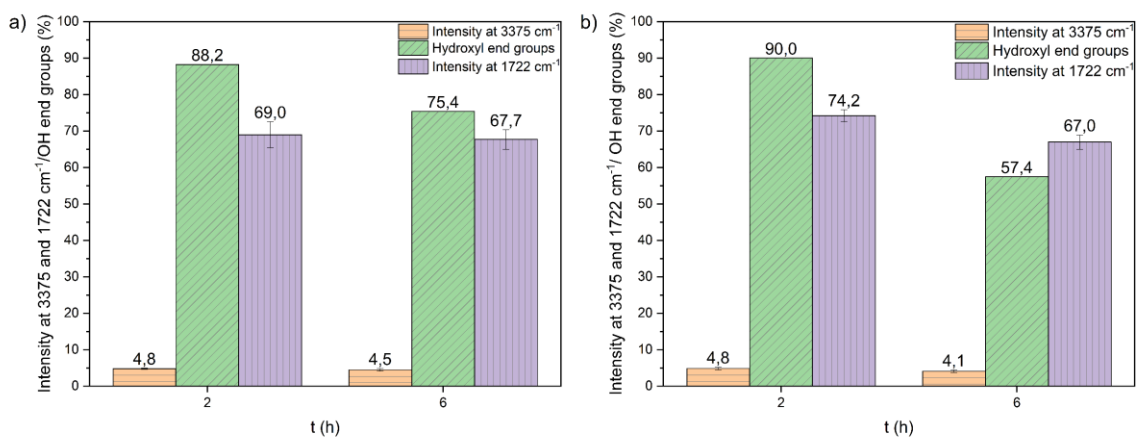


Figure 53. Peak intensity at 3375 cm⁻¹ and 1722 cm⁻¹ and ¹H-NMR-calculated hydroxyl end groups percentage for the prepolymers (a) F-90 compared to D-90 and (b) F-95 compared to D-95

The samples were submitted to GPC, and the following chromatograms were obtained (Figure 54). The longer reaction time negatively affected the polymerization for both 90 and especially 95°C, with all the peaks being shifted to higher elution volumes, indicating lower molecular weight values. More specifically, the \overline{M}_n and \overline{M}_w decreased by 11 and 16%, respectively, both reaching the value of 1600 g mol⁻¹ at 90°C. It can be stated that the system may have reached equilibrium due to increased active end groups consumption. Thus, increased by-product amounts were formed, requiring a higher vacuum to be removed, leading to by-product accumulation within the reacting mass and alcoholysis reactions. It is of high essence that the same conclusions were reached when PBS was submitted for prolonged reaction times at the optimum temperature of 90°C (Chapter 2.4.1.3).

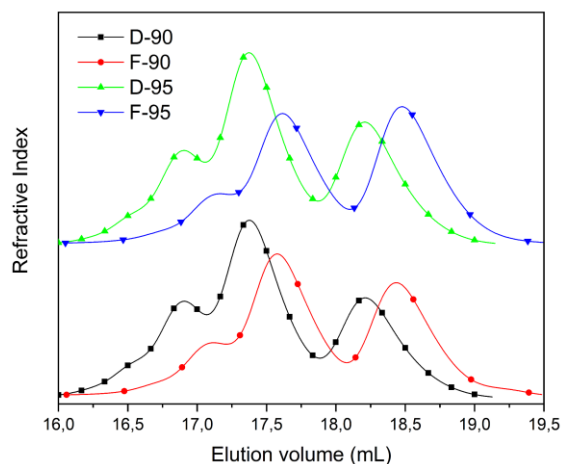


Figure 54. GPC chromatograms for the F-90 and F-95 prepolymers compared to the D-90 and D-95

In order to confirm the hypothesis mentioned above, a supplementary experiment was decided to be conducted. Even though the very extended reaction times at the temperature of 90°C would question the green character of the process due to significant energy requirements, 24 h was tested as the second stage reaction time. Based on the GPC analysis results, the 24 h-product presented similar MW to the 6 h-product, lower than the 2-h product D-90 (Figure 55). An identical trend was monitored in the ¹HNMR results, thus confirming that 2 h is the optimum reaction time for the second prepolymerization stage and higher reaction times do not favor the process.

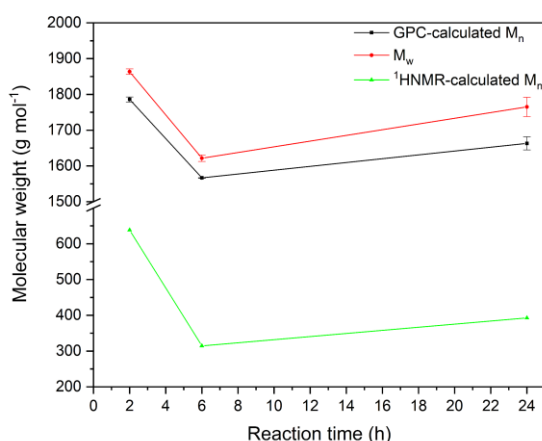


Figure 55. Molecular weights of the D-90, F-90 and F-90_24 prepolymers

As regards 95°C, both \overline{M}_n and \overline{M}_w presented a decrease of 17%, reaching the values of 1500 and 1600 g mol⁻¹, respectively. Thus, the enzyme's time-dependent thermal inactivation beginning at 95°C is confirmed, in line with the FTIR-defined ester content, which was reduced for the prepolymer synthesized at 95°C for 6 hours. It is of high essence that the obtained MW values are slightly higher than the relevant values of the prepolymer synthesized at 95°C under reduced pressure (E-95), indicating the negative effect of the high vacuum (i.e., the unreacted BDO loss, disruption at the reaction equilibrium as the low MW oligomers were sublimated) on the polymerization (see Chapter 3.4.1.3). The same trend was monitored in the ¹HNMR results (Table 12), with the defined MW being significantly lower than the reference sample D-95, implying the enzyme's time-dependent inactivation at 95°C.

The monitored during TGA decomposition temperatures of the samples prepared at 90°C remained similar as expected, in contrast to the $T_{d,5\%}$ that presented significant differences (Figure 56). In line with the GPC results, $T_{d,5\%}$ of F-90 was defined at 159°C, 52°C lower than the reference prepolymer D-90 ($T_{d,5\%}$ 211°C). The supplementary experiment product (reaction time 24 h) presented a higher than F-90 $T_{d,5\%}$ of 199°C, but still lower than the reference prepolymer. As regards the prepolymers prepared at 95°C, similar thermal properties were monitored for them both (2 and 6 h), with $T_{d,5\%}$ at 180-181°C (Table 13), implying that thermal deactivation dominates the system and leads to the formation of products with inferior properties.

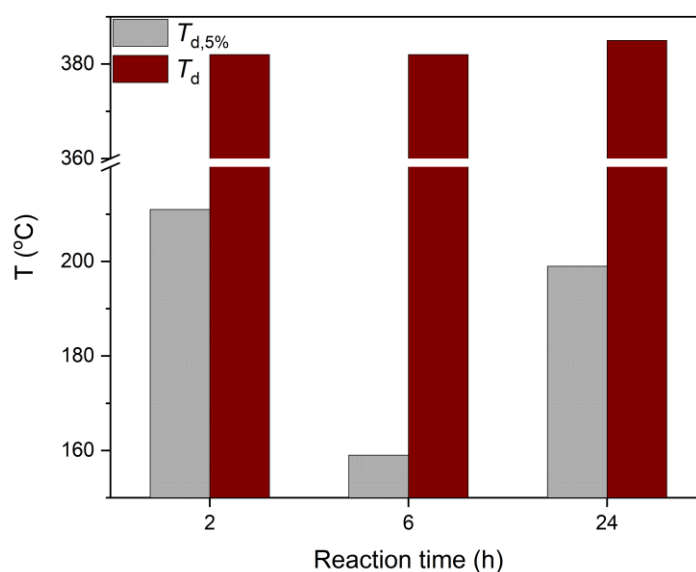


Figure 56. T_d and $T_{d,5\%}$ of the prepolymers D-90, F-90 and F-90_24

3.4.2 Analysis of the scaling-up potential of the optimized PBF enzymatic prepolymerization process: 3 and 6g

The prepolymers synthesized at 90 and 95°C under 200 mbar for 2 h (D-90 and D-95) presented the highest performance in terms of molecular weight (\overline{M}_n 1800 and 1900 g·mol⁻¹) and thermal properties (T_{m2} 75 and 77°C, $T_{d,5\%}$ 211 and 181°C). Even though their characteristics were similar, D-90 was selected to be scaled up (3 and 6 g) as its synthesis reaction temperature was lower (90°C), permitting lower energy requirements in line with the main principles of green chemistry. It is also important that the herein applied process can be considered scalable, considering that it is a low-temperature bulk polymerization technique that does not require multiple solvents for the final product isolation.

Regarding the scaled-up products' macroscopical morphology, D-90_3g was similar to the D-90 and all the synthesized on a small scale (1g) prepolymers, i.e., a sticky yellowish gel (Figure 57a). On the other hand, the D-90_6g was received in a flowing, dark yellow form (Figure 57b), indicating a lower polymerization degree and probably a higher amount of residual DEF having a similar dark yellow color.

The samples were submitted to GPC, and a noticeable decrease in the MW values was monitored compared to the small-scale grade D-90 (Figure 58). The most significant decrease was monitored in the \overline{M}_w of the 6g-scale PBF grade, i.e., 16%. Similar to the PBS scaling-up process, the \overline{M}_n was less affected (10%) compared to the \overline{M}_w , implying that the formation of the longer chains was restricted, probably due to mass transfer limitations that are more intense on large scales. For example, the by-product quantity increases while the vacuum remains constant, leading to reduced removal rates. In agreement with the GPC results, an

identical trend was monitored in the $T_{d,5\%}$ values (Figure 58), defined *via* TGA, in contrast to the maximum decomposition temperatures that remained constant, as they are not dependent on the MW differences.

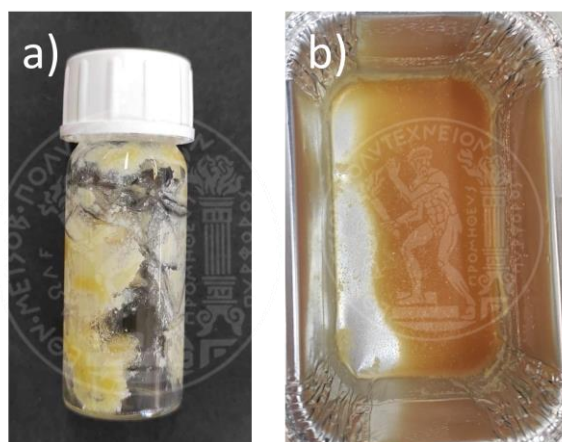


Figure 57. Morphology of the scaled-up prepolymers D-90_3g (a) and D-90_6g (b)

Except for the MW values, the scaled-up prepolymers' OH end groups decreased compared to the small-scale prepolymers. For instance, D-90_3g presented a hydroxyl end group percentage of 65% instead of 88% (OH-end group percentage of D-90). Similarly to the PBS scaling-up process, even though the formation of OH-rich oligomers is expected during lipase-catalyzed polymerization, mainly due to the limited diester accessibility to the active site (attributed to the low internal carbon chain length and the presence of bulky furan rings in the case of DEF), the mass transfer limitations may affect the reactants' concentration leading to a diverse distribution of end groups on larger scales.

Overall, the scaled-up prepolymer, at the scale of 3 g, was selected to be submitted to the following post-polymerization tests (Chapter 5.4.2) due to its similar morphology and MW values with the product of the 1g-scale, D-90.

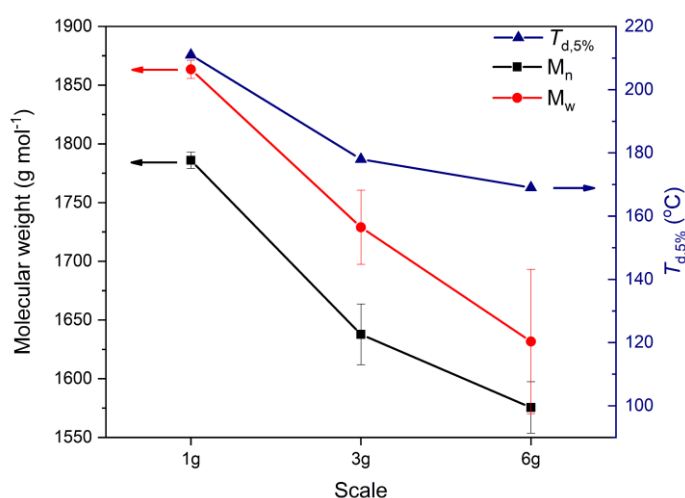


Figure 58. Molecular weights and $T_{d,5\%}$ of the scaled-up prepolymers D-90_3g and D-90_6g compared to D-90

3.5 Conclusions

This chapter examines the ability of immobilized *Candida antarctica* Lipase B as a biocatalyst in a solvent-free system to produce PBF. The enzymatic synthesis was conducted in two stages, with the first at milder conditions (50°C, atmospheric pressure, 24 h) to minimize possible monomers' losses. The second stage's conditions (reaction temperature, pressure, time) were thoroughly investigated.

The examined second-stage reaction temperatures were 75-95°C. All the synthesized prepolymers' structure was verified *via* ¹H-NMR and FTIR, and residual DEF was detected. All the formed prepolymers were found to be OH-rich, especially the ones synthesized at 90 and 95°C (D-90 and D-95, respectively), attributed to the limited DEF accessibility to the active site due to low internal carbon chain length and the presence of bulky furan rings. The molecular weights of the prepolymers synthesized at 90 and 95°C were found to be slightly higher compared to the lower temperatures' products, reaching the values of 1800 and 1900 g·mol⁻¹ (\overline{M}_n and \overline{M}_w , respectively), while two different MW populations were detected. The main advantage of these prepolymers was that the highest molecular weight population maximized at 90°C and slightly decreased at 95°C, probably implying partial loss of the enzyme's reactivity, remaining though higher than 75-85°C. The thermal properties of all the prepolymers were similar, with relatively low melting points (T_{m2} up to 75°C) compared to chemically synthesized PBS grades due to their lower molecular weight values. A two-stage decomposition was monitored for all the prepolymers attributed to the two different MW populations, in line with the open literature.

An assay of the recyclability potential of the enzyme was also conducted, indicating that it cannot be reused, in contrast to other systems analyzed in the open literature aiming at the enzymatic synthesis of aliphatic polyesters. The faster enzyme deactivation for the case of PBF could be attributed to the nature of the monomers (i.e., the presence of furan rings).

The reduced pressure effect was then studied at 90 and 95°C to enhance the by-product (ethanol) removal rate *via* evaporation and diffusion. The applied reduced pressure did not affect the prepolymers synthesized at 90°C but had a negative effect on the prepolymers synthesized at 95°C. The decreased enzyme efficiency probably led to the formation of low MW oligomers sublimated, abruptly interrupting the chain built-up. Thus, the determined MW values were similar at 90°C and decreased at 95°C. On the other hand, the prepolymers' thermal properties were not significantly affected by the reduced pressure.

The reaction time investigation indicated that longer reaction times negatively affected the polymerization for both 90 and especially 95°C. As regards 90°C, it was attributed to by-product accumulation within the reacting particles, leading to alcoholysis reaction. As for 95°C, both \overline{M}_n and \overline{M}_w presented a decrease of 17%, reaching the values of 1500 and 1600 g mol⁻¹,

respectively. Thus, the enzyme's time-dependent thermal inactivation beginning at 95°C was confirmed. The thermal properties of the prepolymer synthesized at 90°C decreased, while at 95°C remained low and constant.

The prepolymer synthesized at 90°C under 200 mbar for 2 h (D-90) was selected to be scaled up (3 and 6 g) thanks to its superior properties compared to the other prepolymers. The herein-applied process was successfully scaled up thanks to its simplicity, as it is a low-temperature bulk polymerization technique that does not require multiple solvents for the final product isolation. The D-90_3g morphology was as expected (yellowish sticky gel), while D-90_6g was received in a flowing, dark yellow form, probably due to a higher amount of residual DEF. The MW values decreased only slightly, especially at the 6g-scale (16% decreased $\overline{M_w}$), indicating the potential for a larger scaling up. The same trend was depicted for the thermal properties of the scaled-up products. Finally, the scaled-up prepolymers' OH end groups decreased compared to the small-scale prepolymers, a phenomenon observed for the case of PBS, too, attributed to mass transfer limitations that may affect the reactants' concentration, leading to a diverse distribution of end groups on larger scales.

Summing up, PBF prepolymers were enzymatically synthesized successfully through a process designed in line with the green chemistry guidelines. The herein-applied, simple process was also proved to be scalable. On that basis, a truly green, free of metal catalyst residues PBF grade can be obtained, potentially used for packaging applications taking advantage of PBF promising barrier properties.

4.1 Introduction

Cutinases are polyester hydrolases that can hydrolyze poly(ethylene terephthalate) (PET) to its monomeric units. Leaf and branch compost cutinase (LCC) presents a relatively high PET hydrolysis activity and thermostability [212], being thus one of the most important enzymes in the developing cutinase-catalyzed PET recycling methods.

Sulaiman *et al.* [213] discovered LCC through a metagenomic screen of DNA from leaf and branch compost. Although the native host of the enzyme is not known, it is of bacterial origin based on its significant sequence identity with several bacterial cutinases (e.g., 52% with *Thermobifida alba* cutinase, *TbC*; 46% identity with *Thermobifida fusca* cutinase, *TfC*). The authors subsequently reported LCC's crystal structure and characterized its structural stability and PET hydrolysis activity. LCC is highly thermostable with a T_m of 86°C, which, in the presence of 20 mM CaCl₂, increases by an additional 12°C. This is the highest cutinase thermostability thus far reported.

Despite its high thermodynamic stability, LCC displays a surprisingly low kinetic stability. Sulaiman *et al.* found the enzyme has half-lives of just 40 min and 7 min at 70°C and 80°C, respectively [213,214]. Shirke *et al.* [212] discovered that LCC displays a high aggregation propensity, primarily contributing to its thermal deactivation. Aggregation is a colloidal property arising when solute-solute (protein-protein) interactions are strong relative to solute-solvent (protein-solvent) interactions. Electrostatic or hydrophobic attractions generally dominate these interactions. Proteins in their native form often display a surface, which, at low concentration and ambient conditions (native conditions), has a low aggregation propensity. However, higher protein concentrations (such as those used for storage) may promote aggregation and lead to formulation challenges. Furthermore, harsh reaction conditions (e.g., pH, chemical, temperatures, agitation) can induce conformational and protonation changes leading to aggregation at lower concentrations [212].

On that basis, a thermostable variant of LCC (LCC^{ICCG}) that exhibits high specificity towards PET and demonstrates remarkable efficiency in depolymerizing amorphized PET waste was developed [215]. Notably, LCC^{ICCG} is the only enzyme to be industrialized for PET biorecycling, with a processing temperature of 72°C, and is expected to be implemented on a large scale soon [216].

Interestingly, even though the wild-type and the thermostable variant have been used in several (PET) hydrolysis studies [212,215,217], they have never been used for the reverse reaction, i.e., polyester synthesis. In this context, the thermostable variant of LCC, LCC^{ICCG}, was examined as a biocatalyst in the PBS synthesis.

4.2 Scope

The main scope of this chapter was to examine the ability of a novel, non-commercially available enzyme, LCC^{ICCG}, known for its plastic degrading activity, to act as a biocatalyst for PBS synthesis for the first time.

In the first part of the chapter, the protein expression and immobilization, as well as the biocatalyst characterization conducted at the Biotechnology Laboratory of NTUA by the Industrial Biotechnology & Biocatalysis group, are presented. The biocatalyst characterization included the investigation of its thermal stability (T_{stab}) and optimum temperature (T_{opt}).

In the second part of the chapter, the products of the conducted enzymatic polymerization attempts were evaluated. The enzymatically synthesized with the immobilized *Candida antarctica* Lipase CALB (N435) PBS at the optimized conditions (i.e., B-90), investigated in Chapter 2, was used as the reference material.

4.3 Experimental

4.3.1 Materials

The materials used for PBS synthesis include the monomers, DES and BDO, and chloroform for the final product isolation, all presented in Chapter 2.3.1.

Regarding the used biocatalyst, a quadruple variant of leaf branch compost cutinase (LCC^{ICCG}, variant F243I/D238C/S283C/Y127G, wild-type LCC UniprotKB ID: G9BY57 excluding the native signal peptide) was heterologously expressed in the bacterium *E. coli* and then immobilized on the carrier EziG³ Amber (EziGTM, Figure 59) (EnginZyme, Sweden) by the Industrial Biotechnology & Biocatalysis group (NTUA), based on the experimental procedures described below. EziG³ is a semi-hydrophilic carrier consisting of controlled porosity glass (CPG) beads.



Figure 59. Controlled porosity glass beads carrier EziG3 Amber (EnginZyme, Sweden)

4.3.2 Experimental procedure of the heterologous expression of the LCC^{ICCG} protein

The selected expression host was *E. coli*, the most widely studied heterologous expression platform. The transformation was conducted based on the heat-shock protocol, i.e.,

recombinant cells (*E. coli* BL21 DE3) and the plasmids (pET22b(+)) containing the gene encoding LCC^{ICCG}) were inserted in an Eppendorf tube at 42°C for 80 s so that the cell membranes could easily permit the plasmids penetration.

The sterilized (121°C, 20 min) nutrient medium with the appropriate selection antibiotic (kanamycin 0.5 $\mu\text{L}\cdot\text{mL}^{-1}$ of nutrient medium) and the recombinant cells were placed in Petri dishes and incubated at 37°C overnight. The transformants were cultured in nutrient medium at 37°C under agitation (180 rpm) and recombinant enzyme expression was induced by the addition of 0.2 mM isopropyl β -D-1-thiogalactopyranoside (IPTG) for 16 h at 16°C. Since the protein expression in bacteria is intracellular, centrifugation was conducted to isolate the bacteria cells. The cells were then resuspended, the membranes disrupted (*via* sonication), and centrifugation was used again to remove the cell debris. The proteins were purified *via* Immobilized Metal Affinity Chromatography and submitted to sodium dodecyl sulphate-polyacrylamide gel electrophoresis to be identified. To receive the protein in a form free of imidazole (used during Immobilized Metal Affinity Chromatography to remove the protein from the columns) residues, dialysis occurs.

4.3.3 Experimental procedure of the protein immobilization on the EziG³ Amber carrier

The immobilization of the protein was conducted using the above-mentioned carrier *via* covalent binding. The carrier EziG³ Amber has Fe(III) particles on its surface, used to create covalent bonds with the His-tag of the recombinant expressed enzymes, leading to their immobilization.

The optimized protocol for the immobilization of LCC^{ICCG} follows. The carrier EziG³ Amber was weighed and suspended in a phosphate buffer 500 mM NaCl pH 7.3, containing the expressed enzyme after purification. The ratio of the enzyme loading to the support material ($W_{\text{enzyme}}/W_{\text{carrier}}$) was optimized to 20%. The mixture was agitated in an orbital shaker (ZHICHENG Analytical Instruments Manufacturing Co LTD, China) at 100 rpm for 3 h at 4°C. The optimized procedure applied resulted in a 77% immobilization yield. At the end of the immobilization procedure, the enzymatic solution was centrifuged, the buffer was removed, and the carrier with the immobilized enzyme was dried through lyophilization. The biocatalyst was received in the form of a free-flowing powder (Figure 60).



Figure 60. Immobilized on the EziG3 Amber carrier LCC^{ICCG}

Calculating the mass of the final carrier and the mass of the immobilized enzyme (calculating the absorbance at 280 nm of the non-immobilized enzyme in the enzymatic solution), loading was defined as equal to 13% $w_{\text{enzyme}}/w_{\text{biocatalyst}}$ and 15% $w_{\text{enzyme}}/w_{\text{carrier}}$. This value is comparable to the commercially available immobilized *Candida antarctica* Lipase CALB, the reported loading of which is 8.5-20% wt ($w_{\text{enzyme}}/w_{\text{carrier}}$), as discussed in Chapter 2.3.1.1.

4.3.4 Biochemical characterization of the immobilized LCC^{ICCG}

4.3.4.1 Experimental procedure to define the esterolytic activity of the biocatalyst

Esterolytic activity of the biocatalyst was assessed through enzymatic reactions with *p*-nitrophenyl laurate *p*NPL, at 35°C for 10 min under agitation (1400 rpm) in an Eppendorf Thermomixer Comfort (Eppendorf, Germany). Reactions consisted of 1 mL substrate solution, containing 1.0 mM of the substrate in 0.1 M phosphate-citrate buffer, 0.125% w·v⁻¹ gum arabic, 1% v/v Triton X-100 pH 6.0, and 0.5 mg of biocatalyst. The release of *p*-nitrophenol (*p*NP) was monitored at 410 nm, in a SpectraMax-250 microplate reader (Molecular Devices, Sunnyvale, CA, USA), connected with the SoftMaxPro software (version 1.1, Molecular Devices, Sunnyvale, CA, USA).

4.3.4.2 Experimental procedure to define the optimal temperature of the biocatalyst

The optimal temperature was assessed through reactions of the biocatalyst with *p*NPL, following the standard *p*NP assay conditions, over a range of temperatures (50-80°C). The release of *p*-nitrophenol (*p*NP) was monitored at 410 nm, in a SpectraMax-250 microplate reader (Molecular Devices, Sunnyvale, CA, USA), connected with the SoftMaxPro software (version 1.1, Molecular Devices, Sunnyvale, CA, USA).

4.3.4.3 Experimental procedure to define the thermostability of the biocatalyst

The thermostability of immobilized LCC^{ICCG} was investigated by assessing the remaining activity on *p*NPL, after incubation of the biocatalyst in 25 mM Tris-HCl, 150 mM NaCl pH 8.0 buffer, at temperatures ranging from 60 to 80°C for a duration of up to 72 h, under standard *p*NP assay conditions.

4.3.5 Enzymatic prepolymerization experimental procedure for poly(butylene succinate) production

Stoichiometric amounts of DES (6 mmol, 1.04 g) and BDO (6 mmol, 0.54 g) were premixed in a round-bottom flask and stirred (75 rpm) at 50-70°C in a rotary evaporator (Rotavapor R-210, Buchi, Switzerland) under atmospheric pressure. The selected biocatalyst concentration was 6.5 % wt (relative to monomers). Given the immobilized LCC^{ICCG} loading ($w_{\text{enzyme}}/w_{\text{carrier}}$), which was 15% (see Chapter 4.3.3), the protein content was calculated at 0.97% wt relative to monomers. This content was selected to be similar to the protein content used for the enzymatic synthesis of PBS with the commercial enzyme N435 (see Chapter 2). In that case, the used biocatalyst concentration was 10% wt relative to monomers; considering a loading ($w_{\text{enzyme}}/w_{\text{carrier}}$) of 10% wt for N435 (see Chapter 2.3.1.1), the protein content was 1% wt relative

to monomers, i.e., similar to the LCC^{ICCG} protein content. After the immobilized LCC^{ICCG} biocatalyst addition, a two-step prepolymerization process was applied (Table 14). The first step was conducted at 50-70°C, under atmospheric pressure for 24 h to minimize BDO losses through limited transesterification reactions. Then, the temperature increased to 80°C and a vacuum of 200 mbar was applied. At the end of the reaction, chloroform was added (4:1 wt relative to monomers) to dissolve the formed polyester and the enzyme was subsequently filtered off. The remaining chloroform was evaporated in a high-vacuum pump (Edwards RV5 Rotary Vane Pump, Edwards, U. K.). The same procedure (first step: 60°C, 24 h and second step: 80°C, 200 mbar, 2h) was applied without biocatalyst for comparison reasons (blank sample).

Table 14. Conditions of PBS enzymatic prepolymerization using the immobilized LCC^{ICCG}

Sample	1 st step			2 nd step		
	T (°C)	P (mbar)	t (h)	T (°C)	P (mbar)	t (h)
L-50	50	1000	24	80	200	2
L-60	60	1000	24	80	200	2
L-70	70	1000	24	80	200	2

4.3.6 Characterization techniques

4.3.6.1 ¹H-NMR Spectroscopy

¹H-NMR was carried out as described in 2.3.3.1.

4.3.6.2 Fourier Transform Infrared Spectroscopy (FTIR)

FTIR was carried out as described in 2.3.3.2.

4.3.6.3 Gel Permeation Chromatography (GPC)

GPC was carried out as described in 2.3.3.3.

4.3.6.4 Thermogravimetric Analysis (TGA)

TGA was carried out as described in 2.3.3.5.

4.4 Results

4.4.1 Biochemical characterization of the immobilized LCC^{ICCG}

The esterolytic activity of the immobilized LCC^{ICCG} on *p*NPL was calculated equal to 0.693 ± 0.080 units·mg_{LCC^{ICCG}}⁻¹. Based on the relevant assay, the immobilized LCC^{ICCG} presented the maximum activity at 60°C (Figure 61a), which was thus considered its optimal temperature. On that basis, the reaction temperature of the first step of the following polymerizations was

investigated in the range of 50-70°C. The long duration of the first step and the atmospheric pressure (no vacuum that could lead to monomers' loss or oligomer sublimation) were the appropriate conditions to examine the real LCC^{ICCG} efficiency on PBS enzymatic polymerization.

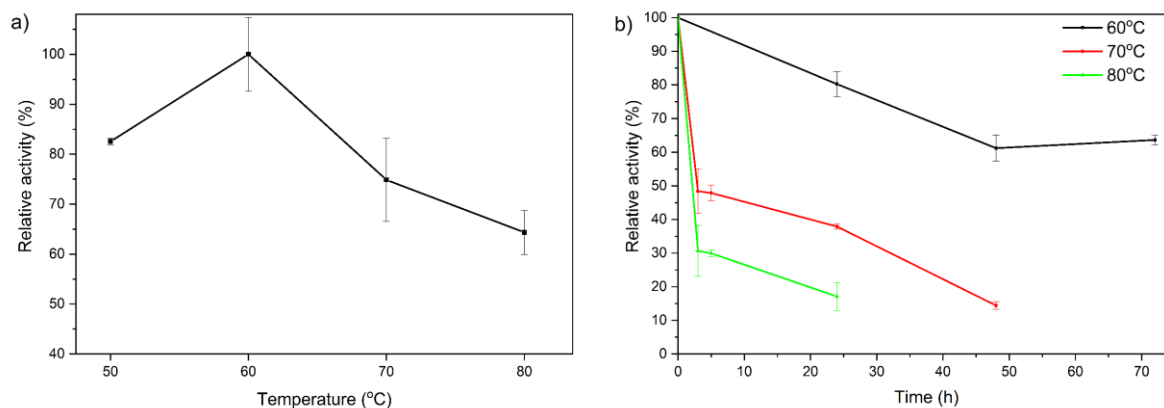


Figure 61. Effect of temperature on the activity (a) and the stability (b) of immobilized LCC^{ICCG} on pNPL.

The effect of temperature on the stability of the immobilized LCC^{ICCG} was also studied, and based on the relevant results, the biocatalyst was found thermally stable at 60°C for the first 24 h of incubation, as the calculated activity loss was less than 20% (Figure 61b). On the other hand, the immobilized LCC^{ICCG} thermal stability at 70°C decreased by almost 60% during the first 24 h. As regards 80°C, the biocatalyst retained only 30% of its activity after the first 3 h of incubation, and it was practically deactivated in 24 h of incubation (relative activity 17%). In this context, the second stage of the following polymerizations was selected to be conducted at 80°C for 2 h under a vacuum of 200 mbar. The selection of these conditions aimed to favor the PBS production by removing the by-product (ethanol) and shifting the reaction equilibrium to the right, thus enhancing the enzymatically synthesized from the first stage oligomers' further reaction.

4.4.2 Enzymatic prepolymerization of PBS using the immobilized LCC^{ICCG}

The blank sample (Figure 62a) and the B-90 PBS prepolymer synthesized with N435 (Figure 62e) were used as reference materials to study the morphology of the immobilized LCC^{ICCG} products. All the prepolymers synthesized with LCC^{ICCG} were in the form of sticky gels (Figure 62b-d), indicating a relatively low degree of polymerization. The product synthesized at 50°C (L-50) presented a liquid-resembling morphology similar to the blank sample, while the products synthesized at 60 and 70°C, L-60 and L-70, presented a drier morphology resembling the reference PBS prepolymer, B-90 [218].

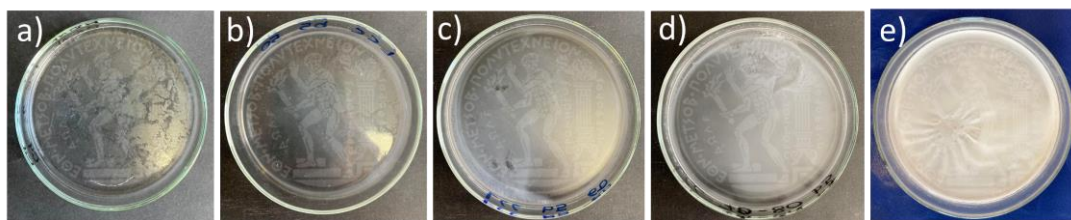


Figure 62. Blank (reference) sample (a), prepolymers synthesized using the immobilized LCC^{ICCG} at 50, 60 and 70°C (b-d), B-90 (e)

All the prepolymers were submitted to ¹H-NMR and FTIR to verify that PBS was successfully formed. PBS repeating unit was verified *via* ¹H-NMR spectroscopy for all the LCC^{ICCG} products (Figure 63). All the determined shifts were identical to the N435 product, B-90, presented in Chapter 2.4.1.1. No residual BDO was detected in the prepolymers, as the hydroxyl end group peak (signal at about 3 ppm, Figure 27) monitored in the BDO spectrum was absent in all prepolymers spectra. As discussed in Chapter 2.4.1.1, since the resonance signal of the end unit (–OH) proton is typically not detectable in polymers' spectra due to intra-molecular hydrogen bonding (e.g., between hydroxyl groups and the ester bonds), its absence in the spectra confirmed no residual unreacted BDO in the prepolymers. In addition, the presence of multiple, distinguished peaks at 4.12 and 1.7 ppm indicates that the expected polymerization degree is higher than the minimum (i.e., \overline{M}_n 1200 g mol⁻¹ and \overline{X}_n 14) above which the ¹H-NMR peaks distinguish, as it is thoroughly discussed in Chapter 2.4.1.1. Regarding the blank sample, the signals corresponding to the e and d protons from the diester, and the diol were hardly detected, presenting significantly lower intensities and different morphology than the prepolymers, probably indicating a monomers' mixture.

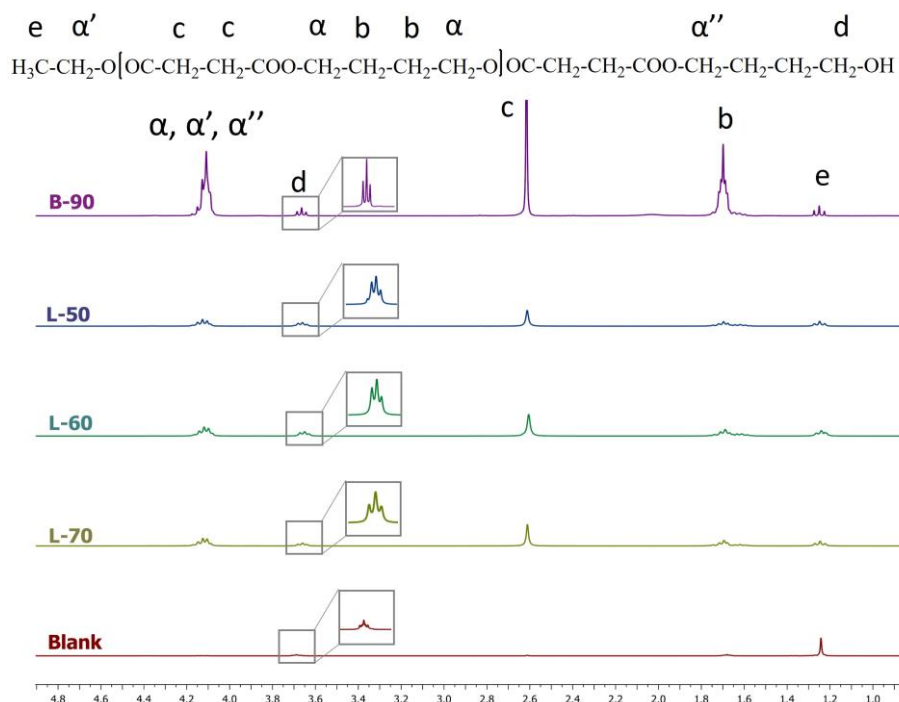


Figure 63. ¹H-NMR spectra of the prepolymers L-50, L-60, L-70, B-90 and the blank (reference) sample

The prepolymers' chemical structure was also verified *via* FTIR and the PBS characteristic peaks, presented in Chapter 2.4.1.1 were monitored (Figure 64). The main difference between the LCC^{ICCG} products and the B-90 sample's spectra is that the latter presents an insignificant baseline shift in contrast to L-prepolymers. As it is thoroughly discussed in Chapter 3.4.1.1, the baseline shift in ATR is a defect fostering stronger signals at lower wavenumbers (due to infrared penetration within the sample depending on the wavenumber), implying surface contact issues. Significant baseline shifts were also observed for the PBF prepolymers (Chapter 3.4.1.1), which, similarly to the L-prepolymers, presented a sticky morphology, probably responsible for inhomogeneity in the surface and thickness of the material submitted to the FTIR measurement. It was thus concluded that the free-flowing powder form of the N435-synthesized PBS provided a high, homogenous surface area, thus eliminating any surface contact issues.

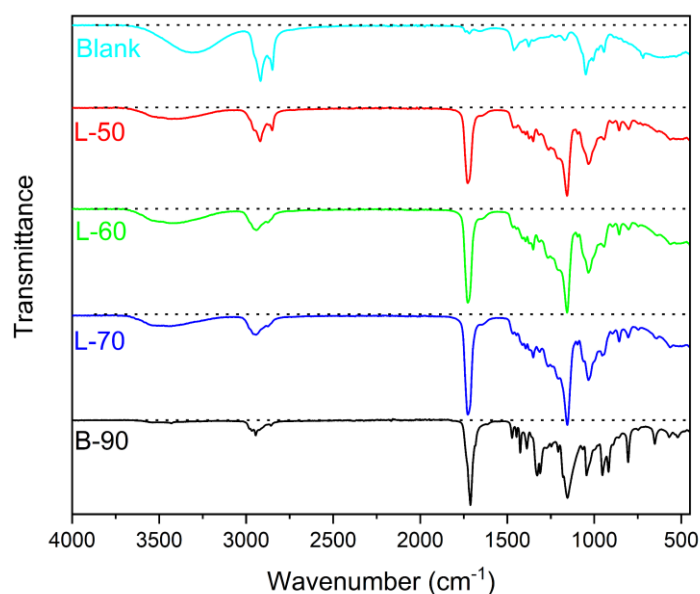


Figure 64. FTIR spectra of the prepolymers L-50, L-60, L-70, B-90 and the blank (reference) sample

Even though there may be surface contact issues, the prepolymers' hydroxyl and carbonyl contents at around 3400 and 1710 cm^{-1} were monitored *via* FTIR in the next step (Figure 65). The OH content was similar for the temperatures of 50 and 60°C, while a small decrease was monitored at 70°C. The same trend was depicted more clearly in the $^1\text{H-NMR}$ results, where a reduction from about 60 (at 50 and 60°C) to 52% (at 70°C) in the OH-end group percentage was monitored. Given that the boiling points of the monomers DES and BDO are similar (217 and 230°C), BDO is probably more prone to evaporation since its molar mass is significantly lower than DES (90 g mol^{-1} instead of 174 g mol^{-1} , respectively). Given that BDO evaporation may begin at the temperature of 70°C, leading to a decreased availability and, thus, less OH-rich oligomers.

Regarding the ester content, the relevant intensity presented a noticeable increase from 50 to 60°C and a slighter increase at 70°C. Considering that the intensity at 1712 cm^{-1} is proportional

to the concentration of the ester bonds along the polymer backbone and at the end of the polymer chain, the monitored increase could be attributed to two reasons: a) since the hydroxyl end groups are decreased, the ester end groups increased. This could indicate that the peak intensity is mainly related to the chain-end ester groups, which is expected since the synthesized PBS grades were oligomers, and the contribution of the ester end-groups to the overall carbonyl stretch C=O band signal intensity is expected to be significant. This scenario came true for the N435-synthesized PBS prepolymers (see Chapter 2.4.1.1). Regarding the second reason, b) the ester end groups are limited because the LCC^{ICCG}-synthesized oligomers are considered OH-rich (hydroxyl end group percentage up to 70%). This means the backbone ester bonds are expected to dominate the 1712 cm⁻¹ signal. A similar trend was monitored for the OH-rich (up to 90%) N435-PBF synthesized prepolymers (see Chapter 3.4.1.1). In that case, the similar ester contents indicated similar molecular weight values. In this scenario, the small increase in the ester content could indicate a small molecular weight increase. Overall, both scenarios a and b may be true.

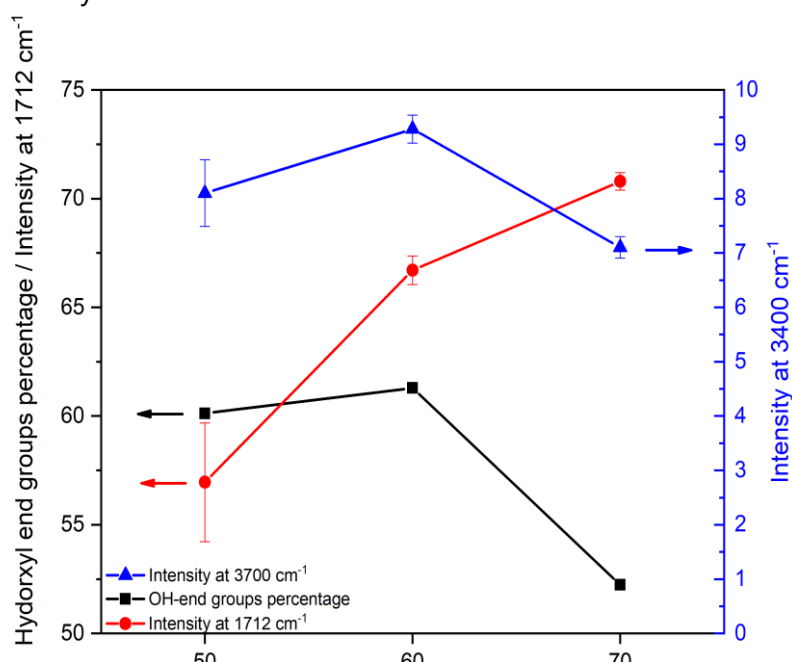


Figure 65. ¹HNMR-calculated OH end groups percentage and peak intensities at 3400 cm⁻¹ and 1712 cm⁻¹ for the prepolymers L-50, L-60 and L-80

The prepolymers synthesized using the immobilized LCC^{ICCG} were then submitted to GPC, and the obtained chromatograms are presented in Figure 66. All the prepolymers presented three distinct populations with different molecular weights. Interestingly, all three populations were detected in the reference, N435-synthesized prepolymers B-90. The obtained chromatograms present significant differences from the blank reference sample's chromatogram; in the blank sample's chromatograms, two broad, low-intensity, distinct peaks were determined, similar to the monomers.

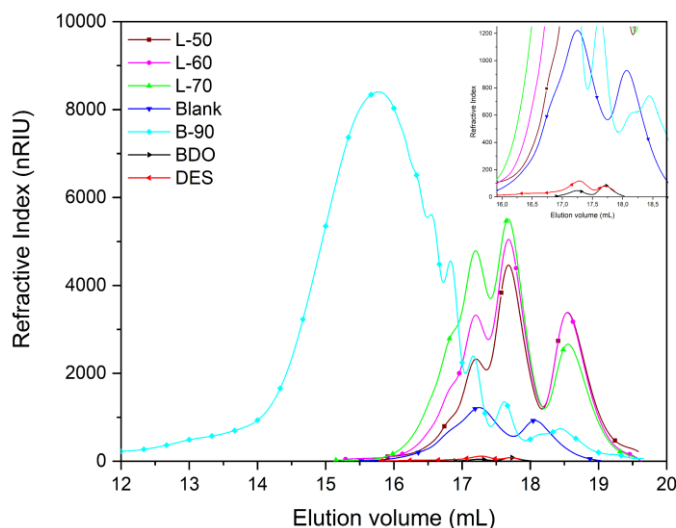


Figure 66. GPC chromatograms of the prepolymers L-50, L-60, L-70, B-90, the blank (reference) sample and the monomers (BDO and DES)

The results of the GPC analysis indicated products of similar MW values, reaching MW values of 1400 g mol^{-1} (\overline{M}_n) and 1500 g mol^{-1} (\overline{M}_w) at 60 and 70°C (Table 15). The similar MW values, especially at 60 and 70°C, could imply that although the enzyme's activity decreases at 70°C, the higher temperature favors the polymerization reactions. All the LCC^{ICCG} products can also be considered monodisperse, as they present narrow MWD with \mathfrak{D} up to 1.33. Their narrow distribution renders them valuable for requiring applications such as biomedical. Especially for applications requiring nanometer-size processing (e.g., pharmaceutical products), narrow molecular weight distributions and precise control of molecular lengths are necessary [219]. Even though biomacromolecules, such as DNA, have uniform molecular lengths (even though their molecular weight is large), in the field of synthetic polymers, it is still difficult to achieve uniform molecular lengths and weights; synthetic polymers typically present a polydispersity in their degree of polymerization which impedes the precise control of their physical properties and material functionalities. Of note, particle size, which is crucial for applications such as drug delivery systems, is influenced by molecular weight distribution.

Table 15. ¹HNMR- and GPC-calculated molecular weights of the polymers L-50, L-60 and L-70

Sample	¹ HNMR-calculated		GPC-calculated	
	\overline{M}_n (g mol ⁻¹)	\overline{M}_n (g mol ⁻¹)	\overline{M}_w (g mol ⁻¹)	(\mathfrak{D})
L-50	300	1300±70	1400±90	1.08
		700±28	800±29	1.14
		300±8	400±11	1.33
L-60	300	1400±16	1500±45	1.07
		800±3	800±2	1.00
		400±1	400±1	1.00
L-70	400	1400±1	1500±4	1.07
		700±2	800±2	1.14
		400±4	400±3	1.00

Even though the molecular weight of the prepolymers presented relatively small deviations, significant differences were observed in the ratios of the intensities of the highest molecular weight population (peak I) and the medium molecular weight population (peak II) compared to the lowest molecular weight (peak III) population intensity (Figure 67). More exactly, when the temperature increased to 70°C, both the higher and medium molecular weight populations maximized compared to the lowest molecular weight population (Figure 67). It can be assumed that, even though the activity of the immobilized LCC^{ICCG} decreased, the polymerization was favored thanks to the increased temperature. The increased temperature probably enhanced the already formed oligomer chains' mobility, thus leading to increased possibilities of recombination. Additionally, at the reaction temperature of 70°C, a quantity of the formed by-product, i.e., ethanol, could have been evaporated (T_b : 78°C).

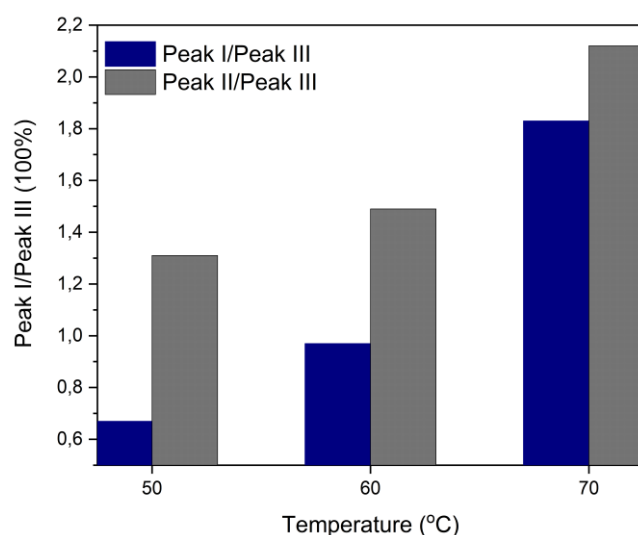


Figure 67. Intensity ratios of peaks I and II of the prepolymers L-50, L-60 and L-70 monitored *via* GPC

The enzymatically synthesized prepolymers' thermal behavior was studied *via* TGA. The monitored decomposition temperatures were similar at about 400°C and slightly higher than the decomposition temperature of the N435-synthesized prepolymer B-90. On the contrary, the $T_{d,5\%}$ values presented an increasing trend with temperature (Table 16), which could be related to the increased amount of the higher molecular weight population as reaction temperature increases.

Table 16. Thermal properties defined *via* TGA of the prepolymers L-50, L-60 and L-70 monitored *via* GPC

Sample	$T_{d,5\%}$ (°C)	T_d (°C)	Residue (%)	
L-50	152	263	397	1.20
L-60	174	285	399	0.90
L-70	224	276	398	0.30

However, the prepolymers decomposition was conducted in two stages, which is unusual for a high-purity PBS grade as the herein synthesized. A supplementary experiment was conducted to investigate the phenomena occurring during the first decomposition stage, and the prepolymers were submitted to a short TGA analysis up to 360°C. The analyzed samples that were received in a solid form were submitted to a GPC analysis. It was concluded that the samples had been post-polymerized, and a significant molecular weight increase was monitored. The obtained chromatogram of the L-60 sample is indicatively presented in Figure 68a, with the monitored peak corresponding to a \overline{M}_n of 3300 g·mol⁻¹ and \overline{M}_w 5600 g·mol⁻¹. Regarding the susceptibility to post-polymerization of the LCC^{ICCG} prepolymers, L-50 and L-60 were found to be more susceptible to post-polymerization compared to L-70, with \overline{M}_n and \overline{M}_w increases of about 150% and 350% (Figure 68b). This trend is probably attributed to the increased amount of the higher molecular weight population in the L-70 sample, meaning decreased concentration of active end groups, that are necessary for the post-polymerization reactions.

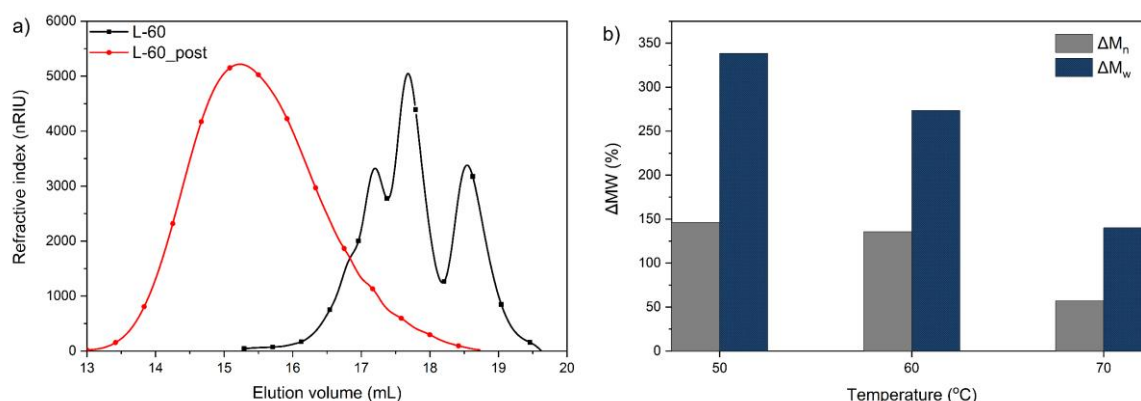


Figure 68. GPC chromatograms of the prepolymer L-60 before and after post-polymerization (a), \overline{M}_n and \overline{M}_w percentage increases after post-polymerization of the prepolymers L-50, L-60, L-70

4.5 Conclusions

This chapter examined the ability of a novel, non-commercially available enzyme to be used as a biocatalyst in a solvent-free system to produce PBS for the first time. Initially, a quadruple variant of the Leaf and branch compost cutinase (LCC), LCC^{ICCG}, was heterologously expressed and immobilized on a controlled-porosity glass carrier at the Biotechnology Laboratory of NTUA by the Industrial Biotechnology & Biocatalysis group. The immobilized biocatalyst was characterized in terms of optimal temperature and thermostability. It was concluded that LCC^{ICCG} presented the maximum activity at 60°C, where it remained thermally stable for 24°C.

The immobilized LCC^{ICCG} was examined as a biocatalyst for PBS synthesis *via* a two-step process. The reaction temperature of the first step was investigated (50-70°C), and it was conducted under atmospheric pressure for 24 h to study the enzyme's efficiency in the polymerization. The second stage was conducted at 80°C, under 200 mbar, for 2 h to favor the polymerization

reaction. PBS was successfully synthesized in all the tested temperatures, confirmed by the $^1\text{H-NMR}$ and FTIR results. The obtained products were in the form of gels, with the ones synthesized at 60 and 70°C being similar to the N435-products (Chapter 2). Interestingly, a significant baseline shift was monitored in the obtained FTIR spectra, indicating crystal contact issues, a phenomenon already observed in the case of the enzymatically synthesized PBF prepolymers also being in a sticky gel form (Chapter 3.4.1.1). The synthesized prepolymers were OH-rich, with a small decrease in the OH content observed at the higher temperature of 70°C. A small increase with the temperature increase was monitored for the ester content. This could be attributed to the reduction of the OH end group percentage and/or an increase in the molecular weight values (i.e., an increase of the ester bonds in the oligomer backbone). Even though the MW of the products were found to be similar, with three distinct populations, reaching the values of 1400 and 1500 g mol^{-1} (\overline{M}_n and \overline{M}_w), the products of higher temperatures had an increased amount of the higher molecular weight population.

One of the most significant advantages of the LCC^{CCG} products is their narrow molecular weight distributions (Đ up to 1.33), rendering them valuable for applications requiring uniform molecular weight lengths, such as bioapplications, including drug delivery systems. Another advantage of the synthesized PBS prepolymers was their susceptibility to post-polymerization, which was revealed during TGA. The monitored $\Delta\overline{M}_n$ and $\Delta\overline{M}_w$ reached the values of 150 and 350%, respectively. The lower temperature prepolymers presented the highest susceptibility, probably due to an increased amount of low molecular weight chains, leading to an increased concentration of active end groups.

Summing up, a novel enzyme, LCC^{CCG} , known for its ability to degrade plastic, was successfully used for the first time as a biocatalyst for synthesizing PBS. The synthesized prepolymers presented several advantages, including narrow molecular weight distributions and increased susceptibility to post-polymerization, rendering them valuable candidates for demanding applications such as drug delivery systems.

Chapter 5: Study of post-polymerization to increase the molecular weight of the enzymatically synthesized prepolymers: Evaluation of different methods and the most critical process parameters

5.1 Introduction

Even though enzymatic polymerization presents numerous advantages, one of its limitations is the difficulty of obtaining polyesters of appropriate molecular weight for the subsequent processing and use [220]. It becomes thus important to combine the method of enzymatic polymerization with adequate finishing steps, in order to upgrade the final products in terms of molecular weight and of thermal properties. An interesting example is the combination of enzymatic synthesis with post-polymerization reactions, such as solid state polymerization (SSP). SSP is an eco-friendly solvent-free polymerization technique, which permits molecular weight (MW) build-up *via* polycondensation reactions in the amorphous regions of semi-crystalline solid prepolymers at temperatures lower than T_m [36,111,127,221], as it is thoroughly described in Chapter 1.2.2. The combination of enzymatic synthesis and SSP has been already examined by the group for different polyesters such as PE 8.12, PE 8.14 and PBS. Vouyiouka *et al.* [111] suggested the following polymerization cycle for the production of the partially renewable polyesters PE 8.12 and PE 8.14: a lipase-catalyzed prepolymerization step, combined with a low-temperature post-polymerization step, in the melt or solid state. Kanelli *et al.* [36] examined the production of PBS and other aliphatic polyesters with the following two-stage procedure: (1) an enzymatic prepolymerization under vacuum, with diphenyl ether as solvent and N435 as biocatalyst and (2) a low-temperature post-polymerization stage in order to upgrade the polyesters properties. Especially for PBS, it was submitted to SSP under vacuum at temperatures close to the prepolymer melting point ($T_m - T_{SSP} = 5 - 10^\circ\text{C}$). The upgrade process was held in two stages, precrystallization and SSP, and resulted in a $\Delta\overline{M}_n$ of 67%, with the \overline{M}_n reaching the value of $6500 \text{ g}\cdot\text{mol}^{-1}$ (initial \overline{M}_n $3910 \text{ g}\cdot\text{mol}^{-1}$). Recently, Comerford *et al.* [102] synthesized enzymatically aliphatic and aromatic oligoesters of \overline{M}_n from 500 to $1000 \text{ g}\cdot\text{mol}^{-1}$, namely poly(butylene adipate) (PBA), poly(butylene isophthalate) (PBI), poly(butylene furanate) (PBF) and poly(butylene pyridinate) (PBP) with N435 in a solvent-free system. The oligoesters/ di-esters were subsequently submitted to a thermal upgrade process, at three temperatures (140, 150 and 180°C) under different surrounding atmospheres (air, vacuum, N_2) resulting in 8.5, 2.6, 3.3 and 2.7 times higher \overline{M}_n values. However, in such studies of post-polymerization, it is important to correlate the melting points of the enzymatically synthesized prepolymers to the selected reaction temperature (T_r) of the finishing step, since post-polymerization kinetics are highly sensitive to the difference between T_m and T_r . Thus, in the most recent results of our group an optimized post-polymerization process, based on a finer tuning of the reaction temperature (T_r) was established and increased polymerization rate with minimum material loss (e.g. oligomers sublimation) and almost null thermal degradation were reached [49]. More precisely, PBS was synthesized enzymatically in the low boiling point isooctane, and submitted to bulk post-polymerization in a TGA chamber serving as a micro-

reactor. Bulk post-polymerization was conducted under nitrogen flow (10 mL·min⁻¹) and resulted in a $\Delta\overline{M}_w$ of 180%, with the achieved \overline{M}_w being 5600 g·mol⁻¹ and the initial ca. 2000 g·mol⁻¹).

5.2 Scope

This chapter's scope was to upgrade the enzymatically synthesized PBS and PBF prepolymers through improving MW and thermal properties while maintaining their truly green character, as the selected upgrade methods are solventless, do not require catalysts, are conducted in low temperatures, and are fully sustainable.

In the first part of this chapter, the enzymatically synthesized PBS on a large scale (20 g) was used as the starting material to examine the efficiency of solid-state and melt post-polymerization. The post-polymerized products were assessed based on their morphology, molecular weight and thermal properties. After identifying the most efficient method, the next goal was to optimize it, i.e., to investigate process parameters, including reaction temperature and time and use an OH-rich prepolymer that could be more susceptible to post-polymerization.

In the second part of this chapter, the enzymatically synthesized and scaled-up (3 g-scale) PBF was also submitted to melt post-polymerization. The main objective was to study the susceptibility of the enzymatically synthesized PBF prepolymer to melt post-polymerization. In this context, a screening study of the reaction temperature of melt post-polymerization was conducted.

5.3 Experimental

5.3.1 Materials

Thanks to the simplicity of the applied post-polymerization methods (i.e., solid-state and melt post-polymerization), the only required materials are the starting prepolymers. On that basis, the herein used materials include the synthesized with N435 on the large scale PBS (B-90_20g, see Chapter 2.4.2), the synthesized with N435 on the large scale PBS with 5% BDO excess (B-90_20g_5%, see Chapter 2.4.3), and the synthesized with N435 on the 3-g scale PBF (D-90_3g, see Chapter 3.4.2).

5.3.2 Post-polymerization experimental procedure for the upgrade of enzymatically synthesized PBS and PBF

All the post-polymerization processes were conducted with the use of ca. 1 g of each prepolymer in a round-bottom flask in a rotary evaporator (Rotavapor R-210, Buchi, Switzerland) under reduced pressure (20 mbar) and stirring (75 rpm). The prepolymer B-90_20g was submitted to SSP and melt post-polymerization. The selected SSP temperature was close

to the initial melting point ($T_m - T_{SSP}$: 7°C) to achieve increased segmental mobility while maintaining the solid state. The total reaction time was 10 h, including a precrystallization step (2 h) and SSP (Table 17). Melt post-polymerization was initially conducted at 110°C, close to the prepolymer melting point, i.e., 12°C above T_m . Then, the most critical parameters of the melt post-polymerization (i.e., reaction time and temperature) were investigated. At the optimized reaction conditions, prepolymer with an excess in BDO (B-90_20g_5%) was also submitted to melt-post polymerization in order to compare its susceptibility to post-polymerization to the stoichiometric B-90_20g. Melt-post polymerization was also tested for the enzymatically synthesized PBF (D-90_3g), and the reaction temperature was investigated (Table 17). At the end of the reactions, the post-polymerized polyesters were cooled at room temperature and stored in a desiccator.

Table 17. Conditions of PBS and PBF prepolymers post-polymerization

Sample	1 st step			2 nd step		
	T (°C)	P(mbar)	t(h)	T(°C)	P(mbar)	t(h)
PBS						
Precrystallization	90	20	2			
S8_95 ¹	95	20	8			
S2_M2 ²	100	20	2	100	20	2
S2_M4	100	20	2	100	20	4
S2_M6	100	20	2	100	20	6
M4_110 ³	110	20	4			
M4_110_5%	110	20	4			
M6_110	110	20	6			
M8_110	110	20	8			
M10_110	110	20	10			
M4_120	120	20	4			
M4_130	130	20	4			
M4_140	140	20	4			
M4_150	150	20	4			
PBF						
M4_85	85	20	4			
M4_95	95	20	4			
M4_105	105	20	4			

¹SX_Y, ²SX_{MZ} and ³MZ_W, where S: sample submitted to SSP, M: sample submitted to melt post-polymerization, X: SSP reaction time (h), Y: SSP reaction temperature (°C), Z: melt post-polymerization reaction time (h), W: melt post-polymerization reaction temperature (°C)

5.3.3 Characterization techniques

5.3.3.1 Gel Permeation Chromatography (GPC)

GPC was carried out as described in 2.4.3. The calibration of the instrument was carried out as described in 2.4.3. The calibration curve was used only for the case of PBS and not PBF due to the lack of Mark-Houwink (K and a) constants for the specific polymer-solvent system.

5.3.3.2 Differential Scanning Calorimetry (DSC) and Thermogravimetric Analysis (TGA)

Differential Scanning Calorimetry (DSC) and Thermogravimetric Analysis (TGA) were conducted as presented in 2.3.3.4 and 2.3.3.5, respectively.

5.4 Results

5.4.1 Study of the enzymatically synthesized PBS post-polymerization methods and key process parameters

5.4.1.1 Assessment of solid-state post-polymerization as an upgrading method

The prepolymer B-90_20g was selected as the starting material for the post-polymerization tests due to its adequate available amount, good thermal performance and morphology to permit applying SSP. A preweighted quantity of about 1 g was used for the following post-polymerization tests and a precrystallization step was introduced before the main SSP process to eliminate possible sintering issues [222], as it is already used for PET and PLA SSP processes. In particular, the precrystallization step was conducted at 90°C under 20 mbar for 2 h, the obtained first heating DSC curve was found sharper compared to the starting material (Figure 69a), while an increase of 4°C in the T_{m1} , reaching 102°C (Table S5), was monitored, indicating a crystal reorganization. Thanks to this T_{m1} increase, the following SSP process was permitted to be conducted at 95°C ($T_{m1} - T_{SSP}$ 7°C) under 20 mbar for 8 h without sintering problems. The SSP product, S8_95, presented slightly upgraded thermal properties compared to the starting prepolymer (Table S5, Figure 69) indicating polymers of similar molecular weights. Indeed, \overline{M}_n increased slightly to 1900 g·mol⁻¹ and \overline{M}_w to 3300 g·mol⁻¹, while dispersity remained almost constant (Table 18).

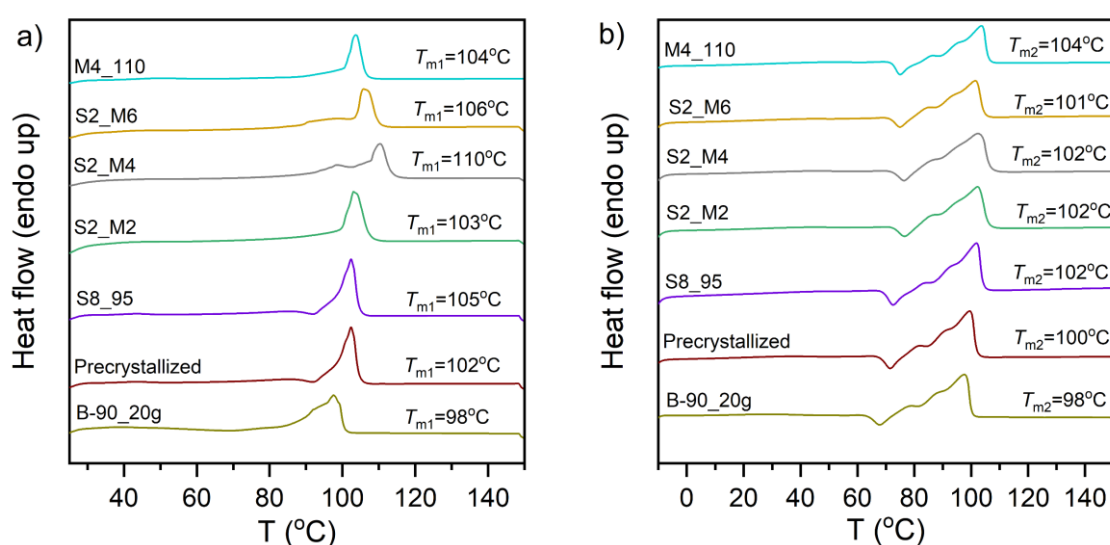


Figure 69. First heating (a) and second heating (b) of the starting material (B-90_20g) and the post-polymerized samples

Table 18. \overline{M}_n , \overline{M}_w and dispersity \mathcal{D} of the enzymatically synthesized and post-polymerized PBS and PBF prepolymers

Sample	\overline{M}_n (g mol ⁻¹)	\overline{M}_w (g mol ⁻¹)	(\mathcal{D})
PBS			
Solid-state post-polymerization			
S8_95	1900	3300	1.7
S2_M2	1700	3000	1.7
S2_M4	1900	3700	1.9
S2_M6	1900	3200	1.7
Melt post-polymerization			
M4_110 (B-90_20 g)	3000	6000	2.0
M4_110 (B-90_20 g_rep)	1700	2600	1.5
M6_110	1700	2600	1.5
M8_110	1500	2400	1.6
M10_110	1400	2300	1.6
M4_120	1700	2600	1.6
M4_130	1700	2200	1.6
M4_140	1200	2200	1.8
M4_150	1400	2300	1.7
M4_110_5%	1800	2800	1.6
PBF			
M4_85	1600	1700	1.1
	800	900	1.0
	400	400	1.0
M4_95	1600	1800	1.1
	900	900	1.0
	400	400	1.0
M4_105	1700	1900	1.1
	800	900	1.0
	400	400	1.0

Since post-polymerization kinetics are highly sensitive to the difference between T_m and T_r , the next approach included the $T_{m1} - T_{SSP}$ reduction up to 2°C. SSP was conducted at 100°C under reduced pressure of 20 mbar after precrystallization. However, after the first two hours of SSP, the sample went from the solid to the melt state (S2_M2). This solid-melt transition is a phenomenon already observed during the polycondensation of various nylon salts [223]. By-

product (water) accumulation within the reacting particles during polycondensation results in the formation of low melting point areas, which eventually overlap, leading to the complete breakdown of the solid structure. In our case, the reaction by-product (ethanol) and any moisture that the prepolymer surface may have absorbed, contribute to the transition from the solid to the melt state. The co-existence of ethanol and water may also synergistically affect the prepolymers' properties; organic solvents like ethanol have been found to swell the polymer matrix and increase chain mobility. Free volume is thus created due to swelling, allowing the water molecules diffusion in the polymeric matrix and thus resulting in hydrolysis [224]. Despite the melt state of the prepolymer, post-polymerization was not significantly favored at 100°C, not even at longer reaction times (e.g., 4 and 6 h, samples S2_M4 and S2_M6). The highest melting point increase by 12°C and 4°C for the first and the second heating respectively was monitored after 4 h of melt polymerization, while the \overline{M}_n and \overline{M}_w increased up to 1900 g·mol⁻¹ and 3700 g·mol⁻¹ respectively (Table 18).

5.4.1.2 Assessment of melt post-polymerization as an upgrading method

In the next step, melt post-polymerization was conducted at 110°C, under reduced pressure of 20 mbar for 4 h. Before melt post-polymerization, drying at 90°C, 20 mbar, for 2 h was conducted to remove any absorbed moisture from the prepolymer. A sharper curve was obtained in the first heating (sample M4_110, Figure 69a), and the melting point reached 104°C, which was maintained during the second heating (Figure 69b), indicating increased molecular weight values compared to previous samples where T_{m2} was at 102°C. Actually, \overline{M}_n reached the value of 3000 g·mol⁻¹ and \overline{M}_w increased to 6000 g·mol⁻¹ with dispersity of 2 (Table 18). The relevant $\Delta\overline{M}_n$ and $\Delta\overline{M}_w$ percentages are 76 and 94%, respectively. In a relevant work of the group, PBS was enzymatically synthesized and then submitted to a two-step bulk post-polymerization (2h at 80°C and 8h at 90°C) in a thermogravimetric analysis (TGA) chamber as a micro-reactor, and a slightly higher $\Delta\overline{M}_w$ (i.e., 126%) was monitored. Even though the herein conducted process' reaction time is almost 50% shorter, and its scale 10 times higher (1 g of starting prepolymer instead of 100 mg), meaning that the mass transfer limitations are more intense, the achieved $\Delta\overline{M}_w$ is comparable to the abovementioned. The high efficiency of the herein-conducted melt-post polymerization could be related to the high vacuum applied, which has been found in some post-polymerization cases more effective than a N₂ flow. Ma *et al.* [225] studied the influence of N₂ flow compared to a high vacuum on the SSP of PET. The researchers found that the SSP rate was enhanced by vacuum compared to nitrogen flow, as the intrinsic viscosity (IV) increased and the end-groups were depleted faster. The superiority of the vacuum system compared to the N₂ was attributed to the solid deposit (sublimates) observed on the cold parts of the reactor walls during SSP-vacuum and not during SSP-N₂. More precisely, the sublimates were found to consist of terephthalic acid (TA), monohydroxyethyl terephthalate (MHET), bishydroxyethyl terephthalate (BHET) and cyclic oligomers, produced by acidolysis, glycolysis and transesterification reactions. Their removal as a sublimate during SSP under vacuum provided a new pathway for the progress of SSP.

The herein post-polymerized PBS was thermally stable with a decomposition temperature of 393°C (Table S6). Even though post-polymerization was conducted in the melt state, it was not thermally downgraded thanks to the relatively low temperature and short reaction times in the melt state.

However, different reaction times and temperatures were tested to increase further the applied melt post-polymerization efficiency. A new batch of the prepolymer B-90_20g was prepared based on the enzymatic prepolymerization process described in Chapter 2.3.2 at the large scale of 20 g to have adequate amounts for the following investigations. The properties of the synthesized prepolymer, B-90_20g_rep, are presented in Tables S1, S2 and S3.

5.4.1.2.1 Investigation of the reaction time effect on the upgrading process

Before the melt post-polymerization, drying (90°C, 20 mbar, 2 h) was conducted for every sample to remove any moisture from the prepolymer and reach comparable results. Reaction time was the first parameter to be investigated, and different reaction times, including 6, 8 and 10 h, for a constant temperature of 110°C, were examined. It is of high risk that polymer thermal degradation may occur when reaction time and/or temperature increases in the melt state. In this context, the post-polymerized samples were submitted to GPC to detect molecular weight changes and TGA to ensure that the examined samples were not thermally downgraded.



Figure 70. Starting material (a) and melt post-polymerized at 110°C PBS samples for 4 h (b), 6 h (c), 8 h (d) and 10 h (e)

The starting material was a free-flowing powder (Figure 70a), while the received post-polymerized samples at 110°C until 6 h were in the form of colorless solid masses, having taken the shape of the reactor (i.e., round-bottom flask) during cooling from the melt (Figure 70b and c). On the contrary, the post-polymerized samples at 110°C for 8 and 10 h were received as sticky gels (Figure 70d and e), probably indicating lower molecular weight values due to degradation. All the post-polymerized samples were weighed at the reaction's end to ensure no sublimation occurred.

In line with the macroscopical observations, GPC indicated that \overline{M}_n presented the maximum increase (ca. 13%) at the reaction time of 4 h, accompanied by a small decrease in the \mathcal{D} , indicating a more homogeneous distribution of the achieved molecular weights (Figure 71).

Similar \overline{M}_n and \overline{M}_w values were obtained at 6 h of post-polymerization, probably implying that the system reached equilibrium. The MW changes were less intense for the \overline{M}_w , even though the trend was similar: increase at 4 h and similar MW at 6 h. This behavior can be attributed to the fact that the shorter chains present increased mobility compared to the longer ones, thus increasing the possibility of them coming into contact so that their end groups can react and lead to increased MW values.

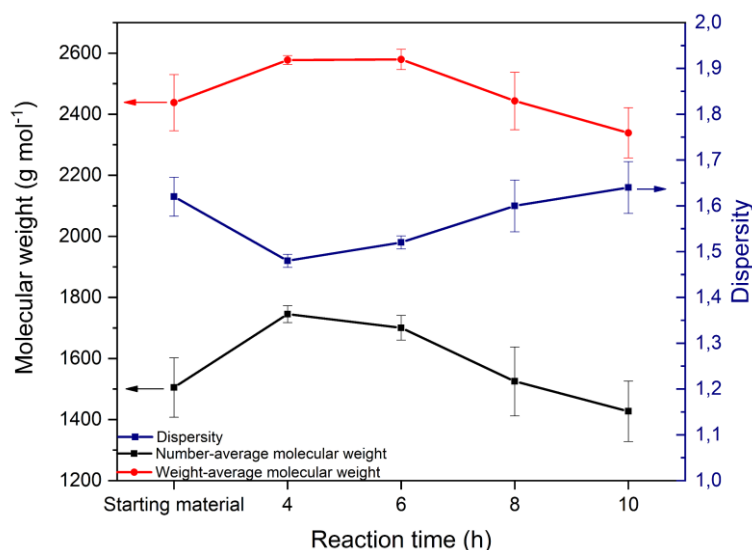


Figure 71. Molecular weights (\overline{M}_n , \overline{M}_w) and dispersity $\overline{M}_w/\overline{M}_n$ of the post-polymerized PBS prepolymers as a function of reaction time

When the reaction time was further increased (i.e., 8 and 10 h), a drop in the MW values \overline{M}_n and \overline{M}_w was monitored, along with an increase in the dispersity, revealing the inhomogeneity of the samples. Interestingly, the calculated standard deviations of the \overline{M}_n , \overline{M}_w and $\overline{M}_w/\overline{M}_n$ were also increased compared to the relevant values of the 4- and 5-h products, also suggesting the inhomogeneity of the products. Given these, the downgrade of the samples for reaction times higher than 6 h is indicated and could be attributed to thermal degradation of the prepolymer, considering that the process was conducted for prolonged times under vacuum (20 mbar), not under an inert (e.g., nitrogen) atmosphere. The two competitive reactions (post-polymerization and thermal degradation) seem to be in balance for the first 6 h, but for higher reaction times (>6h), thermal degradation seems to dominate. The fact that \overline{M}_w was again less affected (decreased) compared to \overline{M}_n , is due to the increased susceptibility of the shorter chains to the downgrade processes, as (a) they present increased mobility, rendering them more prone to degradation reactions, and (b) they can promote the formed by-products diffusion due to their shorter lengths compared to the longer ones. The thermal degradation mechanism is expected to be similar to the oxidative degradation mechanism, which has been studied to an extent in the open literature.

Studying the oxidative mechanisms of polymers, including PBS, is challenging as the molecules formed in oxidation processes are often very reactive, do not accumulate, and are present only in minor amounts among the reaction products, requiring a high sensitivity to be monitored. However, one of the most well-established PBS thermo-oxidative decomposition pathways is

Chapter 5: Study of post-polymerization to increase the molecular weight of the enzymatically synthesized prepolymers: Evaluation of different methods and the most critical process parameters presented by Rizzarelli and Carroccio [226]. In the first step, a hydroperoxide intermediate is formed *via* a hydrogen abstraction from the methylene group adjacent to the PBS ester linkage. Due to instability, this intermediate undergoes further reaction with the elimination of a hydroxyl radical and then, the radical formed subtracts a hydrogen radical to form a hydroxyl ester. Rearrangement reactions follow, and oligomers bearing succinic acid, 4-hydroxy butanoic aldehyde or/and acid end groups are produced (Figure 72). Rizzarelli and Carroccio [226] submitted synthetic and commercial PBS (\overline{M}_w 93000 and 101000 g·mol⁻¹, respectively) to thermo-oxidation at 170°C in atmospheric air for up to 6 h. A significant decrease in the \overline{M}_w (about 50%) was monitored after the first hour for the synthesized grade. In the commercial PBS grade, decomposition started after two hours, which was attributed to the probable presence of a heat stabilizer.

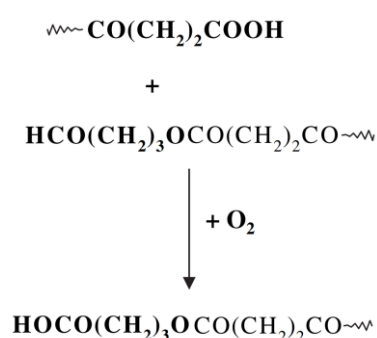


Figure 72. Oligomeric products of PBS thermo-oxidative decomposition [226]

Regarding the thermal stability of the products, the monitored T_d values remained almost constant for every post-polymerized sample until 10 h (Figure 73); similarly, the char residues remained almost constant and lower than 1.5% (Table S6). On the other hand, the $T_{d,5\%}$, which is more sensitive to MW changes, presented a different behavior; it remained almost stable at 4 h and slightly increased at 6 h, while a significant decrease was observed for higher reaction times (decrease up to 46°C for 10 h, Table S6).

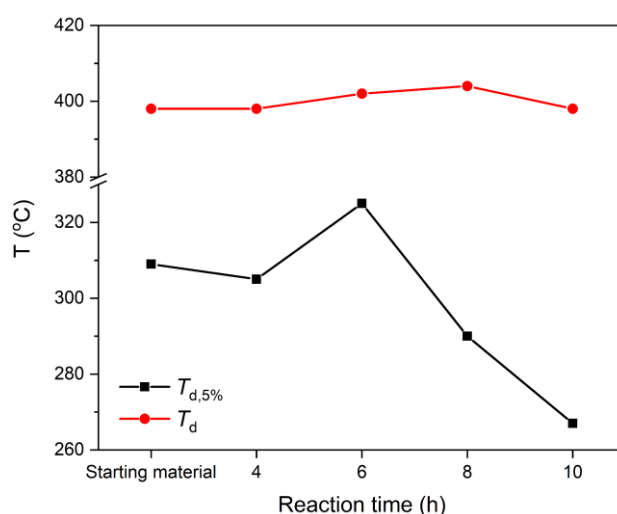


Figure 73. T_d and $T_{d,5\%}$ of the post-polymerized PBS prepolymers as a function of reaction time

The monitored $T_{d,5\%}$ evolution with time, in line with the abovementioned GPC results, suggests that competitive phenomena occur. For the first 6 h of the reaction, melt-post polymerization dominates the system, while after 6 h, the decomposition reactions seem to dominate, and the product's degradation becomes more intense.

5.4.1.2.2 Investigation of the reaction temperature effect on the upgrading process

The next melt post-polymerization parameter to be examined was the reaction temperature. The drying step (90°C, 20 mbar, 2 h) was conducted for every sample before the melt post-polymerization. Considering the above-presented results, the investigated reaction window was 110 – 150°C for a constant reaction time of 4 h.

Regarding the macroscopical morphology of the post-polymerized samples, they were received as colorless solid masses, having taken the shape of the reactor (i.e., round-bottom flask) during cooling from the melt, except for the samples post-polymerized at 140 and 150°C (Figure 74). These high-temperature samples were received as sticky gels; the 150°C sample was also yellowish, indicating thermal degradation (Figure 74f). All the post-polymerized samples were weighed at the reaction's end to ensure no sublimation occurred.



Figure 74. Starting material (a) and melt post-polymerized for 4h PBS samples at 110°C (b), 120°C (c), 130°C (d), 140°C (e), and 150°C (f)

Based on the GPC results, a clear increase in the MW was monitored only for the sample post-polymerized at 110°C (Figure 75), already discussed in Chapter 5.5.1.2.1. Also, the small decrease in the \mathfrak{D} indicates an increased homogeneity of the MW of the sample. When the temperature increased up to 130°C, the MW didn't seem to be negatively or positively affected. When the temperature was further increased at 140°C, there was a clear reduction in both \overline{M}_n and \overline{M}_w to values lower than the starting material, indicating degradation (thermal or thermo-oxidative) of the sample. The MW reduction was more intense when the reaction temperature reached 150°C, in agreement with the sticky, yellowish morphology of the sample M4_150. Increased \mathfrak{D} were monitored for the temperatures of 140 and 150°C also indicating inhomogeneity of the samples due to degradation. It is of high interest that the \overline{M}_w of the sample post-polymerized at 150°C presented a significantly high standard deviation, especially compared to the relevant \overline{M}_n deviation. This difference could indicate the occurrence of competitive phenomena; at that high temperatures the oligomer chains probably have

sufficient mobility to come in contact and promote their end group reaction, leading to the formation of several high molecular weight chains. At the same time, thermal or thermo-oxidative degradation occurs, tending to lower the MW averages. The simultaneous occurrence of these competitive phenomena could lead to increased \overline{M}_w deviations, since \overline{M}_w is mostly affected by the higher molecular weight chains.

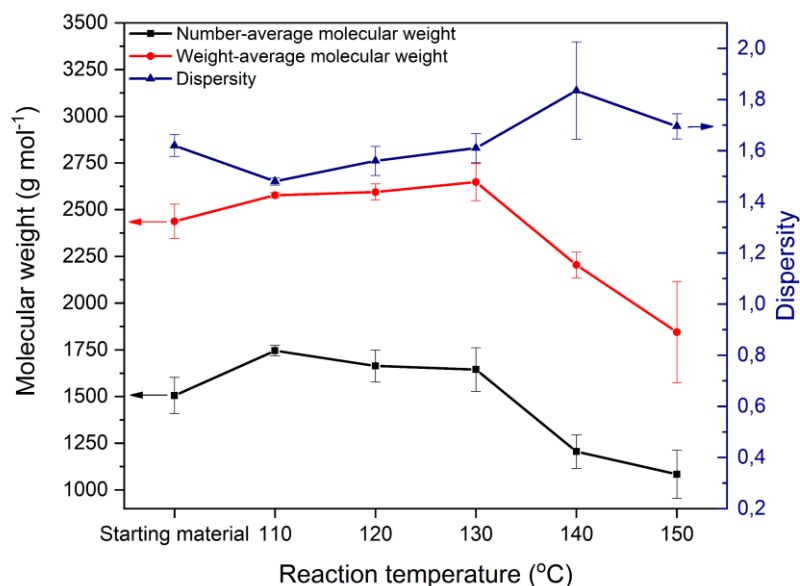


Figure 75. Molecular weights (\overline{M}_n , \overline{M}_w) and dispersity \overline{D} of the post-polymerized PBS prepolymers as a function of reaction temperature

The post-polymerized PBS samples were also submitted to TGA, and the monitored $T_{d,5\%}$ and T_d are presented in Figure 76. As expected, $T_{d,5\%}$ was slightly affected by reaction temperature until 130°C and a significant decrease of 62°C was monitored at 150°C (Table S6), in total agreement with the MW decrease, evidenced by GPC. This trend can also be observed in the zoomed graphs in Figure 77 (a and b); the mass loss rate gradually increased with the increase in reaction temperature until 130°C, and a remarkable increase was monitored at 150°C.

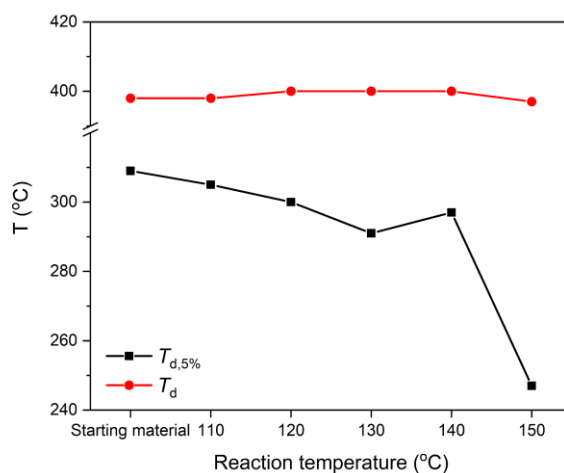


Figure 76. T_d and $T_{d,5\%}$ of the post-polymerized PBS prepolymers as a function of reaction temperature

Even though the decomposition temperature determined at the maximum rate of weight loss was not affected by the melt-post polymerization temperature, remaining almost stable, the decomposition profile significantly changed for the case of 150°C. More specifically, the post-polymerized up to 140°C samples presented a single-stage decomposition profile, similar to the starting material's (Figure 77a and b). On the contrary, the M4_150 sample presented a two-stage decomposition profile, with the first step at 323 and the second at 397°C. As thoroughly discussed in Chapter 2.4.1.3., in a work of the group [49], it has been found that the enzymatically synthesized PBS grades with \overline{M}_n lower than 1000 g·mol⁻¹ present a two-stage decomposition. On the contrary, higher molecular weight grades ($\overline{M}_n > 1000$ g·mol⁻¹) decompose in a single-stage process. This trend seems to be confirmed also for the herein post-polymerized PBS grades, as the M4_150 sample's \overline{M}_n was defined at about the critical value of 1000 g·mol⁻¹.

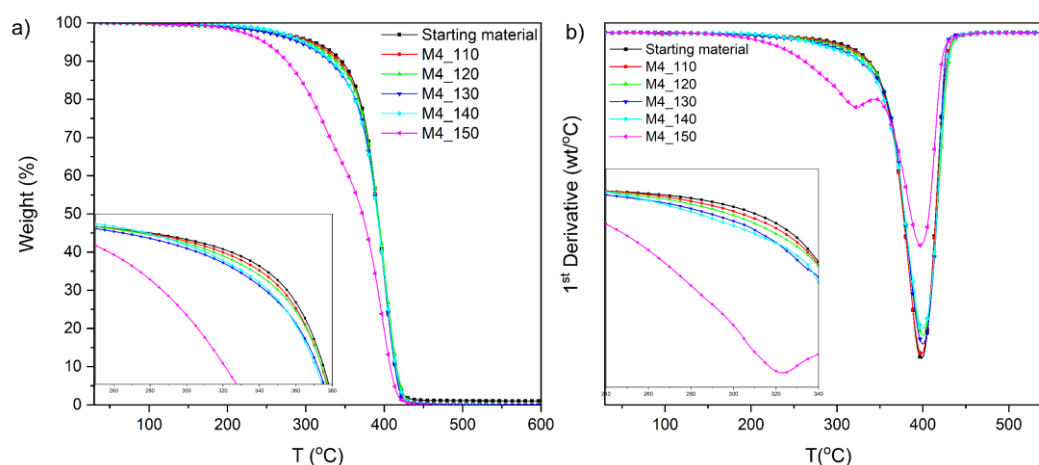


Figure 77. TGA curves and 1st derivatives of the post-polymerized PBS prepolymers as a function of reaction temperature

Except for the abovementioned MW dependence, the different decomposition stages could also be related to different reactions, leading to different decomposition products. In our case, the first stage at 323°C could also be attributed to different products formed during the thermal or thermo-oxidative degradation. In contrast, the second stage corresponds to the thermal degradation of the material. The degradation mechanism is also expected to be similar to oxidative mechanisms. Hiller *et al.* [227] used a commercial PBS grade in a stabilized (with a bio-additive with antioxidant properties) and neat form to submit them to TGA in nitrogen and oxidative atmospheres and compare their degradation behaviors. Focusing on the neat PBS grade, its decomposition occurred in one stage at about 400°C under the nitrogen atmosphere, which was attributed to the thermal decomposition of the material. On the contrary, a three-stage decomposition occurred in the presence of oxygen. The first stage monitored at 330°C, was attributed to thermo-oxidative degradation; this peak almost completely disappeared for the stabilized PBS with the abovementioned antioxidant. The second stage, close to 400°C, presented the greatest intensity, and it was due to the material thermal decomposition, as in

the nitrogen atmosphere. The third stage presented a very weak 1st derivative peak at 480°C and was associated with the oxidation of residues from previous degradative reactions.

5.4.1.2.3 Investigation of the OH-end group concentration effect on the upgrading process

As described in Chapter 2.4.3, PBS grades with 5, 10 and 20% BDO molar excess were synthesized. The molar excess of 20% led to high OH-end group concentrations (up to 81%) but had a negative effect on the \overline{M}_w (35% decreased compared to the stoichiometric prepolymer B-90_20g) which was also depicted in its sticky morphology. On the contrary, 5 and 10% excess led to increased OH-end group concentrations (64 and 70%, respectively) without significantly affecting the MW of the prepolymer. Considering the similar properties of the 5 and 10% excess products, the first one was selected to be submitted to the following melt post-polymerization at the optimum conditions 110°C, 4 h, 20 mbar (Table 17, sample M4_110_5%). The drying step (90°C, 20 mbar, 2 h) was also conducted before the melt post-polymerization to reach results comparable with the M4_110 (Chapter 5.4.1.1).

The post-polymerized sample was first submitted to GPC and the results are presented in Figure 78. The number-average molecular weight remained almost unaffected, in contrast to the weight-average molecular weight, which presented an increase of about 17%, reaching the value of 2800 g·mol⁻¹. This \overline{M}_w increase led to a slight increase in the dispersity of the sample, from 1.3 to 1.6 (Table 18). The main conclusions that can be reached based on GPC are the following: first, the fact that only the \overline{M}_w increased, implies that long chains were mainly formed during melt post-polymerization. Second, the increased OH end group percentage (64%) did not favor the post-polymerization compared to the stoichiometric grade (OH end group percentage 52%). It is also indicated that the herein applied two-stage enzymatic polymerization process does not lead to significant BDO losses, that should be replenished.

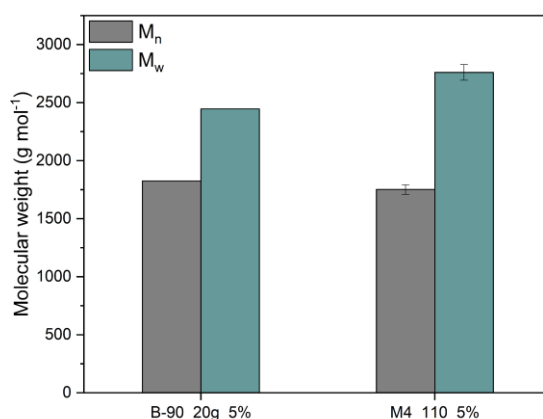


Figure 78. Molecular weights (\overline{M}_n , \overline{M}_w) of the PBS prepolymer synthesized with 5% BDO excess before and after post-polymerization at 110°C for 4 h

To explain the abovementioned observations, we must focus on the reactions occurring during the post-polymerization. Jacquél *et al.* [23] used a BDO excess of 5% to synthesize PBS in the

presence of different metal catalysts in a two-stage process consisting of an esterification and a trans-esterification step. Given the BDO excess, OH-rich PBS oligomers were expected to be formed during esterification. As the researchers stated, efficient trans-esterification or inefficient trans-reactions may follow. The mechanism of a typical efficient trans-esterification involving hydroxyl-terminated PBS, leading to chain growth, is presented in Figure 79. It is defined as a nucleophilic attack on the carbon bearing ester function by the oxygen of a hydroxyl chain end. However, other trans-reaction pathways exist, many of which do not lead to a molar mass increase. These pathways, for instance, could include exchanging an ester- and a hydroxyl-end group between two polymer chains; more precisely, if the oxygen of a hydroxyl chain end (chain a) attacks the ester end group bond of another chain (chain b), the OH may get attached to the chain (a), while the ester end group to the chain (b). Trans-reactions like this decrease the overall rate of the chain growth.

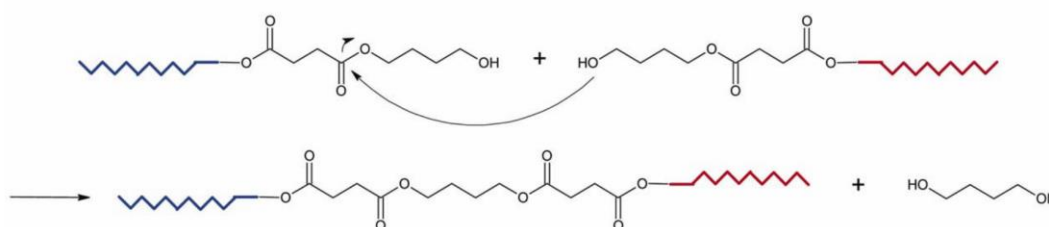


Figure 79. Mechanism of efficient PBS trans-esterification [23]

On that basis, the monitored increased \overline{M}_w values can be attributed to the fact that the longer chains, having an increased number of ester bonds compared to the shorter ones, have an increased possibility to be attacked by a hydroxyl chain end, leading to efficient trans-esterification and chain growth. The general low efficiency of the post-polymerization using the OH-rich prepolymer could be attributed to the formation of BDO as the by-product during efficient trans-esterification (Figure 79). BDO is harder to remove from the reacting mass than ethanol, which is more volatile and is formed during the trans-esterification of an ester- and a hydroxyl-terminated chain. In addition to that, BDO's higher carbon content compared to ethanol hinders its diffusion into the reacting mass. Consequently, BDO (and other by-products) accumulation within the reacting particles is highly probable, hindering the equilibrium shift towards polymerization and rendering the oligomers susceptible to downgrade.

Even though the attempt to use an OH-rich prepolymer for the post-polymerization wasn't proved as effective, the product was also submitted to TGA to confirm no thermal degradation. The post-polymerized grade M4_110_5% presented a T_d of 400°C and a single-stage decomposition, similar to the starting material B-90_20g_5%, implying no degradation. As regards the $T_{d,5\%}$, it was found to be 55°C higher than the starting material, reaching the value of 297°C (Table S6), which could be attributed to its increased \overline{M}_w . Interestingly, when the stoichiometric grade B-90_20g was post-polymerized under the same conditions (see Chapter 5.5.1.2), no increase in the $T_{d,5\%}$ was monitored, even though the MW increased by far more (i.e., $\Delta\overline{M}_n$ and $\Delta\overline{M}_w$ 76 and 94%, respectively). The delay of the decomposition process of the

OH-rich post-polymerized product can be probably due to intermolecular interactions (e.g., hydrogen bonding between the BDO hydroxyl groups that are abundant and ester bonds) requiring additional energy to decompose.

5.4.2 Screening study of the enzymatically synthesized PBF melt post-polymerization: reaction temperature effect on the process

Considering the low efficiency of the SSP to increase the molecular weight of the enzymatically synthesized PBS (see Chapter 5.5.1.1) by more than 30% and the fact that sterical factors (due to higher carbon content and the bulky furan rings of PBF) along with the extremely high OH-end groups percentages that have been monitored for PBF prepolymers (see Chapter 3.4.1.1) may further hinder the post-polymerization process (see Chapter 5.4.1.3), solid-state post-polymerization was excluded from the analysis. Focusing on the melt post-polymerization, which seems more appropriate for PBF thanks to the increased chain mobility, some screening tests were conducted to study the susceptibility of the PBF prepolymers. The examined temperature window was 85-105°C (Table 17), as it is important to eliminate the possibility of thermal degradation of the prepolymer and to keep the energy requirements as low as possible.

The post-polymerized prepolymers presented a similar macroscopical morphology to the starting material (D-90_3g), i.e., sticky, yellowish gel without any indications of degradation. All the post-polymerized grades during GPC presented three different peaks attributed to three different MW populations (Table 18). Peak III, corresponding to a MW of 400 g·mol⁻¹, is attributed to the residual DEF (see Chapter 3.5.1.1). The lower molecular weight PBF population (Peak II) was not significantly affected by the post-polymerization process (Table 18), in contrast to the higher molecular weight population, which was influenced by the reaction temperature (Figure 80). At the temperature of 85°C, the obtained MW and dispersity values were identical to the starting material's, indicating that the post-polymerization was ineffective, probably due to the limited mobility of the oligomer's chains. On the other hand, when the reaction temperature increased to 95°C, a molecular weight increase of about 6% was depicted in the \overline{M}_w , which reached the value of 1700 g·mol⁻¹. No change was monitored for the \overline{M}_n at the same temperature. When further increasing the reaction temperature, a more noticeable MW increase was monitored for both the \overline{M}_n and \overline{M}_w , at 6 and 12%, respectively, while the number-average polymerization degree reached 16. The fact that the \overline{M}_w is more affected than \overline{M}_n , and higher \overline{M}_w increases are achieved, implies that the longer oligomer chains are more reactive than the shorter ones. Considering the increased OH-end groups percentage of the PBF prepolymers, it could be stated that, as in the case of PBS melt post-polymerization (see Chapter 5.4.1.2.3), the formation of BDO as the by-product during efficient trans-esterification (Figure 79) delays the polymerization growth. This phenomenon is due to the BDO's lower volatility than ethanol and higher carbon content, limiting its removal and diffusion into the reacting mass. Thus, BDO accumulation within the reacting particles is highly probable,

meaning that the equilibrium shift towards polymerization does not promote, and the formed oligomers are susceptible to downgrade.

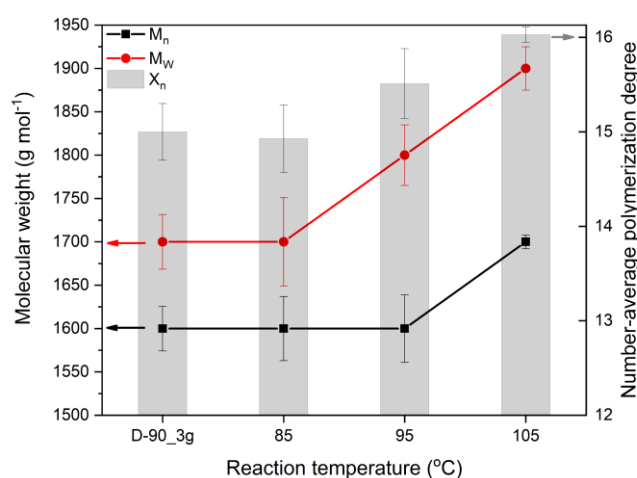


Figure 80. \overline{M}_n , \overline{M}_w and X_n of the post-polymerized PBF prepolymers at 85, 95 and 105°C

The post-polymerized products were also submitted to TGA to investigate their thermal behavior. Even though the thermal properties were generally similar, with the post-polymerized at 95°C grade presenting slightly improved thermal characteristics compared to the other grades and the starting material (Table S6), the reaction temperature affected the products' decomposition profiles and char residues. All the PBF grades presented two-stage decomposition profiles, with, however, quantitative differences (Figure 81).

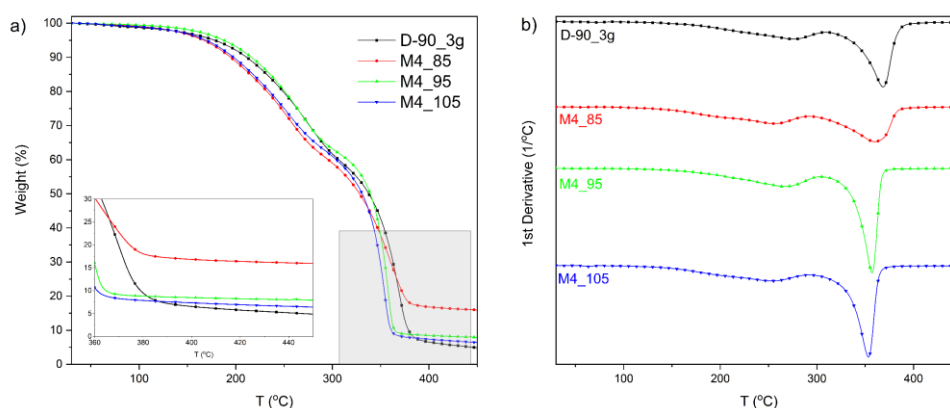


Figure 81. TGA curves and 1st derivatives of the post-polymerized PBF prepolymers as a function of reaction temperature

Part of the first decomposition step, monitored in the 200–300°C range, is attributed to the residual DEF as discussed in Chapter 3.4.1.1. As the reaction temperature increases from 85 to 95°C, the relevant first derivative peak becomes weaker (Figure 81b). Specifically, at the end of the first decomposition step, weight losses of 39.3%, 34.4% and 32.9% were monitored for 85, 95 and 105°C, respectively. This trend could indicate smaller residual DEF quantities in the samples as the temperature increases. More exactly, as the temperature increased, the existing OH-rich oligomers probably gained enough mobility to react with the residual DEF, which was

thus consumed. It is important to note that the abovementioned trend of the post-polymerized grades is an indication and cannot be compared to the starting material D-90_3g, as in this first decomposition step participate both the residual DEF and the lower molecular weight PBF populations that may have been affected by the applied post-polymerization process.

Another interesting observation is that the melt post-polymerization process affects the post-polymerized grades' residue defined at 600°C. The highest residue (15.1 %) was monitored for the sample post-polymerized at 85°C, followed by the grade post-polymerized at 95°C (7.3%) and the sample post-polymerized at 105°C (5.5%, Table 18, Figure 81a). The starting material presented a residue of 4.8% (Table 13). It could be stated that the ineffective post-polymerization reaction at 85°C led to the formation of by-products containing furan moieties that remain thermally stable at even higher temperatures. For instance, Monti *et al.* [228] submitted a commercial furan resin to TGA under a nitrogen environment, and the defined residue at 900°C was 50 %. As the reaction temperature increases, and given the OH-rich nature of the PBF prepolymers, the possibilities of efficient trans-esterification, i.e., nucleophilic attack on the carbon bearing ester function by the oxygen of a hydroxyl chain end (see Chapter 5.4.1.2.3), increases. As described in Chapter 5.4.1.2.3, the by-product of efficient trans-esterification is the linear BDO, which is not thermally stable and does not contribute to the final residue.

5.5 Conclusions

The enzymatically synthesized and scaled-up PBS prepolymer B-90_20g (T_{m1} 98°C, \overline{M}_n 1700 g·mol⁻¹, \overline{M}_w 3100 g·mol⁻¹) was used as the starting material for the post-polymerization tests. SSP was the first method to be examined, and a precrystallization step (90°C, 20 mbar, 2 h) was introduced before the main SSP to eliminate possible sintering issues. This step led to a crystal reorganization of the PBS chains and T_{m1} increase to 102°C. Thanks to this increase, the following SSP process was conducted at 95°C ($T_{m1} - T_{SSP}$ 7°C), which, however, was not found to be effective as the molecular weights increased slightly (\overline{M}_n 1900 g·mol⁻¹, \overline{M}_w 3300 g·mol⁻¹).

Since post-polymerization kinetics are highly sensitive to the difference between T_m and T_r , the next approach included the $T_{m1} - T_{SSP}$ reduction up to 2°C. However, after the first two hours of SSP, a solid-melt transition phenomenon occurred, probably due to the co-existence of ethanol (by-product) and water (absorbed moisture). Despite the melt state of the prepolymer, post-polymerization was not significantly favored at 100°C, not even at longer reaction times (i.e., 4 and 6 h) that were tested. In this context, we focused on the melt post-polymerization of PBS, conducted at 110°C under reduced pressure of 20 mbar for 4h. Before melt post-polymerization, drying at 90°C, 20 mbar, for 2 h was conducted to remove any possible absorbed moisture from the prepolymer. The melt-post polymerization was effective as a sharper curve was obtained in the first heating, and the melting point reached 104°C, which was maintained during the second heating. As regards the molecular weights, the achieved $\Delta\overline{M}_n$ and $\Delta\overline{M}_w$ percentages were 76 and 94%, respectively. On that basis, the reaction time and

temperature of melt post-polymerization were then investigated. The reaction time and temperature examined windows were 4 to 10 h (at 110°C) and 110 to 150°C (for 4 h). It was concluded that competitive phenomena occur during the process. Until 6 h, melt-post polymerization dominates the system, while after 6 h, the decomposition reactions seem to dominate, and the product's degradation becomes more intense. As regards the temperature investigation, PBS remained stable until 130°C, while thermal (or thermo-oxidative) degradation occurred at higher temperatures, especially at 150°C. It was concluded that 110°C and 4 h were the most appropriate conditions, balancing the required prepolymer's upgrade and the process's energy requirements as low as possible.

The last parameter of the PBS melt post-polymerization to be examined was using a prepolymer with increased OH-end groups, especially the grade synthesized with 5% BDO molar excess, leading to 64% OH-end groups. The increased OH end group percentage (64%) did not significantly favor the post-polymerization compared to the stoichiometric grade (OH end group percentage 52%); it was attributed to the formation of BDO as the by-product during efficient trans-esterification, which is harder to diffuse into the reacting mass and remove from the reacting mass than ethanol. As a result, BDO (and other by-products) accumulation within the reacting particles is highly probable, hindering the equilibrium shift towards polymerization and rendering the oligomers susceptible to downgrade.

Finally, the enzymatically synthesized and scaled-up (3 g) PBF grade was submitted to melt post-polymerization at three different temperatures (85, 95 and 105°C). Its susceptibility to post-polymerization was confirmed, especially at 105°C; the monitored $\Delta\overline{M}_n$ and $\Delta\overline{M}_w$ were 6 and 12%, respectively, and an increasing trend was observed. Regarding the thermal properties, the post-polymerized at 105°C grade presented a less intense first decomposition step, indicating that DEF consumption was favored at this temperature. Additionally, its lower char residue could imply the occurrence of efficient trans-esterification reactions leading to the formation of by-products such as BDO, not-containing furan moieties and not contributing to higher char residues, as it was monitored on the lower post-polymerized grades (at 85 and 95°C).

Summing up, a low-temperature melt post-polymerization process was proved the most appropriate for the enzymatically synthesized and scaled-up (20 g scale) PBS prepolymer upgrade, and it was optimized. The enzymatically synthesized PBF prepolymer presented susceptibility to melt post-polymerization, and even though further investigation is required, the results were encouraging. Given the above, a green method conducted at low temperatures, not requiring solvents and catalysts, was established for both the aliphatic and the alipharomatic, enzymatically synthesized PBS and PBF prepolymers, capable of maintaining their sustainable character.

Chapter 6: End-use case study of the enzymatically synthesized and post-polymerization PBS: evaluation of suitability as a matrix for active agent encapsulation

6.1 Introduction

As is thoroughly discussed in Chapter 1.3, conventionally synthesized PBS, PLA, cellulose acetate phthalate (CAP), poly(ϵ -caprolactone) (PCL) and poly (D, L- lactide-co-glycolide) (PLGA) have been tested as carriers in controlled release systems, including active food packaging applications [139,140,229,230].

However, the main drawback of using conventional synthesized polymer grades, and especially PBS, is the requirement of metal catalysts in amounts between 100 and 1500 ppm, e.g., Ti 100–360 ppm, Sb 350–450 ppm, and Sn 450–1500 ppm [23]. These metal contents can be a significant drawback, especially for the food packaging industry, considering that according to the compostable and biodegradable polymers packaging standards, heavy metals should not exceed the maximum allowable level of 150 mg kg⁻¹ (i.e., 150 ppm) on dry substance [20]. An alternative approach to producing high molecular PBS is the combination of polycondensation with a finishing step of chain extension [169]. A chain extender with two functional groups reacts with the terminal –OH or –COOH of PBS and couples two PBS chains. However, the biosafety and biodegradability of PBS can be negatively affected and, thus, impair the use of the chain-extended PBS as a food-contacting material [161].

The most common methods to remove metal-based catalyst residues from polymers, especially when destined for food packaging applications, include solvent extraction and leaching. However, these methods require several steps and many organic solvents and acids. Modern approaches that have been found effective, such as using a high-pressure CO₂/water binary system as a green solvent to dissolve and remove zinc-based catalysts from polymers, present high operation costs and need to be further optimized [20].

An alternative, novel approach could be using a polymer grade synthesized without metal catalysts, such as through enzymatic polymerization. In enzymatic polymerization, non-toxic enzymes are used as catalysts, and they do not have to be completely removed from the final product, as they are harmless for humans and the environment. Additionally, enzymatically synthesized polymers can be considered truly green, combining green properties (e.g., biological origin and biodegradability) and a sustainable production process. On that basis, thanks to its high quality and purity, an enzymatically synthesized PBS grade could be a promising candidate carrier in controlled release systems, including active food packaging applications and to the best of our knowledge, an enzymatically synthesized PBS grade has never been examined for controlled release systems in the open literature.

The mostly encapsulated active compounds are antioxidants, including polyphenol bioactive agents such as curcumin, essential oils and resveratrol, since oxidation is one of the main causes

of food spoilage. Antioxidants, when used in food packaging, prevent oxidation. Detrimental effects such as vitamin degradation and loss of essential fatty acids, which decrease the nutritional value of the food, are also prevented [231]. It is important to mention, though, that every upcoming technology must be critically evaluated and constantly improved. For example, there may be safety issues such as the package's components (i.e., (bio)polymer and/or other additives) migration to the food, which could risk human health [154]. Another challenge is establishing the optimal concentration distribution of antioxidants around the food to match the release kinetics with the oxidation kinetics of the food.

6.2 Scope

The main objective of this Chapter was to assess for the first time the suitability of the enzymatically synthesized PBS to form nanoparticles acting as a matrix for active agent encapsulation.

In this context, the enzymatically synthesized and upgraded PBS grade M4_110 (B-90_20g) was used as the starting material and in the first part of the chapter, blank PBS nanoparticles were formed to evaluate the effectiveness of the process. The naturally occurring antioxidant flavonoid, naringin was selected as a hydrophobic active agent to be encapsulated. Naringin-loaded nanoparticles were thus formed, and their main characteristics, including mean hydrodynamic diameter, zeta potential, encapsulation efficiency, and thermal properties, were assessed.

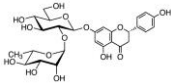
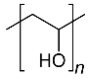
In the second part of the Chapter, the naringin-loaded PBS nanoparticles were submitted to *in vitro* release experiments to evaluate their capability to act as a matrix in encapsulation systems. The scope was to monitor the system's release rate, considering the matrix's low molecular weight. All the nanoparticle formulations and experiments were conducted in collaboration with the research team of the Organic Chemistry Laboratory, NTUA.

6.3 Experimental

6.3.1 Materials

The PBS grade used as a matrix for the encapsulation was the enzymatically synthesized and upgraded (melt post-polymerization at 110°C) M4_110 (B-90_20g). Table 18 and Tables S5 and S6 briefly present its thermal characteristics and molecular weights. Naringin (MW 580 g·mol⁻¹) and poly(vinyl alcohol) (PVA, MW 72000 g·mol⁻¹) were purchased from Tokyo Chemical Industry (Japan) and ITW Reagents (Italy), respectively (Table 19). Acetone (purity ≥ 99.5%) was purchased from KaloChem (Greece). All chemicals were used without further purification.

Table 19. Compounds used for naringin encapsulation in PBS

Compound	Molecular Formula	Structure	MW (g·mol ⁻¹)	Other characteristics	Supplier
Naringin	C ₂₇ H ₃₂ O ₁₄		580.5	Purity >95%	Tokyo Chemical Industry, Japan
PVA	[CH ₂ CH(OH)] _n		72000	DH 85 – 89%	ITW Reagents, Italy

6.3.2 Experimental procedure of naringin encapsulation in enzymatically synthesized and upgraded PBS

PBS nanoparticles were prepared according to the emulsification-solvent evaporation technique. For a loading 40% (mass of naringin per mass of polymer used, wt), PBS (300 mg) was dissolved in chloroform (30 mL) and naringin (120 mg) in acetone (9 mL). The organic solutions were mixed and added in an aqueous solution of PVA (1% w·v⁻¹). The mixture was submitted to sonication (160 Watt, for 6 min). The emulsion was left in an incubator (37°C, 100 rpm) overnight for solvent evaporation. The nanoparticles were recovered by five runs of centrifugation (20000 rpm, 20 min, 4°C) to entirely remove residual PVA. The supernatant from the first centrifugation run was stored at room temperature for indirect quantification of compound encapsulation efficiency. The nanoparticles were finally submitted to freeze-drying and stored in a desiccator. Unloaded (blank) nanoparticles were prepared using the same procedure without the addition of naringin. The process yield was calculated based on Eq. (1) in Chapter 2.3.2 where w_{exp} is the mass of the obtained nanoparticles after freeze-drying (g), and w_{theor} the theoretical weight of the nanoparticles, namely the sum of the initial polymer mass and the initial naringin mass (g).

6.3.3 Experimental procedure of *in vitro* naringin release

In vitro release of naringin from the polymeric nanoparticles was conducted using the dialysis method. Experiments were conducted by dispersing 26 mg of loaded nanoparticles into 5 mL of water and adding the dispersions in SEVAPOR® membranes (pore diameter approx. 25 Å). The membranes were immersed in beakers containing 40 mL phosphate buffer (pH 7.4) under magnetic stirring at 25°C ± 1°C. The amount of naringin released in each beaker was determined using UV–Vis spectroscopy.

6.3.4 Characterization techniques

6.3.4.1 Dynamic Light Scattering (DLS)

Mean particle size, polydispersity index (PDI) and ζ-potential of loaded and blank nanoparticles were determined *via* Dynamic Light Scattering (DLS) technique using a Zetasizer Nano ZS

(Malvern Instruments, UK, Figure 82). The samples were prepared by dispersing 0.2 mL of nanoparticle suspension in water (4 mL), resulting in off-white opaque aqueous suspensions. All measurements were performed in triplicate at $25 \pm 1^\circ\text{C}$.



Figure 82. Zetasizer Nano ZS

6.3.4.2 Encapsulation efficiency determination

The encapsulation efficiency (EE%) was determined using UV–Vis spectroscopy (Figure 83). For that purpose, the supernatant from the first centrifugation run, during the preparation of loaded nanoparticles, was decanted and the naringin content was determined using UV–Vis spectroscopy (λ_{max} 280 nm) and the Eq. (10) obtained by a relevant calibration curve (R^2 0.9995).

$$\text{Abs} = 8.6319 \cdot C + 0.0306 \quad (10)$$

where Abs: the intensity of the absorbance and C: the naringin concentration in $\text{mg}\cdot\text{mL}^{-1}$.



Figure 83. Jasco V – 770, Spectrophotometer (JASCO UK Limited, UK)

6.3.4.3 Differential Scanning Calorimetry (DSC) and Thermogravimetric Analysis (TGA)

Differential scanning calorimetry (DSC) measurements were performed in the system described in 2.3.3.4. Heating was conducted from 20 to 255°C , under N_2 flow ($20 \text{ mL}\cdot\text{min}^{-1}$), with a $10^\circ\text{C}\cdot\text{min}^{-1}$ rate. Thermogravimetric analysis (TGA) was conducted as presented in 2.3.3.5.

6.4 Results

6.4.1 Formation of enzymatically synthesized PBS nanoparticles for naringin encapsulation

Unloaded PBS nanoparticles were first formed to evaluate the effectiveness of the herein applied procedure. The nanoparticles' mean hydrodynamic diameter was about 470 nm (Table 20). The herein formed nanoparticles' polydispersity index was 0.76, indicating a broad size distribution [232], probably attributed to agglomeration. Zeta potential was found to be -8.5 mV. The negative charge of PBS is attributed to its ester end groups $C_2H_5O^-$ ($pK_a = 3.6$) that deionize in water, leading to negative charges in the polymer [233]. The absolute zeta potential value (>30 mV) indicates a suspension with aggregation tendency [229,234], in agreement with the aforementioned results.

Naringin-loaded PBS nanoparticles were formed in the next step. The process yield was 71%, similar to the unloaded nanoparticles' (Table 20). The encapsulation efficiency was 68%, slightly higher than analogous encapsulation systems reported in the literature (e.g., naringin encapsulation in PMMA nanoparticles, EE 60%) [235]. The nanoparticles' size and ζ -potential were similar to those of the unloaded nanoparticles, while their polydispersity index (0.4) indicated a more homogenous nanoparticle population.

Table 20. Characterization of unloaded (Blank) and naringin-loaded PBS nanoparticles: particle size, polydispersity index (PDI), ζ -potential, encapsulation efficiency (EE), process yield

	Size (nm)	PDI	ζ -Potential (mV)	EE (%)	Process yield (%)
Unloaded PBS nanoparticles (Blank)	473±53.7	0.76±0.04	-8.5±0.4	-	68
Naringin-loaded PBS nanoparticles	450.8±13.6	0.40±0.03	-12.1±0.2	68	71

The following DSC and TGA results verified that the encapsulation was successful. Naringin presented two endotherms, a broader one at $60 - 130^\circ C$ and a sharper one at $160^\circ C$ (Figure 84a). The first one probably corresponds to the loss of water molecules [236], while the second is the melting endotherm. These endotherms are present in the physical mixture of PBS-naringin, weaker and shifted at $120 - 140^\circ C$ and $150^\circ C$ but with the same morphology (Figure 84b). The naringin peaks' shift to higher temperatures in the physical mixture can be attributed to the substances' intermolecular interactions, i.e., hydrogen bonding between the naringin hydroxyl groups ($-OH$) and PBS ester bonds, requiring additional energy to melt. Based on the loaded nanoparticles DSC curve, naringin was encapsulated as amorphous in PBS nanoparticles. The transition from a crystalline to an amorphous state of an active agent after encapsulation is typical and observed in different encapsulation systems, including naringin-loaded alginate microspheres [237] and curcumin-loaded lipid nanoparticles [238]. This

phenomenon could be attributed to the stresses (e.g., mechanical pressure) exerted on the active agent during encapsulation. For instance, the ultrasound energy applied during sonication could cause the naringin crystalline structure deformation. Additionally, the main endotherm of the PBS matrix of the loaded nanoparticles (102°C) was broader vs. unloaded particles, probably due to the loss of encapsulated naringin’s water molecules starting at lower temperatures. The endothermic peak of the loaded nanoparticles’ thermogram at 194°C is attributed to residual PVA [239]. The blank nanoparticles’ DSC curve was sharp, and the calculated crystallinity was 54%, while an exothermic peak appeared at 74°C, revealing an increased tendency of PBS to crystallize. The crystallinity of the matrix is considered a key factor for controlled release, with amorphous polymers facilitating the active agent’s diffusion, thus accelerating the release rate [240]. As a highly crystalline polymer (x_c ca. 60%), PBS presents generally low degradation and release rates [159,241].

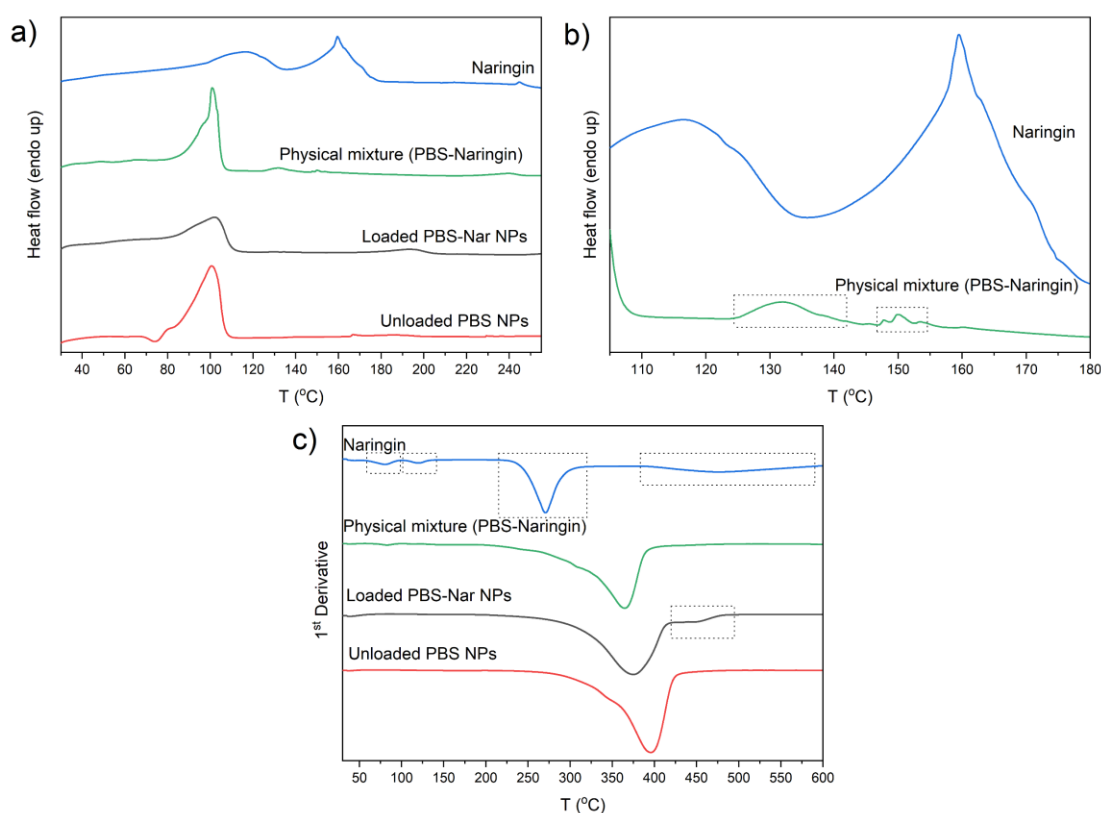


Figure 84. (a) DSC (1st heating), (b) zoomed DSC (1st heating) and (c) TGA (1st derivative) of Naringin (blue), physical mixture of PBS-Naringin (green), naringin-loaded and unloaded PBS nanoparticles (grey and red respectively)

Regarding TGA results, naringin presented four different decomposition stages (Figure 84c); the first two (80 and 120°C) are attributed to the water loss in agreement with the relevant DSC results. The main naringin decomposition occurred at 271°C, and the final decomposition stage was depicted as a broad peak from 410 to 500°C. The naringin water loss is also monitored in the physical mixture. However, the main naringin decomposition stages (271°C and 410 – 500°C) are not distinct, confirming PBS and naringin molecules interaction in the physical mixture in agreement with the abovementioned DSC results. The main decomposition peak of

the physical mixture is monitored at 365°C, between naringin and pure PBS decomposition peaks (Table S6), as expected. The loaded nanoparticles presented two distinct decomposition stages; the first is the main decomposition peak monitored at 375°C (10°C higher than the physical mixture), indicating a different topology between the loaded nanoparticles and the physical mixture. The second one, monitored at 420 – 480°C, is attributed to residual PVA, also evidenced by DSC.

$T_{d,5\%}$ values also confirmed the different topologies of the loaded nanoparticles and the substances' physical mixture. Loaded nanoparticles presented $T_{d,5\%}$ at 269°C, namely 74°C higher than the physical mixture ($T_{d,5\%}$ 195°C) and 35°C lower than the unloaded nanoparticles ($T_{d,5\%}$ 303°C). The higher $T_{d,5\%}$ of the loaded nanoparticles compared to the physical mixture, indicated the naringin's uniform distribution within the PBS matrix preventing localized heating, and thus delaying thermal degradation compared to the physical mixture of the substances. The lower $T_{d,5\%}$ of the loaded nanoparticles compared to the unloaded, is due to the water loss of the naringin in the loaded nanoparticles during heating. Overall, the $T_{d,5\%}$ values of all the nanoparticles were decreased compared to the pure PBS matrix ($T_{d,5\%}$ 317°C, Table S6), even for the unloaded particles, where no different chemical composition exists. This phenomenon is attributed to the size of the particles, as polymers' properties are strongly affected by surface effects and/or chain confinement and mobility and are considerably different for bulk and nano-sized grades [126,242].

6.4.2 *In vitro* release tests of the encapsulated in enzymatically synthesized PBS nanoparticles naringin

The naringin-loaded nanoparticles were then submitted to preliminary *in vitro* release experiments at 25°C and pH 7.4. These conditions were selected, as food storage (shells, warehouses) or transportation may occur at room temperature, and bacterial growth is enhanced near neutral pH. The release profile is presented in Figure 85.

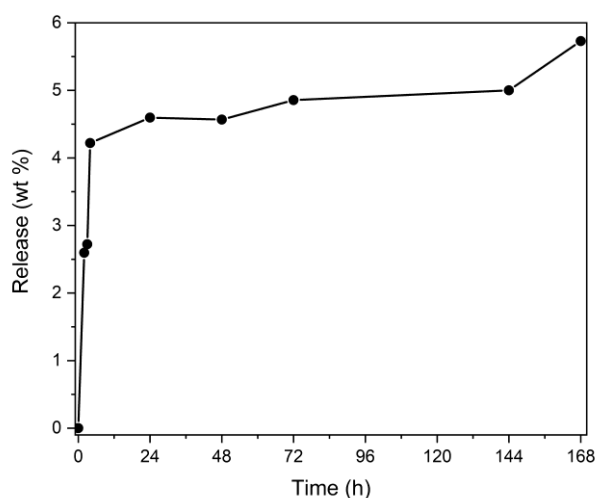


Figure 85. *In vitro* release profile of PBS nanoparticles loaded with naringin (pH 7.4, T=25°C)

During the first 4 h, a burst effect was observed during which almost 4.5% of naringin was released. The burst release is usually caused by the active agents' fast desorption at the surface, and a sustained release is expected to follow [241]. Actually, a plateau was reached until 114 h, and an increasing tendency was monitored at 168 h, reaching a value of almost 6%.

The predominant release mechanism affects the release rate, which has been slow in our system (6% for seven days) and should be further investigated as osmosis, diffusion, polymer swelling, and polymer erosion/degradation may contribute to the release process [243]. PBS, though, degrades slowly compared to other biodegradable polymers, and thus, the release is often dominated by the active agent's diffusion from the polymer matrix, making it thus appropriate for very long-term release systems [159]. In this context, Brunner *et al.* [159] used a commercial PBS grade to form microcapsules and investigated the controlled release of a hydrophilic and a hydrophobic bioactive agent (i.e., bovine serum albumin (BSA) and all-trans retinoic acid (atRA), respectively). BSA was released at 6% after 3 weeks and atRA at 9% after 42 days. Based on the herein results, it could be considered that diffusion is the predominant mechanism until 144 h, and PBS hydrolysis is the following predominant mechanism, becoming more intense after 144 h. Overall, the encapsulated naringin release confirms that the enzymatically synthesized PBS can be used as a matrix, especially for long-term release systems, despite its low molecular weight.

6.5 Conclusions

The applied procedure's effectiveness was first evaluated with the formation of unloaded PBS nanoparticles. The obtained nanoparticles' mean hydrodynamic diameter was 470 nm, and an aggregation tendency was indicated by the increased PDI and the absolute zeta potential value (>30 mV).

Naringin-loaded nanoparticles were formed, and the defined encapsulation efficiency was higher than analogous encapsulation systems reported in the literature (68% instead of 60% for naringin-loaded PMMA nanoparticles). During DSC, it was found that even though naringin is crystalline, it was encapsulated as amorphous, attributed to the stresses exerted on the active agent during encapsulation (e.g., ultrasound energy). The loaded nanoparticles presented two distinct decomposition stages; the first, attributed to the main decomposition at 375°C (10°C higher than the physical mixture), indicated a different topology between the loaded nanoparticles and the physical mixture. The second one, monitored at 420 – 480°C, was attributed to residual PVA, also evidenced by DSC. Additionally, loaded nanoparticles presented $T_{d,5\%}$ 74°C higher than the physical mixture, indicating the naringin's uniform distribution within the PBS matrix, preventing localized heating and thus delaying thermal degradation.

After confirming the enzymatically synthesized PBS's suitability to act as a matrix in encapsulation systems, preliminary *in vitro* release tests were conducted. It was indicated that after 168 h, almost 6% of naringin was released and confirmed that the herein enzymatically

synthesized PBS is a promising candidate carrier in controlled release systems, especially for long-term release applications, despite its low molecular weight.

7.1 General Conclusions

The present research work dealt with the enzymatic prepolymerization and post-polymerization of the bio-based polymers poly(butylene succinate) (PBS) and poly(butylene 2,5-furandicarboxylate) (PBF), thus shedding light on the relevant research area and increasing the selected polymers' research and industrial interest.

In the first part of the research, dealing with enzymatic prepolymerization of bio-based prepolymers (Chapters 2 and 3), the immobilized *Candida antarctica* Lipase B (N435) was used as a biocatalyst in solvent-free systems. PBS and PBF were enzymatically synthesized *via* a two-stage process. The first step was conducted at milder conditions (40 or 50°C, atmospheric pressure, 24 h) to minimize possible monomers' losses. The second stage's conditions (reaction temperature, pressure, time) were thoroughly investigated.

The reaction time investigation was the first to occur (set of samples A and D, for PBS and PBF, respectively, Figure 86). The main achieved characteristics assessed were the molecular weight (MW) values and the prepolymers' thermal properties. For both systems, 90 and 95°C were indicated as the most promising reaction temperatures. The PBS achieved \overline{M}_n and \overline{M}_w reached 2300 and 5000 g·mol⁻¹, respectively (sample A-90), while PBF presented lower MW values up to 1800 and 1900 g·mol⁻¹ (D-90). Especially in the case of PBF, two molecular weight populations were monitored, with the percentage of the highest molecular weight population significantly increasing at 90°C. The highest monitored melting temperatures (T_m) and crystallinities of PBS were 107°C (sample A-95), close to commercial PBS grades' T_m (ca. 114°C) and 73 % (sample A-90). On the contrary, PBF prepolymers reached T_m values of 77°C (D-95), significantly lower than the reported values of chemically synthesized PBF grades (164-173°C), attributed to the low molecular weights. The defined crystallinities were low, i.e., up to 14% for D-90. The higher MW and improved thermal properties achieved for PBS compared to PBF are attributed to the different structures of the prepolymers' repeating units. Due to the presence of the bulky furan rings, DEF accessibility to the enzyme's active site is limited. Thus, the reaction rate is significantly lower, leading to the formation of lower MW oligoesters, apparently with poorer thermal properties.

The reduced pressure (set of samples B and E, Figure 86) had a slightly positive or no effect at 90°C, with the \overline{M}_n and \overline{M}_w reaching the values 2500 and 6700 g·mol⁻¹ for PBS (B-90) and remaining constant at 1800 and 1900 g·mol⁻¹ for PBF (E-90). It was thus indicated that the by-product removal *via* evaporation and diffusion is facilitated by the aliphatic character of PBS and hindered by the ring presence in the PBF repeating unit. At 95°C, the reduced pressure negatively affected both PBS and PBF prepolymers (B-95 and E-95, respectively). This was mainly attributed to the decreased enzyme efficiency due to thermal deactivation, leading to lower molecular weight oligomers and their extended sublimation, interrupting chain built-up

more abruptly. The PBF thermal properties were not significantly affected by the by-product removal rate through vacuum application, indicating that the chemical reaction mainly controls the process. On the contrary, the PBS prepolymer synthesized at 95°C (B-95) presented poor thermal properties and stability compared to A-95 (e.g., $T_{d,5\%}$ 272°C and 326°C, respectively), attributed to its decreased MW.

Increased reaction times at 90 and 95°C negatively affected PBS and PBF enzymatic prepolymerizations (set of samples C and F, Figure 86). The prepolymers' decreased MW at 90°C indicate that the chemical reaction reached equilibrium (due to high active end groups consumption) and increased by-product amounts were formed, requiring a higher vacuum to be removed. The by-product accumulation within the reacting mass led to susceptible to alcoholysis oligomers. At 95°C, the observed MW decreases are attributed to more intense thermal deactivation of the enzyme. The PBS prepolymer C-95 presented notably lower thermal properties compared to the reference prepolymer A-95, attributed to its significantly lower MW. On the contrary, the PBF prepolymer's F-95 thermal properties were not significantly affected by the reaction time, confirming that at 95°C, thermal deactivation dominates the system and products of inferior properties are formed independently of the reaction time.

Thanks to the simplicity of the applied processes (low-temperature bulk polymerization technique, not requiring multiple solvents for the final product isolation), both the prepolymers were synthesized at larger scales at their optimal synthesis conditions (PBS: 90°C, 20 mbar, 2 h and PBF: 90°C, 200 mbar, 2h). Up to 20 g PBS (B-90_20g) and 6 g PBF (D-90_6g) were received for the first time, thus filling the relevant gap in the open literature. For the case of PBS, the scaled-up polymers' molecular weight values were found to be lower compared to the smaller scale grades due to mass transfer limitations that are more intense on large scales, while for PBF, the MW values decreased only slightly (16% decreased \overline{M}_w for the 6-g product), indicating the potential for a larger scaling up.

In the last part of the enzymatic prepolymerization investigation (Chapter 4), a novel, non-commercially available enzyme known for its ability to degrade plastic was used as a biocatalyst in a solvent-free system to produce PBS for the first time. An immobilized, thermostable variant of the Leaf and branch compost cutinase (LCC), LCC^{ICCG}, was thus used as a biocatalyst in a two-step process. In contrast to the N435 investigation, the reaction temperature of the first step was herein investigated (50-70°C, atmospheric pressure, 24 h) to study the enzyme's efficiency in the polymerization. The second stage was conducted at 80°C, under 200 mbar, for 2 h to favour the polymerization reaction. PBS was successfully synthesized in all the tested temperatures, and even though the MW of the products were found to be similar (set of samples L, Figure 86), with three distinct populations, reaching 1400 and 1500 g mol⁻¹ (\overline{M}_n and \overline{M}_w), the products of higher temperatures had an increased amount of the higher molecular weight population. The achieved MW values and thermal properties were significantly lower than the products' of the commercial enzyme N435. For instance, $T_{d,5\%}$ reached the value of 224°C, i.e., 103°C lower than the B-90. However, the synthesized prepolymers presented several

advantages, including narrow molecular weight distributions (\mathcal{D} up to 1.33), rendering them valuable candidates for high-demanding applications such as drug delivery systems.

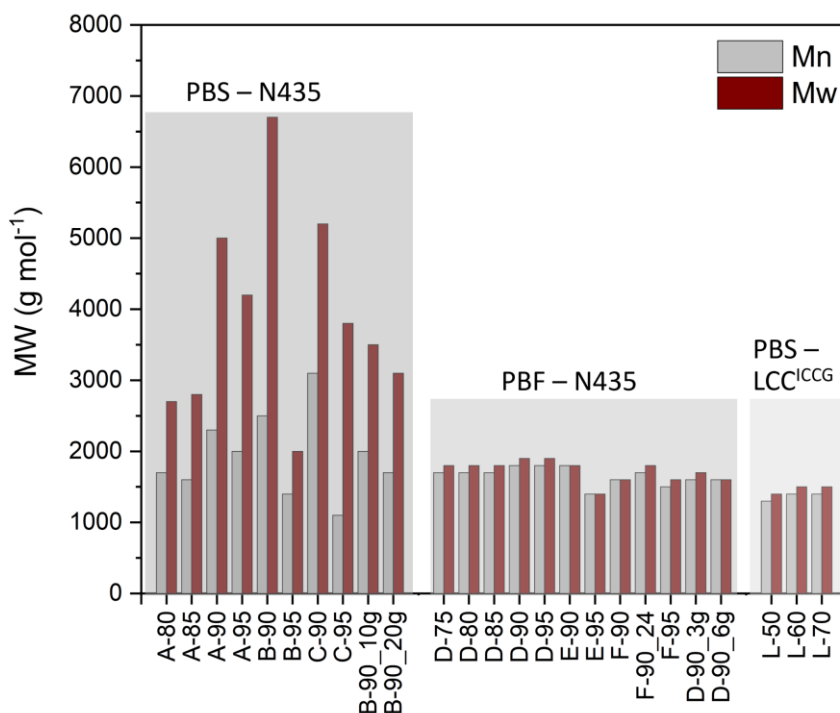


Figure 86. Total molecular weights of the enzymatically synthesized prepolymers PBS and PBF. Reaction temperature investigation: set of samples A, D and L; Pressure investigation: set of samples: B and E; Reaction time investigation: set of samples C and F.

In the second part of this research (Chapter 5), we focused on upgrading the enzymatically synthesized prepolymers through post-polymerization. In the case of PBS, the N435-synthesized and scaled-up (20 g) prepolymer B-90_20g and the LCC^{LCCG}--synthesized prepolymers (L-50, L-60, L-70) were used as starting materials (Figure 87). In the case of PBF, the scaled-up (3 g) prepolymer D-90_3g was the starting material (Figure 87). The PBS B-90_20g prepolymer was first submitted to SSP at 95°C ($T_m - T_{SSP} = 7^\circ\text{C}$), and a precrystallization step (90°C, 20 mbar, 2 h) was introduced before the main SSP to eliminate possible sintering issues. SSP was not found to be effective as the molecular weights increased slightly (S-95). The next approach included the $T_m - T_{SSP}$ reduction up to 2°C and was conducted at 100°C. After the first 2 h of SSP, a solid-melt transition phenomenon occurred, probably due to the co-existence of ethanol (by-product) and water (absorbed moisture). Despite the melt state of the prepolymer, post-polymerization was not significantly favored, not even at longer reaction times that were tested (S2_M2, S2_M4 and S2_M6). On that basis, B-90_20g was submitted to melt post-polymerization, conducted at 110°C under reduced pressure of 20 mbar for 4 h (M4_110), with the addition of a drying step to remove any possible absorbed moisture from the prepolymer. The melt-post polymerization was effective, and the achieved $\Delta\overline{M}_n$ and $\Delta\overline{M}_w$ percentages were 76 and 94 %, respectively. On that basis, the reaction time and temperature of melt post-polymerization were then investigated. The reaction time and temperature examined windows were 4 to 10 h (at 110°C) and 110 to 150°C (for 4 h). It was concluded that

competitive phenomena occur during the process. Until 6 h, melt-post polymerization dominates the system, while after 6 h, the decomposition reactions seem to dominate, and the product's degradation becomes more intense. As regards the temperature investigation, PBS remained stable until 130°C, while thermal (or thermo-oxidative) degradation occurred at higher temperatures, especially at 150°C. It was concluded that 110°C and 4 h were the most appropriate conditions, balancing the required prepolymer's upgrade and the process's energy requirements as low as possible. The last parameter of the PBS melt post-polymerization to be examined was using a prepolymer with increased OH-end groups, especially the grade synthesized with 5% BDO molar excess, leading to 64 % OH-end groups. The increased OH end group percentage (64 %) did not significantly favour the post-polymerization, probably due to the formation of BDO as the by-product during efficient trans-esterification, which is harder to diffuse into the reacting mass and remove from the reacting mass than ethanol. The PBS grades synthesized with LCC^{ICCG} were submitted to post-polymerization using a TGA chamber as micro-reactor. The post-polymerization process was conducted under nitrogen flow and the prepolymers were heated up to 360°C. The post-polymerized samples were received in a solid form and the monitored \overline{M}_n and $\Delta\overline{M}_w$ reached 150 and 350 %, corresponding to \overline{M}_n and \overline{M}_w values of 3300 g·mol⁻¹ and \overline{M}_w 5600 g·mol⁻¹. The increased susceptibility of the LCC^{ICCG}-synthesized prepolymers was thus proved.

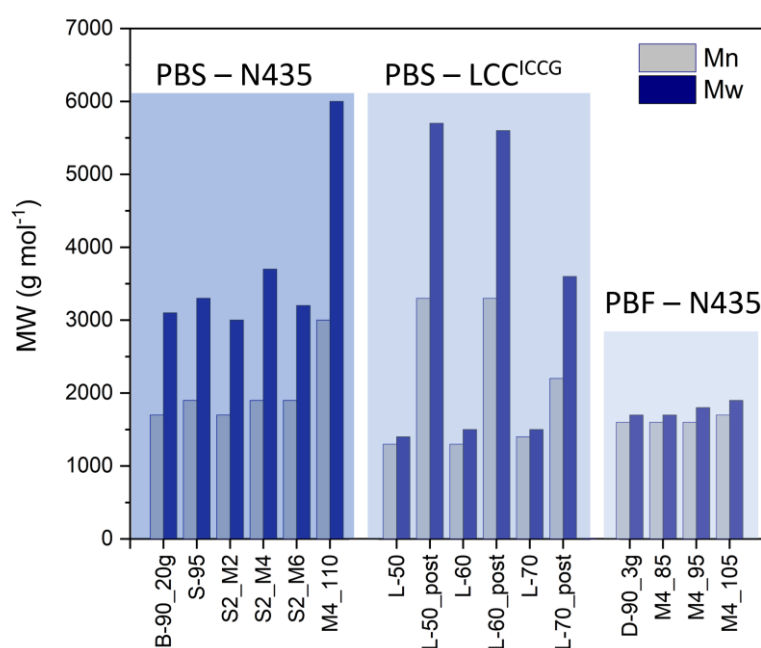


Figure 87. Total molecular weights of the post-polymerized PBS and PBF

Considering the SSP ineffectiveness on PBS, and the PBF structural peculiarity (bulky furan rings) and high hydroxyl end group percentages, that may hinder SSP, PBF was only submitted to melt post-polymerization. Three different temperatures were examined (85, 95 and 105°C) and despite the relatively low monitored molecular weight increases ($\Delta\overline{M}_n$ and $\Delta\overline{M}_w$ 6 and 12

%, respectively) its susceptibility to post-polymerization was confirmed, especially at 105°C. In addition, an increasing trend was observed.

The enzymatically synthesized, scaled-up and upgraded PBS was examined as a carrier for controlled release systems using the naturally occurring antioxidant flavonoid, naringin, as a model compound to be encapsulated. Unloaded nanoparticles were firstly successfully formed (hydrodynamic diameter ca. 470 nm), and an aggregation tendency was indicated by the increased polydispersity index (PDI) and the absolute zeta potential value (>30 mV). Naringin-loaded nanoparticles were formed and the defined encapsulation efficiency was higher than analogous encapsulation systems reported in the literature (68 % instead of 60 % for naringin-loaded PMMA nanoparticles). The system's controlled release was assessed *via* preliminary *in vitro* release experiments. Despite its low molecular weight, the enzymatically synthesized and upgraded PBS was a promising candidate carrier in controlled release systems, especially for long-term release applications.

7.2 Future Research

In the framework of this research, a combination of a synthetic (enzymatic prepolymerization) and upgrading (low-temperature post-polymerization) process to produce bio-based polymers was established. The selected polymers submitted to this route were poly(butylene succinate) (PBS) and poly(butylene 2,5-furandicarboxylate) as representatives of aliphatic and aliphatic bio-based polyesters. Even though the herein suggested route was effective, it could be useful to examine its universality by submitting different bio-based polymers, such as poly(lactic acid) and poly(propylene 2,5-furandicarboxylate) (PPF), to it. PPF, an FDCA-based polyester with higher barrier properties, is a promising packaging material expected to rise soon.

Some more detailed suggestions for future work follow, addressing every part of this research.

Enzymatic prepolymerization of PBS and PBF

- Regarding the further optimization of the enzymatic prepolymerization, the reaction time of the first stage could be investigated with the aim of further reducing energy consumption in line with the main green chemistry principles.
- The scalability of the enzymatic polymerization processes to produce PBS and PBF was proved. However, further scaling up should be considered for both PBS and PBF, with the appropriate parameters fine-tuning (e.g., enzyme concentration).
- Since the cutinase LCC^{ICCG} was found effective for the enzymatic polymerization of PBS, new enzymes, such as the *Humicola insolens* cutinase, could also be examined. LCC^{ICCG} and other novel enzymes could also be tested in the FDCA-polyesters production.

Post-polymerization of PBS and PBF

- Melt post-polymerization was proved effective for PBS; however, the applied process could be further investigated regarding the surrounding environment. For instance, post-polymerization could be conducted under an N₂-atmosphere.
- Melt post-polymerization was found promising for PBF; the reaction temperature, time, and surrounding environment should be investigated.

PBS usage as a carrier for drug delivery systems

- PBS was found effective as a carrier for drug delivery systems; however, more *in vitro* release experiments must be conducted to monitor naringin release for longer times since a slow release profile was revealed.
- Different active agents may be tested under different conditions (i.e., pH, temperature), aiming at (food) packaging and biomedical applications, as the high purity of PBS renders it promising for usage in this field, too.

References

- [1] H. Nakajima, P. Dijkstra, K. Loos, The recent developments in biobased polymers toward general and engineering applications: Polymers that are upgraded from biodegradable polymers, analogous to petroleum-derived polymers, and newly developed, *Polymers (Basel)*. 9 (2017) 1–26. <https://doi.org/10.3390/polym9100523>.
- [2] P. Anastas, N. Eghbali, *Green Chemistry: Principles and Practice*, *Chem. Soc. Rev.* 39 (2010) 301–312. <https://doi.org/10.1039/b918763b>.
- [3] M.A. Dubé, S. Salehpour, Applying the Principles of Green Chemistry to Polymer Production Technology, *Macromol. React. Eng.* 8 (2014) 7–28. <https://doi.org/10.1002/mren.201300103>.
- [4] R.P. Babu, K. O'Connor, R. Seeram, Current progress on bio-based polymers and their future trends, *Prog. Biomater.* 2 (2013) 8. <https://doi.org/10.1186/2194-0517-2-8>.
- [5] R.A. Ilyas, S.M. Sapuan, A. Kadier, M.S. Kalil, R. Ibrahim, M.S.N. Atikah, N.M. Nurazzi, A. Nazrin, C.H. Lee, M.N. Faiz Norrrahim, N.H. Sari, E. Syafri, H. Abrial, L. Jasmani, M.I.J. Ibrahim, *Properties and Characterization of PLA, PHA, and Other Types of Biopolymer Composites*, Elsevier Inc., 2020. <https://doi.org/10.1016/b978-0-12-819661-8.00008-1>.
- [6] M. Savioli Lopes, A.L. Jardini, R. Maciel Filho, Poly (lactic acid) production for tissue engineering applications, *Procedia Eng.* 42 (2012) 1402–1413. <https://doi.org/10.1016/j.proeng.2012.07.534>.
- [7] T.U. Rehman, L.A. Shah, M. Khan, M. Irfan, N.S. Khattak, Zwitterionic superabsorbent polymer hydrogels for efficient and selective removal of organic dyes, *RSC Adv.* 9 (2019) 18565–18577. <https://doi.org/10.1039/c9ra02488c>.
- [8] T. Aziz, H. Fan, F.U. Khan, R. Ullah, F. Haq, M. Iqbal, A. Ullah, Synthesis of Carboxymethyl Starch-Bio-Based Epoxy Resin and their Impact on Mechanical Properties, *Zeitschrift Fur Phys. Chemie.* 234 (2020) 1759–1769. <https://doi.org/10.1515/zpch-2019-1434>.
- [9] C. Li, H. Fan, T. Aziz, C. Bittencourt, L. Wu, D.Y. Wang, P. Dubois, Biobased Epoxy Resin with Low Electrical Permissivity and Flame Retardancy: From Environmental Friendly High-Throughput Synthesis to Properties, *ACS Sustain. Chem. Eng.* 6 (2018) 8856–8867. <https://doi.org/10.1021/acssuschemeng.8b01212>.
- [10] J.H. Song, R.J. Murphy, R. Narayan, G.B.H. Davies, Biodegradable and compostable alternatives to conventional plastics, *Philos. Trans. R. Soc. B Biol. Sci.* 364 (2009) 2127–2139. <https://doi.org/10.1098/rstb.2008.0289>.
- [11] A.S. Luyt, S.S. Malik, Can Biodegradable Plastics Solve Plastic Solid Waste Accumulation?, in: S.M. Al-Salem (Ed.), *Plast. to Energy*, William Andrew Publishing, 2019: pp. 403–423. <https://doi.org/https://doi.org/10.1016/B978-0-12-813140-4.00016-9>.
- [12] E. Rudnik, D. Briassoulis, Comparative Biodegradation in Soil Behaviour of two Biodegradable Polymers Based on Renewable Resources, *J. Polym. Environ.* 19 (2011) 18–39. <https://doi.org/10.1007/s10924-010-0243-7>.
- [13] G. Gallet, R. Lempiäinen, S. Karlsson, Characterization by solid phase microextraction-gas chromatography-mass spectrometry of matrix changes of poly(L-lactide) exposed to outdoor soil environment, *Polym. Degrad. Stab.* 71 (2000) 147–151. [https://doi.org/10.1016/S0141-3910\(00\)00165-8](https://doi.org/10.1016/S0141-3910(00)00165-8).
- [14] T. Narancic, S. Verstichel, S. Reddy Chaganti, L. Morales-Gamez, S.T. Kenny, B. De Wilde, R. Babu Padamati, K.E. O'Connor, Biodegradable Plastic Blends Create New Possibilities for End-

- of-Life Management of Plastics but They Are Not a Panacea for Plastic Pollution, *Environ. Sci. Technol.* 52 (2018) 10441–10452. <https://doi.org/10.1021/acs.est.8b02963>.
- [15] M. Hans, H. Keul, M. Moeller, Ring-opening polymerization of DD-lactide catalyzed by novozyme 435, *Macromol. Biosci.* 9 (2009) 239–247. <https://doi.org/10.1002/mabi.200800236>.
- [16] R. García-Arrazola, D.A. López-Guerrero, M. Gimeno, E. Bárzana, Lipase-catalyzed synthesis of poly-L-lactide using supercritical carbon dioxide, *Polym. Adv. Technol.* 19 (2008) 1396–1400. <https://doi.org/10.1016/j.supflu.2009.08.014>.
- [17] R. Auras, B. Harte, S. Selke, An overview of polylactides as packaging materials, *Macromol. Biosci.* 4 (2004) 835–864. <https://doi.org/10.1002/mabi.200400043>.
- [18] G. Li, M. Zhao, F. Xu, B. Yang, X. Li, X. Meng, L. Teng, F. Sun, Y. Li, Synthesis and Biological Application of Polylactic Acid, *Molecules.* 25 (2020). <https://doi.org/10.3390/molecules25215023>.
- [19] X. Montané, J.M. Montornes, A. Nogalska, M. Olkiewicz, M. Giamberini, R. Garcia-Valls, M. Badia-Fabregat, I. Jubany, B. Tylkowski, Synthesis and synthetic mechanism of Polylactic acid, *Phys. Sci. Rev.* 5 (2020) 20190102.
- [20] B. Bahramian, Y. Ma, R. Rohanzadeh, W. Chrzanowski, F. Dehghani, A new solution for removing metal-based catalyst residues from a biodegradable polymer, *Green Chem.* 18 (2016) 3740–3748. <https://doi.org/10.1039/c5gc01687h>.
- [21] K. Masutani, Y. Kimura, PLA Synthesis and Polymerization, in: A. Jiménez, M. Peltzer, R. Ruseckaite (Eds.), *Poly(Lactic Acid) Sci. Technol. Process. Prop. Addit. Appl.*, Royal Society of Chemistry, Cambridge, United Kingdom, 2014: pp. 3–36.
- [22] C.S. Hege, S.M. Schiller, Non-toxic catalysts for ring-opening polymerizations of biodegradable polymers at room temperature for biohybrid materials, *Green Chem.* 16 (2014) 1410–1416. <https://doi.org/10.1039/c3gc42044b>.
- [23] N. Jacquél, F. Freyermouth, F. Fenouillot, A. Rousseau, J.P. Pascault, P. Fuertes, R. Saint-Loup, Synthesis and properties of poly(butylene succinate): Efficiency of different transesterification catalysts, *J. Polym. Sci. Part A Polym. Chem.* 48 (2011) 5301–5312. <https://doi.org/10.1002/pola.25009>.
- [24] D.N. Bikiaris, D.S. Achilias, Synthesis of poly(alkylene succinate) biodegradable polyesters, Part II: Mathematical modelling of the polycondensation reaction, *Polymer (Guildf.)* 49 (2008) 3677–3685. <https://doi.org/10.1016/j.polymer.2008.06.026>.
- [25] C.D. Papaspyrides, S. Vouyiouka, I.N. Georgousopoulou, S. Marinkovic, B. Estrine, C. Joly, P. Dole, Feasibility of Solid-State Postpolymerization on Fossil- and Bio-Based Poly(butylene succinate) Including Polymer Upcycling Routes, *Ind. Eng. Chem. Res.* 55 (2016) 5832–5842. <https://doi.org/10.1021/acs.iecr.6b00588>.
- [26] A. Pellis, M. Malinconico, A. Guarneri, L. Gardossi, Renewable polymers and plastics : Performance beyond the green, *N. Biotechnol.* 60 (2021) 146–158. <https://doi.org/10.1016/j.nbt.2020.10.003>.
- [27] Y. Jiang, K. Loos, Enzymatic synthesis of biobased polyesters and polyamides, *Polymers (Basel)*. 8 (2016). <https://doi.org/10.3390/polym8070243>.
- [28] K. Loos, R. Zhang, I. Pereira, B. Agostinho, H. Hu, D. Maniar, A Perspective on PEF Synthesis , Properties , and End-Life, 8 (2020) 1–18. <https://doi.org/10.3389/fchem.2020.00585>.

- [29] L. Lalanne, G.S. Nyanhongo, G.M. Guebitz, A. Pellis, Biotechnological production and high potential of furan-based renewable monomers and polymers, *Biotechnol. Adv.* 48 (2021) 107707. <https://doi.org/10.1016/j.biotechadv.2021.107707>.
- [30] A.P.S. Brogan, K.P. Sharma, A.W. Perriman, S. Mann, Enzyme activity in liquid lipase melts as a step towards solvent-free biology at 150 °C, *Nat. Commun.* 5 (2014). <https://doi.org/10.1038/ncomms6058>.
- [31] B.D. Ribeiro, A.M. De Castro, M.A.Z. Coelho, D.M.G. Freire, Production and use of lipases in bioenergy: A review from the feedstocks to biodiesel production, *Enzyme Res.* 2011 (2011). <https://doi.org/10.4061/2011/615803>.
- [32] A. Douka, S. Vouyiouka, L.M. Papaspyridi, C.D. Papaspyrides, A review on enzymatic polymerization to produce polycondensation polymers: The case of aliphatic polyesters, polyamides and polyesteramides, *Prog. Polym. Sci.* 79 (2018) 1–25. <https://doi.org/10.1016/j.progpolymsci.2017.10.001>.
- [33] A. Pellis, J.W. Comerford, A.J. Maneffa, M.H. Sipponen, J.H. Clark, T.J. Farmer, Elucidating enzymatic polymerisations: Chain-length selectivity of *Candida antarctica* lipase B towards various aliphatic diols and dicarboxylic acid diesters, *Eur. Polym. J.* 106 (2018) 79–84. <https://doi.org/10.1016/j.eurpolymj.2018.07.009>.
- [34] V. Ferrario, A. Pellis, M. Cespugli, G.M. Guebitz, L. Gardossi, Nature inspired solutions for polymers: Will cutinase enzymes make polyesters and polyamides greener?, *Catalysts.* 6 (2016) 205. <https://doi.org/10.3390/catal6120205>.
- [35] J. Ichi Kadokawa, S. Kobayashi, Polymer synthesis by enzymatic catalysis, *Curr. Opin. Chem. Biol.* 14 (2010) 145–153. <https://doi.org/10.1016/j.cbpa.2009.11.020>.
- [36] M. Kanelli, A. Douka, S. Vouyiouka, C.D. Papaspyrides, E. Topakas, L.M. Papaspyridi, P. Christakopoulos, Production of biodegradable polyesters via enzymatic polymerization and solid state finishing, *J. Appl. Polym. Sci.* 131 (2014) 2–9. <https://doi.org/10.1002/app.40820>.
- [37] Y. Yu, D. Wu, C. Liu, Z. Zhao, Y. Yang, Q. Li, Lipase/esterase-catalyzed synthesis of aliphatic polyesters via polycondensation: A review, *Process Biochem.* 47 (2012) 1027–1036. <https://doi.org/10.1016/j.procbio.2012.04.006>.
- [38] Y. Hu, W.A. Daoud, K.K.L. Cheuk, C.S.K. Lin, Newly developed techniques on polycondensation, ring-opening polymerization and polymer modification: Focus on poly(lactic acid), *Materials (Basel)*. 9 (2016). <https://doi.org/10.3390/ma9030133>.
- [39] Rahmayetty, Y. Whulanza, Sukirno, S.F. Rahman, E.A. Suyono, M. Yohda, M. Gozan, Use of *Candida rugosa* lipase as a biocatalyst for L-lactide ring-opening polymerization and polylactic acid production, *Biocatal. Agric. Biotechnol.* 16 (2018) 683–691. <https://doi.org/10.1016/j.bcab.2018.09.015>.
- [40] M. Takwa, M.W. Larsen, K. Hult, M. Martinelle, Rational redesign of *Candida antarctica* lipase B for the ring opening polymerization of d,d-lactide, *Chem. Commun.* 47 (2011) 7392–7394. <https://doi.org/10.1039/c1cc10865d>.
- [41] S. Målberg, A. Finne-Wistrand, A.C. Albertsson, The environmental influence in enzymatic polymerization of aliphatic polyesters in bulk and aqueous mini-emulsion, *Polymer (Guildf)*. 51 (2010) 5318–5322. <https://doi.org/10.1016/j.polymer.2010.09.016>.
- [42] H.Ö. Düşkünkörür, A. Bégué, E. Pollet, V. Phalip, Y. Güvenilir, L. Avérous, Enzymatic ring-opening (co)polymerization of lactide stereoisomers catalyzed by lipases. Toward the in situ synthesis of organic/inorganic nanohybrids, *J. Mol. Catal. B Enzym.* 115 (2015) 20–28.

- <https://doi.org/10.1016/j.molcatb.2015.01.011>.
- [43] S.W. Duchiron, E. Pollet, S. Givry, L. Avérous, Mixed systems to assist enzymatic ring opening polymerization of lactide stereoisomers, *RSC Adv.* 5 (2015) 84627–84635. <https://doi.org/10.1039/c5ra18954c>.
- [44] F. Guzmán-Lagunes, A. López-Luna, M. Gimeno, E. Bárzana, Enzymatic synthesis of poly-l-lactide in supercritical R134a, *J. Supercrit. Fluids.* 72 (2012) 186–190. <https://doi.org/10.1016/j.supflu.2012.08.017>.
- [45] S. Chanfreau, M. Mena, J.R. Porrás-Domínguez, M. Ramírez-Gilly, M. Gimeno, P. Roquero, A. Tecante, E. Bárzana, Enzymatic synthesis of poly-L-lactide and poly-L-lactide-co-glycolide in an ionic liquid, *Bioprocess Biosyst. Eng.* 33 (2010) 629–638. <https://doi.org/10.1007/s00449-009-0388-8>.
- [46] H. Zhao, G.A. Nathaniel, P.C. Merenini, Enzymatic ring-opening polymerization (ROP) of lactides and lactone in ionic liquids and organic solvents: Digging the controlling factors, *RSC Adv.* 7 (2017) 48639–48648. <https://doi.org/10.1039/c7ra09038b>.
- [47] D. Omay, Y. Guvenilir, Synthesis and characterization of poly(d,l-lactic acid) via enzymatic ring opening polymerization by using free and immobilized lipase, *Biocatal. Biotransformation.* 31 (2013) 132–140. <https://doi.org/10.3109/10242422.2013.795148>.
- [48] M. Mena, K. Shirai, A. Tecante, E. Bárzana, M. Gimeno, Enzymatic syntheses of linear and hyperbranched poly-L-lactide using compressed R134a–ionic liquid media, *J. Supercrit. Fluids.* 103 (2015) 77–82. <https://doi.org/10.1016/j.supflu.2015.04.024>.
- [49] C. Gkountela, M. Rigopoulou, E.M. Barampouti, S. Vouyiouka, Enzymatic prepolymerization combined with bulk post-polymerization towards the production of bio-based polyesters: The case of poly(butylene succinate), *Eur. Polym. J.* 143 (2021) 110197. <https://doi.org/10.1016/j.eurpolymj.2020.110197>.
- [50] V. Lassalle, M. Ferreira, Lipase-catalyzed synthesis of polylactic acid: an overview of the experimental aspects, *J. Chem. Technol. Biotechnol.* 83 (2008) 1493–1502. <https://doi.org/10.1002/jctb>.
- [51] Rahmayetty, D.R. Barleany, E. Suhendi, B. Prasetya, T. Andiyani, Poly(lactic acid) Synthesis via Direct Polycondensation Method Using *Candida rugosa* Lipase Catalyst, *World Chem. Eng. J.* 1 (2017) 70–74.
- [52] T. Panyachanakul, T. Lomthong, W. Lorliam, J. Prajanbarn, S. Tokuyama, V. Kitpreechavanich, S. Krajangsang, New insight into thermo-solvent tolerant lipase produced by *Streptomyces* sp. A3301 for re-polymerization of poly (DL-lactic acid), *Polymer (Guildf).* 204 (2020) 122812. <https://doi.org/10.1016/j.polymer.2020.122812>.
- [53] B. Yeniad, H. Naik, A. Heise, Lipases in polymer chemistry, *Adv. Biochem. Eng. Biotechnol.* 125 (2011) 69–95. https://doi.org/10.1007/10_2010_90.
- [54] M. Nikulin, V. Švedas, Prospects of using biocatalysis for the synthesis and modification of polymers, *Molecules.* 26 (2021) 1–37. <https://doi.org/10.3390/molecules26092750>.
- [55] A. Pellis, E. Herrero Acero, V. Ferrario, D. Ribitsch, G.M. Guebitz, L. Gardossi, The Closure of the Cycle: Enzymatic Synthesis and Functionalization of Bio-Based Polyesters, *Trends Biotechnol.* 34 (2016) 316–328. <https://doi.org/10.1016/j.tibtech.2015.12.009>.
- [56] D.G. Filho, A.G. Silva, C.Z. Guidini, Lipases: sources, immobilization methods, and industrial applications, *Appl. Microbiol. Biotechnol.* 103 (2019) 7399–7423.

- <https://doi.org/10.1007/s00253-019-10027-6>.
- [57] N.F. Mokhtar, R. Noor, Z. Raja, A. Rahman, N. Dina, M. Noor, The Immobilization of Lipases on Porous Support by Adsorption and Hydrophobic Interaction Method, *Catalysts*. 10 (2020) 1–17.
- [58] M. Noel, D. Combes, Effects of temperature and pressure on *Rhizomucor miehei* lipase stability, *J. Biotechnol.* 102 (2003) 23–32. [https://doi.org/10.1016/S0168-1656\(02\)00359-0](https://doi.org/10.1016/S0168-1656(02)00359-0).
- [59] A. Kundys, E. Białocka-Florjańczyk, A. Fabiszewska, J. Małajowicz, *Candida antarctica* Lipase B as Catalyst for Cyclic Esters Synthesis, Their Polymerization and Degradation of Aliphatic Polyesters, *J. Polym. Environ.* 26 (2018) 396–407. <https://doi.org/10.1007/s10924-017-0945-1>.
- [60] F.C. Loeker, C.J. Duxbury, R. Kumar, W. Gao, R.A. Gross, S.M. Howdle, Enzyme-Catalyzed Ring-Opening Polymerization of ϵ -Caprolactone in Supercritical Carbon Dioxide, *Macromolecules*. 37 (2004) 2450–2453. <https://doi.org/10.1021/ma001252n>.
- [61] Y. Poojari, J.S. Beemat, S.J. Clarkson, Enzymatic synthesis of poly(ϵ -caprolactone): Thermal properties, recovery, and reuse of lipase B from *Candida antarctica* immobilized on macroporous acrylic resin particles, *Polym. Bull.* 70 (2013) 1543–1552. <https://doi.org/10.1007/s00289-013-0916-1>.
- [62] W. Adhami, Y. Bakkour, C. Rolando, Polylactones synthesis by enzymatic ring opening polymerization in flow, *Polymer (Guildf)*. 230 (2021) 124040. <https://doi.org/10.1016/j.polymer.2021.124040>.
- [63] C. Luna, D. Luna, F.M. Bautista, R. Estevez, J. Calero, A. Posadillo, A.A. Romero, E.D. Sancho, Application of enzymatic extracts from a CALB standard strain as biocatalyst within the context of conventional biodiesel production optimization, *Molecules*. 22 (2017). <https://doi.org/10.3390/molecules22112025>.
- [64] K.C.N.R. Pedro, J.M. Parreira, I.N. Correia, C.A. Henriques, M.A.P. Langone, Enzymatic biodiesel synthesis from acid oil using a lipase mixture, *Quim. Nova*. 41 (2018) 284–291. <https://doi.org/10.21577/0100-4042.20170180>.
- [65] E. Yilmaz, M. Soylak, Type of green solvents used in separation and preconcentration methods, *INC*, 2020. <https://doi.org/10.1016/b978-0-12-818569-8.00005-x>.
- [66] A. Pellis, F.P. Byrne, J. Sherwood, M. Vastano, J.W. Comerford, T.J. Farmer, Safer bio-based solvents to replace toluene and tetrahydrofuran for the biocatalyzed synthesis of polyesters, *Green Chem.* 21 (2019) 1686–1694. <https://doi.org/10.1039/c8gc03567a>.
- [67] D.R. Joshi, N. Adhikari, An Overview on Common Organic Solvents and Their Toxicity, *J. Pharm. Res. Int.* 28 (2019) 1–18. <https://doi.org/10.9734/jpri/2019/v28i330203>.
- [68] Y. Gu, F. Jérôme, Bio-based solvents: An emerging generation of fluids for the design of eco-efficient processes in catalysis and organic chemistry, *Chem. Soc. Rev.* 42 (2013) 9550–9570. <https://doi.org/10.1039/c3cs60241a>.
- [69] K. Häckl, W. Kunz, Some aspects of green solvents, *Comptes Rendus Chim.* 21 (2018) 572–580. <https://doi.org/10.1016/j.crci.2018.03.010>.
- [70] L. Gardella, D. Furaro, M. Galimberti, O. Monticelli, On the development of a facile approach based on the use of ionic liquids: preparation of PLLA (sc-PLA)/high surface area nano-graphite systems, *Green Chem.* 17 (2015) 4082–4088.
- [71] Knez, E. Markočič, M. Leitgeb, M. Primožič, M. Knez Hrnčič, M. Škerget, Industrial applications

- of supercritical fluids: A review, *Energy*. 77 (2014) 235–243. <https://doi.org/10.1016/j.energy.2014.07.044>.
- [72] M. Yoshizawa-Fujita*, C. Saito, Y. Takeoka, M. Rikukawa, Lipase-catalyzed polymerization of L-lactide in ionic liquids, *Polym. Adv. Technol.* 19 (2008) 1396–1400. <https://doi.org/10.1002/pat>.
- [73] J.L. Kaar, A.M. Jesionowski, J.A. Berberich, R. Moulton, A.J. Russell, Impact of ionic liquid physical properties on lipase activity and stability, *J. Am. Chem. Soc.* 125 (2003) 4125–4131. <https://doi.org/10.1021/ja028557x>.
- [74] T. Horváth, K. Marossy, T.J. Szabó, Ring-opening polymerization and plasticization of poly(L-lactic acid) by adding of glycerol-dioleate, *J. Therm. Anal. Calorim.* 147 (2022) 2221–2227. <https://doi.org/10.1007/s10973-020-10540-1>.
- [75] S.N. Vouyiouka, C.D. Papaspyrides, Mechanistic Aspects of Solid-State Polycondensation, *Polym. Sci. A Compr. Ref.* 4 (2012) 857–874. <https://doi.org/10.1016/B978-0-444-53349-4.00126-6>.
- [76] A. Wcislek, A.S. Olalla, A. McClain, A. Piegat, P. Sobolewski, J. Puskas, M. El Fray, Enzymatic degradation of poly(butylene succinate) copolyesters synthesized with the use of *Candida antarctica* lipase B, *Polymers (Basel)*. 10 (2018) 688. <https://doi.org/10.3390/polym10060688>.
- [77] A. Guinault, C. Sollogoub, S. Domenek, A. Grandmontagne, V. Ducruet, Influence of crystallinity on gas barrier and mechanical properties of PLA food packaging films, *Int. J. Mater. Form.* 3 (2010) 603–606. <https://doi.org/10.1007/s12289-010-0842-9>.
- [78] Y.Y. Linko, M. Lämsä, X. Wu, E. Uosukainen, J. Seppälä, P. Linko, Biodegradable products by lipase biocatalysis, *J. Biotechnol.* 66 (1998) 41–50. [https://doi.org/10.1016/S0168-1656\(98\)00155-2](https://doi.org/10.1016/S0168-1656(98)00155-2).
- [79] R.C. Rodrigues, R. Fernandez-Lafuente, Lipase from *Rhizomucor miehei* as an industrial biocatalyst in chemical process, *J. Mol. Catal. B Enzym.* 64 (2010) 1–22. <https://doi.org/10.1016/j.molcatb.2010.02.003>.
- [80] V. Hevilla, A. Sonseca, C. Echeverría, A. Muñoz-Bonilla, M. Fernández-García, Enzymatic Synthesis of Polyesters and Their Bioapplications: Recent Advances and Perspectives, *Macromol. Biosci.* 2100156 (2021) 1–28. <https://doi.org/10.1002/mabi.202100156>.
- [81] M. El Fray, B. Gradzik, Synteza Enzymatyczna Poli (Bursztynianu Butylenu) (Pbs) Katalizowana Lipazą B Ze Szczepu *Candida* Obiecujący Materiał Dla Enzymatic Synthesis of Poly (Butylene Succinate) (Pbs) Catalyzed By Lipase B From *Candida Antarctica* : a New Promising Material, *Eng. Biomater.* 115 (2012) 26–31.
- [82] A. Sonseca, A. McClain, J.E. Puskas, M. El Fray, Kinetic studies of biocatalyzed copolyesters of poly(butylene succinate)(PBS)containing fully bio-based dilinoleic diol, *Eur. Polym. J.* 116 (2019) 515–525. <https://doi.org/10.1016/j.eurpolymj.2019.04.038>.
- [83] O. Misset, A. van Dijk, Diagnosing the inactivating process of enzymes, in: A. Ballesteros, F.J. Plou, J.L. Iborra, P.J. Halling (Eds.), *Stab. Stab. Biocatal.*, Elsevier Masson SAS, 1998: pp. 3–18. [https://doi.org/10.1016/S0921-0423\(98\)80003-8](https://doi.org/10.1016/S0921-0423(98)80003-8).
- [84] Y. Jiang, A.J.J. Woortman, G.O.R. Alberda van Ekenstein, K. Loos, Enzyme-catalyzed synthesis of unsaturated aliphatic polyesters based on green monomers from renewable resources, *Biomolecules*. 3 (2013) 461–480. <https://doi.org/10.3390/biom3030461>.
- [85] S. Sugihara, K. Toshima, S. Matsumura, New strategy for enzymatic synthesis of high-

- molecular-weight poly(butylene succinate) via cyclic oligomers, *Macromol. Rapid Commun.* 27 (2006) 203–207. <https://doi.org/10.1002/marc.200500723>.
- [86] H. Azim, A. Dekhterman, Z. Jiang, R.A. Gross, *Candida antarctica* Lipase B catalyzed synthesis of poly(butylene succinate): Shorter chain building blocks also work, *Biomacromolecules.* 7 (2006) 3093–3097. <https://doi.org/10.1021/bk-2008-0999.ch019>.
- [87] D. Pospiech, R. Choińska, D. Flugrat, K. Sahre, D. Jehnichen, A. Korwitz, P. Friedel, A. Werner, B. Voit, Enzymatic Synthesis of Poly(alkylene succinate)s: Influence of Reaction Conditions, Processes. 9 (2021) 499. <http://dx.doi.org/10.1016/j.cattod.2014.11.010>.
- [88] K. Nasr, J. Meimoun, A. Favrelle-Huret, J. De Winter, J.M. Raquez, P. Zinck, Enzymatic polycondensation of 1,6-hexanediol and diethyl adipate: A statistical approach predicting the key-parameters in solution and in bulk, *Polymers (Basel).* 12 (2020) 1907. <https://doi.org/10.3390/POLYM12091907>.
- [89] S. An, J. Zhu, D. Lu, Z. Liu, Lipase-catalyzed synthesis and characterization of high-molecular-weight PBS, *Huagong Xuebao/CIESC J.* 64 (2013) 1855–1861.
- [90] A. Burgard, M.J. Burk, R. Osterhout, S. Van Dien, H. Yim, Development of a commercial scale process for production of 1,4-butanediol from sugar, *Curr. Opin. Biotechnol.* 42 (2016) 118–125. <https://doi.org/10.1016/j.copbio.2016.04.016>.
- [91] M. Sokołowska, M. El Fray, “Green” Poly(Butylene Succinate-co-Dilinoleic Succinate) Copolymers Synthesized Using *Candida antarctica* Lipase B (CAL-B) as Biocatalyst, *Proceedings.* 69 (2020) 33. <https://doi.org/10.3390/cgpm2020-07221>.
- [92] L. Ren, Y. Wang, J. Ge, D. Lu, Z. Liu, Enzymatic synthesis of high-molecular-weight poly(butylene succinate) and its copolymers, *Macromol. Chem. Phys.* 216 (2015) 636–640. <https://doi.org/10.1002/macp.201400550>.
- [93] S. Bhatia, Introduction to enzymes and their applications, in: *Introd. to Pharm. Biotechnol. Vol. 2 Enzym. Proteins Bioinforma.*, IOP SCIENCE, Bristol, UK, 2018: pp. 1–29. <https://doi.org/10.1088/978-0-7503-1302-5ch1>.
- [94] H. Uyama, K. Inada, S. Kobayashi, Lipase-catalyzed synthesis of aliphatic polyesters by polycondensation of dicarboxylic acids and glycols in solvent-free system, *Polym. J.* 32 (2000) 440–443. <https://doi.org/10.1295/polymj.32.440>.
- [95] F. Elias Guckert, C. Sayer, D. de Oliveira, P.H. Hermes de Araújo, B. Francisco Oechsler, Synthesis of polybutylene succinate via Lipase-Catalyzed Transesterification: Enzyme Stability, reuse and PBS properties in bulk polycondensations, *Eur. Polym. J.* 179 (2022). <https://doi.org/10.1016/j.eurpolymj.2022.111573>.
- [96] I.N. Georgousopoulou, S. Vouyiouka, P. Dole, C.D. Papaspyrides, Thermo-mechanical degradation and stabilization of poly(butylene succinate), *Polym. Degrad. Stab.* 128 (2016) 182–192. <https://doi.org/10.1016/j.polymdegradstab.2016.03.012>.
- [97] J. Carlos Morales-Huerta, A. Martínez De Ilarduya, S. Muñoz-Guerra, Poly(alkylene 2,5-furandicarboxylate)s (PEF and PBF) by ring opening polymerization, *Polymer (Guildf).* 87 (2016) 148–158. <https://doi.org/10.1016/j.polymer.2016.02.003>.
- [98] G.-J.M. Gruter, T.B. van Aken, Making an Impact: Sustainable Success Stories, in: T.J. Clark, A.S. Pasternak (Eds.), *How to Commer. Chem. Technol. a Sustain. Futur.*, 1st ed., John Wiley & Sons Ltd, 2021: pp. 263–270. <https://doi.org/10.1002/9781119604860.ch14c>.
- [99] L. Papadopoulos, A. Zamboulis, N. Kasmi, M. Wahbi, C. Nannou, D.A. Lambropoulou, M.

- Kostoglou, G.Z. Papageorgiou, D.N. Bikiaris, Investigation of the catalytic activity and reaction kinetic modeling of two antimony catalysts in the synthesis of poly(ethylene furanoate), *Green Chem.* 23 (2021) 2507–2524. <https://doi.org/10.1039/d0gc04254d>.
- [100] J. Zhu, J. Cai, W. Xie, P.H. Chen, M. Gazzano, M. Scandola, R.A. Gross, Poly(butylene 2,5-furan dicarboxylate), a biobased alternative to PBT: Synthesis, physical properties, and crystal structure, *Macromolecules.* 46 (2013) 796–804. <https://doi.org/10.1021/ma3023298>.
- [101] N. Pouloupoulou, N. Guigo, N. Sbirrazzuoli, D.G. Papageorgiou, D.N. Bikiaris, G.N. Nikolaidis, G.Z. Papageorgiou, Towards increased sustainability for aromatic polyesters: Poly(butylene 2,5-furandicarboxylate) and its blends with poly(butylene terephthalate), *Polymer (Guildf).* 212 (2021) 123157. <https://doi.org/10.1016/j.polymer.2020.123157>.
- [102] J.W. Comerford, F.P. Byrne, S. Weinberger, T.J. Farmer, G.M. Guebitz, L. Gardossi, A. Pellis, Thermal upgrade of enzymatically synthesized aliphatic and aromatic oligoesters, *Materials (Basel).* 13 (2020). <https://doi.org/10.3390/ma13020368>.
- [103] Y. Jiang, A.J.J. Woortman, G.O.R. Alberda Van Ekenstein, K. Loos, A biocatalytic approach towards sustainable furanic-aliphatic polyesters, *Polym. Chem.* 6 (2015) 5198–5211. <https://doi.org/10.1039/c5py00629e>.
- [104] D. Maniar, Y. Jiang, A.J.J. Woortman, J. van Dijken, K. Loos, Furan-Based Copolyesters from Renewable Resources: Enzymatic Synthesis and Properties, *ChemSusChem.* 12 (2019) 990–999. <https://doi.org/10.1002/cssc.201802867>.
- [105] D. Maniar, F. Silvianti, V.M. Ospina, A.J.J. Woortman, J. van Dijken, K. Loos, On the way to greener furanic-aliphatic poly(ester amide)s: Enzymatic polymerization in ionic liquid, *Polymer (Guildf).* 205 (2020) 122662. <https://doi.org/10.1016/j.polymer.2020.122662>.
- [106] Y. Jiang, D. Maniar, A.J.J. Woortman, K. Loos, Enzymatic synthesis of 2,5-furandicarboxylic acid-based semi-aromatic polyamides: Enzymatic polymerization kinetics, effect of diamine chain length and thermal properties, *RSC Adv.* 6 (2016) 67941–67953. <https://doi.org/10.1039/c6ra14585j>.
- [107] F. Silvianti, D. Maniar, L. Boetje, K. Loos, Green Pathways for the Enzymatic Synthesis of Furan-Based Polyesters and Polyamides, *ACS Symp. Ser.* 1373 (2020) 3–29. <https://doi.org/10.1021/bk-2020-1373.ch001>.
- [108] C.D. Papaspyrides, A.D. Porfyrus, S. Vouyiouka, R. Rulkens, E. Grolman, G. Vanden Poel, Solid state polymerization in a micro-reactor: The case of poly(tetramethylene terephthalamide), *J. Appl. Polym. Sci.* 133 (2016) 1–14. <https://doi.org/10.1002/app.43271>.
- [109] A.D. Porfyrus, C.D. Papaspyrides, R. Rulkens, E. Grolman, Direct solid state polycondensation of tetra- and hexa-methylenediammonium terephthalate: Scaling up from the TGA micro-reactor to a laboratory autoclave, *J. Appl. Polym. Sci.* 134 (2017) 1–11. <https://doi.org/10.1002/app.45080>.
- [110] C.D. Papaspyrides, S.N. Vouyiouka, Fundamentals of Solid State Polymerization, in: *Solid State Polym.*, 2009: pp. 1–37. <https://doi.org/10.1002/9780470451830.ch1>.
- [111] S.N. Vouyiouka, E. Topakas, A. Katsini, C.D. Papaspyrides, P. Christakopoulos, A green route for the preparation of aliphatic polyesters via lipase-catalyzed prepolymerization and low-temperature postpolymerization, *Macromol. Mater. Eng.* 298 (2013) 679–689. <https://doi.org/10.1002/mame.201200188>.
- [112] C.I. Gkountela, D. Markoulakis, M. Mathioudaki, I. Pitterou, A. Detsi, S.N. Vouyiouka, Scalable enzymatic polymerization and low-temperature post-polymerization of poly(butylene

- succinate): Process parameters and application, *Eur. Polym. J.* 198 (2023) 112423. <https://doi.org/10.1016/j.eurpolymj.2023.112423>.
- [113] V. Filgueiras, S.N. Vouyiouka, C.D. Papaspyrides, E.L. Lima, J.C. Pinto, Solid-state polymerization of poly(ethylene terephthalate): The effect of water vapor in the carrier gas, *Macromol. Mater. Eng.* 296 (2011) 113–121. <https://doi.org/10.1002/mame.201000201>.
- [114] J. Zimmerman, M.I. Kohan, Nylon – Selected Topics, *J. Polym. Sci. Part A Polym. Chem.* 39 (2001) 2565–2570.
- [115] S. Vouyiouka, P. Theodoulou, A. Symeonidou, C.D. Papaspyrides, R. Pfaendner, Solid state polymerization of poly(lactic acid): Some fundamental parameters, *Polym. Degrad. Stab.* 98 (2013) 2473–2481. <https://doi.org/10.1016/j.polymdegradstab.2013.06.012>.
- [116] D.N. Bikiaris, D.S. Achilias, Synthesis of poly(alkylene succinate) biodegradable polyesters I. Mathematical modelling of the esterification reaction, *Polymer (Guildf)*. 47 (2006) 4851–4860. <https://doi.org/10.1016/j.polymer.2006.04.044>.
- [117] K. Shinno, M. Miyamoto, Y. Kimura, Y. Hirai, H. Yoshitome, Solid-State Postpolymerization of L-Lactide Promoted by Crystallization of Product Polymer: An Effective Method for Reduction of Remaining Monomer, *Macromolecules*. 30 (1997) 6438–6444. <https://doi.org/10.1021/ma9704323>.
- [118] S.-I. Moon, I. Taniguchi, M. Miyamoto, Y. Kimura, C.-W. Lee, Synthesis and Properties of High-Molecular-Weight Poly(L-Lactic Acid) by Melt/Solid Polycondensation under Different Reaction Conditions, *High Perform. Polym.* 13 (2001) S189–S196. <https://doi.org/10.1088/0954-0083/13/2/317>.
- [119] S.-I. Moon, C.-W. Lee, I. Taniguchi, M. Miyamoto, Y. Kimura, Melt/solid polycondensation of L-lactic acid: an alternative route to poly(L-lactic acid) with high molecular weight, *Polymer (Guildf)*. 42 (2001) 5059–5062. [https://doi.org/https://doi.org/10.1016/S0032-3861\(00\)00889-2](https://doi.org/https://doi.org/10.1016/S0032-3861(00)00889-2).
- [120] H. Xu, M. Luo, M. Yu, C. Teng, S. Xie, The Effect of Crystallization on the Solid State Polycondensation of Poly(L-lactic Acid), *J. Macromol. Sci. Part B.* 45 (2006) 681–687. <https://doi.org/10.1080/00222340600770400>.
- [121] H. Nanavati, K. Vimal, Method for producing lactic acid polymers of high crystallinity and molecular weight., WO2009007989A2, 2010. <https://patentimages.storage.googleapis.com/1f/68/32/c9611fbae13fe1/WO2009007989A2.pdf>.
- [122] V. Katiyar, H. Nanavati, High molecular weight poly (L-lactic acid) clay nanocomposites via solid-state polymerization, *Polym. Compos.* 32 (2011) 497–509. <https://doi.org/https://doi.org/10.1002/pc.21069>.
- [123] K. Fukushima, M. Hirata, Y. Kimura, Synthesis and Characterization of Stereoblock Poly(lactic acid)s with Nonequivalent D/L Sequence Ratios, *Macromolecules*. 40 (2007) 3049–3055. <https://doi.org/10.1021/ma070156k>.
- [124] K. Fukushima, Y. Kimura, An efficient solid-state polycondensation method for synthesizing stereocomplexed poly(lactic acid)s with high molecular weight, *J. Polym. Sci. Part A Polym. Chem.* 46 (2008) 3714–3722. <https://doi.org/https://doi.org/10.1002/pola.22712>.
- [125] R. Pfaendner, C. Papaspyrides, P.C. Diamanti, S. Vouyiouka, K. Chronaki, A. Porfyrus, Method for manufacturing aliphatic polyesters, aliphatic polyester and use of phosphorous-containing organic additives, WO 2018/224672 A1, 2018.

- [126] K. Chronaki, D.M. Korres, C.D. Papaspyrides, S. Vouyiouka, Poly(lactic acid) microcapsules: Tailoring properties via solid state polymerization, *Polym. Degrad. Stab.* 179 (2020) 109283. <https://doi.org/10.1016/j.polymdegradstab.2020.109283>.
- [127] F. Jbilou, I.N. Georgousopoulou, S. Marinkovic, S. Vouyiouka, C.D. Papaspyrides, B. Estrine, P. Dole, A. Cottaz, C. Joly, Intelligent monitoring of solid state polymerization via molecular rotors: The case of poly(butylene succinate), *Eur. Polym. J.* 78 (2016) 61–71. <https://doi.org/10.1016/j.eurpolymj.2016.03.005>.
- [128] N. Kasmi, G.Z. Papageorgiou, D.S. Achilias, D.N. Bikiaris, Solid-State polymerization of poly(Ethylene Furanoate) biobased Polyester, II: An efficient and facile method to synthesize high molecular weight polyester appropriate for food packaging applications, *Polymers (Basel)*. 10 (2018) 1–21. <https://doi.org/10.3390/polym10050471>.
- [129] Y. Chebbi, N. Kasmi, M. Majdoub, G.Z. Papageorgiou, D.S. Achilias, D.N. Bikiaris, Solid-state polymerization of poly(ethylene furanoate) biobased polyester, III: Extended study on effect of catalyst type on molecular weight increase, *Polymers (Basel)*. 11 (2019). <https://doi.org/10.3390/polym11030438>.
- [130] D.S. Achilias, A. Chondroyiannis, M. Nerantzaki, K.-V. Adam, Z. Terzopoulou, G.Z. Papageorgiou, D.N. Bikiaris, Solid State Polymerization of Poly(Ethylene Furanoate) and Its Nanocomposites with SiO₂ and TiO₂, *Macromol. Mater. Eng.* 302 (2017) 1700012. <https://doi.org/https://doi.org/10.1002/mame.201700012>.
- [131] R.J.I. Knoop, W. Vogelzang, J. Van Haveren, D.S. Van Es, High molecular weight poly(ethylene-2,5-furanoate); Critical aspects in synthesis and mechanical property determination, *J. Polym. Sci. Part A Polym. Chem.* 51 (2013) 4191–4199. <https://doi.org/10.1002/pola.26833>.
- [132] S. Hong, K.-D. Min, B.-U. Nam, O.O. Park, High molecular weight bio furan-based co-polyesters for food packaging applications: synthesis, characterization and solid-state polymerization, *Green Chem.* 18 (2016) 5142–5150. <https://doi.org/10.1039/C6GC01060A>.
- [133] N. Kasmi, M. Majdoub, G.Z. Papageorgiou, D.S. Achilias, D.N. Bikiaris, Solid-state polymerization of poly(ethylene furanoate) biobased polyester, I: Effect of catalyst type on molecularweight increase, *Polymers (Basel)*. 9 (2017). <https://doi.org/10.3390/polym9110607>.
- [134] M.B. Banella, J. Bonucci, M. Vannini, P. Marchese, C. Lorenzetti, A. Celli, Insights into the Synthesis of Poly(ethylene 2,5-Furandicarboxylate) from 2,5-Furandicarboxylic Acid: Steps toward Environmental and Food Safety Excellence in Packaging Applications, *Ind. Eng. Chem. Res.* 58 (2019) 8955–8962. <https://doi.org/10.1021/acs.iecr.9b00661>.
- [135] E. Gabirondo, B. Melendez-Rodriguez, C. Arnal, J.M. Lagaron, A. Martínez De Ilarduya, H. Sardon, S. Torres-Giner, Organocatalyzed closed-loop chemical recycling of thermo-compressed films of poly(ethylene furanoate), *Polym. Chem.* 12 (2021) 1571–1580. <https://doi.org/10.1039/d0py01623c>.
- [136] L. Papadopoulos, E. Xanthopoulou, G.N. Nikolaidis, A. Zamboulis, D.S. Achilias, G.Z. Papageorgiou, D.N. Bikiaris, Towards High Molecular Weight Furan-Based Polyesters: Solid State Polymerization Study of Bio-Based Poly(Propylene Furanoate) and Poly(Butylene Furanoate), *Materials (Basel)*. 13 (2020). <https://doi.org/10.3390/ma13214880>.
- [137] S.D.F. Mihindukulasuriya, L.-T. Lim, Nanotechnology development in food packaging: A review, *Trends Food Sci. Technol.* 40 (2014) 149–167. <https://doi.org/10.1016/j.tifs.2014.09.009>.

- [138] R. Sandhir, A. Yadav, A. Sunkaria, N. Singhal, Nano-antioxidants: An emerging strategy for intervention against neurodegenerative conditions, *Neurochem. Int.* 89 (2015) 209–226. <https://doi.org/10.1016/j.neuint.2015.08.011>.
- [139] C. Pinto Reis, R.J. Neufeld, Ribeiro António J., F. Veiga, Nanoencapsulation I. Methods for preparation of drug-loaded polymeric nanoparticles, *Nanomedicine Nanotechnology, Biol. Med.* 2 (2006) 8–21. <https://doi.org/https://doi.org/10.1016/j.nano.2005.12.003>.
- [140] S. Sahani, Y.C. Sharma, Advancements in applications of nanotechnology in global food industry, *Food Chem.* 342 (2021) 128318. <https://doi.org/10.1016/j.foodchem.2020.128318>.
- [141] Nanotechnology-Over a Decade of Progress and Innovation, (2020). <https://www.fda.gov/media/140395/download> (accessed April 25, 2022).
- [142] N. Chausali, J. Saxena, R. Prasad, Recent trends in nanotechnology applications of bio-based packaging, *J. Agric. Food Res.* 7 (2022) 100257. <https://doi.org/https://doi.org/10.1016/j.jafr.2021.100257>.
- [143] A.A. Yaqoob, H. Ahmad, T. Parveen, A. Ahmad, M. Oves, I.M.I. Ismail, H.A. Qari, K. Umar, M.N. Mohamad Ibrahim, Recent Advances in Metal Decorated Nanomaterials and Their Various Biological Applications: A Review, *Front. Chem.* 8 (2020) 1–23. <https://doi.org/10.3389/fchem.2020.00341>.
- [144] K. Kızılbey, Optimization of Rutin-Loaded PLGA Nanoparticles Synthesized by Single-Emulsion Solvent Evaporation Method, *ACS Omega.* 4 (2019) 555–562. <https://doi.org/10.1021/acsomega.8b02767>.
- [145] S.M.A. Sadat, S.T. Jahan, A. Haddadi, Effects of Size and Surface Charge of Polymeric Nanoparticles on in Vitro and in Vivo Applications, *J. Biomater. Nanobiotechnol.* 07 (2016) 91–108. <https://doi.org/10.4236/jbnb.2016.72011>.
- [146] A. Zielińska, F. Carreiró, A.M. Oliveira, A. Neves, B. Pires, D.N. Venkatesh, A. Durazzo, M. Lucarini, P. Eder, A.M. Silva, A. Santini, E.B. Souto, Polymeric Nanoparticles: Production, Characterization, Toxicology and Ecotoxicology, *Molecules.* 25 (2020) 3731. <https://doi.org/10.3390/molecules25163731>.
- [147] J.K. Patel, Y. V. Pathak, Emerging technologies for nanoparticle manufacturing, 2021. <https://doi.org/10.1007/978-3-030-50703-9>.
- [148] Y. Wang, P. Li, T.T.D. Tran, J. Zhang, L. Kong, Manufacturing techniques and surface engineering of polymer based nanoparticles for targeted drug delivery to cancer, *Nanomaterials.* 6 (2016). <https://doi.org/10.3390/nano6020026>.
- [149] M. Paranjpe, C.C. Müller-Goymann, Nanoparticle-Mediated Pulmonary Drug Delivery: A Review, *Int. J. Mol. Sci.* 15 (2014) 5852–5873. <https://doi.org/10.3390/ijms15045852>.
- [150] E.T. Baran, N. Özer, V. Hasirci, Poly(hydroxybutyrate-co-hydroxyvalerate) nanocapsules as enzyme carriers for cancer therapy: an in vitro study, *J. Microencapsul.* 19 (2002) 363–376. <https://doi.org/10.1080/02652040110105355>.
- [151] L.F. Santos, I.J. Correia, A.S. Silva, J.F. Mano, Biomaterials for drug delivery patches, *Eur. J. Pharm. Sci.* 118 (2018) 49–66. <https://doi.org/https://doi.org/10.1016/j.ejps.2018.03.020>.
- [152] K.K. Kuorwel, M.J. Cran, J.D. Orbell, S. Buddhadasa, S.W. Bigger, Review of Mechanical Properties, Migration, and Potential Applications in Active Food Packaging Systems Containing Nanoclays and Nanosilver, *Compr. Rev. Food Sci. Food Saf.* 14 (2015) 411–430. <https://doi.org/https://doi.org/10.1111/1541-4337.12139>.

References

- [153] G. Fuertes, I. Soto, R. Carrasco, M. Vargas, J. Sabattin, C. Lagos, Intelligent Packaging Systems: Sensors and Nanosensors to Monitor Food Quality and Safety, *J. Sensors*. 2016 (2016) 4046061. <https://doi.org/10.1155/2016/4046061>.
- [154] P.R. Salgado, L. Di Giorgio, Y.S. Musso, A.N. Mauri, Recent Developments in Smart Food Packaging Focused on Biobased and Biodegradable Polymers, *Front. Sustain. Food Syst.* 5 (2021) 1–30. <https://doi.org/10.3389/fsufs.2021.630393>.
- [155] A.E. Kapetanakou, P.N. Skandamis, Applications of active packaging for increasing microbial stability in foods: Natural volatile antimicrobial compounds, *Curr. Opin. Food Sci.* 12 (2016) 1–12. <https://doi.org/10.1016/j.cofs.2016.06.001>.
- [156] Ł. Łopusiewicz, M. Zdanowicz, S. Macieja, K. Kowalczyk, A. Bartkowiak, Development and Characterization of Bioactive Poly(butylene-succinate) Films Modified with Quercetin for Food Packaging Applications, *Polymers (Basel)*. 13 (2021). <https://doi.org/10.3390/polym13111798>.
- [157] N. Mohamad, M.M. Mazlan, I.S.M.A. Tawakkal, R.A. Talib, L.K. Kian, M. Jawaid, Characterization of Active Polybutylene Succinate Films Filled Essential Oils for Food Packaging Application, *J. Polym. Environ.* (2021). <https://doi.org/10.1007/s10924-021-02198-z>.
- [158] S. Mallardo, V. De Vito, M. Malinconico, M.G. Volpe, G. Santagata, M.L. Di Lorenzo, Poly(butylene succinate)-based composites containing β -cyclodextrin/d-limonene inclusion complex, *Eur. Polym. J.* 79 (2016) 82–96. <https://doi.org/10.1016/j.eurpolymj.2016.04.024>.
- [159] C.T. Brunner, E.T. Baran, E.D. Pinho, R.L. Reis, N.M. Neves, Performance of biodegradable microcapsules of poly(butylene succinate), poly(butylene succinate-co-adipate) and poly(butylene terephthalate-co-adipate) as drug encapsulation systems, *Colloids Surfaces B Biointerfaces*. 84 (2011) 498–507. <https://doi.org/10.1016/j.colsurfb.2011.02.005>.
- [160] P. Hariraksapitak, O. Suwanton, P. Pavasant, P. Supaphol, Effectual drug-releasing porous scaffolds from 1,6-diisocyanatohexane-extended poly(1,4-butylene succinate) for bone tissue regeneration, *Polymer (Guildf)*. 49 (2008) 2678–2685. <https://doi.org/10.1016/j.polymer.2008.04.006>.
- [161] J. Xu, B. Guo, Microbial Succinic Acid, Its Polymer Poly(butylene succinate), and Applications, in: G.-Q. Chen (Ed.), *Microbiol. Monogr.*, Springer-Verlag, Heidelberg, 2009: pp. 347–388. https://doi.org/10.1007/978-3-642-03287-5_14.
- [162] L.R. Almeida, A.R. Martins, E.M. Fernandes, M.B. Oliveira, V.M. Correlo, I. Pashkuleva, A.P. Marques, A.S. Ribeiro, N.F. Durães, C.J. Silva, G. Bonifácio, R.A. Sousa, A.L. Oliveira, R.L. Reis, New biotextiles for tissue engineering: Development, characterization and in vitro cellular viability, *Acta Biomater.* 9 (2013) 8167–8181. <https://doi.org/10.1016/j.actbio.2013.05.019>.
- [163] H. Li, J. Chang, A. Cao, J. Wang, In vitro evaluation of biodegradable poly(butylene succinate) as a novel biomaterial, *Macromol. Biosci.* 5 (2005) 433–440. <https://doi.org/10.1002/mabi.200400183>.
- [164] H. Wang, J. Ji, W. Zhang, Y. Zhang, J. Jiang, Z. Wu, S. Pu, P.K. Chu, Biocompatibility and bioactivity of plasma-treated biodegradable poly(butylene succinate), *Acta Biomater.* 5 (2009) 279–287. <https://doi.org/10.1016/j.actbio.2008.07.017>.
- [165] 2 Ribeiro V P1, 2, Ribeiro A S3, Silva C J 3, Durães N F3, Bonifácio G4, Correlo V M 1, 2, Marques A P1, 2, Sousa R A1, 2, Oliveira A L1, 2, 5[†], Reis R L1, Evaluation of Novel 3D Architectures Based on Knitting Technologies for Engineering Biological Tissues, 5220 (2013).
- [166] M. Ojansivu, L. Johansson, S. Vanhatupa, I. Tamminen, M. Hannula, J. Hyttinen, M. Kellomäki,

- S. Miettinen, Knitted 3D Scaffolds of Polybutylene Succinate Support Human Mesenchymal Stem Cell Growth and Osteogenesis, *Stem Cells Int.* 2018 (2018) 1–11. <https://doi.org/10.1155/2018/5928935>.
- [167] European Green Deal: Putting an end to wasteful packaging, boosting reuse and recycling, *Eur. Com. Press Release.* (2022). https://ec.europa.eu/commission/presscorner/detail/en/ip_22_7155.
- [168] O. Platnieks, S. Gaidukovs, V. Kumar Thakur, A. Barkane, S. Beluns, Bio-based poly (butylene succinate): Recent progress, challenges and future opportunities, *Eur. Polym. J.* 161 (2021) 110855. <https://doi.org/10.1016/j.eurpolymj.2021.110855>.
- [169] M.I. Peñas, Synthesis of Poly (Butylene Succinate), *Sch. Community Encycl.* (2022). <https://encyclopedia.pub/entry/20774>.
- [170] S.A. Rafiqah, A. Khalina, A.S. Harmaen, I.A. Tawakkal, K. Zaman, M. Asim, M.N. Nurrazi, C.H. Lee, A review on properties and application of bio-based poly(Butylene succinate), *Polymers (Basel)*. 13 (2021) 1–28. <https://doi.org/10.3390/polym13091436>.
- [171] M. Gigli, M. Fabbri, N. Lotti, R. Gamberini, B. Rimini, A. Munari, Poly(butylene succinate)-based polyesters for biomedical applications: A review, *Eur. Polym. J.* 75 (2016) 431–460. <https://doi.org/10.1016/j.eurpolymj.2016.01.016>.
- [172] C. Ortiz, M.L. Ferreira, O. Barbosa, J.C.S. Dos Santos, R.C. Rodrigues, Á. Berenguer-Murcia, L.E. Briand, R. Fernandez-Lafuente, Novozym 435: The “perfect” lipase immobilized biocatalyst?, *Catal. Sci. Technol.* 9 (2019) 2380–2420. <https://doi.org/10.1039/c9cy00415g>.
- [173] B. Chen, J. Hu, E.M. Miller, W. Xie, M. Cai, R.A. Gross, *Candida antarctica* Lipase B chemically immobilized on epoxy-activated micro- and nanobeads: Catalysts for polyester synthesis, *Biomacromolecules*. 9 (2008) 463–471. <https://doi.org/10.1021/bm700949x>.
- [174] T. Siódmiak, D. Mangelings, Y. Vander Heyden, M. Ziegler-Borowska, M.P. Marszałł, High Enantioselective Novozym 435-Catalyzed Esterification of (R,S)-Flurbiprofen Monitored with a Chiral Stationary Phase, *Appl. Biochem. Biotechnol.* 175 (2015) 2769–2785. <https://doi.org/10.1007/s12010-014-1455-4>.
- [175] A. Mahapatro, B. Kalra, A. Kumar, R.A. Gross, Lipase-catalyzed polycondensations: Effect of substrates and solvent on chain formation, dispersity, and end-group structure, *Biomacromolecules*. 4 (2003) 544–551. <https://doi.org/10.1021/bm0257208>.
- [176] T. Debuissy, E. Pollet, L. Avérous, Enzymatic Synthesis of a Bio-Based Copolyester from Poly(butylene succinate) and Poly((R)-3-hydroxybutyrate): Study of Reaction Parameters on the Transesterification Rate, *Biomacromolecules*. 17 (2016) 4054–4063. <https://doi.org/10.1021/acs.biomac.6b01494>.
- [177] X. Yongxiang, X. Jun, L. Dehua, G. Baohua, X. Xuming, Synthesis and Characterization of Biodegradable Poly(butylene succinate-co-propylene succinate)s, *J. Appl. Polym. Sci.* 109 (2008) 1881–1889. <https://doi.org/10.1002/app>.
- [178] X. Chen, X. Liu, J. Lei, L. Xu, Z. Zhao, F. Kausar, X. Xie, X. Zhu, Y. Zhang, W.Z. Yuan, Synthesis, clustering-triggered emission, explosive detection and cell imaging of nonaromatic polyurethanes, *Mol. Syst. Des. Eng.* 3 (2018) 364–375. <https://doi.org/10.1039/c7me00118e>.
- [179] A.M. Bhayo, R. Abdul-Karim, S.G. Musharraf, M.I. Malik, Synthesis and characterization of 4-arm star-shaped amphiphilic block copolymers consisting of poly(ethylene oxide) and poly(ϵ -caprolactone), *RSC Adv.* 8 (2018) 28569–28580. <https://doi.org/10.1039/c8ra05000g>.

References

- [180] L. Kang-Jen, NMR Studies of Polymer Solutions. VII. Effects of Chain Length on Polymer NMR Measurements, *Die Makromol. Chemie.* 126 (1969) 187–196.
- [181] P.N. Adams, D.C. Apperley, A.P. Monkman, A comparison of the molecular weights of polyaniline samples obtained from gel permeation chromatography and solid state ¹⁵N n.m.r. spectroscopy, *Polymer (Guildf).* 34 (1993) 328–332. [https://doi.org/10.1016/0032-3861\(93\)90085-O](https://doi.org/10.1016/0032-3861(93)90085-O).
- [182] V.C. da Costa, E.R.F. dos Santos, F.G. de Souza, Poly(Butylene Succinate) Molar Mass Calculation by GPC and ¹H-NMR, *Macromol. Symp.* 398 (2021) 1–7. <https://doi.org/10.1002/masy.202000216>.
- [183] J.U. Izunobi, C.L. Higginbotham, Polymer molecular weight analysis by ¹H NMR spectroscopy, *J. Chem. Educ.* 88 (2011) 1098–1104. <https://doi.org/10.1021/ed100461v>.
- [184] C.I. Gkountela, S.N. Vouyiouka, Enzymatic Polymerization as a Green Approach to Synthesizing Bio-Based Polyesters, *Macromol.* 2 (2022) 30–57. <https://doi.org/10.3390/macromol2010003>.
- [185] A. Kumar, R.A. Gross, *Candida antarctica* Lipase B catalyzed polycaprolactone synthesis: Effects of organic media and temperature, *Biomacromolecules.* 1 (2000) 133–138. <https://doi.org/10.1021/bm990510p>.
- [186] Y. Jiang, D. Maniar, A.J.J. Woortman, G.O.R. Alberda Van Ekenstein, K. Loos, Enzymatic Polymerization of Furan-2,5-Dicarboxylic Acid-Based Furanic-Aliphatic Polyamides as Sustainable Alternatives to Polyphthalamides, *Biomacromolecules.* 16 (2015) 3674–3685. <https://doi.org/10.1021/acs.biomac.5b01172>.
- [187] Z. Liang, P. Pan, B. Zhu, T. Dong, Y. Inoue, Mechanical and Thermal Properties of Poly(butylene succinate)/Plant Fiber Biodegradable Composite, *J. Appl. Polym. Sci.* 115 (2010) 3559–3567. <https://doi.org/10.1002/app>.
- [188] D.K. Song, Y.K. Sung, Synthesis and characterization of biodegradable poly(1,4-butanediol succinate), *J. Appl. Polym. Sci.* 56 (1995) 1381–1395. <https://doi.org/10.1002/app.1995.070561102>.
- [189] K. Chrissafis, K.M. Paraskevopoulos, D.N. Bikiaris, Effect of molecular weight on thermal degradation mechanism of the biodegradable polyester poly(ethylene succinate), *Thermochim. Acta.* 440 (2006) 166–175. <https://doi.org/10.1016/j.tca.2005.11.002>.
- [190] M. Unger, C. Vogel, H.W. Siesler, Molecular weight dependence of the thermal degradation of poly(ϵ -caprolactone): A thermogravimetric differential thermal fourier transform infrared spectroscopy study, *Appl. Spectrosc.* 64 (2010) 805–809. <https://doi.org/10.1366/000370210791666309>.
- [191] G. Guidotti, M. Soccio, M.C. García-Gutiérrez, T. Ezquerra, V. Siracusa, E. Gutiérrez-Fernández, A. Munari, N. Lotti, Fully Biobased Superpolymers of 2,5-Furandicarboxylic Acid with Different Functional Properties: From Rigid to Flexible, High Performant Packaging Materials, *ACS Sustain. Chem. Eng.* 8 (2020) 9558–9568. <https://doi.org/10.1021/acssuschemeng.0c02840>.
- [192] A.F. Sousa, C. Vilela, A.C. Fonseca, M. Matos, C.S.R. Freire, G.-J.M. Gruter, J.F.J. Coelho, A.J.D. Silvestre, Biobased polyesters and other polymers from 2,5-furandicarboxylic acid: a tribute to furan excellency, *Polym. Chem.* 6 (2015) 5961–5983. <https://doi.org/10.1039/C5PY00686D>.
- [193] M. Soccio, M. Costa, N. Lotti, M. Gazzano, V. Siracusa, E. Salatelli, P. Manaresi, A. Munari, Novel fully biobased poly(butylene 2,5-furanoate/diglycolate) copolymers containing ether linkages: Structure-property relationships, *Eur. Polym. J.* 81 (2016) 397–412. <https://doi.org/10.1016/j.eurpolymj.2016.06.022>.

- [194] L. Sipos, A process for preparing a polymer having a 2,5-furandicarboxylate moiety within the polymer backbone and such (co)polymers, WO2010077133A1, 2010. <https://patentimages.storage.googleapis.com/02/4c/30/78987d25d4e56c/WO2010077133A1.pdf>.
- [195] M. Jiang, Q. Liu, Q. Zhang, C. Ye, G. Zhou, A series of furan-aromatic polyesters synthesized via direct esterification method based on renewable resources, *J. Polym. Sci. Part A Polym. Chem.* 50 (2012) 1026–1036. <https://doi.org/10.1002/pola.25859>.
- [196] J. Ma, Y. Pang, M. Wang, J. Xu, H. Ma, X. Nie, The copolymerization reactivity of diols with 2,5-furandicarboxylic acid for furan-based copolyester materials, *J. Mater. Chem.* 22 (2012) 3457–3461. <https://doi.org/10.1039/C2JM15457A>.
- [197] L. Lalanne, G.S. Nyanhongo, G.M. Guebitz, A. Pellis, Biotechnological production and high potential of furan-based renewable monomers and polymers, *Biotechnol. Adv.* 48 (2021) 107707. <https://doi.org/10.1016/j.biotechadv.2021.107707>.
- [198] G.Z. Papageorgiou, V. Tsanaktis, D.G. Papageorgiou, S. Exarhopoulos, M. Papageorgiou, D.N. Bikiaris, Evaluation of polyesters from renewable resources as alternatives to the current fossil-based polymers. Phase transitions of poly(butylene 2,5-furan-dicarboxylate), *Polymer (Guildf)*. 55 (2014) 3846–3858. <https://doi.org/https://doi.org/10.1016/j.polymer.2014.06.025>.
- [199] C.I. Gkountela, O. Plaggese, S.N. Vouyiouka, Enzymatic prepolymerization combined with bulk post-polymerization towards the production of bio-based polyesters: The case of poly(butylene 2,5-furandicarboxylate), (n.d.).
- [200] M. Montejo, A. Navarro, G.J. Kearley, J. Vázquez, J.J. López-González, Intermolecular charge transfer and hydrogen bonding in solid furan, *J. Am. Chem. Soc.* 126 (2004) 15087–15095. <https://doi.org/10.1021/ja040130y>.
- [201] T.P. Kainulainen, T.I. Hukka, H.D. Özeren, J.A. Sirviö, M.S. Hedenqvist, J.P. Heiskanen, Utilizing Furfural-Based Bifuran Diester as Monomer and Comonomer for High-Performance Bioplastics: Properties of Poly(butylene furanoate), Poly(butylene bifuranoate), and Their Copolyesters, *Biomacromolecules*. 21 (2020) 743–752. <https://doi.org/10.1021/acs.biomac.9b01447>.
- [202] K. Loos, R. Zhang, I. Pereira, B. Agostinho, H. Hu, D. Maniar, N. Sbirrazzuoli, A.J.D. Silvestre, N. Guigo, A.F. Sousa, A Perspective on PEF Synthesis, Properties, and End-Life, *Front. Chem.* 8 (2020) 1–18. <https://doi.org/10.3389/fchem.2020.00585>.
- [203] C. Signoret, A.S. Caro-Bretelle, J.M. Lopez-Cuesta, P. Ienny, D. Perrin, Alterations of plastics spectra in MIR and the potential impacts on identification towards recycling, *Resour. Conserv. Recycl.* 161 (2020). <https://doi.org/10.1016/j.resconrec.2020.104980>.
- [204] X. Zhang, J. Wang, High molecular weight poly (butylene terephthalate-co- butylene 2 , 5- furan dicarboxylate) copolyesters : From synthesis to thermomechanical and barrier properties, *J. Appl. Polym. Sci.* (2020) 1–12. <https://doi.org/10.1002/app.49365>.
- [205] J. Wang, X. Liu, J. Zhu, Y. Jiang, Copolyesters based on 2,5-furandicarboxylic acid (FDCA): Effect of 2,2,4,4-tetramethyl-1,3-cyclobutanediol units on their properties, *Polymers (Basel)*. 9 (2017) 1–15. <https://doi.org/10.3390/polym9090305>.
- [206] J.C. Morales-Huerta, A.M. de Ilarduya, S. Muñoz-Guerra, Partially renewable poly(butylene 2,5-furandicarboxylate-co-isophthalate) copolyesters obtained by ROP, *Polymers (Basel)*. 10 (2018). <https://doi.org/10.3390/polym10050483>.

References

- [207] J. Wang, X. Liu, Z. Jia, L. Sun, J. Zhu, Highly crystalline polyesters synthesized from furandicarboxylic acid (FDCA): Potential bio-based engineering plastic, *Eur. Polym. J.* 109 (2018) 379–390. <https://doi.org/10.1016/j.eurpolymj.2018.10.014>.
- [208] E. Bianchi, M. Soccio, V. Siracusa, M. Gazzano, S. Thiyagarajan, N. Lotti, Poly(butylene 2,4-furanoate), an Added Member to the Class of Smart Furan-Based Polyesters for Sustainable Packaging: Structural Isomerism as a Key to Tune the Final Properties, *ACS Sustain. Chem. Eng.* 9 (2021) 11937–11949. <https://doi.org/10.1021/acssuschemeng.1c04104>.
- [209] M. Mitsubishi, Process for purifying 1,4-butanediol by melt crystallisation, EP0885864A1, 1998. <https://patentimages.storage.googleapis.com/69/18/b5/86017ae2358ce9/EP0885864A1.pdf>.
- [210] T.M.R. Maria, A.J. Lopes Jesus, M.E.S. Eusébio, Glass-forming ability of butanediol isomers, *J. Therm. Anal. Calorim.* 100 (2010) 385–390. <https://doi.org/10.1007/s10973-009-0633-z>.
- [211] S. Weinberger, A. Pellis, J.W. Comerford, T.J. Farmer, G.M. Guebitz, Efficient physisorption of candida antarctica lipase B on polypropylene beads and application for polyester synthesis, *Catalysts.* 8 (2018). <https://doi.org/10.3390/catal8090369>.
- [212] A.N. Shirke, C. White, J.A. Englaender, A. Zwarzyz, G.L. Butterfoss, R.J. Linhardt, R.A. Gross, Stabilizing Leaf and Branch Compost Cutinase (LCC) with Glycosylation: Mechanism and Effect on PET Hydrolysis, *Biochemistry.* 57 (2018) 1190–1200. <https://doi.org/10.1021/acs.biochem.7b01189>.
- [213] S. Sulaiman, S. Yamato, E. Kanaya, J.-J. Kim, Y. Koga, K. Takano, S. Kanaya, Isolation of a Novel Cutinase Homolog with Polyethylene Terephthalate-Degrading Activity from Leaf-Branch Compost by Using a Metagenomic Approach, *Appl. Environ. Microbiol.* 78 (2012) 1556–1562. <https://doi.org/10.1128/AEM.06725-11>.
- [214] S. Sulaiman, D.-J. You, E. Kanaya, Y. Koga, S. Kanaya, Crystal Structure and Thermodynamic and Kinetic Stability of Metagenome-Derived LC-Cutinase, *Biochemistry.* 53 (2014) 1858–1869. <https://doi.org/10.1021/bi401561p>.
- [215] V. Tournier, C.M. Topham, A. Gilles, B. David, C. Folgoas, E. Moya-Leclair, E. Kamionka, M.-L. Desrousseaux, H. Texier, S. Gavalda, M. Cot, E. Guémard, M. Dalibey, J. Nomme, G. Cioci, S. Barbe, M. Chateau, I. André, S. Duquesne, A. Marty, An engineered PET depolymerase to break down and recycle plastic bottles, *Nature.* 580 (2020) 216–219. <https://doi.org/10.1038/s41586-020-2149-4>.
- [216] K. Makryniotis, E. Nikolaivits, C. Gkountela, S. Vouyiouka, E. Topakas, Discovery of a polyesterase from *Deinococcus maricopensis* and comparison to the benchmark LCCICCG suggests high potential for semi-crystalline post-consumer PET degradation, *J. Hazard. Mater.* 455 (2023) 131574. <https://doi.org/https://doi.org/10.1016/j.jhazmat.2023.131574>.
- [217] R. Xue, Y. Chen, H. Rong, R. Wei, Z. Cui, J. Zhou, W. Dong, M. Jiang, Fusion of Chitin-Binding Domain From Chitinolytic bacter *meiyuanensis* SYBC-H1 to the Leaf-Branch Compost Cutinase for Enhanced PET Hydrolysis, *Front. Bioeng. Biotechnol.* 9 (2021) 1–9. <https://doi.org/10.3389/fbioe.2021.762854>.
- [218] C. Gkountela, K. Makryniotis, I. Spanos, E. Topakas, S.N. Vouyiouka, Enzymatic prepolymerization of poly(butylene succinate) using a thermostable variant of the Leaf and branch compost cutinase (LCC), along with melt post-polymerization as a finishing step, (n.d.).
- [219] K. Takahashi, Advanced reference materials for the characterization of molecular size and weight, *JPhys Mater.* 3 (2020). <https://doi.org/10.1088/2515-7639/aba6f5>.

- [220] A. Pellis, E. Herrero Acero, L. Gardossi, V. Ferrario, G.M. Guebitz, Renewable building blocks for sustainable polyesters: new biotechnological routes for greener plastics, *Polym. Int.* 65 (2016) 861–871. <https://doi.org/10.1002/pi.5087>.
- [221] C. Vouyiouka, S. Papaspyrides, Solid State Polymerization, in: S.N.V. Papaspyrides (Ed.), *Encycl. Polym. Sci. Technol.*, 4th ed., John Wiley & Sons, New Jersey, 2009: pp. 1–32.
- [222] T.Y. Kim, E.A. Lofgren, S.A. Jabarin, Solid-state polymerization of poly(ethylene terephthalate). I. Experimental study of the reaction kinetics and properties, *J. Appl. Polym. Sci.* 89 (2003) 197–212. <https://doi.org/10.1002/app.11903>.
- [223] C.D. Papaspyrides, Solid state polyamidation processes, *Polym. Int.* 29 (1992) 293–298. <https://doi.org/10.1002/pi.4990290409>.
- [224] F. Iñiguez-Franco, R. Auras, G. Burgess, D. Holmes, X. Fang, M. Rubino, H. Soto-Valdez, Concurrent solvent induced crystallization and hydrolytic degradation of PLA by water-ethanol solutions, *Polym. (United Kingdom)*. 99 (2016) 315–323. <https://doi.org/10.1016/j.polymer.2016.07.018>.
- [225] Y. Ma, U.S. Agarwal, D.J. Sikkema, P.J. Lemstra, Solid-state polymerization of PET: influence of nitrogen sweep and high vacuum, *Polymer (Guildf)*. 44 (2003) 4085–4096. [https://doi.org/https://doi.org/10.1016/S0032-3861\(03\)00408-7](https://doi.org/https://doi.org/10.1016/S0032-3861(03)00408-7).
- [226] P. Rizzarelli, S. Carroccio, Thermo-oxidative processes in biodegradable poly(butylene succinate), *Polym. Degrad. Stab.* 94 (2009) 1825–1838. <https://doi.org/https://doi.org/10.1016/j.polymdegradstab.2009.06.007>.
- [227] B.T. Hiller, J.L. Azzi, M. Rennert, Improvement of the Thermo-Oxidative Stability of Biobased Poly(butylene succinate) (PBS) Using Biogenic Wine By-Products as Sustainable Functional Fillers, *Polymers (Basel)*. 15 (2023). <https://doi.org/10.3390/polym15112533>.
- [228] M. Monti, H. Hoydonckx, F. Stappers, G. Camino, Thermal and combustion behavior of furan resin/silica nanocomposites, *Eur. Polym. J.* 67 (2015) 561–569. <https://doi.org/https://doi.org/10.1016/j.eurpolymj.2015.02.005>.
- [229] M. Kesente, E. Kavetsou, M. Roussaki, S. Blidi, S. Loupassaki, S. Chanioti, P. Siamandoura, C. Stamatogianni, E. Philippou, C. Papaspyrides, S. Vouyiouka, A. Detsi, Encapsulation of olive leaves extracts in biodegradable PLA nanoparticles for use in cosmetic formulation, *Bioengineering*. 4 (2017). <https://doi.org/10.3390/bioengineering4030075>.
- [230] M. Roussaki, A. Gaitanarou, P.C. Diamanti, S. Vouyiouka, C. Papaspyrides, P. Kefalas, A. Detsi, Encapsulation of the natural antioxidant aureusidin in biodegradable PLA nanoparticles, *Polym. Degrad. Stab.* 108 (2014) 182–187. <https://doi.org/10.1016/j.polymdegradstab.2014.08.004>.
- [231] L. Kuai, F. Liu, B. Sen Chiou, R.J. Avena-Bustillos, T.H. McHugh, F. Zhong, Controlled release of antioxidants from active food packaging: A review, *Food Hydrocoll.* 120 (2021) 106992. <https://doi.org/10.1016/j.foodhyd.2021.106992>.
- [232] S. Betala, M. Mohan Varma, K. Abbulu, Formulation and evaluation of polymeric nanoparticles of an antihypertensive drug for gastroretention, *J. Drug Deliv. Ther.* 8 (2018) 82–86. <https://doi.org/10.22270/jddt.v8i6.2018>.
- [233] M. Wiśniewska, V. Bogatyrov, I. Ostolska, K. Szewczuk-Karpisz, K. Terpiłowski, A. Nosal-Wiercińska, Impact of poly(vinyl alcohol) adsorption on the surface characteristics of mixed oxide Mn_xO_y-SiO₂, *Adsorption*. 22 (2016) 417–423. <https://doi.org/10.1007/s10450-015-9696-2>.

References

- [234] J. Varshosaz, S. Eskandari, M. Tabbakhian, Freeze-drying of nanostructure lipid carriers by different carbohydrate polymers used as cryoprotectants, *Carbohydr. Polym.* 88 (2012) 1157–1163. <https://doi.org/10.1016/j.carbpol.2012.01.051>.
- [235] J. Secerli, Ş. Adatepe, S. Altuntas, G.R. Topal, O. Erdem, M. Bacanlı, In vitro toxicity of naringin and berberine alone, and encapsulated within PMMA nanoparticles, *Toxicol. Vitro.* 89 (2023) 105580. <https://doi.org/10.1016/j.tiv.2023.105580>.
- [236] L.M. Cordenonsi, R.M. Sponchiado, S.C. Campanharo, C.V. Garcia, R.P. Raffin, E.E.S. Schapoval, STUDY OF FLAVONOIDS PRESENT IN POMELO (*Citrus Maxima*) BY DSC, UV-VIS, IR, ¹H AND ¹³C NMR AND MS, *Drug Anal. Res.* 1 (2017) 31–37. <https://doi.org/10.22456/2527-2616.74097>.
- [237] H. Wang, H. Hu, X. Zhang, L. Zheng, J. Ruan, J. Cao, X. Zhang, Preparation, Physicochemical Characterization, and Antioxidant Activity of Naringin–Silk Fibroin–Alginate Microspheres and Application in Yogurt, *Foods.* 11 (2022) 2147. <https://doi.org/10.3390/foods11142147>.
- [238] J. Chen, W.T. Dai, Z.M. He, L. Gao, X. Huang, J.M. Gong, H.Y. Xing, W.D. Chen, Fabrication and evaluation of curcumin-loaded nanoparticles based on solid lipid as a new type of colloidal drug delivery system, *Indian J. Pharm. Sci.* 75 (2013) 178–184.
- [239] R.K. Tubbs, Melting Point and Heat of Fusion of Poly(vinyl Alcohol), *J. Polym. Sci. Part A.* 3 (1965) 4181–4189.
- [240] H. Hu, R. Zhang, J. Wang, W. Bin Ying, J. Zhu, Synthesis and Structure-Property Relationship of Biobased Biodegradable Poly(butylene carbonate- co-furandicarboxylate), *ACS Sustain. Chem. Eng.* 6 (2018) 7488–7498. <https://doi.org/10.1021/acssuschemeng.8b00174>.
- [241] S. Papadimitriou, G.Z. Papageorgiou, F.I. Kanaze, M. Georganakis, D.N. Bikiaris, Nanoencapsulation of nimodipine in novel biocompatible poly(propylene-co- butylene succinate) aliphatic copolyesters for sustained release, *J. Nanomater.* 2009 (2009) 1–11. <https://doi.org/10.1155/2009/716242>.
- [242] A. Kamtsikakis, E. Kavetsou, K. Chronaki, E. Kiosidou, E. Pavlatou, A. Karana, C. Papaspyrides, A. Detsi, A. Karantonis, S. Vouyiouka, Encapsulation of antifouling organic biocides in poly(Lactic acid) nanoparticles, *Bioengineering.* 4 (2017). <https://doi.org/10.3390/bioengineering4040081>.
- [243] M. Sanopoulou, K.G. Papadokostaki, Controlled drug release systems: Mechanisms and kinetics, *Biomed. Membr. (Bio)Artificial Organs.* (2017) 1–33. https://doi.org/10.1142/9789813223974_0001.

Appendix 1. Supplementary results

Table S 1. ^1H NMR- and GPC-calculated \overline{M}_n , \overline{M}_w and dispersity \mathcal{D} of the enzymatically synthesized PBS prepolymers.

Sample	^1H NMR-calculated		GPC-calculated	
	\overline{M}_n (g mol $^{-1}$)	\overline{M}_n (g mol $^{-1}$)	\overline{M}_w (g mol $^{-1}$)	(\mathcal{D})
A-80	1000	1700	2700	1.6
A-85	1000	1600	2800	1.8
A-90	1200	2300	5000	2.2
A-95	1500	2000	4200	2.1
B-90	1200	2500	6700	2.7
B-95	800	1400	2000	1.5
C-90	1500	3100	5200	1.7
C-95	700	1100	3800	1.6
B-90_10g	1000	2000	3500	1.7
B-90_20g	1100	1700	3100	1.8
B-90_20g_rep	n.d.	1500	2400	1.6
B-90_20g_5%	800	1800	2400	1.3
B-90_20g_10%	700	1800	2400	1.3
B-90_20g_20%	600	1600	2000	1.3

Table S 2. Thermal properties (DSC) of the enzymatically synthesized PBS prepolymers

Sample	1 st heating		Cooling				2 nd heating					
	T_{m1} (°C)	ΔH_{m1} (J/g)	T_c (°C)	ΔH_c (J/g)	x_c (%)	T_{cc} (°C)	ΔH_{cc} (J/g)	T_{m2} (°C)	ΔH_{m2} (J/g)	x_{cf} (%)		
A-80	93	104	53	80	72	68	4	77	84	93	81	70
A-85	97	101	55	82	74	70	6	79	88	96	81	68
A-90	104	88	61	81	73	77	8	87	95	103	88	73
A-95	107	99	64	81	73	81	12	92	100	107	86	67
B-90	106	95	64	81	73	80	10	91	99	105	87	70
B-95	82	111	45	84	76	58	2	67	75	83	72	63
C-90	108	107	65	85	78	82	14	94	101	107	91	70
C-95	77	64	38	73	66	50	0	60	69	76	62	56
B-90_10g	103	86	57	71	64	74	7	85	94	103	72	59
B-90_20g	98	85	55	78	70	68	8	77	88	98	79	64
B-90_20g_rep	100	95	57	84	76	72	10	83	92	99	85	68
B-90_20g_5%	97	75	54	68	62	69	7	79	88	98	67	61
B-90_20g_10%	99	91	53	78	70	71	8	80	89	97	68	54
B-90_20g_20%	96	62	49	66	60	65	5	74	84	94	58	52

Table S 3. Thermal properties (TGA) of the enzymatically synthesized PBS prepolymers.

Sample	$T_{d,5\%}$ (°C)	T_d (°C)	Residue (%)
A-80	308	398	1.39
A-85	310	382	2.42
A-90	303	396	3.83
A-95	326	385	1.84
B-90	327	384	2.13
B-95	272	382	1.67
C-90	331	383	2.29
C-95	236	383	1.09
B-90_10g	301	387	1.44
B-90_20g	315	384	1.40
B-90_20g_rep	309	398	0.99
B-90_20g_5%	242	400	0.13
B-90_20g_10%	264	401	0.50
B-90_20g_20%	233	401	0.17

Table S 4. Thermal properties (DSC) of the enzymatically synthesized PBF prepolymers

Sample	1 st heating			Cooling			2 nd heating				
	T_{m1} (°C)	ΔH_{m1} (J/g)	T_c (°C)	ΔH_c (J/g)	x_c (%)	T_{cc} (°C)	ΔH_{cc} (J/g)	T_{m2} (°C)	ΔH_{m2} (J/g)		
D-75											
D-80	48	79	10	25	20	7	5	27	16	74	15
D-85	37	74	14	7	-	-	-	16	10	65	7
D-90	48	72	14	14	18	2	2	31	19	75	14
D-95	52	(69) 77	8	9	22	6	5	30	15	(43) 77	12

Table S 5. Thermal properties (DSC) of the enzymatically synthesized and post-polymerized PBS prepolymers

Sample	1 st heating		Cooling				2 nd heating			x_c (%)	
	T_{m1} (°C)	ΔH_{m1} (J/g)	T_c (°C)	ΔH_c (J/g)	T_{cc} (°C)	ΔH_{cc} (J/g)	T_{m2} (°C)	ΔH_{m2} (J/g)			
	Post-polymerization										
Precrystallized	102	65	57	79	71	9	82	90	99.5	79	63
	Solid-state post-polymerization										
S8_95	105	74	54	73	72	11	84	93	102	77	60
S2_M2	103	71	61	79	76	6	87	94	102	77	64
S2_M4	110	67	59	75	76	10	86	96	102	66	51
S2_M6	106	62	59	67	75	8	85	93	101	63	50
	Melt post-polymerization										
M4_110 (B-90_20 g)	104	59	56	56	75	9	87	94	104	60	46

Table S 6. Thermal properties (TGA) of the enzymatically synthesized and post-polymerized PBS and PBF prepolymers

Sample	$T_{d,5\%}$ (°C)	T_d (°C)	Residue (%)
PBS			
Precrystallized	294	379	1.47
Solid-state post-polymerization			
S8_95	312	394	0.17
S2_M2	282	380	6.73
S2_M4	295	381	0.92
S2_M6	298	379	2.81
Melt post-polymerization			
M4_110 (B-90_20 g)	317	393	1.1
M4_110 (B-90_20 g_rep)	305	398	0.3
M6_110	325	402	0.3
M8_110	290	404	0
M10_110	267	398	1.5
M4_120	300	400	0
M4_130	291	400	0
M4_140	298	400	0.7
M4_150	247	323 397	0.9
M4_110_5%	297	400	2.8
PBF			
M4_85	167	256 360	15.1
M4_95	187	266 357	7.3
M4_105	169	253 353	5.5

Appendix 2: Table of Figures

Figure 1. Mechanism of the hydrolysis reaction of ester bonds catalyzed by esterases and lipases [31].	8
Figure 2. Enzymatic ROP of lactide (eROP) (a) and polycondensation of lactic acid (b).	9
Figure 3. Mechanism of the lipase-catalyzed ROP of lactones: Formation of the acyl-enzyme intermediate (a); Initiation (b); Propagation (c).	10
Figure 4. Reaction pathways for enzymatic ring-opening polymerization of lactide: Water reaction (a); Cyclisation reaction (b); Chain Coupling reaction (c).	12
Figure 5. Oligomers chain-end activation (a) and nucleophilic activation of lactide (b).	12
Figure 6. Enzymatic polycondensation in the presence of CALB. *I) Tetrahedral intermediate, *II) acyl-enzyme complex (AEC), *III) tetrahedral intermediate [80].	21
Figure 7. Proposed copolymerization mechanism of CALB-catalyzed formation of P(FMF-co-DOF) [99].	29
Figure 8. Solid state polymerization: Two-phase model.	33
Figure 9. Change of viscosity-average molecular weight with respect to reaction temperature during SSP under flowing nitrogen nitrogen for 32h, with starting PLA grades of $M_v < 25000 \text{ g}\cdot\text{mol}^{-1}$ [115].	36
Figure 10. Mapping of the susceptibility of PBS prepolymers to SSP [25].	38
Figure 11. Melting point change of different PBS grades in the course of SSP [127].	40
Figure 12. Evolution of the intrinsic viscosity (η) with time during SSP of PBF at different temperatures. The continuous line represents simulation results [136].	41
Figure 13. Evolution of hydroxyl ($-\text{OH}$) end-groups concentration with time during SSP at different temperatures. The continuous line represents simulation results [136].	41
Figure 14. Evolution of the crystallinity degree with time and temperature of SSP for (a) PBF and (b) PPF [136].	42
Figure 15. Different types of nanocarriers (nanoparticles) serve as drug delivery [143].	43
Figure 16. Different possibilities of the drug association with nanospheres and nanocapsules [146].	44
Figure 17. Schematic representation of the solvent evaporation method [146].	45
Figure 18. Schematic representation of the emulsification/solvent diffusion method [146].	45
Figure 19. Schematic representation of the emulsification/reverse salting-out method [146].	46
Figure 20. Schematic illustration of the nanoprecipitation method [146].	47
Figure 21. Schematic diagram of active and intelligent packaging concepts [154].	48
Figure 22. Spectrometer Platinum-ATR ALFA II Bruker	59
Figure 23. Agilent 1260 Infinity II instrument.	59
Figure 24. Mettler DSC 1 STARe System	60
Figure 25. Mettler TGA 1 STARe System.	61
Figure 26. ^1H NMR spectra of the prepolymers A-80, A-85, A-90 and A-95	62
Figure 27. ^1H NMR spectra of the prepolymer B-90 and the monomers BDO and DES	63

Figure 28. ¹ H-NMR- and GPC-calculated M_n and X_n of the A-80, A-85, A-90 and A-95 prepolymers.....	64
Figure 29. FTIR spectra of the prepolymers A-80 (a), A-85 (b), A-90 (c) and A-95 (d).....	65
Figure 30. ¹ H-NMR-calculated ester end groups percentage (eq.4) and peak intensities (transmittance percentage) at 1712 and 3400 cm^{-1} for the prepolymers A-80, A-85, A-90, A-95.....	66
Figure 31. Temperature coefficient (a) and the ratios of the constants of the 2 nd order kinetics (k_2/k_{2_ref}).....	67
Figure 32. First heating (a), cooling (b) and second heating (c) of the prepolymers A-80, A-85, A-90 and A-95.	68
Figure 33. Crystallization temperature (T_c) and melting point from the second heating (T_{m2}) of the prepolymers A-80, A-85, A-90 and A-95.....	69
Figure 34. TGA curves and 1 st derivatives of the prepolymers A-80, A-85, A-90 and A-95.	70
Figure 35. 2 nd heating DSC thermogram of B-90 and the monomer BDO (a) and 1 st derivative of the TGA curve of B-90, DES and BDO (b).	70
Figure 36 Morphology of the enzymes at the end of the reactions for the production of the prepolymers B-95 (a), C-95 (d), B-90 (e) and C-90 (f). Morphology of the prepolymers C-90 (b) and C-95 (c)	71
Figure 37. Cooling (a) and second heating (b) of the prepolymers A-95, B-95 and C-95.	72
Figure 38. First heating (a), cooling (b) and second heating (c) of the prepolymer B-90 and the scaled-up prepolymers (10 and 20 g)	75
Figure 39. Peak intensity at 3400 cm^{-1} , ¹ H-NMR-calculated hydroxyl end groups percentage and the analytically calculated slopes for the prepolymers B-90_20g, B-90_20g_5%, B-90_20g_10% and B-90_20g_20%.....	76
Figure 40. Number-average molecular weight values defined by GPC and ¹ H-NMR (a) and weight-average molecular weight values and dispersity values (b).....	77
Figure 41. ¹ H-NMR spectra of the prepolymer D-90, the blank sample, the monomers, and the monomers' mixture. The signals in boxes are zoomed in Figure 21.....	86
Figure 42. Zoomed ¹ H-NMR spectra of the prepolymer D-90, the blank sample, the monomers DEF, BDO and the monomers' mixture for the e (a), a and a' (b), c and c' (c) protons' shifts. .	87
Figure 43. Morphology of the prepolymer D-90 and the relevant blank sample	88
Figure 44. FTIR spectrum of the prepolymer D-90 (a) compared to the blank sample, the monomers DEF, BDO and the monomers' mixture (b).	88
Figure 45. ¹ H-NMR-calculated BDO end groups percentage and peak intensities at 3375 cm^{-1} (a) and 1722 cm^{-1} (b) for the prepolymers D-75, D-80, D-85, D-90, D-95.	89
Figure 46. GPC chromatograms of the prepolymers D-75, D-80, D-85, D-90, D-95.	91
Figure 47. Intensity ratios of peaks I and II of the prepolymers D-75, D-80, D-85, D-90, and D-95, monitored <i>via</i> GPC.....	92
Figure 48. Molecular weights (M_n and M_w) and number-average polymerization degree of the prepolymers D-75, D-80, D-85, D-90 and D-95 (Peak I).	93

Figure 49. DSC curves of the monomers BDO, DEF and the prepolymer D-90 before and after washing with hexane: (a) first heating; (b) cooling; (c) second heating..... 96

Figure 50. TGA curves of the monomers BDO, DEF, monomers' mixture and the prepolymer D-90 before and after washing with hexane: (a) weight curves; (b) 1st derivatives..... 98

Figure 51. Initial activity of N435 compared to the defined activity at the end of the PBF enzymatic prepolymerization reactions at 80, 85, 90 and 95°C..... 98

Figure 52. Peak intensity at 3375 cm⁻¹ and 1722 cm⁻¹ and ¹H-NMR-calculated hydroxyl end groups percentage for the prepolymers (a) E-90 compared to D-90 and (b) E-95 compared to D-95 101

Figure 53. Peak intensity at 3375 cm⁻¹ and 1722 cm⁻¹ and ¹H-NMR-calculated hydroxyl end groups percentage for the prepolymers (a) F-90 compared to D-90 and (b) F-95 compared to D-95 103

Figure 54. GPC chromatograms for the F-90 and F-95 prepolymers compared to the D-90 and D-95 103

Figure 55. Molecular weights of the D-90, F-90 and F-90_24 prepolymers..... 104

Figure 56. T_d and T_{d,5%} of the prepolymers D-90, F-90 and F-90_24 105

Figure 57. Morphology of the scaled-up prepolymers D-90_3g (a) and D-90_6g (b) 106

Figure 58. Molecular weights and T_{d,5%} of the scaled-up prepolymers D-90_3g and D-90_6g compared to D-90 106

Figure 59. Controlled porosity glass beads carrier EziG3 Amber (EnginZyme, Sweden)..... 110

Figure 60. Immobilized on the EziG3 Amber carrier LCC^{ICCG} 111

Figure 61. Effect of temperature on the activity (a) and the stability (b) of immobilized LCC^{ICCG} on pNPL..... 114

Figure 62. Blank (reference) sample (a), prepolymers synthesized using the immobilized LCC^{ICCG} at 50, 60 and 70°C (b-d), B-90 (e) 115

Figure 63. ¹HNMR spectra of the prepolymers L-50, L-60, L-70, B-90 and the blank (reference) sample 115

Figure 64. FTIR spectra of the prepolymers L-50, L-60, L-70, B-90 and the blank (reference) sample 116

Figure 65. ¹HNMR-calculated OH end groups percentage and peak intensities at 3400 cm⁻¹ and 1712 cm⁻¹ for the prepolymers L-50, L-60 and L-80..... 117

Figure 66. GPC chromatograms of the prepolymers L-50, L-60, L-70, B-90, the blank (reference) sample and the monomers (BDO and DES) 118

Figure 67. Intensity ratios of peaks I and II of the prepolymers L-50, L-60 and L-70 monitored via GPC 119

Figure 68. GPC chromatograms of the prepolymer L-60 before and after post-polymerization (a), *Mn* and *Mw* percentage increases after post-polymerization of the prepolymers L-50, L-60, L-70..... 120

Figure 69. First heating (a) and second heating (b) of the starting material (B-90_20g) and the post-polymerized samples..... 125

Figure 70. Starting material (a) and melt post-polymerized at 110°C PBS samples for 4 h (b), 6 h (c), 8 h (d) and 10 h (e).....	128
Figure 71. Molecular weights (M_n , M_w) and dispersity \mathcal{D} of the post-polymerized PBS prepolymers as a function of reaction time	129
Figure 72. Oligomeric products of PBS thermo-oxidative decomposition [226]	130
Figure 73. T_d and $T_{d,5\%}$ of the post-polymerized PBS prepolymers as a function of reaction time	130
Figure 74. Starting material (a) and melt post-polymerized for 4h PBS samples at 110°C (b), 120°C (c), 130°C (d), 140°C (e), and 150°C (f)	131
Figure 75. Molecular weights (M_n , M_w) and dispersity \mathcal{D} of the post-polymerized PBS prepolymers as a function of reaction temperature	132
Figure 76. T_d and $T_{d,5\%}$ of the post-polymerized PBS prepolymers as a function of reaction temperature	132
Figure 77. TGA curves and 1 st derivatives of the post-polymerized PBS prepolymers as a function of reaction temperature	133
Figure 78. Molecular weights (M_n , M_w) of the PBS prepolymer synthesized with 5% BDO excess before and after post-polymerization at 110°C for 4 h.....	134
Figure 79. Mechanism of efficient PBS trans-esterification [23]	135
Figure 80. M_n , M_w and X_n of the post-polymerized PBF prepolymers at 85, 95 and 105°C ..	137
Figure 81. TGA curves and 1 st derivatives of the post-polymerized PBF prepolymers as a function of reaction temperature	137
Figure 82. Zetasizer Nano ZS.....	143
Figure 83. Jasco V – 770, Spectrophotometer (JASCO UK Limited, UK)	143
Figure 84. (a) DSC (1 st heating), (b) zoomed DSC (1 st heating) and (c) TGA (1 st derivative) of Naringin (blue), physical mixture of PBS-Naringin (green), naringin-loaded and unloaded PBS nanoparticles (grey and red respectively).....	145
Figure 85. In vitro release profile of PBS nanoparticles loaded with naringin (pH 7.4, T=25°C)	146
Figure 86. Total molecular weights of the enzymatically synthesized prepolymers PBS and PBF. Reaction temperature investigation: set of samples A, D and L; Pressure investigation: set of samples: B and E; Reaction time investigation: set of samples C and F.....	151
Figure 87. Total molecular weights of the post-polymerized PBS and PBF.....	152

Appendix 3: Table of Tables

Table 1. Structures of PLA, PBS and PBF.....	6
Table 2. Literature data on the enzymatic polymerization of PLA.....	14
Table 3. Literature data on the enzymatic polymerization of PBS.....	24
Table 4. Literature data on the enzymatic polymerization of furan-based polymers	28
Table 5. Indicative literature conditions for melt synthesized PLA solid state polymerization [115].....	35
Table 6. Active agents incorporated in PBS matrices, incorporation methods and formulations	50
Table 7. Compounds used for the prepolymerization of PBS	56
Table 8. Calculated activity values of N435, based on the different protein contents.....	57
Table 9. Conditions of PBS enzymatic prepolymerization	58
Table 10. Compounds used for the prepolymerization of PBF	82
Table 11. Conditions of PBF enzymatic prepolymerization	83
Table 12. ¹ HNMR- and GPC-calculated M_n , M_w and dispersity \bar{D} of the enzymatically synthesized PBF prepolymers.....	94
Table 13. Thermal properties (TGA) of the enzymatically synthesized PBF prepolymers.....	97
Table 14. Conditions of PBS enzymatic prepolymerization using the immobilized LCC ^{ICCG}	113
Table 15. ¹ HNMR- and GPC-calculated molecular weights of the polymers L-50, L-60 and L-70	118
Table 16. Thermal properties defined via TGA of the prepolymers L-50, L-60 and L-70 monitored via GPC.....	119
Table 17. Conditions of PBS and PBF prepolymers post-polymerization	124
Table 18. M_n , M_w and dispersity \bar{D} of the enzymatically synthesized and post-polymerized PBS and PBF prepolymers.....	126
Table 19. Compounds used for naringin encapsulation in PBS	142
Table 20. Characterization of unloaded (Blank) and naringin-loaded PBS nanoparticles: particle size, polydispersity index (PDI), ζ -potential, encapsulation efficiency (EE), process yield	144